

**PERFORMANCE AND MODELING OF  
GASIFICATION PROCESS IN A FLUIDIZED BED  
GASIFIER**

**A Thesis  
Submitted to the College of Engineering  
of Alnahrain University in Partial Fulfillment of the  
Requirements for the Degree of  
Master of Science  
in  
Chemical Engineering**

**by  
ISRAA KARAM ABED  
B.Sc. in Chemical Engineering 2009**

**Dhu Al-Qi'da  
October**

**1433  
2012**

## Certification

I certify that this thesis entitled “**Performance and Modeling of Gasification Process in a Fluidized Bed Gasifier**” was prepared by **Israa Karam Abed** under my supervision at Alnahrain University / College of Engineering in partial fulfillment of the requirements for the degree of Master of Science in Chemical Engineering.

Signature:



Name: Asst. Prof. Dr. Basim O. Hasan  
( Supervisor)

Date:

22 / 10 / 2012

Signature:



Name: Asst. Prof. Dr. Basim O. Hasan  
(Head of Department)

Date:

22 / 10 / 2012

## Certificate

We certify, as an examining committee, that we have read this thesis entitled "Performance and Modeling of Gasification Process in a Fluidized Bed Gasifier", examined the student **Israa Karam Abed** in its content and found it meets the standard of thesis for the degree for the degree of Master of Science in Chemical Engineering.

Signature:



Name: Asst. Prof. Dr. Basim O. Hasan

(Supervisor)

Date:

21 / 10 / 2012

Signature:



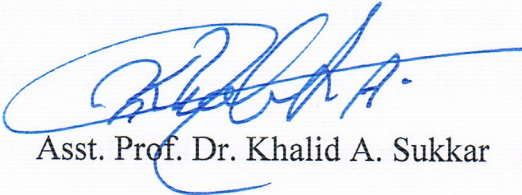
Name: Asst. Prof. Dr. Khalid M. Mousa

(Member)

Date:

22 / 10 / 2012

Signature:



Name: Asst. Prof. Dr. Khalid A. Sukkar

(Member)

Signature:



Name: Prof. Dr. Aprael S. Yaro

(Chairman)

Date:

21 / 10 / 2012

Date:

21 / 10 / 2012

Approval of the college of Engineering

Signature:



Name: Prof. Dr. Muhsin J. Jweeg  
(Dean)

Date:

31 / 10 / 2012

## Abstract

The present work is concerned with the study of the mechanisms of gasification reactions to produce biogas by the gasification of coal and algae, and co-gasification of coal-algae and coal-grape seeds in a spouted fluidized bed gasifier under different operating conditions. Theoretically, an isothermal model is established to calculate the concentration profile of the produced gas components inside the gasifier.

The experimental work was conducted to gasify coal, algae, coal + algae biomass, and coal + grape seeds biomass with silica sand as a bed material in a spouted fluidized bed gasifier consists of cylindrical column with 77 mm inside diameter and 1.165 m height connecting to a fuel hoppers, heater, air flow meter, ash collector, and water rotameter. The effect of different variables on the carbon conversion and biogas production were studied such as bed temperature, steam to fuel ratio S/F, air to fuel ratio A/F, and biomass to coal ratio.

In coal gasification experiments the concentration of CO<sub>2</sub> was found to decrease with increasing temperature at lower coal feed rate, while H<sub>2</sub>, CO, and CH<sub>4</sub> concentrations increased with temperature increase. Increasing the coal feed rate results in an increase in the compositions of the produced CO<sub>2</sub>, CO, H<sub>2</sub>, and CH<sub>4</sub> with bed temperature increase.

Using the steam with air as a gasification agent prevents bed agglomeration to occur. Increasing the ratio of steam to fuel results in an increase in the concentrations of CO<sub>2</sub>, H<sub>2</sub> and CH<sub>4</sub> and decrease in CO concentration. At lower bed temperature the concentration of H<sub>2</sub> increased with increasing the ratio of A/F while at higher bed temperature increasing the ratio of A/F decreased the concentration of H<sub>2</sub>. The optimum operating conditions, in coal gasification, were identified to occur with A/F = 1.8, S/F = 0.75 and T = 850 °C. These conditions resulted in a producer gas with the highest extent of carbon conversion of 92.9% and the optimum H<sub>2</sub>:CO ratio of 2.197 for Fischer-Tropsch synthesis.

Co-gasification of coal-grape seeds biomass revealed that the bed temperature is the most influential parameter on the carbon conversion while the biomass to coal ratio (B/C) has the less effect on carbon conversion.

Theoretically, an isothermal model for calculating concentration profile of the gases inside the gasifier was established. The mass transport model for the species was obtained from differential mass balance to obtain the differential equations describing the system. Finite difference numerical technique was employed to solve these equations using Matlab (R2011a) that has been built to solve for the whole investigated range of temperature and flow velocity.

Good agreement was obtained between theoretical model and experimental results.

# List of Contents

## Content

		Page
Abstract		I
List of Contents		III
Notations		VII
List of Tables		XI
List of Figures		XIV
<b>Chapter One : Introduction</b>		<b>1</b>
1.1	Introduction	1
1.2	Aim of this Work	3
<b>Chapter Two : Literature Survey</b>		<b>4</b>
2.1	Gasification	4
2.1.1	Introduction	4
2.1.2	Effect of fuel moisture content on gasification	5
2.2	Gasification Reactions	6
2.2.1	Gasification products	8
2.3	Gasification Processes	8
2.3.1	Air gasification	9
2.3.2	Steam gasification	9
2.3.3	Oxygen gasification	10
2.3.4	Hydrogen gasification	10
2.4	Gasification Reactors	10
2.4.1	Fixed Bed Gasifiers	11
2.4.2	Fluidized Bed Gasifiers	11
2.4.2.1	Fluidize Bed Gasifiers Types	12
2.4.2.1.1	Bubbling Fluidized Bed Gasifier	12
2.4.2.1.2	Circulating Fluidized Bed Gasifier	12
2.4.2.1.3	Spouted Fluidized Bed Gasifier	14
2.4.3	Indirect Fluidized Bed Gasifier	14
2.5	Geldart Classification of Particles	15
2.6	Characteristics of Spouted Fluidized Bed	16
2.6.1	The phenomena of Fluidization	16
2.6.2	Minimum fluidization velocity	17
2.6.3	Minimum spouting velocity ( $U_{ms}$ )	19
2.7	Fossil Fuel	20
2.7.1	Introduction	20
2.7.2	Coal	21
2.7.2.1	Coal production	22
2.8	Biomass	22
2.8.1	Introduction	22
2.8.2	Biomass algae	23

2.8.3	Types of Algae	24
2.8.3.1	Macro-algae	24
2.8.3.2	Micro-algae	24
2.9	Hydrogen	25
2.9.1	Hydrogen Production methods	25
2.9.1.1	Coal gasification	25
2.9.2.	Biomass Sources	26
2.10	Modelling	28
2.10.1	Introduction	28
<b>Chapter Three : Theoretical Modeling</b>		<b>34</b>
3.1	Simulation of gas – solid system model	34
3.1.1	Steady – State model assumptions	34
3.2	Steady – state model equations	34
3.2.1	Mass balance to obtain the continuity equation in the gas phase	34
3.2.2	Gas – phase equations for the spout and annulus regions	37
3.2.3	Gas – Solid interface	40
3.3	Solution procedure of the modeling equations	42
3.3.1	Boundary conditions	42
3.3.2	Calculation procedure	43
<b>Chapter Four : Experimental Work</b>		<b>46</b>
4.1	Materials	46
4.1.1	Bed material	46
4.1.2	Fuel	46
4.1.3	Gasification agents	47
4.1.4	Nitrogen	47
4.1.5	Cooling water	48
4.2	Bed material and fuel sieving	48
4.3	Moisture content of the fuel	48
4.4	Steam calibration	49
4.5	Minimum fluidization velocity	49
4.6	Leaching of algae	50
4.6.1	Composition materials of algae	51
4.7	Feeding velocity of the fuel	51
4.8	Spouted bed gasification Unit Description	52
4.8.1	Gasifier	52
4.8.2	Furnace	52
4.8.3	Fuel hoppers	53
4.8.4	Temperature controllers and pressure transmitters	53
4.8.5	Heater	53
4.8.6	Ash collector	54
4.9	The studied operating conditions	55
4.9.1	Coal gasification experiments	55
4.9.2	Co – gasification experiments	56

4.10	Procedure of gasification experiments	58
4.11	Composition measurement	60
4.11.1	Scanning Electron Microscope	60
4.11.2	Gas Chromatography	61
<b>Chapter Five : Results and Discussions</b>		<b>62</b>
5.1	Minimum fluidization velocity	62
5.2	Gasification of coal	62
5.2.1	Effect of temperature	63
5.2.2	Effect of steam to fuel ratio	73
5.2.3	Effect of air to fuel ratio	81
5.2.4	Carbon conversion	86
5.3	Algae gasification	88
5.3.1	Co-gasification (Coal-Algae, gasification)	90
5.4	Co-gasification (coal-grape seeds gasification)	92
5.4.1	Determination of Percentage Contribution of Individual Variables.	94
5.4.2	Determination of Best Experimental Condition by the Taguchi Method	97
5.4.3	Effect of different variable levels on the average gas compositions	100
5.5	Theoretical modelling	104
5.5.1	Distribution of gas compositions in the gasifier	104
5.5.2	Comparison of Experimental and Isothermal Model results	109
5.5.3	Checking the validity of the predicted isothermal Model	110
<b>Chapter Six: Conclusions and Recommendations</b>		<b>114</b>
6.1	Conclusions	114
6.2	Recommendations for the Future Work	116
<b>References</b>		<b>117</b>
<b>Appendices</b>		
<b>Appendix A: Experimental Data</b>		<b>A-1</b>
<b>Appendix B: Experimental calculations</b>		<b>B-1</b>
<b>Appendix C: Kinetic rate expressions and fuel compositional information</b>		<b>C-1</b>
<b>Appendix D: Theoretical calculations</b>		<b>D-1</b>
<b>Appendix E: SEM analysis results</b>		<b>E-1</b>
<b>Appendix F: Carbon conversion results for coal-grape seeds gasification</b>		<b>F-1</b>

## Notations

Symbols		Unit
A	Cross sectional area of the differential element	$m^2$
$A_a$	Annulus area	$m^2$
$A_c$	Area of column	$m^2$
$a_i$	Number of carbon molecules in the produced gas	-
$A_s$	Spout area	$m^2$
$A_r$	Archimede's number	-
$C_1, C_2$	Constants in equation (2.5)	-
$C_i$	Concentration of gas at node $i$	$k.mole/m^3$
$C_{i+1}$	Concentration of gas at node $i+1$	$k.mole/m^3$
$C_{i-1}$	Concentration of gas at node $i-1$	$k.mole/m^3$
$C_{ib}$	Concentration of the gas phase in the bulk	$k.mole/m^3$
$C_{is}$	Concentration of the gas on the solid fuel surface	$k.mole/m^3$
$cp_i$	Heat capacity of component $i$	$kJ/kmol.K$
$D_b$	Bed diameter	m
$D_c$	Column diameter	m
$D_i$	Gas diffusivity	$m^2/s$
$D_e$	Gas effective diffusivity	$m^2/s$
$d_p$	Particle diameter	m
$d_{in}$	Gas inlet diameter	m
$D_s$	Spout diameter	m
$D_{sm}$	Minimum spouting diameter	m
$F_a$	fraction of ash in coal	-
$F_c$	carbon fraction in coal	-
$f_{lossi}$	spout gas divergence function for component $i$	$kmol/ m.s$
$F_w$	fraction of moisture in coal	-
$g$	gravitational constant	$m/s^2$
$H$	Bed height	m
$H_c$	Height of column	m
$h$	Height above base of gasifier	m
$H_m$	Maximum spoutable height	m
$h_M$	Height of spouted bed	m
$h_p$	Heat-transfer coefficient for particle to spout gas heat transfer	$kW/ m^2.K$
$h_{wr}$	Wall heat transfer coefficient	$W/ m^2.K$
$k_{ea}$	Particle effective thermal conductivity	$W/ m. K$
$L_e$	length of entrainment region	m
$M_c$	Molar mass of carbon	$kg/k.mol$
$N_c$	Number of gaseous components	-
$N_1$	Number of collocation points in entrainment region	-
$Q$	Volumetric gas flow rate	$m^3/s$
$Q_p^j$	Gas flow rate after temperature correction	$m^3/s$

$Q_p^A$	Gas flow rate after gasification reactions	$m^3/s$
$Q_s$	Gas flow rate at the spout after temperature correction	$m^3/s$
R	Gasifier column radius	m
$Re_{mf}$	Reynolds number at minimum fluidization	-
$(Re_o)_{ms}$	Reynolds number at minimum spouting	-
$r_{ij}$	Reaction rate for component i in reaction j	$kmol/m^3.s$
$r_p$	Radius of the fuel particle	m
Rg	Ideal gas constant	J/mol.K
$T_a$	Gas temperature in the annular	K
$T_E$	Gasifier exit temperature	K
$T_g$	Gas temperature	K
$T_p$	Particle temperature	K
$T_R$	Reference temperature	K
$T_w$	Wall temperature	K
t	Time	s
U	Superficial gas velocity	m/s
u	Interstitial gas velocity	m/s
$u_a$	Annulus gas velocity	m/s
$u_{in}$	Injection gas velocity	m/s
$u_{mf}$	Minimum fluidization gas velocity	m/s
$u_{ms}$	Minimum spouting gas velocity	m/s
$u_s$	Gas velocity at the spout	m/s
$U_w$	overall heat-transfer coefficient for heat transfer from annular wall to spout gas	$kW/m^2.K$
v	Volume of the element	$m^3$
$V_a$	Superficial annular particle velocity	m/s
$V_s$	Superficial spout particle velocity	m/s
$W_1$	Weight of the solid fuel sample before drying	kg
$W_2$	Weight of the solid fuel sample before drying	kg
$W_s$	Solids flow rate	mole/s
$X_C$	Carbon conversion	-
$x_i$	Composition of the produce gas from GC	-
$X_i$	Molar fraction of gas composition	-
$Y_{k,A}^j$	molar concentration after temperature correction	$mol/m^3$
z	Axial distance from gas inlet	m

## Greek Letters

$\Delta H$	heat of reaction for reaction	kJ/kmol
$\eta$	Viscosity of air	kg/m.s
$\varnothing_k(T_b)$	devolatilization gas yield of species <i>k</i> as a function of bed temperature	kg.mol/ kg coal
$\varepsilon$	Porosity of the bed	-
$\lambda, \mu, \alpha, \beta, \gamma, \delta$	Exponents in equation (2.8)	-
$\varepsilon_a$	Porosity of the bed at the annulus	-
$\varepsilon_{mf}$	Porosity of the bed at minimum fluidization velocity	-
$\varepsilon_s$	Voidage in the spout	-
$\mu_g$	Viscosity of gas	kg/m.s
$\rho_g$	Density of gas	kg/m <sup>3</sup>
$P_p$	particle density	kg/m <sup>3</sup>
$\tau$	Tortuosity factor	-

## Abbreviations

A/F	Air to Fuel ratio
B/C	Biomass to Coal ratio
BFG	Bubbling Fluidized Bed Gasifier
CFB	Circulating Fluidized Bed
CFD	Computational Fluid Dynamics
GC	Gas Chromatography
IEA	International Energy Agency
PT	Pressure tapping
S/B	Steam to Biomass ratio
S/F	Steam to Fuel ratio
TC	Temperature Controllers
TCD	Thermal Conductivity Detector

## List of Tables

Table	Title	Page
(2-1)	Gasification exothermic reactions	7
(2-2)	Gasification endothermic reactions	7
(2-3)	Correlations for $U_{mf}$ and $Re_{mf}$	18
(2-4)	Parameters used in Wen and Yu type equations for minimum fluidization velocity	19
(2-5)	Correlations for minimum spouting velocity	20
(2-6)	Fitted constants for minimum spouting velocity equation	20
(4-1)	moisture content of the used fuels	49
(4-2)	Studied operating conditions for coal gasification experiments	56
(4-3)	Design experiments, with four parameters at three-levels, for the production of biogas	57
(4-4)	Orthogonal array used to design experiments with four parameters at three-levels	57
(4-5)	Experiments for the parameters and levels shown in Table 4-3	57
(5-1)	Gasification reactions	63
(5-2)	% Carbon conversion, MSD, and S/N ratios for the nine set of gasification experiments	95
(5-3)	Mean S/N ratios	96
(5-4)	Difference between two levels	96
(5-5)	% Contribution for each variable	96
(5-6)	Theoretical and experimental producer gas compositions at the bed exit	109
(5-7)	Producer gas compositions at the bed exit results from the completed model and the compositions obtained by Lucas et al., (1991) model	111
(A-1)	Experimental results for run with coal feed rate = 1.6 kg/h, S/F ratio= 0.5, and bed Temperature = 850 °C	A-1
(A-2)	Experimental results for run with coal feed rate = 1.6 kg/h, S/F ratio= 0.75, and bed Temperature = 850 °C	A-1
(A-3)	Experimental results for run with coal feed rate = 1.6 kg/h, S/F ratio= 0.5, and bed Temperature = 820 °C	A-2
(A-4)	Experimental results for run with coal feed rate = 1.6 kg/h, S/F ratio= 0.75, and bed Temperature = 820 °C	A-3
(A-5)	Experimental results for run with coal feed rate = 1.43 kg/h, S/F ratio= 0.75, and bed Temperature = 850 °C	A-3
(A-6)	Experimental results for run with coal feed rate = 1.43 kg/h, S/F ratio= 0.5, and bed Temperature = 850 °C	A-4

(A-7)	Experimental results for run with coal feed rate = 1.43 kg/h, S/F ratio= 0.75, and bed Temperature = 820 °C	A-4
(A-8)	Experimental results for run with coal feed rate = 1.43 kg/h, S/F ratio= 0.5, and bed Temperature = 820 °C	A-5
(A-9)	Experimental results for run with coal feed rate = 1.28 kg/h, S/F ratio= 0.5, and bed Temperature = 850 °C	A-6
(A-10)	Experimental results for run with coal feed rate = 1.28 kg/h, S/F ratio= 0.75, and bed Temperature = 850 °C	A-6
(A-11)	Experimental results for run with coal feed rate = 1.28 kg/h, S/F ratio= 0.5, and bed Temperature = 820 °C	A-7
(A-12)	Experimental results for run with coal feed rate = 1.28 kg/h, S/F ratio= 0.75, and bed Temperature = 820 °C	A-8
(A-13)	Experimental results for run with coal feed rate = 1.43 kg/h, S/F ratio= 0, and bed Temperature = 850 °C	A-8
(A-14)	Operating conditions for coal gasification experiments and % carbon conversion at each run	A-9
(A-15)	Compositions for gases result from co – gasification experiment with 10% algae + 90% coal, with S/F and A/F ratios of 0.5 and 2 respectively	A-9
(A-16)	Average S/N ratios at different S/F ratios	A-10
(A-17)	Average S/N ratios at different A/F ratios	A-11
(A-18)	Average S/N ratios at different B/C ratios	A-11
(A-19)	Average S/N ratios at different bed temperatures	A-12
(A-20)	Average carbon conversion results at different S/F ratios	A-12
(A-21)	Average carbon conversion results at different A/F ratios	A-13
(A-22)	Average carbon conversion results at different B/C ratios	A-13
(A-23)	Average carbon conversion results at different bed temperatures	A-14
(A-24)	Average gas compositions at different S/F ratios	A-15
(A-25)	Average gas compositions at different A/F ratios	A-15
(A-26)	Average gas compositions at different B/C ratios	A-16
(A-27)	Average gas compositions at different bed temperatures	A-16
(A-28)	Experimental results for the best coal-grape seeds experiment with A/F = 2.5, S/F ratio= 0.75, B/C =0.05, and bed Temperature = 850 °C	A-17
(B-1)	Experimental results of pressure drop values for each superficial gas velocity	B-1
(B-2)	Calibration data of water flow rate and mass flow rate	B-3
(B-3)	Experimental results for the feed settling velocity experiment	B-3
(B-4)	Experimental results for the volatile and non-volatile in the algae	B-4

(C-1)	Gasification reaction rates expressions	C-1
(C-2)	Coal compositional information	C-2
(C-3)	Grape seeds biomass compositional information	C-3
(D-1)	Values of bed porosity at the spout, and gas annulus velocities $u_a$	D-5
(E-1)	Compositions of the materials in the selected section in Fig. E-1	E-1
(E-2)	Compositions of the materials in the selected part in Fig. E-2	E-2
(E-3)	Compositions of the materials in the selected part in Fig. E-3	E-3
(E-4)	Compositions of the materials in the selected part in Fig. E-4	E-3
(E-5)	Compositional information for the selected sections in Figure E-9a, b, c, and d	E-8

## List of Figures

Figure	Title	page
(2-1)	Moisture scale for gasification	6
(2-2)	Gasification Steps	6
(2-3)	Fluidised Bed Gasifiers; a: Bubbling Fluidized Bed Gasifier; b: Circulating Fluidized Bed Gasifier; c: Spouting Fluidized Bed Gasifier; and d: Gas Indirect Gasifier.	13
(2-4)	Geldart classification of particles according to fluidization properties	16
(2-5)	Pressure drop in flow through packed and fluidized beds	17
(2-6)	Schematic draw of spouted bed	18
(2-7)	Coal consumed for electricity	22
(2-8)	Oil Yields of Feedstocks for Biofuel from EarthTrends	23
(3-1)	Schematic sketch for the gasifier and the gas cell taken to make the balance	35
(3-2)	Schematic diagram of the spout fluidized bed gasifier	39
(3-3)	Schematic sketch of the solid particle surrounded by the boundary layer	40
(3-4)	Schematic sketch of the element taken in the boundary layer	41
(3-5)	Two dimensional finite difference net work of node (i,n)	44
(4-1)	a. Bed material b. Brown Coal c. Algae d. Grape seeds	47
(4-2)	photographic picture for the used Shaker	48
(4-3)	Photographic picture of microalgae solution	50
(4-4)	Photographic picture of algae cake settled after leaching	50
(4-5)	Photographic picture of dried algae	50
(4-6)	Algae samples for burning	51
(4-7)	photographic picture for the spouted bed gasification unit	54
(4-8)	Schematic sketch for the Spouted bed gasification unit	55
(4-9)	Photographic picture of the Scanning Electron Microscope	60
(4-10)	Gas Chromatography	61
(5-1)	Relation between bed pressure drop and air superficial velocity at 25 °C	62
(5-2)	Effect of bed temperature on the molar hydrogen compositions at coal feeding rate of 1.28 kg/h, 0.5 S/F	64
(5-3)	Effect of bed temperature on the molar hydrogen compositions at coal feeding rate of 1.28 kg/h, 0.75 S/F	64
(5-4)	Effect of bed temperature on the molar compositions of the produced gas component at run of 1.28 kg/h coal feed rate	65

(5-5)	Effect of bed temperature on the molar compositions of the produced gas component at run of 1.28 kg/h coal feed rate	66
(5-6)	Effect of bed temperature on the molar hydrogen compositions at coal feeding rate of 1.43 kg/h, 0.5 S/F	67
(5-7)	Effect of bed temperature on the molar hydrogen compositions at coal feeding rate of 1.43 kg/h, 0.75 S/F	68
(5-8)	Effect of bed temperature on the molar compositions of the produced gas component at run of 1.43 kg/h coal feed rate	68
(5-9)	Effect of bed temperature on the molar compositions of the produced gas component at run of 1.43 kg/h coal feed rate	69
(5-10)	Effect of bed temperature on the molar hydrogen compositions at coal feeding rate of 1.6 kg/h, 0.5 S/F	70
(5-11)	Effect of bed temperature on the molar hydrogen compositions at coal feeding rate of 1.6 kg/h, 0.75 S/F	70
(5-12)	Effect of bed temperature on the molar compositions of the produced gas component at run of 1.6 kg/h coal feed rate	71
(5-13)	Effect of bed temperature on the molar compositions of the produced gas component at run of 1.6 kg/h coal feed rate	72
(5-14)	Produced gas component distribution at the first hour of 1.43kg/h coal feed rate and 0 S/F, at 850 °C	73
(5-15)	Photographic picture of the agglomerate collected after the run	74
(5-16)	Effect of S/F ratio on the molar hydrogen compositions at coal mass rate of 1.28 kg/h, 820 °C	75
(5-17)	Effect of S/F ratio on the molar hydrogen compositions at coal mass rate of 1.28 kg/h, 850 °C	76
(5-18)	Effect of S/F ratio on the molar compositions of CO <sub>2</sub> , CO, and CH <sub>4</sub> at coal mass rate of 1.28 kg/h	77
(5-19)	Effect of S/F ratio on the molar compositions of hydrogen at coal mass rate of 1.43 kg/h and 820 °C	77
(5-20)	Effect of S/F ratio on the molar compositions of hydrogen at coal mass rate of 1.43 kg/h and 850 °C	78
(5-21)	Effect of S/F ratio on the molar compositions of CO <sub>2</sub> , CO, and CH <sub>4</sub> at coal mass rate of 1.43 kg/h	79
(5-22)	Effect of S/F ratio on the molar compositions of hydrogen at coal mass rate of 1.6 kg/h	79
(5-23)	Effect of S/F ratio on the molar compositions of CO <sub>2</sub> , CO, and CH <sub>4</sub> at coal mass rate of 1.6 kg/h	80

(5-24)	Effect of A/F ratio on the molar compositions of hydrogen at S/F of 0.5 and 820 °C	81
(5-25)	Effect of A/F ratio on the molar compositions of hydrogen at S/F of 0.75 and 820 °C	82
(5-26)	Effect of A/F ratio on the molar compositions of hydrogen at S/F of 0.5 and 850 °C	82
(5-27)	Effect of A/F ratio on the molar compositions of hydrogen at S/F of 0.75 and 850 °C	83
(5-28)	Effect of A/F on the molar composition of CO <sub>2</sub> at S/F ratios of 0.5, and 0.75	84
(5-29)	Effect of A/F on the molar composition of CO at S/F ratios of 0.5 and 0.75	85
(5-30)	Effect of A/F on the molar composition of CH <sub>4</sub> at S/F ratios of 0.5 and 0.75	86
(5-31)	Carbon conversion values for coal gasification experiments	87
(5-32)	Producer gas molar compositions from (algae-coal) gasification	91
(5-33)	Blockages in the outer tubes of the gasifier	91
(5-34)	Molar compositions of producer gas component result from Co-gasification	93
(5-35)	Percentage contribution of individual variables on variation carbon conversion	97
(5-36)	Effect of bed temperature at different levels on the mean S/N ratio	98
(5-37)	Effect of changing the S/F ratios on the S/N ratio	98
(5-38)	Effect of changing A/F ratio on the S/N ratio	99
(5-39)	Effect of changing the B/C ratios on the S/N	99
(5-40)	Effect of A/F ratio on the average gas compositions	101
(5-41)	Effect of S/F ratio on the average gas compositions	101
(5-42)	Effect of bed temperature on the average gas compositions	102
(5-43)	Effect of B/C ratio on the average gas compositions	103
(5-44)	Theoretical concentration profiles for oxygen in the spout and the annulus	105
(5-45)	Theoretical concentration profiles for carbon dioxide in the spout and the annulus	106
(5-46)	Theoretical concentration profiles for carbon monoxide in the spout and the annulus	107
(5-47)	Theoretical concentration profiles for steam in the spout and the annulus	108
(5-48)	Theoretical concentration profiles for hydrogen in the spout and the annulus	109
(5-49)	Experimental and theoretical concentration profiles for	110

	CO <sub>2</sub> , CO, H <sub>2</sub> , and O <sub>2</sub> at the bed exit	
(5-50)	CO, CO <sub>2</sub> , and H <sub>2</sub> concentration at the bed exit in both annulus and spout regions resulting from the completed model and Lucas et al., (1991) model	111
(5-51)	Average CO, CO <sub>2</sub> , and H <sub>2</sub> compositions at the bed exit in both annulus and spout regions resulting from the completed model and Lucas et al., (1991) model	112
(5-52)	Bed porosity with the bed height	112
(5-53)	Gas – phase velocity profile at the annulus region	113
(B-1)	Relation between the mass flow rate of the water and rotameter readings	B-3
(B-2)	Relation between feed settler velocity and the weight of fuel	B-4
(E-1)	Micrograph of SEM secondary electronic image for a section of agglomerate	E-1
(E-1a)	Micrograph of SEM secondary electronic image for section (A) in Figure E-1	E-1
(E-1b)	Peaks of the materials included in the selected section in Fig. E-1	E-1
(E-2)	Micrograph of SEM secondary electronic image for a section of agglomerate	E-2
(E-2a)	Micrograph of SEM secondary electronic image for the selected section in Fig. E-2	E-2
(E-2b)	Peaks of the materials included in the selected part of Fig. E-2	E-2
(E-3)	Micrograph of a SEM backscattered image of a section of agglomerate	E-3
(E-4)	Micrograph of a SEM backscattered image of a section of agglomerate	E-3
(E-5)	Micrographs of SEM secondary electronic images of agglomerate	E-4
(E-6)	Micrographs of SEM secondary electronic images of agglomerate	E-5
(E-7)	Micrographs of SEM back scattered electron images	E-5
(E-8)	Micrographs of SEM back scattered electron images	E-6
(E-8a)	Micrographs of SEM back-scattered electron images zoom-in for section 1 in Fig. E-8	E-6
(E-9)	Micrographs of SEM back-scattered electron images for the bed material, with the results of analysis for the selected sections in images a, b, c, and d.	E-7
(E-10)	Micrographs of SEM secondary- electron images and the composition of each component result from analysis in sections 1 and 2 of raw algae before leaching	E-8
(E-10a)	Peaks for the compositions of raw algae before leaching	E-9

(E-10b)	at section 1 in Fig.E-10 taken under SE detector Peaks for the compositions of raw algae before leaching	E-9
(E-11)	at section 2 in Fig.E-10 taken under SE detector Micrographs of SEM secondary- electron images and the composition of each component result from analysis in the selected sections of raw algae after leaching	E-10
(E-11a)	Peaks for the compositions in the selected section in Fig. E-11 of raw algae after leaching taken under SE detector	E-10
(F-1)	Effect of changing A/F ratio on carbon conversion	F-1
(F-2)	Effect of changing S/F ratio on carbon conversion	F-2
(F-3)	Effect of changing the bed temperature on carbon conversion	F-2
(F-4)	Effect of changing the B/C ratio on carbon conversion	F-3

# Chapter One

## Introduction

### 1.1 Introduction

The global warming crisis has become a major and ever increasing issue in the fast pace, heavily industrialized world we live in today. As the population living on this planet increases and the acceptable standard of living gets higher, energy demand is expected to increase and with it the consumption of fossil fuels and production of greenhouse gases (**Agency, 2011**), therefore more and more attentions have been paid to the clean coal technology, among which the coal gasification is one of the critical technologies for the efficient utilization of coal (**Yu et al., 2007**). The use of biomass as a source of energy has been further enhanced in recent years and special attention has been paid to biomass gasification (**Arnavat et al., 2010**). The New Policies Scenario proposed by the International Energy Agency (IEA) has predicted a world primary demand for energy increase of 40% between 2009 and 2035. This is expected to result in an energy related carbon dioxide emission increase of 20% and a long term rise in global temperature of approximately 3.5 °C (**Agency, 2011**).

Gasification can be broadly defined as the thermochemical conversion of a solid or liquid carbon-based material (feedstock) into a combustible gaseous product (combustible gas) by the supply of a gasification agent (another gaseous compound), this process can be done in an up-draft, down draft, fluidized bed and entrained flow gasifiers. The thermochemical conversion changes the chemical structure of the biomass by means of high temperature. The gasification agent allows the feedstock to be quickly converted into gas by means of different heterogeneous reactions. The combustible gas contains CO<sub>2</sub>, CO, H<sub>2</sub>, CH<sub>4</sub>, trace amounts of higher hydrocarbons, inert gases present in the gasification agent, various contaminants such as small char particles, ash and tars (**Di, 2000**).

The produced gas mixture from gasification process is called producer gas. Producer gas can be used to run internal combustion engines, can be used as substitute for furnace oil in direct heat applications, in gas turbines for producing electricity or shaft power, and can be used to produce, in an economically viable way, methanol – an extremely attractive chemical which is useful both as fuel for heat engines as well as chemical feedstock for industries (**Rajvanshi, 1986; Salam and Bhattacharya, 2006**).

Spouted beds, originally invented in Canada by **Mathur and Gishler (1955)** as an alternative to fluidized beds for handling coarse particles, are now widely applied in various physical operations such as drying, coating and granulation. The distinctive advantages of spouted beds as reactors for various chemical processes are also well recognized in recent years. In addition to their ability to handle coarse particles, spouted beds also possess certain structural and flow characteristics that are very desirable in some chemical reaction systems. Consequently, increasing attention has been paid to the application of spouted beds as chemical reactors, including as combustion reactors, coal gasification reactors, catalytic partial oxidation reactors, catalytic oxidative coupling reactors, catalytic polymerization reactors, and pyrolysis reactors (**Du et al., 2006**).

Numerical simulation is an effective technology to model and optimize the performance of gasifiers. It also provides the best method for the gasifier scale up investigations. Many improvements have been developed to simulate the coal gasification process (**Li et al., 2009**). Due to the increasing interest in gasification, several models have been proposed in order to explain and understand this complex process, and the design, simulation, optimization and process analysis of gasifiers have been carried out (**Arnavat et al., 2010**). There has been little information on coal gasification in spout-fluid bed (**Li et al., 2009**).

## **1.2 Aims of This Work**

The present work consists of two parts; theoretical and experimental.

1. Predict a theoretical isothermal model of spouting fluidized bed gasifier for gasification (gas-solid) system.
2. Study gasification process experimentally of different fuels such as coal, algae, co-gasification (coal + algae biomass), and co-gasification (coal + grape seeds biomass) at different operating conditions.

# Chapter Two

## Literature Survey

### 2.1 Gasification

#### 2.1.1 Introduction

Gasification is a more than century old technology, which flourished before and during the Second World War. The technology disappeared soon after the Second World War when liquid fuel (petroleum based) became easily available. During the 20th century, the gasification technology roused intermittent and fluctuating interest among the researchers. However, today with rising prices of fossil fuel and increasing environmental concern, this technology has regained interest and has been developed as a more modern and sophisticated technology. The energy in biomass or any other organic matter is converted by gasification process to combustible gases (mixture of CO, CH<sub>4</sub> and H<sub>2</sub>), with char, water, and condensable as minor products. The producer gas leaves the reactor with pollutants and, therefore, requires cleaning to satisfy requirements for engines. Mixed with air, the cleaned producer gas can be used in gas turbines (in large scale plants), gas engines, gasoline or diesel engines (**Abdul Salam et al., 2010**).

Gasification is a flexible, commercially proven and efficient technology, a building block for production of a range of high-value products including clean power, synthetic fuels, and chemicals, from lower value feedstock (**Abadie and Chamorro, 2009**). It is a process in which combustible materials are partially oxidized or partially combusted. Gasification processes operate in an oxygen-lean environment (**Belgiorno et al., 2002**).

The quantity and composition of the volatile compounds produced by gasification depend on the reactor temperature and type, the characteristics of the fuel, and the degree to which various chemical reactions occur within the process (**Sadaka et al., 2002; Ciferno and Marano, 2002**).

Almost any carbonaceous or biomass fuel can be gasified under experimental or laboratory conditions. Different types of gasifying agents can be used like steam, steam + oxygen, air + steam, O<sub>2</sub>-enriched air (**Abdullah and Yusup, 2010; Narvaez et al., 1996**).

Nowadays, gasification is the main technology for biomass conversion to energy and an attractive alternative for the thermal treatment of solid waste. The number of different uses of gas shows the flexibility of gasification and therefore allows it to be integrated with several industrial processes, as well as power generation systems also it is widely used to produce commercial fuels and chemicals. Current developments in the chemical manufacturing and petroleum refinery industries show that use of gasification facilities to produce synthesis gas, methanol, gasoline or diesel, and ethanol will continue to rise (**Belgiorno et al., 2002; Hsu, 2011; Zhang et al., 2009**).

### **2.1.2 Effect of fuel moisture content on gasification**

Fuel moisture content differs by fuel type. Fuels with high moisture content lower the reactor temperatures due to the amount of energy needed to dry the fuel, which results in the production of lower energy syngas and lower yields of syngas (**Knoef, 2008**).

Theoretically, almost all kinds of biomass with moisture content of 5-30% can be gasified as shown in Figure 2-1, however not every biomass fuel can lead to the successful gasification. Most of the development work is carried out with common fuels such as coal, charcoal and wood. It was recognized that fuel properties such as solid surface, size, shape as well as moisture content, volatile matter, and carbon content influence gasification (**Turare, 2002**).

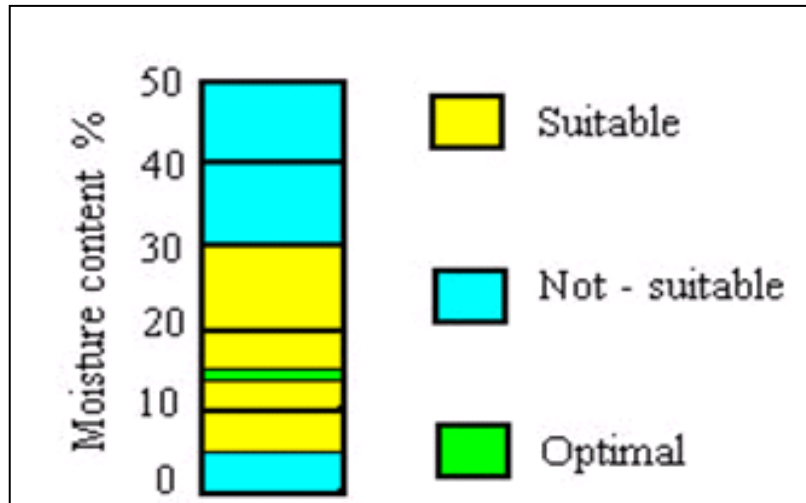


Figure 2-1 Moisture scale for gasification, (Turare, 2002).

## 2.2 Gasification Reactions

The chemistry of gasification is complex. The process of gasification proceeds primarily via a two-step process, pyrolysis followed by gasification, Figure 2-2. Pyrolysis is the decomposition of the biomass and/or coal feedstock by heat. This step, also known as devolatilization, is endothermic and produces 75 to 90% volatile materials in the form of gaseous and liquid hydrocarbons. The remaining nonvolatile material, containing high carbon content, is referred to as char (Bridgwater and Evans, 1993).

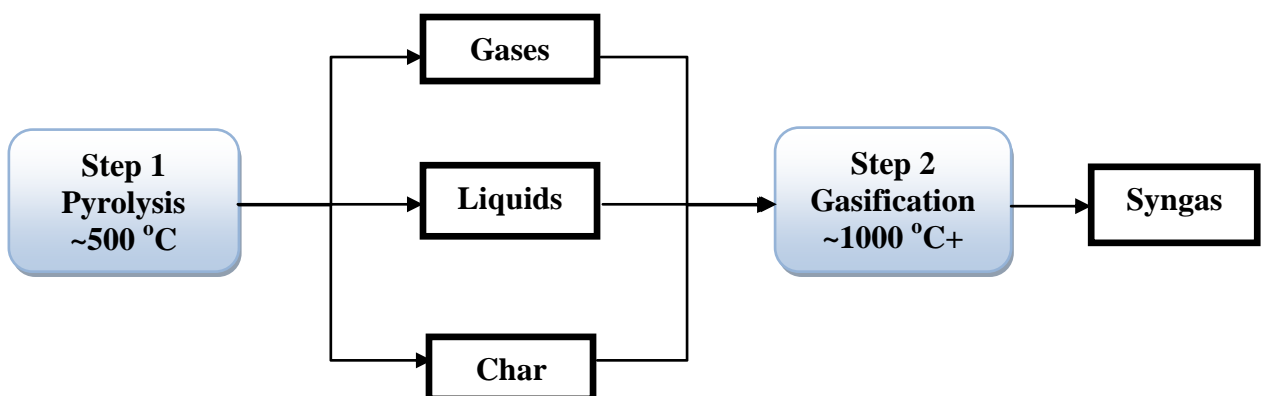


Figure 2-2 Gasification Steps (Ciferno and Marano, 2002)

The volatile hydrocarbons and char are subsequently converted to syngas in the second step gasification. Reactions involved in this step are listed below:

1. Exothermic reactions, which involves the following reactions:
  - a. Combustion reactions producing CO<sub>2</sub> and CO and release thermal energy, which are both needed for gasification reactions. The combustion reactions are faster than other gasification reactions and they occur first rapidly consuming the oxygen, Table 2-1 (**Basu, 2006**).
  - b. Methanation and Shift conversion reactions, Table 2-1.
2. Endothermic reactions, these gasification reactions are water-gas reaction, steam methane reforming reaction, and Boudouard reaction, Table 2-2.

**Table 2-1** Gasification exothermic reactions (Heiskanen, 2011; Ciferno, and Marano, 2002)

Reactions	Reaction heat , MJ/kmol	Equation Number
Basic combustion reactions		
$C + \frac{1}{2} O_2 \rightarrow CO$	-111	(1)
$CO + \frac{1}{2} O_2 \rightarrow CO_2$	-283	(2)
$C + O_2 \rightarrow CO_2$	-394	(3)
Methanation reaction		
$C + 2H_2 \rightarrow CH_4$	-75	(4)
Shift conversion		
$CO + H_2O \leftrightarrow CO_2 + H_2$	-41	(5)

**Table 2-2** Gasification endothermic reactions (Heiskanen, 2011; Ciferno, and Marano, 2002)

Reactions	Reaction heat, MJ/kmol	Equation Number
Boudouard reaction		
$C + CO_2 \rightarrow 2CO$	+172	(6)

Water gas reaction		
$C + H_2O \rightarrow CO + H_2$	+131	(7)
Steam methane reforming reaction		
$CH_4 + H_2O \leftrightarrow CO + 3H_2$	+206	(8)

### 2.2.1 Gasification products

Gasification of biomass resulting in production of combustible gases with char, water, and condensable as minor products combustible gases produced are called producer or syngas as follows:

**Producer gas:** is a mixture of gases produced by the gasification of organic material such as biomass at relatively low temperatures (700 to 1000 °C). Producer gas is composed of carbon monoxide (CO), hydrogen (H<sub>2</sub>), carbon dioxide (CO<sub>2</sub>) and typically a range of hydrocarbons such as methane (CH<sub>4</sub>) with nitrogen from the air. Producer gas can be burned as a fuel gas such as in a boiler for heat or in an internal combustion gas engine for electricity generation or combined heat and power (CHP). The composition of the gas can be modified by manipulation of gasification parameters (**Lim and Alimuddin, 2007**).

**Synthesis Gas (Syngas):** A combustible mixture of hydrogen and carbon monoxide (CO). Synthesis gas is the product of the full conversion of a carbon feedstock (coal, oil, natural gas, and biomass) into the most basic components of hydrogen and carbon monoxide. Synthesis gas is widely produced from coal and natural gas as the first step in the creation of numerous synthetic compounds including plastics, ammonia fertilizers, synthetic diesel fuel and chemicals. Syngas can also be converted into methane (CH<sub>4</sub>) in a methanation process (**Taglia, 2010**).

### 2.3 Gasification Processes

During gasification, the material is heated to a high temperature, which causes a series of physical and chemical changes that result in the evolution of

volatile products and carbonaceous solid residues. The gasification process uses an agent, air, oxygen, hydrogen or steam to convert carbonaceous materials into gaseous products (**Basu, 2006**).

### **2.3.1 Air gasification**

**Ergudenler, (1993)** studied the effect of air flow rate on the gas quality and quantity during air gasification of wheat straw in a fluidized bed gasifier. The results showed that at equivalence ratio of 0.25, the mole fraction of the combustible component achieved their maximum.

**Cao et al., (2005)** demonstrated a fluidized bed air gasification system using sawdust. Two individual regions of pyrolysis, gasification, and combustion of biomass combined in one reactor. The primary air stream and the biomass feedstock were introduced into the gasifier from the bottom and the top, respectively. Secondary air was injected into the upper region of the reactor to maintain elevated temperature; the fuel gas was produced at a rate of about 3.0 Nm<sup>3</sup>/kg biomass and heating value of about 5.0 MJ/Nm<sup>3</sup>. The concentration of hydrogen, carbon monoxide and methane in the fuel gas produced were 9.27%, 9.25% and 4.21%, respectively.

### **2.3.2 Steam gasification**

**Boateng et al., (1992)** determined the effects of reactor temperature and steam to biomass ratio on producer gas composition, heating value and energy recovery. The produced gas, which is rich in hydrogen, had been found to have a heating value ranging from 11.1 MJ/m<sup>3</sup> at temperature of 700 °C to 12.1 MJ/m<sup>3</sup> at temperature of 800°C. Energy recovery varied from 35-59% within the same temperature range.

**Mermoud et al., (2005)** studied charcoal steam gasification of beech charcoal spheres of different diameters 10-30 mm at different temperatures 830-1030 °C. Results show a very slow reaction at 830 °C. A difference in gasification rate as high 6.5 to 1 was observed between temperatures at 1030 and 830°C. Experiments carried out with mixtures of H<sub>2</sub>O/N<sub>2</sub> at 10%, 20%, and 40% mol of steam confirmed

that oxidant partial pressure influences gasification. A gasification rate of 1.9 was obtained for H<sub>2</sub>O partial pressure varying from 0.4 to 0.1 atm.

### **2.3.3 Oxygen gasification**

**Tillman, (1987)** gasified municipal solid waste in an oxygen gasifier. The feedstock (shredded and magnetically sorted) was fed into the top of the gasifier and the oxygen was fed at the bottom. Pyrolytic char was combusted with the oxygen at the bottom of the gasifier providing enough thermal energy to produce temperatures in the range of 1593-1704 °C and to produce a molten slag from all noncombustible materials. The maximum mole fraction of the produced gas for CO, H<sub>2</sub>, CO<sub>2</sub> and CH<sub>4</sub> recorded were 44%, 31%, 13% and 4%, respectively. The maximum heating value was 10.6 MJ/Nm<sup>3</sup>.

### **2.3.4 Hydrogen gasification**

**Weil et al., (1978)** used preheated hydrogen mixed with peat at the entrance of fluidized bed gasifier. The reactor was operated as an entrained flow reactor in an isothermal or a constant heat-up mode. Increasing the temperature from 426 °C to 760 °C increased carbon monoxide and hydrocarbon gases from 8% to 18% and 41% to 63%, respectively.

## **2.4 Gasification Reactors**

Gasification reactors can be generally classified into two broad categories; namely, fixed bed and fluidized bed. Fluidized bed gasifiers are more flexible in the selection of fuel type. It can gasify various types of biomass without much difficulty and has high carbon conversion rates as well as high heat transfer rates (**Lim and Alimuddin, 2007**). Fluidized bed gasification performs better than fixed bed gasification to reduce ash-related problems since the bed temperature of fluidized bed gasification can be kept uniformly below the ash slagging temperature (**Abdul Salam et al, 2010**).

### **2.4.1 Fixed Bed Gasifiers**

The fixed bed gasification system consists of a reactor / gasifier with a gas cooling and cleaning system. The fixed bed gasifier has a bed of solid fuel particles through which the gasifying media and gas move either up or down. It is the simplest type of gasifier consisting of usually a cylindrical space for fuel and gasifying media with a fuel feeding unit, an ash removal unit and a gas exit. It is made up of firebricks, steel or concrete. In the fixed bed gasifier the fuel bed moves slowly down the reactor as the gasification occurs. The fixed bed gasifiers are of simple construction and generally operate with high carbon conversion. There are three basic fixed bed designs, Updraft, Downdraft and Cross-draft Gasifiers (Chopra and Jain, 2007).

### **2.4.2 Fluidized Bed Gasifiers**

A Fluidized Bed Gasifier has a bed made of an inert material (such as sand, ash or char) that acts as a heat transfer medium. In this design, the bed is initially heated and the fuel introduced when the temperature has reached the appropriate level. The bed material transfers heat to the fuel and blows the reactive agent through a distributor plate at a controlled rate. Unlike fixed bed gasifiers, fluidized bed gasifiers have no distinct reaction zones and drying, pyrolysis, and gasification occur simultaneously during mixing (Lim and Alimuddin, 2008).

The advantages of fluidize bed gasifiers are:

1. Strong gas-to-solids contact.
2. Excellent heat transfer characteristics.
3. Better temperature control.
4. Large heat storage capacity.
5. Good degree of turbulence.
6. High volumetric capacity.

The disadvantages are the large pressure drop, particle entrainment, and erosion of the reactor body (**Lettner et al., 2007**).

### **2.4.2.1 Fluidize Bed Gasifiers Types**

Fluidized Bed Gasifiers are classified by their configuration and the velocity of the reactive agent. It consists of bubbling, circulating and spouted fluidized beds.

#### **2.4.2.1.1 Bubbling Fluidized Bed Gasifier**

In bubbling fluidized beds, granular material is fed into a vessel through which an upward flow of gas passes at a flow rate where the pressure drop across the particles is sufficient to support their weight (incipient fluidization). In bubbling fluidization (at relatively low fluidization velocity just above the minimum fluidization velocity), the gas in excess of that needed for minimum fluidization passes through the bed in the form of bubbles. Bubbles grow by coalescence as they rise in the bed. At the bed surface, the bubbles burst causing a shower of bed solids to leave the bed surface and enter the freeboard, at which the carryover occurs. Bubbling fluidized bed gasifiers (BFG) has potential for rural electrification projects especially in third world countries where biomass supplies are abundant from agricultural, wood industries and where electricity supply from the grid is not available, Figure 2-3a (**Lim and Alimuddin, 2008**).

#### **2.4.2.1.2 Circulating Fluidized Bed Gasifier**

If the gas velocity in a bubbling fluidized bed is further increased, more particles will be entrained in the gas stream and leave the reactor. Eventually the transport velocity for most of the particles is reached, and the vessel can be quickly emptied of solids unless additional particles are fed to the base of the reactor. If the solids leaving the vessel are returned through an external collection system, the system is called a circulating or fast fluidized bed (CFB) system. The streams of

particles moving upward in the reactor are at solid concentrations well above that for dilute phase transport. Compared to conventional furnaces, circulating beds have a higher processing capacity, better gas-solid contact, and the ability to handle cohesive solids that might otherwise be difficult to fluidize in bubbling fluidized beds. Despite these advantages, circulating fluidized beds are still less commonly used than bubbling models, primarily because their height restricts their applications in terms of cost analysis, Figure 2-3b (Brown, 2006).

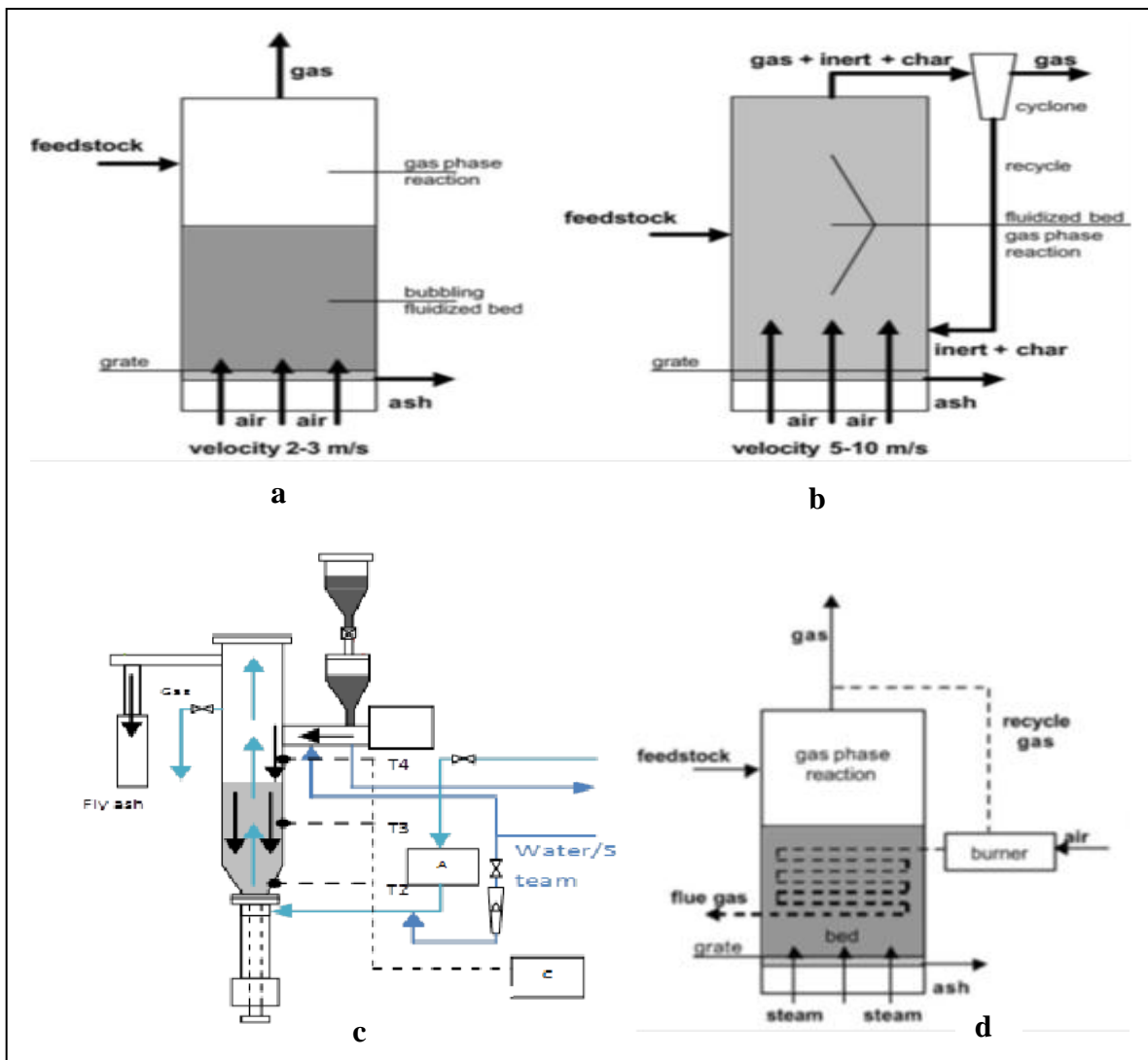


**Figure 2-3** Fluidised Bed Gasifiers; **a**: Bubbling Fluidized Bed Gasifier; **b**: Circulating Fluidized Bed Gasifier; **c**: Spouting Fluidized Bed Gasifier; and **d**: Gas Indirect Gasifier (Craig and Margaret, 1996).

### 2.4.2.1.3 Spouted Fluidized Bed Gasifier

The bed is filled with relatively coarse particulate solids, **Geldart group D**. Fluid is injected vertically through a centrally located small opening at the base of the vessel. If the fluid injection rate is high enough, the resulting high velocity jet causes a stream of particles to rise rapidly in a hollowed central core within the bed of solids. These particles, after reaching somewhat above the peripheral bed level, rain back onto the annular region between the hollowed core and the column wall, where they slowly travel downward and, to some extent, inward as a loosely packed bed. As the fluid travels upward, it flares out into the annulus. The overall bed thereby becomes a composite of a dilute phase central core with upward moving solids entrained by a concurrent flow of fluid and a dense phase annular region with counter region with counter-current percolation of the fluid. The central core is called a spout and the peripheral annular region is referred to as the annulus. The term fountain denotes the mushroom-shaped zone above the level of the annulus. To enhance motions of the solids and eliminate dead spaces at the bottom of the vessel, it is common to use a diverging conical base with fluid injection at the truncated apex of the cone, Figure 2-3c (**Hoque and Bhattacharya, 2001; Thamavithya et al., 2010**). Spout-Fluid Beds have been of increasing interest in the petrochemical, chemical and metallurgic industries since spout-fluid beds can reduce some of the limitations of both spouting and fluidization by superimposing the two type of system (**Zhong, 2005**).

### 2.4.3 Indirect Fluidized Bed Gasifier

Indirect gasifiers are the reactors used for the steam indirect gasification and are grouped as char indirect gasifiers and gas indirect gasifiers depending on the type of internal energy source. The main advantage of indirect gasification is the high quality of the combustible gas produced in contrast with greater investment and maintenance cost of the reactor. Therefore it is necessary to improve the quality

of gas with the adoption of a highly efficient energy recovery system, Figure 2-3d (Craig and Margaret, 1996).

## 2.5 Geldart Classification of Particles

Geldart (1973) observed the nature of particles fluidizing. He categorized his observations by particle diameter versus the relative density difference between the fluid phase and the solid particles. Geldart identified four regions in which the fluidization character can be distinctly defined, Figure 2-4.

**Group A** Small particle size or density less than  $1.4 \text{ g/cm}^3$ . Easily fluidized with smooth fluidization at low gas velocities and controlled bubbling with small bubbles at higher gas velocities. When fluidized by air at ambient conditions, result in a region of non-bubbling fluidization beginning at  $U_{mf}$ , followed by bubbling fluidization as fluidizing velocity increases. Gas bubbles rise faster than the rest of the gas.

**Group B** Are sand like powders which result in vigorous bubbling fluidization under these conditions. Bubbles form as soon as the gas velocity exceeds the minimum fluidization velocity. Majority of gas-solid reactions occur in this regime based on particle size of raw materials.

**Group C** Cohesive or very fine powders. Normal fluidization is difficult for these solids because of interparticle forces that are greater than those resulting from the action of the gas on the particles. In small diameter beds these particles form a plug of solids that rises upward. Powders, very fine, cohesive powders which are incapable of fluidization in the strict sense. Examples: Face powder, flour, and starch.

**Group D** Spoutable, large and/or dense particles. Examples include drying grains, peas, roasting coffee beans, gasifying coals and roasting of metal ores (Yang, 2006).

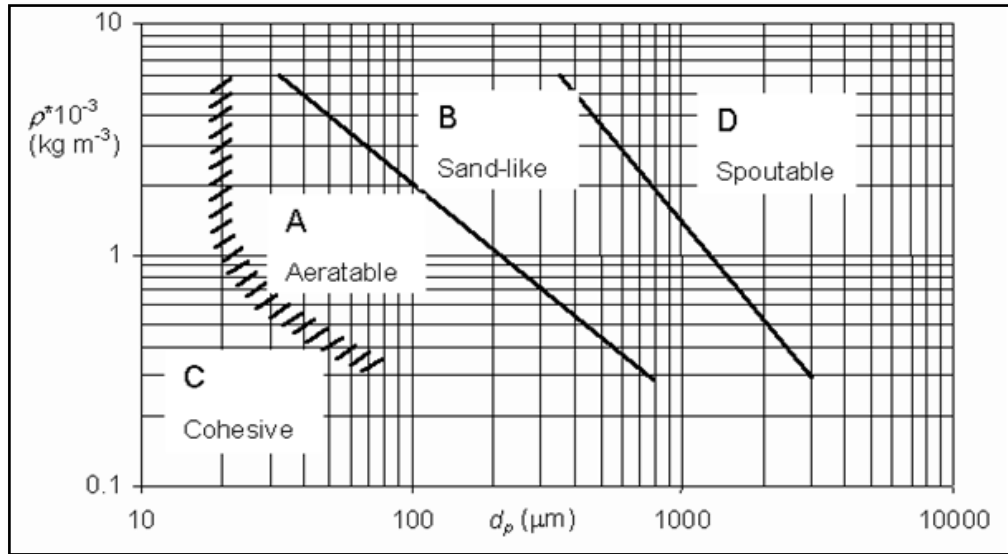


**Figure 2-4** Geldart classification of particles according to fluidization properties (Yang, 2006).

## 2.6 Characteristics of Spouted Fluidized Bed

### 2.6.1 The phenomena of Fluidization

The fluidization principle was first used on an industrial scale in 1922 for the gasification of fine-grained coal. Since then, fluidized beds have been applied in many industrially important processes (Werther, 2012).

Different parameters influence the fluidization characteristics and they can be classified into two major groups comprised of **independent variables** and **dependent variables**. **Independent variables** include fluid properties (e.g., density, viscosity, relative humidity), particle characteristics (e.g., density, size, shape, distribution, surface roughness, and porosity) and equipment related such as direction of fluid flow, distributor plate design, vessel geometry, operating velocity, centrifugal force, temperature, pressure, type of nozzle, etc. **The dependent variables** are basically capillary forces, minimum fluidization velocity, electrostatic forces, bed voltage; Vander Waals forces (Dixit and Shivanand, 2009).

In fluidization an initially stationary bed of solid particles is brought to a “fluidized” state by an upward stream of gas or liquid as soon as the volume flow rate of the fluid exceeds a certain limiting value  $U_{mf}$  (where **mf** denotes minimum fluidization). In the fluidized bed, the particles are held suspended by the fluid

stream; the pressure drop  $\Delta p_{fb}$  of the fluid on passing through the fluidized bed is equal to the weight of the solids minus the buoyancy, divided by the cross sectional area  $A_c$  of the fluidized-bed vessel, Figure 2-5.

$$\Delta p_{fb} = \frac{A_c \cdot H \cdot (1 - \varepsilon) \cdot (\rho_s - \rho_g)}{A_c} \quad (2.1)$$

In Equation (2.1), the porosity  $\varepsilon$  of the fluidized bed is the void volume of the fluidized bed (volume in interstices between grains, not including any pore volume in the interior of the particles) divided by the total bed volume;  $\rho_s$  is the solids apparent density; and  $H$  is the height of the fluidized bed (Werther, 2012).

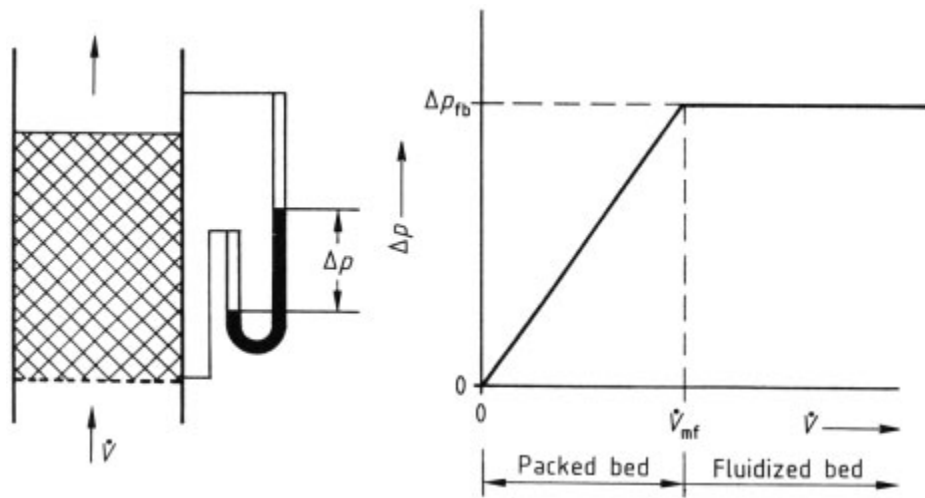


**Figure 2-5** Pressure drop in flow through packed and fluidized beds (Werther, 2012).

### 2.6.2 Minimum fluidization velocity

A minimum velocity is needed to fluidize a bed. If the velocity is too small the bed stays fixed and operates as a packed bed. In spout fluidized beds the favourable properties of both spouted and fluidized beds are combined. Schematic diagram is shown in Figure 2-6. Table 2-3 shows correlations proposed by previous authors for  $U_{mf}$ .

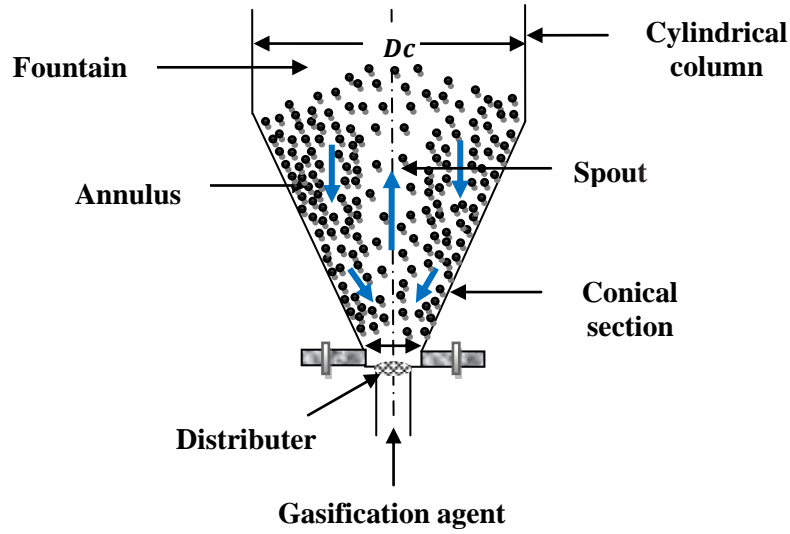


**Figure 2-6** Schematic draw of spouted bed (Smith et al., 1981); (Abdul Salam and Bhattacharya, 2006)

**Table 2-3** Correlations for  $U_{mf}$  and  $Re_{mf}$

Reference	Equations	Equation No.
<b>Jackson and Judd, (1981)</b>	$U_{mf} = \frac{25.7\eta \left\{ \left( 1 + \frac{5.53Ga}{100000} \right)^{0.5} - 1 \right\}}{d_p \rho}$ <p>Where:</p> $Ga = \frac{\rho g d_p^3}{\eta^2} (\rho_s - \rho_g)$	(2.2)
<b>Littman et al., (1981)</b>	$u_{mf} = 42.9(1 - \varepsilon_{mf}) \frac{\mu_g}{\rho_g d_p} \left[ \left\{ 1 + (3.111 * 10^{-4}) * \frac{\varepsilon_{mf}^3 Ar}{(1 - \varepsilon_{mf})^2} \right\}^{\frac{1}{2}} - 1 \right]$ <p>Where:</p> $Ar = \frac{d_p^3 \rho_g (\rho_p - \rho_g) g}{\mu_g^2}$	(2.3)
<b>Thonglimp et al., (1984)</b>	$(Re)_{mf} = (1.95 * 10^{-2}) Ar^{0.66}$	(2.4)

<b>Wen and Yu, (1966)</b>	$Re_{mf} = \sqrt{C_1^2 + C_2 Ar} - C_1$ <p>Where:</p> $NRe = \left( \frac{\rho_g U_{mf} dp}{\mu_g} \right)$ <p>Constants <math>C_1</math> and <math>C_2</math> shown in Table 2-4</p>	(2.5)
---------------------------	---	-------

**Table 2-4** Parameters used in Wen and Yu type equations for minimum fluidization velocity (Abdul Salam and Bhattacharya, 2006)

Reference	Equation parameters	
	$C_1$	$C_2$
<b>Bourgeois and Grenier, (1968)</b>	25.46	0.0384
<b>Grace, (1982)</b>	27.2	0.0408
<b>Thonglimp et al., (1984)</b>	31.6	0.0425
<b>Lucas et al., (1986)</b>	29.5	0.0357
<b>Tannous, (1993)</b>	25.83	0.0430

### 2.6.3 Minimum spouting velocity ( $U_{ms}$ )

The minimum fluid velocity at which a bed will remain in the spouted state, defined as the minimum spouting velocity ( $U_{ms}$ ), depends on solid and fluid properties on one hand and bed geometry on the other. Data on minimum spouting velocity in packed beds as described in literature are scarce. The minimum spouting velocity is measured experimentally by first achieving a spout regime and then decreasing the gas velocity slowly until the spout is no longer permanent, the porosity at that instant will be larger than that for a fixed bed. So, at that instant, when measurements of minimum spouting velocity are made, the porosity of bed is certainly higher than the porosity reported for the fixed bed (**Dogan et al., 2004**). Tables 2-5 and 2-6 list correlations of  $U_{ms}$  proposed by different authors.

**Table 2-5** Correlations for minimum spouting velocity

Reference	Equations	Equation No.
<b>Grbavcic et al., (1976)</b>	$u_{ms} = u_{mf} \left( 1 - \left( 1 - \frac{H}{H_m} \right)^3 \right)$	(2.6)
<b>Wu et al., (1987)</b>	$U_{ms} = 10.6 \left[ \frac{d_p}{D_c} \right]^{1.05} \left[ \frac{d_{in}}{D_c} \right]^{0.266} \left[ \frac{H_c}{D_c} \right]^{-0.095} \left[ \frac{(\rho_p - \rho_g)}{\rho_g} \right]^{0.256} \sqrt{2gH_c}$	(2.7)
<b>Brunello et al., (1974)</b>	$U_{ms} = \lambda(2gH)^\mu \left( \frac{d_p}{D_c} \right)^\alpha \left( \frac{d_{in}}{D_c} \right)^\beta \left( \frac{H}{D_c} \right)^\gamma \left[ \left( \frac{\rho_p - \rho_g}{\rho_g} \right) \right]^\delta$ Constants shown in Table 2-6	(2.8)
<b>Olazar et al., (1993)</b>	$(Re_o)_{ms} = 0.126 Ar^{0.5} \left( \frac{D_b}{d_{in}} \right)^{1.68} \left[ \tan \left( \frac{\gamma}{2} \right) \right]^{-0.57}$	(2.9)

**Table 2-6** Fitted constants for minimum spouting velocity equation (Abdul Salam and Bhattacharya, 2006)

Sources	$\lambda$	$\mu$	$\alpha$	$\beta$	$\gamma$	$\delta$
<b>Mathur and Gishler, (1955)</b>	1.0	0.5	1.0	0.333	0	0.5
<b>Uemaki et al., (1983)</b>	0.977	0.324	0.615	0.274	0	0.324
<b>Wu et al., (1987)</b>	10.6	0.5	1.05	0.266	-0.095	0.256
<b>Choi and Meisen, (1992)</b>	18.5	0.5	1.19	0.373	-0.193	0.263

## 2.7 Fossil Fuel

### 2.7.1 Introduction

Fossil fuels are carbon-based fuels found in the earth's crust that have been formed over millions of years by decomposing remains of plants and animals under intense heat and pressure. Their energy include energy-rich fuels such as coal, petroleum (oil), and natural gas, which have provided the majority of the world's energy supply since the industrial revolution. It is commonly predicted that world consumption will grow by 50 percent during the 2007 to 2030 time period and that the majority of this energy will be supplied by fossil fuels as has been stated by US Energy Information Administration, 2009.

The recent increase in fossil fuel prices and worsening effects of global warming has prompted the use of biomass as a source of energy. Unlike other renewable energy sources that require costly technology, biomass can generate electricity with the same type of equipment and power plants that now burn fossil fuels. However low thermal efficiencies have hindered its development and the main challenge now is to develop low cost high efficiency systems. In 2007, approximately 86 percent of world energy production came from burning fossil fuels. The majority of fossil fuels are used in the electric-power generation, transportation, manufacturing and residential heating industries (**Lim and Alimuddin, 2008**).

### **2.7.2 Coal**

**Coal** is a **fossil fuel** created from the remains of plants that lived and died about 100 to 400 million years ago when parts of the Earth were covered with huge swampy forests. Coal is classified as a non-renewable energy source because it takes millions of years to form. The energy we get from coal today comes from the energy that plants absorbed from the sun millions of years ago. All living plants store solar energy through a process known as photosynthesis. When plants die, this energy is usually released as the plants decay. Under conditions favourable to coal formation, however, the decay process is interrupted, preventing the release of the stored solar energy. The energy is locked into the coal. Millions of years ago, dead plant matter fell into swampy water and over the years, a thick layer of dead plants lay decaying at the bottom of the swamps. Over time, the surface and climate of the Earth changed, and more water and dirt washed in, halting the decay process. The weight of the top layers of water and dirt packed down the lower layers of plant matter. Under heat and pressure, this plant matter underwent chemical and physical changes, pushing out oxygen and leaving rich hydrocarbon deposits. What once had been plants gradually turned into coal (**Secondary and Intermediate Energy ebooks, 2011**).

### 2.7.2.1 Coal production

The world currently consumes over 4000 million tons coal each year. The largest consumers are mainly power generation and steel industry. Cement manufacturing and coal liquefaction are two a medium consumers. A small proportion of coal is also used for various chemical processes. Coal production has increased with 38% the last 20 years. Asia is the fastest growing coal producer, while European production actually has declined. Global coal production is expected to reach 7 billion tonnes in 2030 with China accounting for nearly half the increase. Coal still plays a vital role in the world's primary energy mix, providing 23.5% of global primary energy needs in 2002, 39% of the world's electricity, more than double the next largest source, and an essential input into 64% of the world's steel production (Höök, 2007).

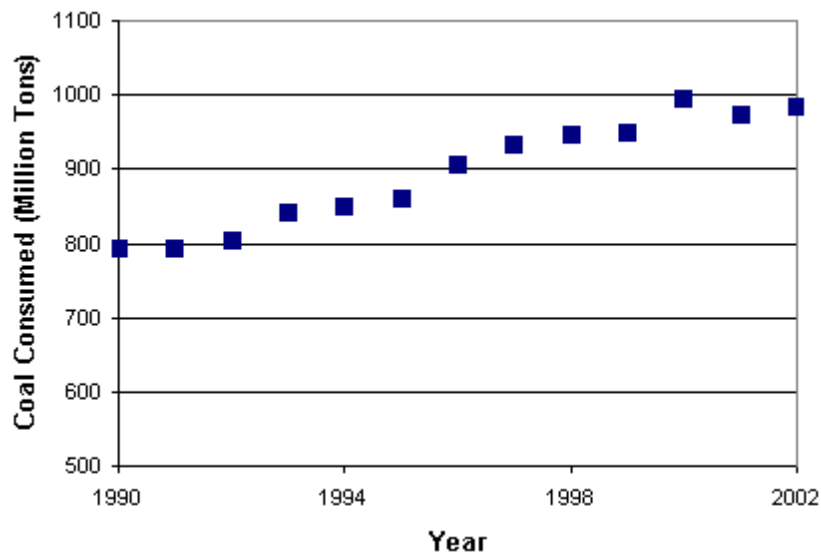


Figure 2-7 Coal consumed for electricity (Höök, 2007).

## 2.8 Biomass

### 2.8.1 Introduction

Biomass is a renewable energy source whose advantages and drawbacks, compared to fossil fuels, are periodically analysed (Goldemberg, 2004). Biomass is an umbrella term used to describe vegetable or animal (biological) sourced energy mass, for example canola and lard. Biomass fuels may be derived from many



sources, including forestry products and residue, agriculture residues, food processing wastes, and municipal and urban wastes (Roos, 2008).

### 2.8.2 Biomass algae

Algae have recently received a lot of attention as a new biomass source for the production of renewable energy. Some of the main characteristics which set algae apart from other biomass sources are that algae can have a high biomass yield per unit of light and area, can have a high oil or starch content (Global bioenergy partnership, 2009).

Algae range from small, single-celled organisms to multi-cellular organisms, some with fairly complex and differentiated form. Algae are usually found in damp places or bodies of water and thus are common in terrestrial as well as aquatic environments. Like plants, algae require primarily three components to grow: sunlight, carbon-dioxide and water. Photosynthesis is an important bio-chemical process in which plants, algae, and some bacteria convert the energy of sunlight to chemical energy (Wagner, 2007; Wen and Michael, 2009).

Algae biomass has the potential to grow yields far higher than any other feedstock currently being used. It has the possibility of a much higher energy yield per unit, so it can be much more efficient (Campbell, 2008).

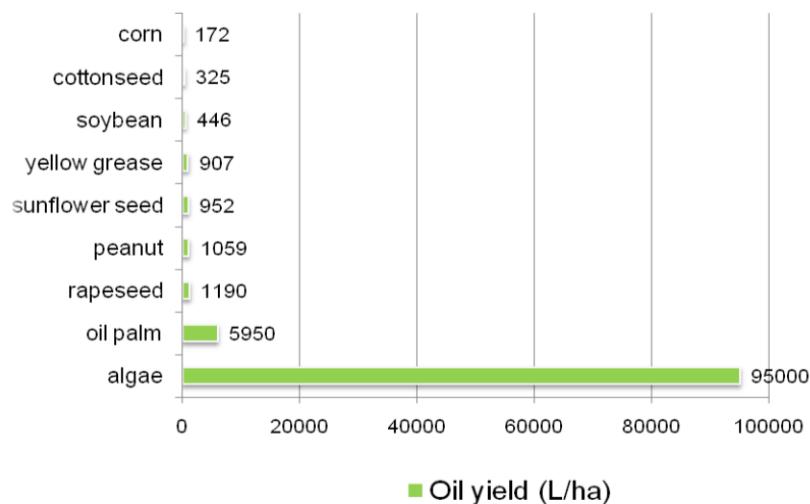


**Figure 2-8** Oil Yields of Feedstocks for Biofuel from EarthTrends (Global bioenergy partnership, 2009).

Algal concentration may vary substantially from sample to sample. The variability can be attributed to spatiotemporal variability of the collection, as well as variability in the processing, storage, and analysis of the sample (**Berkman and Michael, 2007**).

### **2.8.3 Types of Algae**

There are two classifications of algae: macroalgae and microalgae.

#### **2.8.3.1 Macro-algae**

Seaweeds or macro-algae belong to the lower plants, meaning that they do not have roots, stems and leaves. Instead they are composed of a thallus (leaf-like) and sometimes a stem and a foot. Some species have gas-filled structures to provide buoyancy. The big advantage of macro-algae is their huge mass production (**Carlsson et al., 2007**).

#### **2.8.3.2 Micro-algae**

Micro-algae are microscopic photosynthetic organisms that are found in both marine and freshwater environments. Their photosynthetic mechanism is similar to land based plants, but due to a simple cellular structure, and submerged in an aqueous environment where they have efficient access to water, CO<sub>2</sub> and other nutrients, they are generally more efficient in converting solar energy into biomass (**Wagner, 2007**).

The technical potential of macro- and micro-algae for biomass production and greenhouse gas abatement has been recognised for many years, given their ability to use carbon dioxide and the possibility of their achieving higher productivities than land-based crops (**Wellinger, 2009**).

Macro- and micro-algae are currently mainly used for food, in animal feed, in feed for aquaculture and as bio-fertiliser. Biomass from micro-algae is dried and marketed in the human health food market in form of powders or pressed in the form of tablets (**Wen and Michael, 2009**).

## 2.9 Hydrogen

Hydrogen is well known. It is the smallest of all atoms. Promoters praise the energy content of hydrogen. In the past, many have considered the production and use of hydrogen, assuming that it is just another gaseous fuel and can be handled much like natural gas in today's energy economy (**Eliasson and Taylor, 2005**).

### 2.9.1 Hydrogen Production methods

#### 2.9.1.1 Coal gasification

Hydrogen can be produced from coal through a variety of gasification processes (e.g. fixed bed fluidized bed or entrained flow). In practice, high-temperature entrained flow processes are favored to maximize carbon conversion to gas, thus avoiding the formation of significant amounts of char, tars and phenols. A typical reaction for the process is given in the following equation, in which carbon is converted to carbon monoxide and hydrogen.



**Purdy et al. (1984)** made experimental work to gasify New Mexico subbituminous coal with steam and oxygen in a 15.2 cm inside diameter fluidized bed reactor at a pressure of 790 kPa (100 psig) and average bed temperatures between 875 and 990 °C. Material balances were obtained on total mass and major elements (C, H, O, N, S). A simple representation of coal pyrolysis has been added to a previously developed model of gasification and combustion; the resulting model provides good correlations of measured carbon conversions, make gas production rates, and make gas compositions. Approximations that can be used to estimate sulfur conversion and the split between H<sub>2</sub>S and COS in the product gas have also been developed.

**Neogi et al., (1986)** used a bench-scale fluidized bed reactor for the gasification of coal with steam as the fluidizing medium. A mixture of sand and limestone used as the bed material made it possible to gasify a caking coal without the problem of agglomeration. The gas composition and yield of the hydrogen-rich

product gas were studied as a function of temperature. A mathematical model was developed to study the heterogeneous reactions taking place in the reactor and also the transient behaviour of the system.

**Chatterjee, (1995)** studied gasification of high ash India coal in a laboratory-scale, atmospheric fluidized bed gasifier using steam and air as fluidizing media. A one-dimensional analysis of the gasification process has been presented incorporating a two-phase theory of fluidization, char gasification, volatile release and an overall system energy balance. Results are presented on the variation of product gas composition, bed temperature, calorific value and carbon conversion with oxygen and steam feed. Comparison between predicted and experimental data has been presented, and the predictions show similar trends as in the experiments.

**Zedtwitz and Steinfeld, (2005)** studied the steam-gasification of coal in a fluidized-bed or a packed-bed chemical reactor using an external source of concentrated thermal radiation for high-temperature process heat. The authors found that above 1450 K, the product composition consisted mainly of an equimolar mixture of H<sub>2</sub> and CO, a syngas quality that is notably superior than that typically obtained in autothermal gasification reactors (with internal combustion of coal for process heat), besides the additional benefit of the upgraded calorific value.

**Jin, et al., (2010)** applied a supercritical water gasification system with a fluidized bed reactor to investigate the gasification of coal in supercritical water. 24 wt% coal- water- slurry was continuously transported and stably gasified without plugging problems; a hydrogen yield of 32.26 mol/kg was obtained and the hydrogen fraction was 69.78%. The effects of operational parameters upon the gasification characteristics were investigated.

### **2.9.2. Biomass Sources**

**Lv et al., (2002)** investigated the characteristics of biomass air-steam gasification in a fluidized bed for hydrogen-rich gas production through a series of experiments. The effects of reactor temperature, steam-to-biomass ratio,

equivalence ratio ER, and the biomass particle size on gas composition and hydrogen production were investigated. The authors concluded that the higher reactor temperature, the proper ER, proper steam-to-biomass ratio  $S/B$ , and smaller biomass particle size will contribute to more hydrogen production. The highest hydrogen yield, 71g H<sub>2</sub>/ kg biomass (wet basis), was achieved at a reactor temperature of 900 °C,  $S/B$  of 2.70. It was also shown that under proper operating parameters biomass air-steam gasification in a fluidized bed was one effective way for hydrogen-rich gas production.

**Kong et al., (2008)** found that hydrothermal gasification of biomass wastes can be identified as a possible system for producing hydrogen. The authors investigated the decomposition of biomass, as a basis of hydrothermal treatment of organic wastes. To eliminate chars and tars formation and obtain higher yields of hydrogen, catalyzed hydrothermal gasification of biomass wastes was summarized.

**González et al., (2008)** studied the production of hydrogen-rich gas by air/steam and air gasification of olive oil waste was investigated. The study was carried out in a laboratory reactor at atmospheric pressure over a temperature range of 700-900°C using a steam/biomass ratio of 1.2 w/w. The solid, energy and carbon yield (%), gas molar composition and high heating value of the gas (kJ NL<sup>-1</sup>), were determined for all cases and the differences between the gasification process with and without steam were established. The results obtained suggest that the operating conditions were optimized at 900°C in steam gasification (a hydrogen molar fraction of 0.70 was obtained at a residence time of 7 min). The use of both catalysts ZnCl<sub>2</sub> and dolomite resulted positive at 800 °C, especially in the case of ZnCl<sub>2</sub> (attaining H<sub>2</sub> molar fraction of 0.69 at a residence time of 5 min).

## 2.10 Modelling

### 2.10.1 Introduction

Coal gasification is one of the key technologies among current advanced clean coal technologies. Numerical simulation is an effective technology for scale-up and optimizing the performance of gasifiers (**Deng et al., 2008**). Models used for the description of spouted bed reactors are chosen according to the following criteria: (i) desired accuracy, (ii) required computational efforts and (iii) available information on the spouted bed. Any type of model is thus valid within a certain range of operating conditions, depending on the extent to which it simplifies reality (**Mendes et al., 2008**).

**Eng et al., (1989)** developed a multiregion nonisothermal dynamic model predicting the response of spouted fluidized bed reactor with a draft tube to the changes in operational conditions. Validation of the model is carried out by comparison with experimental results obtained from a 11.4-cm-diameter bench-scale reactor and a 20-cm-diameter pilot-scale reactor. Furthermore, the simulation has been used to study the effect of fluctuations in the feed properties and in the energy supplied to the reactor.

The material balance equation describing the gaseous components within the spout is:

$$\frac{dQ_i}{dz} = A_s \varepsilon_s \sum_{j=1}^{N1} r_{ij} - f_{lossi}(z) \quad (2.10)$$

$i=1, Nc$

With boundary conditions of:

$$\text{At } z=0, Q_i = Q_{i0} \quad i=1, Nc$$

Assuming radial uniformity of temperatures within the spout results in the following equation for the spout gas temperature:

$$\frac{dT_g}{dt} = \frac{1}{\varepsilon_s \sum_{i=1}^{Nc} C_i c_{pi}} \left[ \frac{4U_w(T_a - T_g)}{D_s} + \frac{6h_p(1 - \varepsilon_s)(T_p - T_g)}{d_p} - \varepsilon_s \sum_{j=1}^{N1} r_j (\Delta H_j) - \frac{\sum_{i=1}^{Nc} Q_i c_{pi}}{A_s} \frac{dT_g}{dz} \right] \quad (2.11)$$

The accompanying boundary conditions are:

$$\text{At } z = 0 \quad T_g = T_{go}$$

At  $t = 0$   $T_{g(z)} = T_g^0(z)$

A similar energy balance for the spout particles yields the following expression for the spout particle temperature:

$$\frac{dT_p}{dt} = -V_s \frac{dT_p}{dt} - \frac{6h_p(T_p - T_g)}{c_{p_p} \rho_p d_p} + \frac{4\sigma Q_{ap}(T_a^4 - T_p^4)}{c_{p_p} D_s d_p (1 - \epsilon_s)} + \frac{Q_p(T_a - T_p)}{\rho_p A_s L_e (1 - \epsilon_s)} \quad (2.12)$$

The boundary conditions associated with this PDE are:

At  $z=0$   $T_p = T_{ao}$

At  $t=0$   $T_p(z) = T_p^0(z)$

Responses of spout gas temperature profiles are found to exhibit two trends. First, a sudden pseudo steady state is found to appear with a time constant comparable to the residence time of the reacting gases (e.g., 30 ms). Second, long-term responses are found to be dependent upon the dynamics of the annular temperature (e.g., 15 min). Simulations of dynamic responses for various disturbances indicate that short-term dynamic behavior is strongly affected by changes in the inlet gas stream properties. Long-term responses, however, are dependent upon the dynamics of the annular temperature.

**Lucas et al., (1998)** developed a two-region model of a spouted bed gasifier, the model assumes first-order reaction kinetics for the gasification reactions and the spout is treated as a plug flow reactor of fixed diameter with cross flow of gas into the annulus. The annulus region is considered to be a single plug flow reactor. Solids move in plug flow in both annulus and spout, independent of temperature and reaction. The model allows predictions of axial profiles of temperature and gas in the spout and annulus as well as exit gas compositions and overall carbon conversion.

In a given increment of spout height the pyrolysis and char gases are added to the gases from the previous increment in a manner that ensures that the generation is largest at the spout entrance and decreases with spout height. This pattern is achieved by the following equation:

$$Q_p^j = W_s^o (1 - F_a - F_w) M_c \eta \frac{4}{h_M} \phi_k(T_b) * \int_{h_{j-1}}^{h_j} \left[ 1 - \left( \frac{h}{h_M} \right)^{1/3} \right] dh \quad (2.13)$$

The gas flow and gas compositions entering annulus section j are, respectively:

$$Q_A^{\sim j} = Q_A^{j-1} + Q_{SA}^j \quad (2.14)$$

$$Y_{k,A}^{\sim j} = \frac{Y_{k,A}^{j-1} Q_A^{j-1} + Y_{k,S}^j Q_{k,SA}^j}{Q_A^{j-1} + Q_{SA}^j} \quad (2.15)$$

The authors predicted an equation to calculate the average temperature at the gasifier exit:

$$T_E = T_R + \frac{Q_S^M \sum_K Y_{K,S}^M c_{p_k} (T_S^M - T_R) + Q_A^M \sum_K Y_{K,A}^M c_{p_k} (T_A^M - T_R)}{(Q_S^M + Q_A^M) \sum_K Y_{K,A}^M c_{p_k}} \quad (2.16)$$

For ease of computation, the number of streamtubes was reduced to one. Predicted axial composition profiles in the annulus were affected more by the reduction in the number of streamtubes than by the change from isothermal to nonisothermal conditions. The axial profile was shown to depend strongly on the assumed solids recirculation rates. Comparisons made between predicted axial temperature profiles and those measured in a pilot gasifier showed good agreement for both air gasification of a highly reactive sub-bituminous coal and oxygen gasification of a much less reactive anthracite. In the lower spout region where heat losses were large, agreement was poorer.

**Mendes et al., (2008)** modelled a spouted bed reactor operating at high temperature through one dimensional model in which heat transfer has been carefully described at different levels of complexity. The process of coal gasification has been selected to demonstrate the models achievements and predictions have been compared to previous spouted bed reactor experimental results. The authors studied the velocity of particles in the spouted bed and they predicted an equation to calculate the velocity of the solid articles in the annular:

$$V_a(z) = - \frac{A_s V_s}{A_a} \quad (2.17)$$

The conservation equations for the gaseous component j in the spout and annulus were predicted by the authors as follows:

$$\text{Spout region: } A_s u_s \frac{dC_{sj}}{dz} = r_{sj} A_s \quad (2.18)$$

$$\text{Annulus region: } A_a u_a \frac{dC_{aj}}{dz} = r_{aj} A_a + \left[ A_a \frac{du_a}{dz} + u_a \frac{dA_a}{dz} \right] (C_{sj} - C_{aj}) \quad (2.19)$$

Two types of one-dimensional spouted bed reactor models are presented: a pseudo homogeneous model and a heterogeneous one. In the pseudo homogeneous approach, energy balances are function of a unique temperature characteristic of the flow region and representative of both gas and solid phases.

**Pseudo homogeneous approach, spout region:**

$$A_s \left[ \rho_p C_p V_s + \rho_g C_p u_s \right] \frac{dT_s}{dz} = \rho_p C_p \left[ A_s \frac{dV_s}{dz} + V_s \frac{dA_s}{dz} \right] (T_a - T_s) + A_s \sum (-\Delta H) R_g \quad (2.20)$$

**Pseudo homogeneous approach, annulus region:**

$$K_{ea} A_a \frac{d^2 T_a}{dz^2} = A_a (\rho_p C_p V_a + \rho_g C_p u_a) \frac{dT_a}{dz} + \rho_g C_p \left( A_a \frac{du_a}{dz} + u_a \frac{dA_a}{dz} \right) (T_a - T_s) - K_{ea} \frac{dA_a}{dz} \frac{dT_a}{dz} - A_a \sum (-\Delta H) R_g + 2\pi R(z) h_{wr} \quad (2.21)$$

In the heterogeneous approach, four energy balances are written, which correspond to gas and particle temperature fields in each hydrodynamic region of the bed.

**Heterogeneous approach, spout region:**

Gas phase:

$$\rho_g C_p u_s \frac{dT_{sg}}{dz} = h_p \frac{6(1-\varepsilon)}{d_p} [T_{sp} - T_{sg}] + \sum (-\Delta H) R_g \quad (2.22)$$

Solid phase:

$$\rho_p C_p V_s A_s \frac{dT_{sp}}{dz} = A_s h_{ps} \frac{6(1-\varepsilon_s)}{d_p} [T_{sg} - T_{sp}] + \rho_p C_p \left[ A_s \frac{dV_s}{dz} + V_s \frac{dA_s}{dz} \right] (T_{ap} - T_{sp}) + \sum (-\Delta H) R_p \quad (2.23)$$

**Heterogeneous approach, annulus region:**

$$\text{Gas phase: } \rho_g C_p V_a A_a \frac{dT_{ag}}{dz} = A_a h_{ag} \frac{6(1-\varepsilon_a)}{d_p} [T_{ag} - T_{ap}] + \rho_g C_p \left[ A_a \frac{dU_a}{dz} + U_s \frac{dA_a}{dz} \right] (T_{sg} - T_{ag}) + \sum (-\Delta H) R_g \quad (2.24)$$

Solid phase:

$$K_{ea} A_a \frac{d^2 T_{ap}}{dz^2} = A_a h_{pga} \frac{6(1-\varepsilon_a)}{d_p} [T_{ap} - T_{ag}] + \rho_p C_p V_a A_a \frac{dT_{ap}}{dz} - K_{ea} \frac{dA_a}{dz} \frac{dT_{ap}}{dz} + \pi D_c h_w (T_{ap} - T_w) - \sum (-\Delta H) R_g A_a \quad (2.25)$$

The process of coal gasification has been selected to demonstrate the prediction capability of this model. The results selected are from **Lucas et al., (1998)**, who developed a non-isothermal model of a spouted bed gasifier, and from **Salam and Bhattacharya, (2006)**, studied charcoal gasification in two different configurations of spouted bed, comparing bed temperatures, species concentrations at the reactor exit as well as gasification efficiencies. The results obtained with the complete model remain in fairly good agreement with experimental data and showed that the most important reaction pathways of the gasification process have been captured, as well as the most important heat transfer phenomena.

**Deng et al., (2008)** developed a 3D mathematical model to simulate the coal gasification process in a pressurized spout fluid bed. This CFD model is composed of gas-solid hydrodynamics, coal pyrolysis, char gasification, and gas phase reaction submodels.

### **Gas-solid Hydrodynamics:**

Continuity Equations

$$\frac{d}{dt}(\varepsilon_g \rho_g) + \nabla \cdot (\varepsilon_g \rho_g u) = S_{gs} \quad (2.26)$$

$$\frac{d}{dt}(\varepsilon_s \rho_s) + \nabla \cdot (\varepsilon_s \rho_s V_s) = S_{sg} \quad (2.27)$$

### **Momentum Equations:**

For the gas phase

$$\frac{d}{dt}(\varepsilon_g \rho_g u) + \nabla \cdot (\varepsilon_g \rho_g u \cdot u) = -\varepsilon_g \nabla p + \varepsilon_g \rho_g g + \nabla \cdot \varepsilon_g \tau_g - \beta_{gs}(u - u_s) + S_{gs} u_s \quad (2.28)$$

The momentum equation for the solid phase should obtain the reverse source term and can be expressed as follows:

$$\frac{d}{dt}(\varepsilon_s \rho_s V_s) + \nabla \cdot (\varepsilon_s \rho_s V_s V_s) = -\varepsilon_s \nabla p + \varepsilon_s \rho_s g - \nabla \cdot p_s + \nabla \cdot \varepsilon_s \tau_s - \beta_{gs}(u - u_s) + S_{sg} u_s \quad (2.29)$$

### **Energy Equations:**

$$\frac{d}{dt}(\varepsilon_g \rho_g H_g) + \nabla \cdot (\varepsilon_g \rho_g u_g H_g) = \nabla \cdot (\lambda_g \nabla T_g) + Q_{gs} + S_{gs} H_s \quad (2.30)$$

$$\frac{d}{dt}(\varepsilon_s \rho_s H_s) + \nabla \cdot (\varepsilon_s \rho_s u_s H_s) = \nabla \cdot (\lambda_s \nabla T_s) + Q_{sg} + S_{sg} H_s \quad (2.31)$$

The heat exchange between phases can be expressed as a function of the temperature difference and conform to the local balance condition

$$Q_{sg} = -Q_{gs} \quad (2.32)$$

$$Q_{gs} = h_{sg}(T_s - T_g) \quad (2.33)$$

The simulation results of the outlet molar fraction of gas composition are expressed by the area average as below:

$$\bar{X}_i = \frac{1}{Ac} \int X_i dAc \quad (2.34)$$

The authors found that the prediction results are in good agreement with the experimental data. Most of the calculation errors are within the range of 10%. In addition they concluded that CFD modeling can be used for complex fluidized beds coal gasification processes.

# **Chapter Three**

## **Theoretical Modeling**

### **3.1 Simulation of gas – solid system model**

#### **3.1.1 Steady – State model assumptions**

1. Mass transfer by flow occurs in z direction by the stream of gasification agent (air + steam) which passes from the bottom to the top of the gasifier.
2. Mass transfer between gas bulk and particle occurs by diffusion and by convection (bulk flow) in both axial direction (z) and radial direction (r).
3. Close to the particle boundary, mass transfer occurs solely by diffusion through the boundary layer surrounding the solid particles, from the bulk to the surface of the solid particle due to the concentration difference for the reacted species presented in the gas.
4. The reaction occurs on the surface of the solid particle consuming the carbon in the solid fuel and the produced species, which is in gas phase, leave the surface of the solid particle after the reaction has been completed.

#### **3.2 Steady – state model equations**

Modeling equations consist of mass balance equations for the gas – phase in the bulk gas and on the surface of the solid particles.

##### **3.2.1 Mass balance to obtain the continuity equation in the gas phase**

Figure 3-1 shows a schematic diagram of the fluidized bed. Mass balance was carried out over a differential element (Figure 3-1b), in the gas bulk of gasifier. This differential element is a hollow cylindrical shape consists of solid particles.

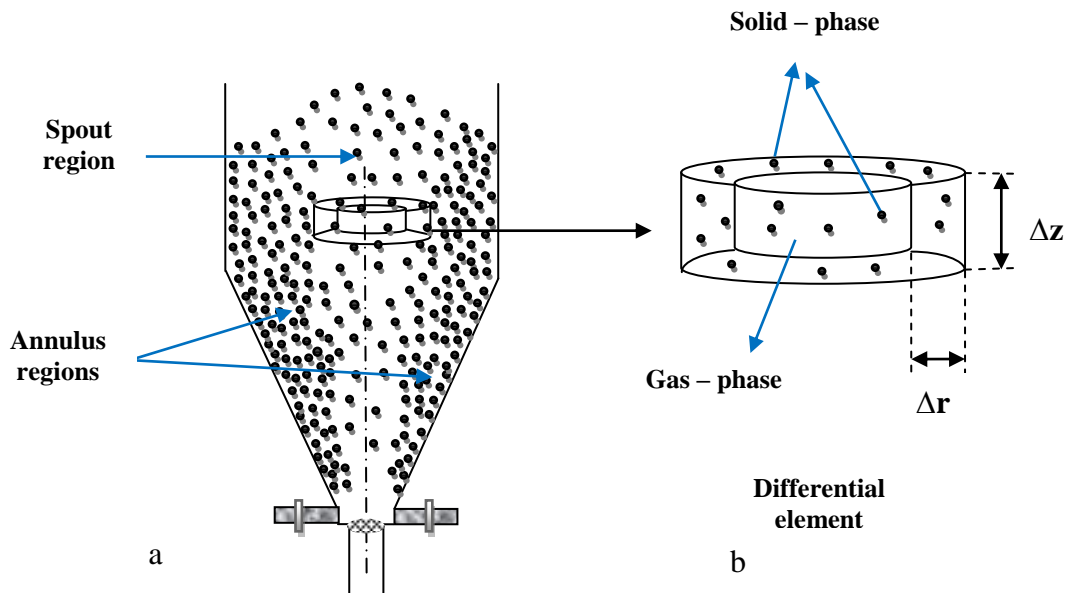


**Figure 3-1** Schematic sketch for the gasifier and the gas cell taken to make the balance

The following inventory rate equation can be written to describe the transformation of the particular conserved quantity of component  $i$ , (Tosun, 2002):

$$[(\text{Rate of mass In}) - (\text{Rate of mass out})]_{\text{by flow}} + [(\text{Rate of mass In}) - (\text{Rate of mass out})]_{\text{by molecular diffusion}} + \text{Generation} = \text{Consumption} + \text{Accumulation} \quad (3.1)$$

The gas enters the gasifier from the bottom and flows in  $z$  - direction; therefore there is mass transfer by bulk flow (convection) in  $z$  - direction. In addition due to the concentration gradient in  $z$  and  $r$  direction, mass transfer occurs by molecular diffusion as well. The detailed steps for the balance are shown as follows:

### **$z$ - direction**

$$\text{Rate of mass in by flow} = Q \cdot C_i$$

$$Q = U \cdot A = u \cdot \epsilon \cdot A$$

**Where:**

Q: Volumetric gas flow rate

U: Superficial gas velocity

$$U = \frac{Q}{A}$$

A: Cross sectional area of the element

$$u = \frac{U}{\epsilon}$$

u: Interstitial gas velocity

$\varepsilon$ : Porosity of the bed,  $\varepsilon = \frac{\text{volume of voids in bed}}{\text{Total volume( void+solid)}}$  , (Darby, 2001)

$$\text{Rate of mass in by flow} = u_z \cdot \varepsilon \cdot 2 \pi r \Delta r C_i \quad (3.2)$$

$$\text{Rate of mass out by flow} = (u_z \cdot \varepsilon \cdot C_i + \frac{d}{dz} u_z \cdot \varepsilon \cdot C_i \cdot \Delta z) 2 \pi r \Delta r \quad (3.3)$$

$$\text{Rate of mass in by molecular diffusion} = N_{iz}|_z 2 \pi r \Delta r \quad (3.4)$$

$$\text{Rate of mass out by molecular diffusion} = N_{iz}|_{z+\Delta z} 2 \pi (r + \Delta r) \Delta r = (N_{iz} + \frac{d}{dz} N_{iz} \cdot \Delta z) 2 \pi (r + \Delta r) \Delta r \quad (3.5)$$

Generation = 0 (No reaction will occur in the gas – phase).

### **r – direction**

$$\text{Rate of mass in by molecular diffusion} = N_{ir}|_r \cdot 2 \pi r \Delta z \quad (3.6)$$

$$\begin{aligned} \text{Rate of mass out by molecular diffusion} &= N_{ir}|_{r+\Delta r} \cdot 2 \pi (r + \Delta r) \Delta z \\ &= (N_{ir} + \frac{d}{dr} N_{ir} \cdot \Delta r) 2 \pi (r + \Delta r) \Delta z \end{aligned} \quad (3.7)$$

$$\text{Accumulation} = \frac{dN_i}{dt} = \left( \frac{dC_i \cdot \varepsilon}{dt} \right) \cdot v$$

Where:

$$v = (A_{out} - A_{in}) \Delta z = \pi [(r + \Delta r)^2 - r^2] \cdot \Delta z = 2 \pi r \cdot \Delta r \cdot \Delta z \text{ hence,}$$

$$\text{Accumulation} = \left( \frac{dC_i \cdot \varepsilon}{dt} \right) 2 \pi r \cdot \Delta r \cdot \Delta z \quad (3.8)$$

Substitute Equations. (3.2), (3.3), (3.4), (3.5), (3.6), (3.7), and (3.8) into equation (3.1):

$$\begin{aligned} &\{[(u_z \cdot \varepsilon \cdot C_i) - (u_z \cdot \varepsilon \cdot C_i + \frac{d}{dz} u_z \cdot \varepsilon \cdot C_i \cdot \Delta z)] 2 \pi r \Delta r\} + \{N_{iz} \cdot 2 \pi r \Delta r - (N_{iz} + \\ &\frac{d}{dz} N_{iz} \cdot \Delta z) 2 \pi (r + \Delta r) \Delta r\} + \{N_{ir} \cdot 2 \pi r \Delta z - (N_{ir} + \frac{d}{dr} N_{ir} \cdot \Delta r) 2 \pi (r + \\ &\Delta r) \Delta z\} = \left( \frac{dC_i \cdot \varepsilon}{dt} \right) 2 \pi r \cdot \Delta r \cdot \Delta z \end{aligned} \quad (3.9)$$

Rearrange the above equation:

$$\begin{aligned} &-\frac{d}{dz} u_z \cdot \varepsilon \cdot C_i \cdot 2 \pi r \cdot \Delta r \cdot \Delta z - \frac{d}{dz} N_{iz} \cdot 2 \pi r \cdot \Delta r \cdot \Delta z - N_{ir} 2 \pi \cdot \Delta r \cdot \Delta z - \\ &\frac{d}{dr} N_{ir} \cdot 2 \pi r \cdot \Delta r \cdot \Delta z = \left( \frac{dC_i \cdot \varepsilon}{dt} \right) 2 \pi r \cdot \Delta r \cdot \Delta z \end{aligned} \quad (3.10)$$

Divide equation (3.10) by  $2 \pi r \cdot \Delta r \cdot \Delta z$

$$-\frac{d}{dz} u_z \cdot \varepsilon \cdot C_i - \frac{d}{dz} N_{iz} - \frac{1}{r} N_{ir} - \frac{d}{dr} N_{ir} = \left( \frac{dC_i \cdot \varepsilon}{dt} \right) \quad (3.11)$$

From Fick's first law, the mass flux (**Kreith and Boehm, 1999**) can be written as:

$$N_{iz} = -D_e \frac{dC_i}{dz}, \quad N_{ir} = -D_e \frac{dC_i}{dr}$$

Where:  $D_e = \frac{\varepsilon}{\tau} D_i$

$D_e$ : is the diffusivity of gas and the subscript e denotes an effective diffusivity that accounts for the presence of the solid material (**Geankoplis, 1998**).

Substitute for  $N_{iz}$  and  $N_{ir}$  into equation (3.11):

$$-\frac{d}{dz} u_z \cdot \varepsilon \cdot C_i - \frac{d}{dz} \left( -\frac{\varepsilon}{\tau} D_i \frac{dC_i}{dz} \right) - \frac{1}{r} \left( -\frac{\varepsilon}{\tau} D_i \frac{dC_i}{dr} \right) - \frac{d}{dr} \left( -\frac{\varepsilon}{\tau} D_i \frac{dC_i}{dr} \right) = \left( \frac{dC_i \cdot \varepsilon}{dt} \right)$$

$\tau$  is the tortuosity factor and it is equal to 1 in the spouted fluidized bed (**Limtrakul, 2003**)

So equation above can be written as follows:

$$\frac{d}{dz} \left( \varepsilon \cdot D_i \frac{dC_i}{dz} \right) + \frac{1}{r} \left( \varepsilon \cdot D_i \frac{dC_i}{dr} \right) + \frac{d}{dr} \left( \varepsilon \cdot D_i \frac{dC_i}{dr} \right) - \frac{d}{dz} u_z \cdot \varepsilon \cdot C_i = \left( \frac{dC_i \cdot \varepsilon}{dt} \right) \quad (3.12)$$

### Boundary conditions:

1. At  $t; r; z = 0$        $C_{ib} = C_{ib}^0$
2. At  $t; r; z = L$        $\left( \frac{dC_{ib}}{dz} \right) = 0$
3. At  $t; z; r = 0$        $\left( \frac{dC_{ib}}{dr} \right) = 0$
4. At  $t; z; r = R$        $\left( \frac{dC_{ib}}{dr} \right) = 0$

Equation (3.12) represents the general continuity equation for the gas – phase species in the bulk.

The spouted bed consists of two regions; spout and annulus regions, Figure (3-1). The spout region lies at the centre of the gasifier and the annulus regions lie around the spout. So, equation (3.12) can be written for the two regions, spout and annulus.

## 3.2.2 Gas – phase equations for the spout and annulus regions

### a- Spout region

Equation (3.12) can be written for the gas – phase at the spout region:

$$\frac{d}{dz} \left( D_i \frac{dC_i \cdot \varepsilon}{dz} \right) + \frac{1}{r} \left( D_i \frac{dC_i \cdot \varepsilon}{dr} \right) + \frac{d}{dr} \left( D_i \frac{dC_i \cdot \varepsilon}{dr} \right) - \frac{d}{dz} u_z \cdot \varepsilon \cdot C_i = \left( \frac{dC_i \cdot \varepsilon}{dt} \right) \quad (3.13)$$

At steady – state  $\left( \frac{dC_i \cdot \varepsilon}{dt} \right) = 0$

So, equation (3.13) becomes:

$$\frac{d}{dz} \left( D_i \frac{dC_i \cdot \varepsilon}{dz} \right) + \frac{1}{r} \left( D_i \frac{dC_i \cdot \varepsilon}{dr} \right) + \frac{d}{dr} \left( D_i \frac{dC_i \cdot \varepsilon}{dr} \right) - \frac{d}{dz} u_z \cdot \varepsilon \cdot C_i = 0 \quad (3.14)$$

Re-arrange equation (3.14):

$$\left( D_i \cdot \varepsilon \frac{d^2 C_i}{dz^2} \right) + 2D_i \frac{dC_i}{dz} \frac{d\varepsilon}{dz} + \left( D_i \cdot C_i \frac{d^2 \varepsilon}{dz^2} \right) - u_z \cdot \varepsilon \frac{dC_i}{dz} - u_z \cdot C_i \frac{d\varepsilon}{dz} + \left( D_i \cdot \varepsilon \frac{d^2 C_i}{dr^2} \right) + \frac{D_i \cdot \varepsilon}{r} \left( \frac{dC_i}{dr} \right) = 0 \quad (3.15)$$

Equation (3.15) can be used to calculate the concentration profile of the gas – phase species in the spout region. The diameter of the spout is calculated in Appendix (D.1) and it is equal to 0.04 m. So, the annulus equivalent diameter is the difference between the column diameter and the spout diameter:

Annulus equivalent diameter = column diameter – spout diameter

Annulus equivalent diameter = (0.077 – 0.04) m = 0.037 m.

The space of annulus on each side will be 0.037/2 = 0.0185 m

The velocity in equation (3.15) is the gas – phase velocity at the spout, and the porosity represents the bed porosity at the spout region which are calculated in Appendix (D.2) and (D.3) respectively.

Figure 3-2 shows the diameter of the spout and the annulus space on each side of the gasifier.

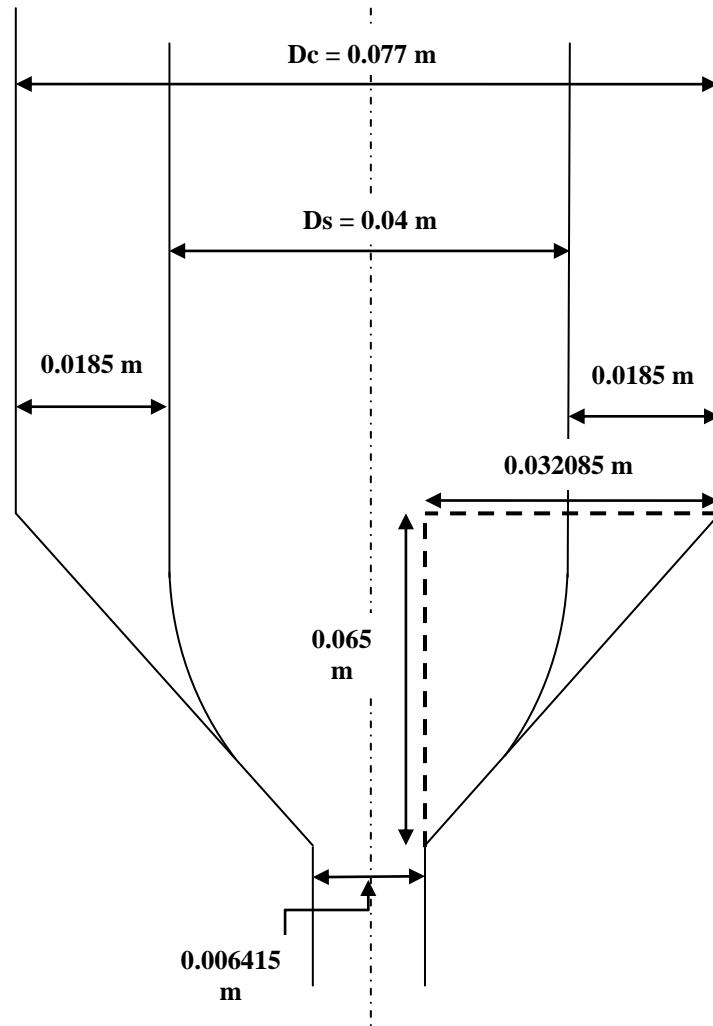


**Figure 3-2** Schematic diagram of the spout fluidized bed gasifier

### **b- Annulus region**

The voidage in the annulus  $\varepsilon_a$  is usually close to the minimum fluidization condition (Lim, et al., 1991; Sanchez et al., 2000):

$$\varepsilon_a = \varepsilon_{mf} = 0.45$$

For the concentration of the gas – phase species at the annulus, equation (3.12) can be arranged as follows:

$$D_i \cdot \varepsilon \frac{d}{dz} \left( \frac{dC_i}{dz} \right) + \frac{D_i \cdot \varepsilon}{r} \left( \frac{dC_i}{dr} \right) + \varepsilon \cdot D_i \frac{d}{dr} \left( \frac{dC_i}{dr} \right) - \varepsilon \frac{d}{dz} u_z \cdot C_i = 0 \quad (3.16)$$

The velocity in equation (3.16) represents the gas – phase velocity in the annulus region and it is calculated in Appendix (D.4).

$$D_i \cdot \varepsilon \frac{d^2 C_i}{dz^2} - \varepsilon \cdot u_z \frac{dC_i}{dz} - \varepsilon \cdot C_i \frac{du_z}{dz} + D_i \cdot \varepsilon \frac{d^2 C_i}{dr^2} + \frac{D_i \cdot \varepsilon}{r} \frac{dC_i}{dr} = 0 \quad (3.17)$$

Equation (3.17) represents the concentration and velocity profile of the gas – phase at the annulus region.

### 3.2.3 Gas – Solid interface

The gas species diffuses from the bulk with concentration of  $C_{ib}$  to the surface of the solid particle through the boundary layer surrounding the particle by molecular diffusion and then reacts on the surface of the particle. The gas concentration on the solid fuel surface is  $C_{is}$ .

The solid particle is surrounded by a boundary layer which is defined as the distance from a solid surface to a position where the concentration of the diffusing species reaches 99% of the bulk concentration. All the resistance to mass transfer is found within this hypothetical stagnant film and the properties (i.e., concentration, temperature) of the fluid at the outer edge of the film are identical to those of the bulk fluid (Fogler, 1999; Geankoplis 1998). Calculation of boundary layer thickness can be shown in Appendix (D.5).

A differential element of thickness =  $\Delta r$  in the boundary layer was taken and a mass balance was done on this element to predict the concentration profile of the gas – phase species in the diffusion boundary layer close to the solid surface.

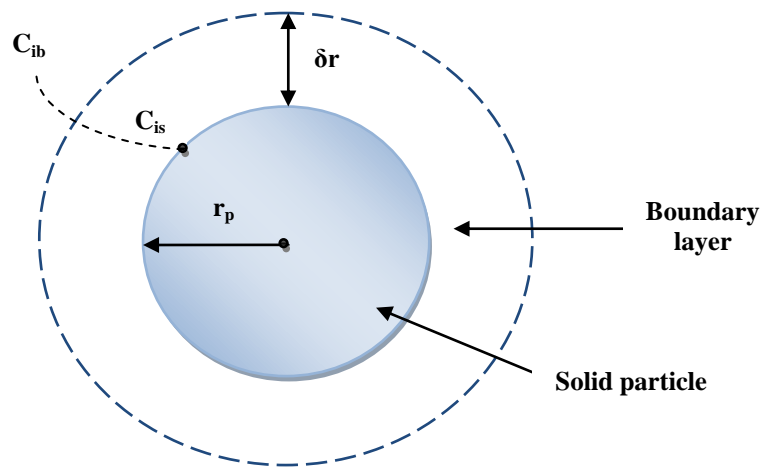


**Figure 3-3** Schematic sketch of the solid particle surrounded by the boundary layer

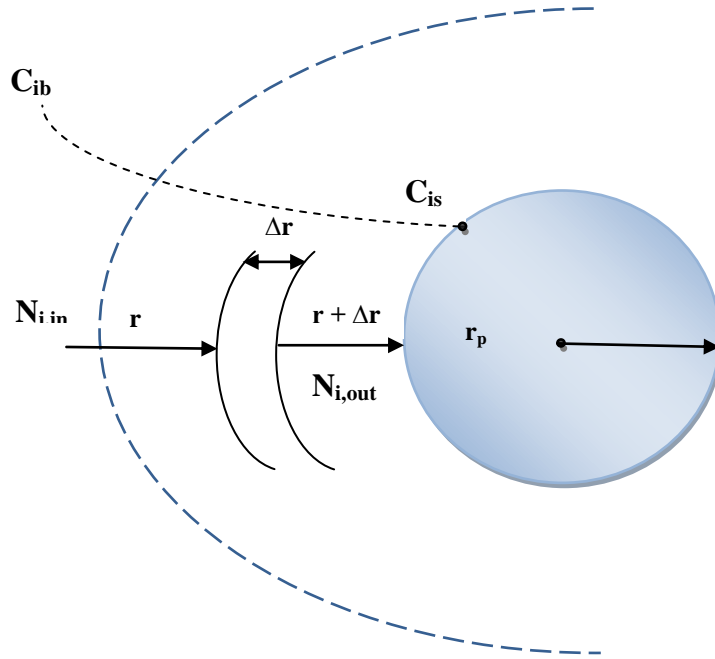


**Figure 3-4** Schematic sketch of the element taken in the boundary layer

$$\text{Rate of mass In} = N_{ir}|_r \cdot 4\pi r^2 \quad (3.18)$$

$$\text{Rate of mass out} = N_{ir}|_{r+\Delta r} \cdot 4\pi(r + \Delta r)^2$$

$$\text{Volume of element} = \frac{4}{3}\pi(r + \Delta r)^3 - \frac{4}{3}\pi r^3$$

$$\text{Rate of mass out} = \left( N_{ir} + \frac{d}{dr} N_{ir} \cdot \Delta r \right) \cdot 4\pi(r + \Delta r)^2 \quad (3.19)$$

$$\text{Rate of consumption} = -R_i \cdot v = -R_i \cdot (1 - \varepsilon) \cdot 4\pi r^2 \Delta r \quad (3.20)$$

$$\text{Rate of accumulation} = \frac{dN_i}{dt} = \left( \frac{dC_i(1-\varepsilon)}{dt} \right) \cdot 4\pi r^2 \Delta r \quad (3.21)$$

Substitute equations (3.18), (3.19), (3.20), and (3.21) into equation (3.1):

$$N_{ir}|_r \cdot 4\pi r^2 - \left( N_{ir} + \frac{d}{dr} N_{ir} \cdot \Delta r \right) \cdot 4\pi(r + \Delta r)^2 - R_i \cdot (1 - \varepsilon) \cdot 4\pi r^2 \Delta r = \left( \frac{dC_i(1-\varepsilon)}{dt} \right) \cdot 4\pi r^2 \Delta r \quad (3.22)$$

Re-arrange equation (3.22)

$$N_{ir}|_r \cdot 4\pi r^2 - N_{ir}|_{r+\Delta r} \cdot 4\pi r^2 - N_{ir}|_r \cdot 8\pi r \Delta r - \frac{d}{dr} N_{ir} 4\pi r^2 \Delta r - \frac{d}{dr} N_{ir} 8\pi r \cdot \Delta r^2 - R_i \cdot (1 - \varepsilon) \cdot 4\pi r^2 \cdot \Delta r = \left( \frac{dC_i(1-\varepsilon)}{dt} \right) \cdot 4\pi r^2 \cdot \Delta r$$

Re-arrange the above equation:

$$-N_{ir}|_r 8 \pi r \Delta r - \frac{d}{dr} N_{ir} 4\pi r^2 \cdot \Delta r - R_i \cdot (1 - \varepsilon) 4\pi r^2 \cdot \Delta r = \left( \frac{dC_i(1-\varepsilon)}{dt} \right) 4\pi r^2 \cdot \Delta r \quad (3.23)$$

Substitute for  $N_{ir}$  and divide equation (3.23) by the volume  $4\pi r^2 \Delta r$ ; at steady state conditions equation (3.23) become

$$D_i \cdot \varepsilon \frac{d^2 C_i}{dr^2} + \frac{2 \cdot D_i \cdot \varepsilon}{r} \frac{dC_i}{dr} - (1 - \varepsilon) \cdot R_i = 0 \quad (3.24)$$

Equation (3.24) represents the continuity equation for gas – phase on the surface of the solid particles. The boundary conditions for this equation are:

**Boundary conditions:**

1. At  $r_p = R_p$   $C_i = C_{i,s}$
2. At  $r_p = 0$   $\left( \frac{dC_i}{dr_p} \right) = 0$

The following cases are studied in the predicted model:

1. Oxygen consumption.
2. Steam consumption.
3. Carbon monoxide production.
4. Carbon dioxide production.
5. Hydrogen production.

$R_i$  in equation (3.24) represents the rate of reaction which occurs on the surface of the solid particles and can be calculated using rate equations presented in Table C-1.

### 3.3 Solution procedure of the modeling equations

#### 3.3.1 Boundary conditions

In order to solve the model equations, boundary conditions are specified. Initial oxygen concentration is calculated from inlet air-flow rate. Initial concentrations of  $CO_2$ ,  $CO$ , and  $H_2$  are assumed to be equal to zero at the gasifier inlet where  $z = 0$ , the  $H_2O$  initial concentration is calculated from inlet steam-flow rate.

### 3.3.2 Calculation procedure

The overall solution strategy of the predicted isothermal model follows the steps described below:

1. The gasifier is divided into two symmetrical sides; starting from the centre of the gasifier where  $r = 0$  to the wall of the gasifier where  $r = R$ , the spout and annulus regions are selected in one side. This side is divided for nodes at equal distances of  $\Delta z = 0.013$  m and equal distances of  $\Delta r = 0.006416$  m. The concentration of the gas – phase in the bulk is calculated at each node in the gasifier by the predicted model equations. The finite difference numerical method was employed to solve the differential equations to obtain the concentration profile under different operating conditions. For the gas – phase species in the spout, equation (3.15) can be written in finite difference form as follows:

$$D_i \cdot \varepsilon \frac{C_{i+1} - 2C_i + C_{i-1}}{\Delta z^2} + 2D_i \frac{C_{i+1} - C_i}{\Delta z} \frac{\varepsilon_{i+1} - \varepsilon_i}{\Delta z} + D_i \cdot C_i \frac{\varepsilon_{i+1} - 2\varepsilon_i + \varepsilon_{i-1}}{\Delta z^2} - u_z \cdot \varepsilon \frac{C_{i+1} - C_i}{\Delta z} + D_i \cdot \varepsilon \frac{C_{i+1} - 2C_i + C_{i-1}}{\Delta r^2} + \frac{D_i \cdot \varepsilon}{r} \frac{C_{i+1} - C_i}{\Delta r} = 0 \quad (3.25)$$

Where:

$$\frac{d^2 C_i}{dz^2} = \frac{C_{i+1} - 2C_i + C_{i-1}}{\Delta z^2}, \quad \frac{d^2 C_i}{dr^2} = \frac{C_{i+1} - 2C_i + C_{i-1}}{\Delta r^2}, \quad \frac{dC_i}{dz} = \frac{C_{i+1} - C_i}{\Delta z}, \quad \frac{dC_i}{dr} = \frac{C_{i+1} - C_i}{\Delta r}$$

$$\frac{d^2 \varepsilon_i}{dz^2} = \frac{\varepsilon_{i+1} - 2\varepsilon_i + \varepsilon_{i-1}}{\Delta z^2}, \quad \frac{d\varepsilon_i}{dz} = \frac{\varepsilon_{i+1} - \varepsilon_i}{\Delta z}$$

Equation (3.25) re-arranged and the following form used in Matlab Program to calculate the concentration of the gas phase in the spout region.

$$C_i = \frac{D_i \cdot \varepsilon \frac{C_{i+1} + C_{i-1}}{\Delta z^2} + 2D_i \frac{C_{i+1}}{\Delta z} \frac{\varepsilon_{i+1} - \varepsilon_i}{\Delta z} - u_z \cdot \varepsilon \frac{C_{i+1}}{\Delta z} + D_i \cdot \varepsilon \frac{C_{i+1} + C_{i-1}}{\Delta r^2} + \frac{D_i \cdot \varepsilon}{r} \frac{C_{i+1}}{\Delta r}}{\varepsilon \frac{2D_i}{\Delta z^2} + 2D_i \frac{\varepsilon_{i+1} - \varepsilon_i}{\Delta z} - D_i \cdot \frac{\varepsilon_{i+1} - 2\varepsilon_i + \varepsilon_{i-1}}{\Delta z^2} - \varepsilon \frac{u_z}{\Delta z} + \varepsilon \frac{2D_i}{\Delta r^2} + \frac{D_i \cdot \varepsilon}{r \cdot \Delta r}}$$

And for the gas – phase species in the annulus, equation (3.17) can be written as:

$$D_i \cdot \varepsilon \frac{C_{i+1} - 2C_i + C_{i-1}}{\Delta z^2} - \varepsilon \cdot u_z \frac{C_{i+1} - C_i}{\Delta z} - \varepsilon \cdot C_i \frac{u_{i+1} - u_i}{\Delta z} + D_i \cdot \varepsilon \frac{C_{i+1} - 2C_i + C_{i-1}}{\Delta r^2} + \frac{D_i \cdot \varepsilon}{r} \frac{C_{i+1} - C_i}{\Delta z} = 0 \quad (3.26)$$

Equation (3.26) re-arranged and the following form used in Matlab Program to calculate the concentration of the gas phase in the annulus region.

$$C_i = \frac{D_i \cdot \varepsilon \frac{C_{i+1} + C_{i-1}}{\Delta Z^2} - u_z \cdot \varepsilon \frac{C_{i+1}}{\Delta Z} + D_i \cdot \varepsilon \frac{C_{i+1} + C_{i-1}}{\Delta r^2} + \frac{D_i \cdot \varepsilon}{r} \frac{C_{i+1}}{\Delta r}}{\varepsilon \frac{2D_i}{\Delta Z^2} - \varepsilon \cdot \frac{u_{i+1} - u_i}{\Delta Z} - \varepsilon \frac{u_z}{\Delta Z} + \varepsilon \frac{2D_i}{\Delta r^2} + \frac{D_i \cdot \varepsilon}{r \cdot \Delta r}}$$

2. The concentration of the gases produced from gasification process is calculated at each node by the predicted model equation for the gas – phase on the solid surface after connecting with the predicted gas – phase equation at each node. Continuity equation for gas – phase on the surface of the solid particles (3.24) can be written in finite difference as follows:

$$D_i \cdot \varepsilon \frac{C_{i+1} - 2C_i + C_{i-1}}{\Delta r^2} + D_i \cdot \varepsilon \frac{6}{d_p} (1 - \varepsilon) \cdot \frac{C_{i+1} - C_i}{\Delta r} - (1 - \varepsilon) \cdot Ri = 0 \quad (3.27)$$

A computer program to solve the modeling equations has been developed using MATLAB (R2011a) to determine the composition of the reacted gas and the produced gas components from gasification process in two regions of the spout fluidized bed gasifier; spout and annulus regions.

The program begins with specifying all parameters that consist of the gas velocity at the spout and annulus regions, porosity, minimum fluidization velocity of the gas, minimum spouting velocity of the gas, bed height, diameter of the spout, and the physical properties of the gasification agent. The gasifier is divided into nodes and the concentration of the gas phase is calculated at each node, also the concentration of the reacted and the produced gases has been calculated at the surface of each fuel particle. Loops of the gas concentration were started, respectively over each node depending on the position of the node (i.e. the axial distance from the gas inlet  $z$ , and the radius of the gasifier  $r$ ).

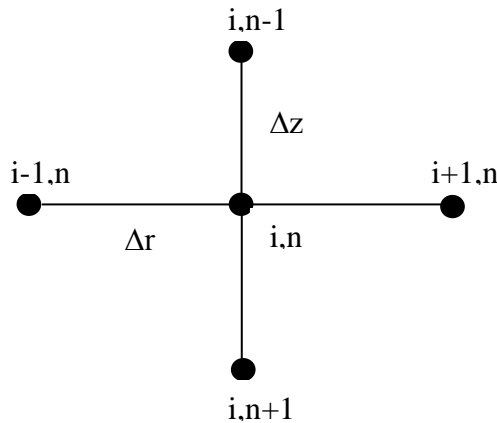


**Figure 3-5** Two dimensional finite difference net work of node (i,n)

At each particle equation (3.27) was applied and the reaction rate equation was taken from Table C-1 depending on the case studied, and the concentration of the gas species is calculated from equation (3.25) for the nodes lie at the spout region and from equation (3.26) for the nodes lie at the annulus region. Finally the concentration profile for the gas consumed and for the produced gas components inside the gasifier were obtained.

# Chapter Four

## Experimental work

### 4.1 Materials

#### 4.1.1 Bed material

Dry sand was used as a bed material with 0.6 - 0.71 mm particle mesh diameter and a density of  $1593.8 \text{ kg/m}^3$ . Two hundred grams of dry sand were added to the reactor in each experiment, the main function of this was to act as a heat carrier medium Figure 4-1a.

#### 4.1.2 Fuel

- a. Brown coal was used as a fuel with a particle mesh of 1 - 3.3 mm diameter and a bulk density of  $672.28 \text{ kg/m}^3$ , as shown in Figure 4-1b. Coal compositional information are shown in Table C-2.
- b. Algae biomass used was 1 - 3.3 mm particle mesh diameter and a bulk density of  $490.47 \text{ kg/m}^3$ . The ash of the algae used was 38% (dry weight basis), as shown in Figure 4-1c. Algae compositional information are presented in Appendix E.
- c. Algae biomass with 1 - 3.3 mm particle mesh diameter was mixed with coal (10% algae + 90% coal) for use in co-gasification experiments.
- d. Grape seeds biomass was used in co-gasification at different percents (5%, 10%, and 25%) with a particle mesh size of 1-3.3 mm diameter and bulk density of  $384.28 \text{ kg/m}^3$ , as shown in Figure 4-1d. Grape seeds compositional information are shown in Table C-3.

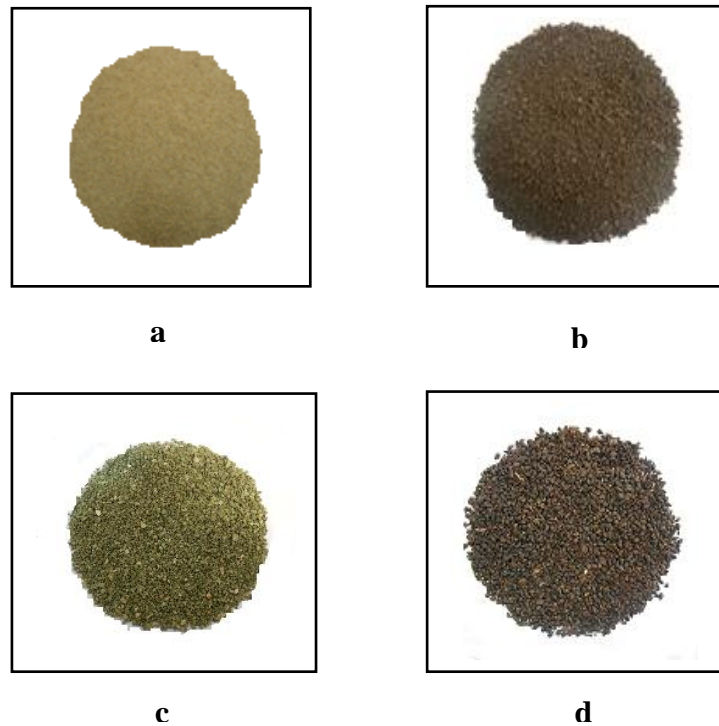


**Figure 4-1 a.** Bed material **b.** Brown Coal **c.** Algae **d.** Grape seeds

### **4.1.3 Gasification agents**

Both compressed air and steam were used together for the gasification at the following conditions:

- a. Air was passed through the air heater at an initial rate of 70 l/min after which it was mixed with steam and injected into the gasifier through the distributor. After the bed temperature reached 400 °C, the air flow rate was reduced to 35 l/min to ensure the bed material will fluidize.
- b. Deionised water was used as a steam source; this was done by calibrating the water rotameter to get the desired steam flow rate.

### **4.1.4 Nitrogen**

Nitrogen was added to the fuel hopper to create an inert environment during start up, shutdown and operation.

### 4.1.5 Cooling water

Deionised cold water was passed through an outside jacket on the screw feeder during the experiments; this was done to ensure the fuel is cold and prevent fuel burning before entering the gasifier.

### 4.2 Bed material and fuel sieving

The particles used as bed material and/or fuel were sieved to separate the desirable particle size. Sieving was done by using the shaker shown in Figure 4-2, in the lab for 10 minutes as shaking time for each sample. The bigger particles were crushed by the crusher and re-sieved again.



Figure 4-2 photographic picture for the used shaker

### 4.3 Moisture content of the fuel

The moisture content of the fuel was calculated by inserting a known weight of the fuel to the oven at 110 °C to insure all the water in the fuel will evaporate. The fuel sample was taken out of the oven after 2 hours and weighed. The moisture content was then calculated using the following equation:

$$\text{Moisture content} = \left( \frac{w_1 - w_2}{w_1} \right) * 100\% \quad (4.1)$$

The same procedure was repeated until the value of moisture content becomes unchanged.

**Table 4-1** moisture content of the used fuels

Fuel	Moisture content
Brown coal	19 % <sup>a</sup> , 15.2% <sup>b</sup>
Biomass algae	17%
Grape seeds biomass	9.5%

a- initial batch of coal, b- second batch of coal

#### 4.4 Steam calibration

The mass of steam needed for each experiment was calculated by calibrated rotameter. This was achieved by collecting the water at selected flow rates for a set period of time (10 minutes) Table B-2. A calibration curve (Figure B-1) was generated and referred to prior to gasification run to obtain the water flow rate required. The steam to fuel (S/F) ratio has been predicted using equation 4.2, this accounts for both the water in the coal and the water added as steam. The fuel mass is measured on a dry weight basis.

$$\frac{S}{F} = \frac{F_S + m_C M_C}{m_C (1 - M_C)} \quad (4.2)$$

Where;  $F_S$  is the flow rate of steam into the bed,  $m_C$  is the mass flow rate of coal into the bed and  $M_C$  is the moisture content of the coal used.

#### 4.5 Minimum fluidization velocity

Minimum fluidization velocity was estimated by running the reactor at different flow rates using air flow meter to measure the flow rate of air. The pressure drop within the reactor was measured by two pressure transmitters, one connected below the bed and the other above the bed. The transmitters were connected with the Fluid-Bed-Furnace control panel which gave a reading for the pressure drop across the bed. The experimental results of minimum fluidization velocity are presented in Table B-1.

## 4.6 Leaching of algae

A mixture of microalgal biomass and coal (10% biomass, 90% coal) was used as fuel for co-gasification experiments. The algae was found to contain high sodium chloride when analysed in the laboratory using the scanning electron microscope. To test for the level of salt present in the algae a sample was immersed in de-mineralized water (conductivity = 0) with agitation (Figure 4-3). After 3 hours the conductivity of the microalgae solution was measured using conductivity electrical meter giving a value of 13.3 mS. The water was replaced three times to insure almost all the salt was dissolved and then the solution was left to settle after which the supernatant was removed and the remaining material was left to dry by sun as shown in Figure 4-4. The algae was then put into the oven to further dry to a moisture content less than 20% (for further analysis and for using in co-gasification experiments).



**Figure 4-3** Photographic picture of microalgae solution

The dried algae was analysed by (Secondary Electron Detector) SE and BSE (Backscattered Electron Detector) and the salt content was found to decrease after leaching. Photographic pictures and peaks for analysis are shown in Appendix E.



**Figure 4-4** Photographic picture of algae cake settled after leaching



**Figure 4-5** Photographic picture of dried algae

The dried algae was sieved as mentioned in fuel sieving part to get the desired algae particle size diameter for gasification experiments.

#### **4.6.1 Composition materials of algae**

A basic analysis was completed to calculate the volatile, salt, and ash components in algae. This was done by placing a known weight of dried leached algae into a furnace at 840 °C for three hours. This combusted all volatile matter leaving behind any non-volatiles, the crucible was then taken out of the furnace and weighed. The sample was then added to de-mineralized water and the conductivity and salinity were measured using conductivity meter to calculate the salt content of the non-volatile matter (which was found to be 3.59 %). From this the ash content was found to be approximately 38%. Calculation procedure for this experiment is shown in Appendix B.5.



**Figure 4-6** Algae samples for burning

#### **4.7 Feeding velocity of the fuel**

The feeding velocity of the fuel was estimated by the following procedure: At room temperature and atmospheric pressure fuel was added to the fuel hopper and then the feeder was turned on, after 10 minutes the feeder was turned off and the amount of fuel inside the column was collected using the discharge cylinder at the bottom of the column. Then the weight of the collected fuel was measured. The same procedure was repeated with different feeding velocities and then fuel feed rate was calculated. The results are shown in Table B-3. A calibration curve similar to that of the water rotameter curve was generated for control of the feed flow rate (only accurate for fuel with a particle size diameter ranging from 1 to 3.35 mm) Figure B-2.

## **4.8 Spouted bed gasification Unit Description**

The gasification experiments were performed in an experimental fluidized bed unit constructed in the laboratory of Chemical Engineering School / University of Adelaide, SA, Australia. A photographic picture and schematic sketch are illustrated in Figures 4-7 and 4-8 respectively. The unit consists of a spouted bed column connected to a nitrogen cylinder, compressor, gas flow meter, H<sub>2</sub>O/steam source, water flow meter, heater, fuel hoppers, fuel motor feeder, furnace, ash collector, pressure transmitter and temperature controllers.

### **4.8.1 Gasifier**

The spouted-bed gasifier consists of two sections: the first section was the lower canister of 40 mm inner diameter with a height of 400 mm. A small perforated stainless-steel cylinder with 50 holes (each 3 mm in diameter) was placed at the injection point of the air/steam stream. This was done to ensure uniform gas distribution. This canister can be used for removing bed material. A very fine mesh was placed between the top of the stainless-steel cylinder and the lower part of the conical base which was used to prevent bed material from falling down during the experiment and also for distributing injected gas. The second section was a 65 mm high conical base, which expands from 10 mm (inner diameter) gas inlet to 77 mm (inner diameter) cylindrical section. The 77 mm cylindrical section was approximately 1.1 m high. A coal feed port was located approximately halfway between the conical base and the viewport. Gas and fine solids exit the vessel, by an exit port, to the gas-handling section.

The gasifier was heated by an electrical furnace which houses the middle section of the reactor. The column was insulated by two layers of Fiberfrax insulation material and the outer walls of the furnace consist of thermal ceramics insulating firebricks.

### **4.8.2 Furnace**

External heating was used during start-up to minimize heat loss from the reactor. The outer walls of the furnace consist of thermal ceramics insulating

firebricks. Two pairs of Kanthal Crusilite electrical heating elements (nominal resistance = 6.0  $\Omega$ ) provide heating. The elements were situated within each corner of the furnace and were suspended vertically from the top plate. Radiation shielding prevents hot spots on the reactor wall, which would otherwise occur because of the close proximity of the elements.

### **4.8.3 Fuel hoppers**

Fuel was fed above the bed halfway between the conical base and the viewport, via a pair of lock-hoppers and a screw feeder. Nitrogen was used to ensure an inert atmosphere within the hoppers and to provide backpressure to prevent steam from condensing in the feed line, and thus, causing blockages. The coal feed line was water-cooled near the entrance to the reactor.

### **4.8.4 Temperature controllers and pressure transmitters**

Thermocouples type-K (3.0 mm outer diameter) were used to measure the temperature at various locations along the centreline of the reactor. Thermocouples are labeled sequentially from TC<sub>1</sub> to TC<sub>4</sub> at the following locations: TC<sub>1</sub> is just below the conical distributor, and TC<sub>2</sub>, TC<sub>3</sub>, and TC<sub>4</sub> are 35, 65, and 105 mm above the gas inlet, respectively. Pressure tapings are located 15 mm below the gas inlet (PT<sub>1</sub>) and 190 mm above the gas inlet (PT<sub>2</sub>). The absolute pressure at PT<sub>1</sub> is measured using a Wika pressure transmitter. The bed pressure drop was measured between PT<sub>1</sub> and PT<sub>2</sub> using an ABB Kent Deltapi K series electronic transmitter. Both pressure transmitters provide 4-20 mA signal to a Mann Industries PM350 industrial process monitor. Temperatures and pressure signals were monitored using a Pico Technology eight-channel data logger (model TC-08) and logged at 1 Hz using the supplied PicoLog software.

### **4.8.5 Heater**

A Leister CH-6056 Sarnen heater was used to heat up the compressed dry air prior to mixing with the water. Heater temperature was controlled from the Fluid-Bed-Furnace control panel.

#### 4.8.6 Ash collector

A canister was connected to the top of gasifier column to collect the ash entrained. The ash canister can be removed during the operation and emptied to prevent excess build up.



**Figure 4-7** photographic picture for the spouted bed gasification unit.

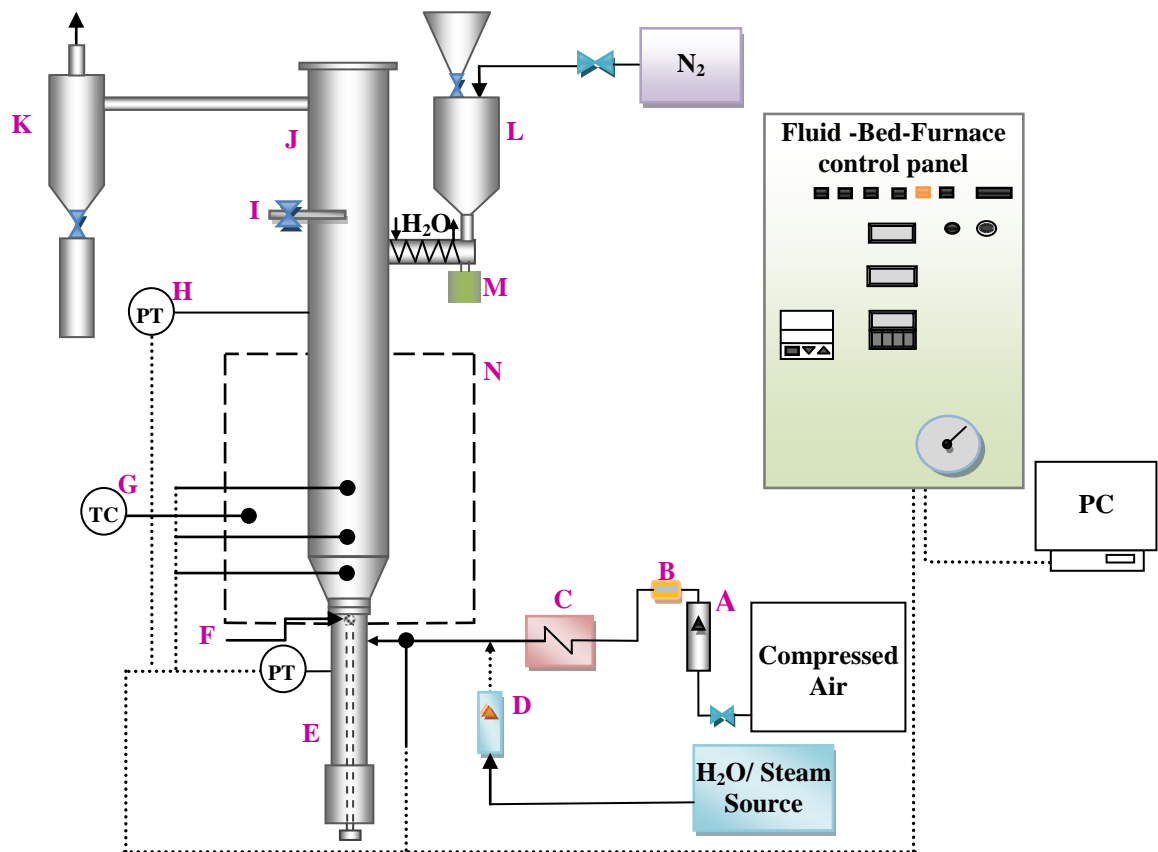


**Figure 4-8** Schematic sketch for the Spouted bed gasification unit

**A:** air flow meter; **B:** digital air flow meter; **C:** air heater; **D:** water flow meter; **E:** bed material discharge cylinder; **F:** distributor; **G:** temperature controllers; **H:** pressure transmitters; **I:** sampling port; **J:** spouted column; **K:** ash collector; **L:** fuel hopper; **M:** motor feeder; **N:** furnace.

## 4.9 The studied operating conditions

### 4.9.1 Coal gasification experiments

The experiments were carried out at two different temperatures 820 °C and 850 °C, steam to fuel (S/F) ratios of 0, 0.5 and 0.75, and air to fuel (A/F) ratios of 1.6, 1.8, and, 2. All the operating conditions were changed until reached to the optimum conditions that give the highest carbon conversion. The steam to air ratio was adjusted through the steam flow rate and air to fuel by changing the fuel feed flow rate. The studied conditions for coal gasification are shown in Table 4-2.

**Table 4-2** Studied operating conditions for coal gasification experiments

Run	Air /Fuel (w/w)	Steam /Fuel (w/w)	Fuel rate (kg/h)	Temperature °C
1	1.6	0.5	1.609	820
2	1.8	0.5	1.43	820
3	2	0.5	1.28	820
4	1.6	0.75	1.609	820
5	1.8	0.75	1.43	820
6	2	0.75	1.28	820
7	1.6	0.5	1.609	850
8	1.8	0.5	1.43	850
9	2	0.5	1.28	850
10	1.6	0.75	1.609	850
11	1.8	0.75	1.43	850
12	2	0.75	1.28	850

#### 4.9.2 Co – gasification experiments

The design of co-gasification experiment used a statistical technique to investigate the effects of various parameters included in experimental study and to determine their optimal combination. The design of the experiment by the Taguchi method uses a set of orthogonal arrays for performing of the fewest experiments. That is, the Taguchi method involves the determination of a large number of experimental situations, described as orthogonal arrays, to reduce the errors and enhance the efficiency and reproducibility of the experiments. Orthogonal arrays are a set of tables of numbers, which can be used to efficiently accomplish optimal experimental designs by considering a number of experimental situations (Mahamuni et al., 2010). An experimental design methodology adopting the Taguchi approach was employed in this study, with the orthogonal array design used to screen the effects of four parameters, including the steam to fuel ratio, air to

fuel ratio, percent of biomass used and reaction temperature, on the production of biogas.

**Table 4-3** Design experiments, with four parameters at three-levels, for the production of biogas.

parameter	levels		
	1	2	3
<b>A</b> Steam to Fuel (S/F) ratio	0.25	0.5	0.75
<b>B</b> Air to Fuel (A/F) ratio	2.1	2.3	2.5
<b>C</b> Biomass to Coal (B/C) ratio	0.05	0.11	0.25
<b>D</b> Temperature, °C	800	820	850

**Table 4-4** Orthogonal array used to design experiments with four parameters at three-levels.

Experiment NO.	Parameters and their levels			
	S/F ratio	A/F ratio	B/C ratio	Temperature
1	1	1	1	1
2	1	2	2	2
3	1	3	3	3
4	2	1	2	3
5	2	2	3	1
6	2	3	1	2
7	3	1	3	2
8	3	2	1	3
9	3	3	2	1

**Table 4-5** Experiments for the parameters and levels shown in Table 4-3.

Experiment NO.	Parameters and their levels			
	S/F ratio	A/F ratio	B/C ratio	Temperature, °C
1	0.25	2.1	0.05	800
2	0.25	2.3	0.11	820
3	0.25	2.5	0.25	850
4	0.5	2.1	0.11	850

5	0.5	2.3	0.25	800
6	0.5	2.5	0.05	820
7	0.75	2.1	0.25	820
8	0.75	2.3	0.05	850
9	0.75	2.5	0.11	800

#### **4.10 Procedure of gasification experiments:**

##### **A. Before each experiment**

1. The bed was ensured to be free of any solids from the previous run.
2. The screw feeder and hopper must be free of contaminants. The screw feeder was turned on with no coal in the hopper to allow any contaminants to be completely removed.
3. The furnace walls must be in place before switching on the heating elements.
4. All valves were ensured to be correctly opened / closed as appropriate.

##### **B. Requirements of experiments**

1. Fuel was prepared beforehand: sieving, drying, and weighing.
2. Inert material (sand) required as fluidising medium.

##### **C. The experimental procedure**

The experimental procedure for running the gasification unit includes the following steps:

1. Air-dried fuel was inserted into the hopper, and pre-determined amount of bed material added into the reactor through the top, then top of reactor sealed with flange system.
2. Nitrogen was fed to the fuel hopper.
3. Screw feeder cooling water was turned on.
4. Air flow was set at 70 l/min to start fluidization of the bed material.

5. Air preheater and heating elements were turned on to pre-heat the furnace and bed to the desired temperatures.
6. The contactor, control element, and power point were turned on from the fluid-bed-furnace control panel.
7. The computer connected to the control panel was turned on and software PicoLog started to record the furnace, bed, and freeboard temperatures and pressure drop inside the gasifier. During the reaction the temperature can be changed to the required value using the control panel by either choosing a set point temperature for  $T_{\text{furnace}}$  or by increasing or decreasing the air heater temperature or steam flow rate as appropriate.
8. Steam needed for the run to use with air as gasification agent, the water valve was turned on at a flow rate to obtain the ratio of steam required. The water was mixed with air out from the heater, thus water can be evaporated due to the high air temperature.
9. Once the temperature has reached desired level, the fuel feeding was started at the desired rate by turning on the screw feeder, and the speed of fuel feeder was dependent on the mass of fuel needed for each experiment.
10. The gas flow rate was decreased to 35 l/min when the temperature of the bed reaches 400 °C, to control the bed at minimum fluidization case.
11. After bed temperature be 450 °C fuel was fed to the gasifier, so gasification process will start and the temperature of the bed started to increase gradually until reaches the desired reaction temperature, then steam starting to pass through the gasifier.
12. When the steady state has been reached, gas samples were drawn four times after each hour from the reactor by the gas sampling port.

#### **D. Shut down Procedure**

1. Once the experiment has completed, heating elements and air preheater were switched off, and then the air completely (slump the bed) switched off to reduce the temperature to ambient conditions over time.

2. Once cool, cooling water for feeder was turned off, also the nitrogen flow to the hopper was turned off and the contents of bed were removed by discharging the solids at the bottom.

## 4.11 Composition Measurement

### 4.11.1 Scanning Electron Microscope

The raw algae before and after leaching, agglomerate from coal gasification, agglomerate from algae gasification, and bed material from algae gasification were examined by a scanning electron microscope (Figure 4-10) located at the Adelaide Microscopy/Medical School, SA, Australia.

For this process a small sample was inserted inside the microscope and two detectors were used; SE detector (Secondary Electron Detector) and BSE (Backscattered Electron Detector). SE is used to investigate the structural nature of the material and BSE for the variation in elemental composition. The BSE detector works based on elemental “hardness”, the harder the element is, the higher the level of electron reflection will be resulting in a lighter shade in the image obtained. Figures, peaks, and compositions of the analyzed samples under SE and BSE detectors are shown in Appendix E.

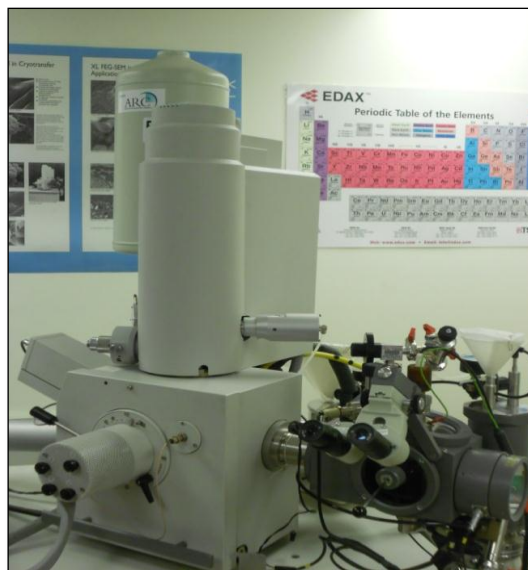


**Figure 4-9** Photographic picture of the Scanning Electron Microscope

### 4.11.2 Gas Chromatography

Agilent 3000 Micro Gas Chromatograph was used to analyse gas samples with thermal-conductivity detector (TCD). The major advantage of GC over other separation techniques is the high selective ability to separate volatile components from the gas mixture. The oven temperature of the gas chromatography is programmed at inlet temperature of 90 °C and raised to 108 °C. Injection time was 25 seconds and rotation time was 2 minutes. The carrier gases used for chromatographic analysis were pure helium and argon, Cerity NDS for Chemical QA/QC software was used to analyze the samples and produce molar concentrations from the peaks obtained.



**Figure 4-10** Gas Chromatography

# Chapter five

## Results and Discussions

### 5.1 Minimum fluidization velocity

The minimum fluidization velocity was obtained by measuring the pressure drop across the bed at different superficial velocities and plotting the results. The results are listed in Table B-1.

Figure (5-1) shows the values of air superficial velocity with changing the pressure drop. The value of minimum fluidization velocity is found to be equal to 0.09 m/s at 25 °C, and 0.135 m/s at 400 °C for the particle diameter of 0.6-0.71 mm. The value of minimum fluidization velocity is corrected at 400 °C as shown in Appendix B.2.

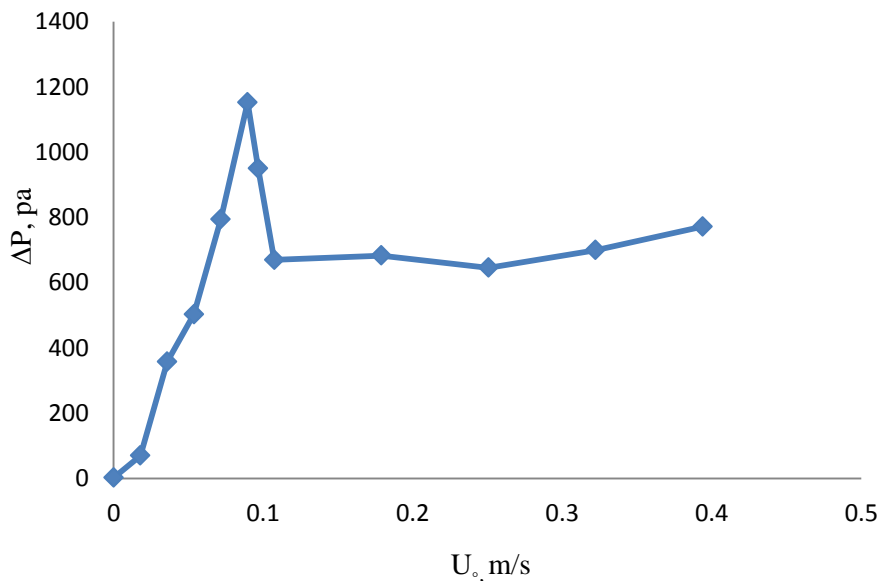


**Figure 5-1** Relation between bed pressure drop and air superficial velocity at 25 °C

### 5.2 Gasification of coal

The fraction of carbon converted during gasification and the amount of each major component found in the producer gas allow the conclusion of how gasification reactions are behaving in the reactor. Table 5-1 lists the gasification reaction.

**Table 5-1** Gasification reactions (Heiskanen, 2011; Ciferno, and Marano, 2002)

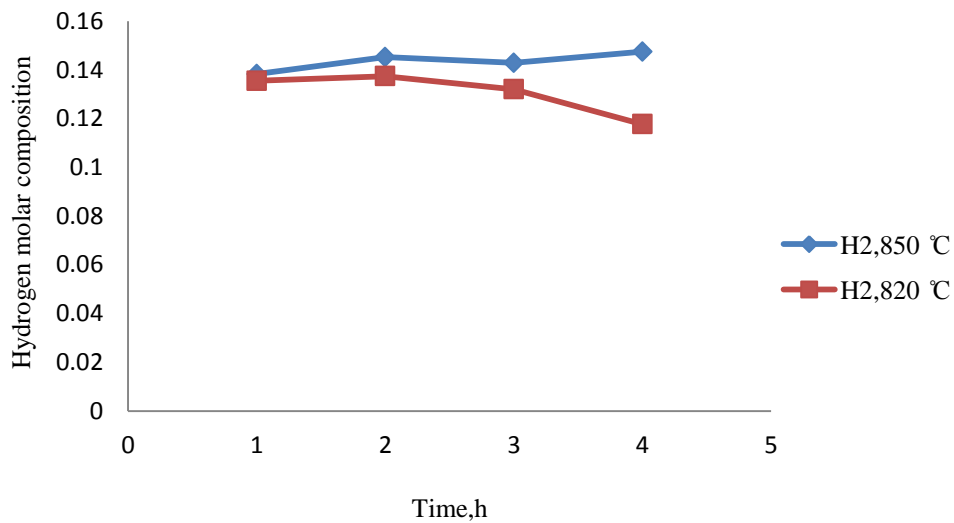
<b>Exothermic Reactions</b>	<b>Reaction number</b>
$C + 0.5 O_2 \rightarrow CO$	(1)
$CO + 0.5 O_2 \rightarrow CO_2$	(2)
$C + O_2 \rightarrow CO_2$	(3)
$C + 2H_2 \rightarrow CH_4$	(4)
$CO + H_2O \leftrightarrow CO_2 + H_2$	(5)
<b>Endothermic Reactions</b>	
$C + CO_2 \rightarrow 2CO$	(6)
$C + H_2O \rightarrow CO + H_2$	(7)
$CH_4 + H_2O \leftrightarrow CO + 3H_2$	(8)

### 5.2.1 Effect of temperature

Reaction temperature is one of the most important operating parameters affecting the performance of coal gasification.

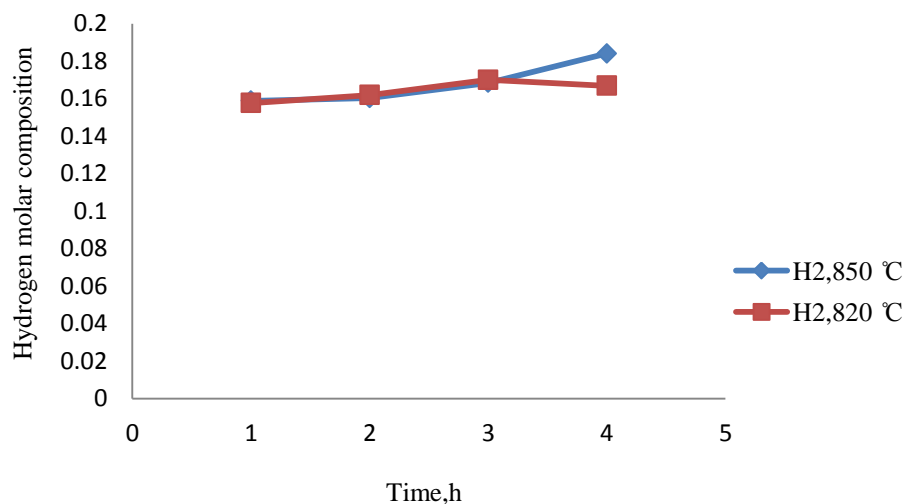
The temperature of the bed increases rapidly after fuel feeding. This increase is happening from the homogenous mixing of the bed material (which acts as a heat carrier medium) with the fuel inside the gasifier, and also due to the heat produced from a limited amount of combustion present in the gasifier. In the present study the gasifier operated with different temperature values (820 and 850) °C to study the mechanism of gasification reactions at these temperatures.

Figure 5-2 shows the variation of produced molar hydrogen composition with time at coal feeding rate of 1.28 kg/h, S/F=0.5, and at bed temperature of 850 °C and 820 °C, respectively. Running the gasifier with a feed flow rate of 1.28 kg/h and a S/F ratio of 0.5 results in a maximum molar composition of hydrogen of 0.1374 at 820 °C and with the same coal rate, and S/F ratio, the maximum molar composition of hydrogen produced is 0.147 at 850 °C.



**Figure 5-2** Effect of bed temperature on the molar hydrogen compositions at coal feeding rate of 1.28 kg/h, 0.5 S/F

Figure 5-3 shows the variation of molar composition of the produced hydrogen with time, in case of coal feeding rate of 1.28 kg/h, S/F=0.75, and at 850 °C and 820 °C, respectively. When running with coal feeding rate of 1.28 kg/h, and the same value of S/F=0.75, but changing temperature from 850 °C to 820 °C in both cases, the produced molar hydrogen composition increases giving values of 0.17 and 0.184 at 820 °C and 850 °C respectively.

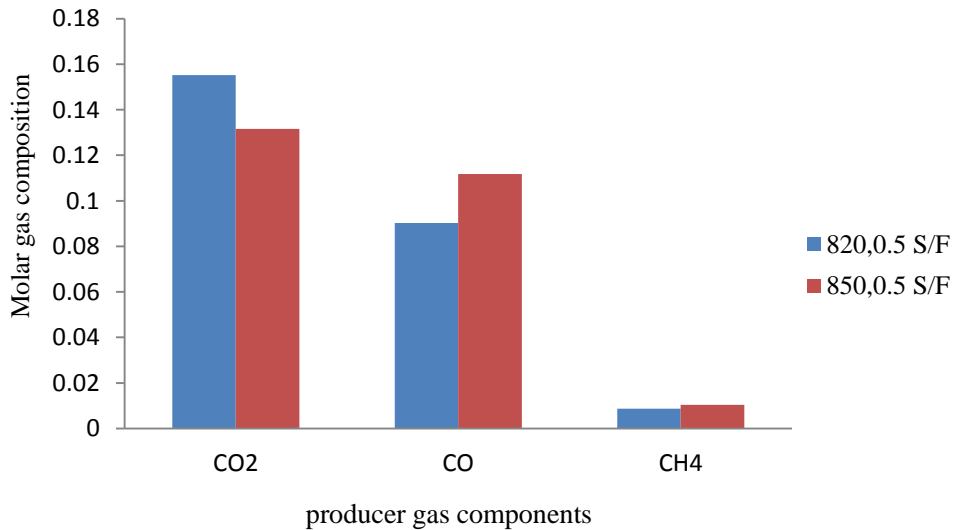


**Figure 5-3** Effect of bed temperature on the molar hydrogen compositions at coal feeding rate of 1.28 kg/h, 0.75 S/F

At 850 °C the molar composition of hydrogen was noticed to increase with time and it's maximum value was obtained at the end of experiment; i.e. after four

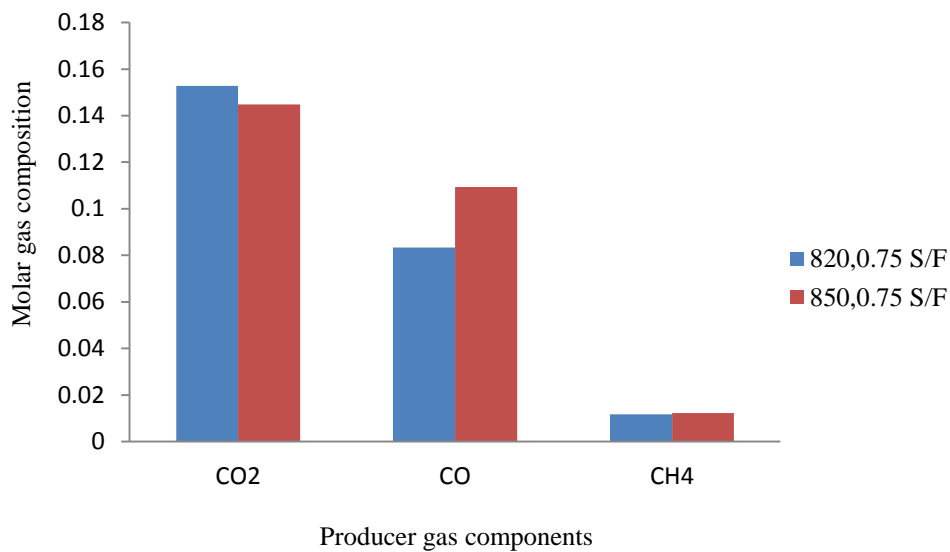
hours reaction time. This happens due to increase the heat inside the gasifier resulting in consumption of the rest of steam and unconverted carbon by reactions 7 and 8 and that explains the trends of hydrogen curves in Figure 5-2 and 5-3. While at 820 °C the molar composition of the produced hydrogen starting to increase and then decreased at reaction time of 3 hours and continue to slightly decrease until the end of experiment, and the molar composition of CH<sub>4</sub> increases with time and that is happening due to consuming of the excess hydrogen in the gasifier by reaction 4 and 8 producing more CH<sub>4</sub>.

Figure 5-4 shows the molar composition of CO<sub>2</sub>, CO, and CH<sub>4</sub> produced when running the gasifier with 1.28 kg/h, 0.5 S/F at 850 °C and 820 °C, respectively.



**Figure 5-4** Effect of bed temperature on the molar compositions of the produced gas component at run of 1.28 kg/h coal feed rate

The same coal feed rate of 1.28 kg/h with increasing the S/F to 0.75 is performed with two different temperatures 850 °C and 820 °C, the molar compositions of CO<sub>2</sub>, CO, and CH<sub>4</sub> produced in this case are shown in Figure 5-5.



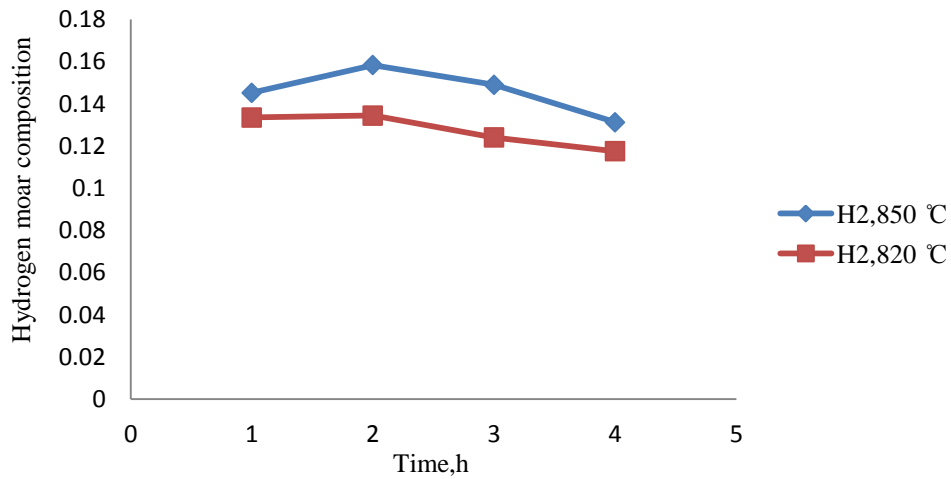
**Figure 5-5** Effect of bed temperature on the molar compositions of the produced gas component at run of 1.28 kg/h coal feed rate

The produced CO<sub>2</sub> is found to decrease with increasing temperature from average molar composition of 0.155138 at 820 °C, 0.5 S/F ratio to 0.13154 at 850 °C, 0.5 S/F ratio and from 0.156027 at 820 °C, 0.75 S/F ratio to 0.144742 at 850 °C, 0.75 S/F ratio, while the produced CO and CH<sub>4</sub> is increasing with temperature. The average molar compositions for CO are 0.090319 and 0.111742 at 820 °C, 0.5 S/F ratio and 850 °C, 0.5 S/F ratio respectively (Figure 5-4). When increasing the S/F ratio to 0.75 the average molar composition of CO increases from 0.08331 to 0.109389 at 820 and 850 °C respectively. CH<sub>4</sub> average molar compositions are increasing from 0.008779 at 820 °C, 0.5 S/F ratio to 0.010384 at 850 °C, 0.5 S/F ratio and at 0.75 S/F ratio the average molar compositions of CH<sub>4</sub> is increased from 0.011679 to 0.01219 at 820 °C and 850 °C respectively (Figure 5-5).

The experimental results reveal that the composition of CO<sub>2</sub> decreases with temperature in case of 1.28 kg/h coal feed rate while the concentrations of CO and CH<sub>4</sub> increase. This occurs because of the increase in heat within the reactor driving the reaction to the right producing more CO. Also, reaction 1 is favoured over reaction 3 so at higher temperatures due to the lower heat of reaction. This will result in an increase in the carbon converted to CO and decrease in the carbon converted to CO<sub>2</sub>. An increase in the hydrogen produced in reaction 5 will increase

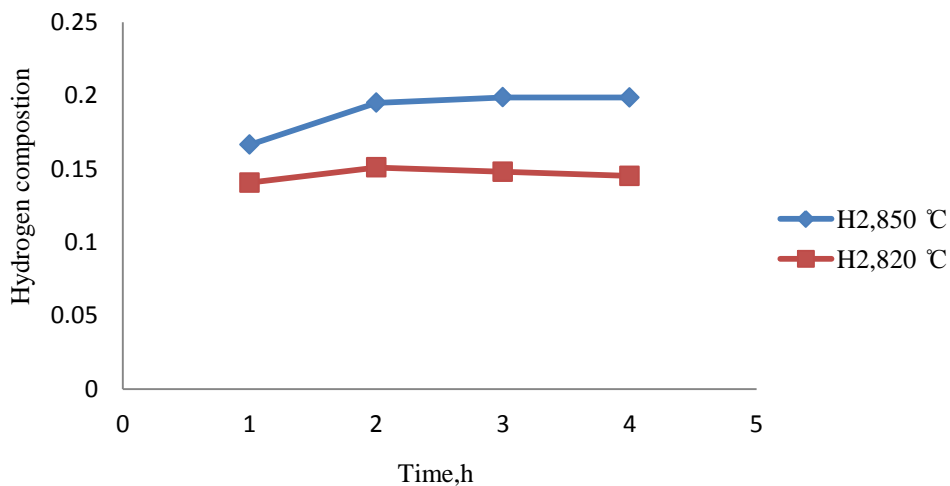
the conversion of carbon to  $\text{CH}_4$  by reaction 4. In addition, the excess CO present in the system will drive reaction 8 to the left producing more  $\text{CH}_4$ . The tendency of  $\text{CO}_2$  decrease and CO and  $\text{CH}_4$  increase with temperature increase has been found by **González et al., (2008)**.

Figure 5-6 shows the variation of produced molar hydrogen composition with time at coal feeding rate of 1.43 kg/h, S/F=0.5, and at 850 °C and 820 °C, respectively. The molar hydrogen compositions in the runs performed with 1.43 kg/h mass rate of coal and 0.5 S/F, at both 820 °C and 850 °C, are 0.1343 and 0.1582 respectively.



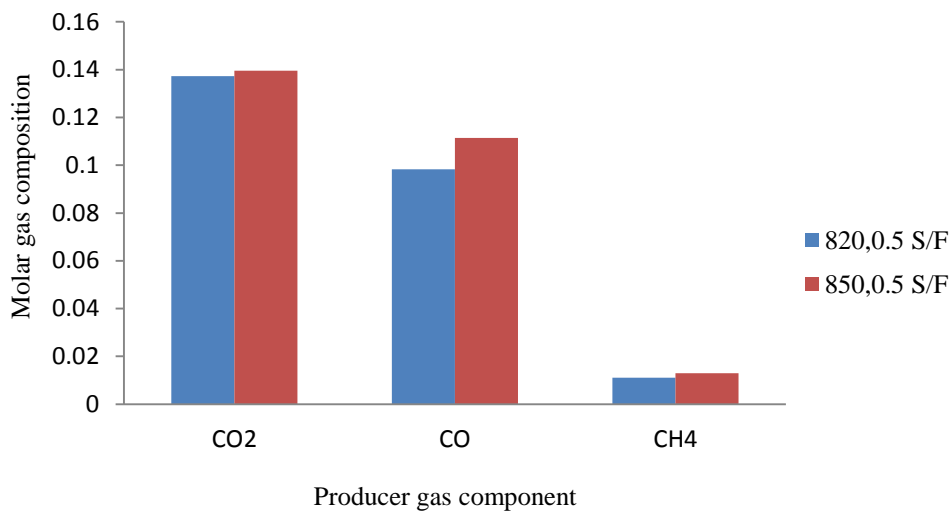
**Figure 5-6** Effect of bed temperature on the molar hydrogen compositions at coal feeding rate of 1.43 kg/h, 0.5 S/F

Figure 5-7 shows the variation of produced molar hydrogen composition with time at coal feeding rate of 1.43 kg/h, S/F=0.75, and at 820 °C and 850 °C, the compositions of hydrogen are 0.15107 and 0.1989 at 820 °C and 850 °C respectively. The molar hydrogen composition increased with increasing temperature at the same ratio of steam to fuel and the same mass of coal used with both runs.



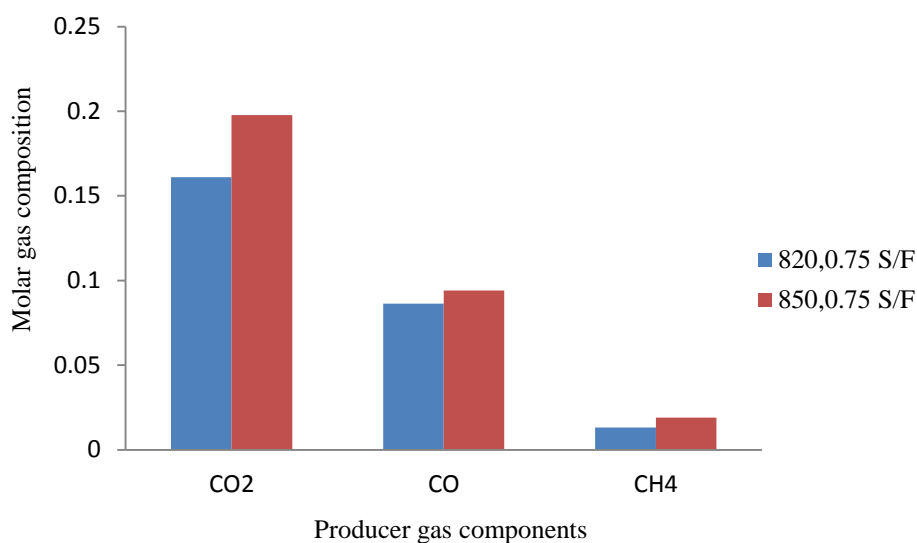
**Figure 5-7** Effect of bed temperature on the molar hydrogen compositions at coal feeding rate of 1.43 kg/h, 0.75 S/F

Figure 5-8 shows the molar composition of CO<sub>2</sub>, CO, and CH<sub>4</sub> produced when running the gasifier with 1.43 kg/h, 0.5 S/F at 850 °C and 820 °C, respectively.



**Figure 5-8** Effect of bed temperature on the molar compositions of the produced gas component at run of 1.43 kg/h coal feed rate

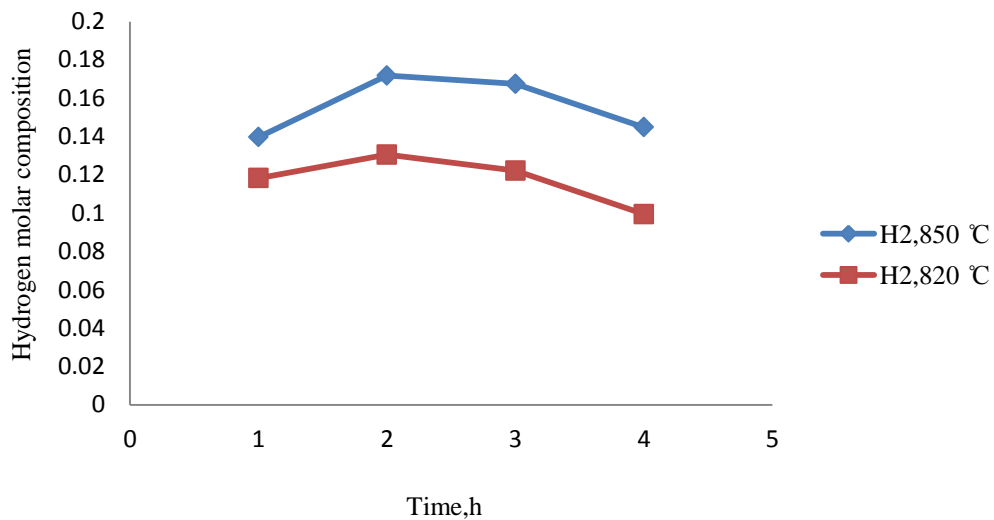
The same coal feed rate of 1.43 kg/h with increasing the S/F to 0.75 is performed with two different temperatures 850 °C and 820 °C. The molar compositions of CO<sub>2</sub>, CO, and CH<sub>4</sub> produced in this case are shown in Figure 5-9. The molar compositions of CO<sub>2</sub>, CO, and CH<sub>4</sub> increasing with temperature increase.



**Figure 5-9** Effect of bed temperature on the molar compositions of the produced gas component at run of 1.43 kg/h coal feed rate

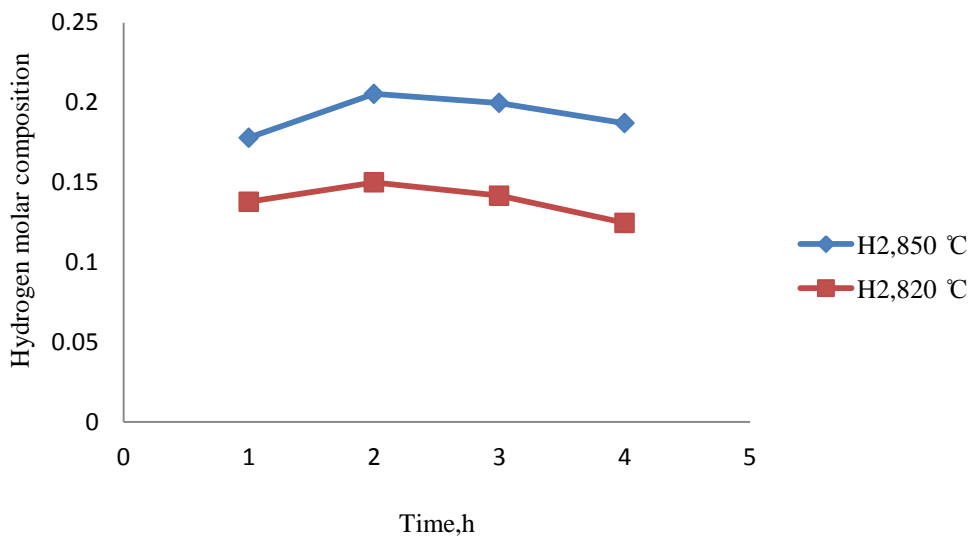
The average molar compositions of CO<sub>2</sub>, CO, and CH<sub>4</sub> increasing with temperature increase. At 0.5 S/F ratio the CO<sub>2</sub> average molar compositions obtained are 0.13729, and 0.139534 at 820 and 850 °C respectively, while at 0.75 S/F ratio the average molar compositions of CO<sub>2</sub> are 0.161112 and 0.19764 at 820 and 850 °C respectively. The average CO molar compositions at 0.5 S/F ratio are 0.098326 at 820 and 0.111467 at 850 °C, and their average compositions obtained at 0.75 S/F ratio are 0.086391 and 0.094026 at 820 and 850 °C respectively. CH<sub>4</sub> average molar compositions are increasing from 0.011086 at 820 °C, 0.5 S/F ratio to 0.012946 at 850 °C, 0.5 S/F ratio and at 0.75 S/F ratio the average molar compositions of CH<sub>4</sub> increased from 0.013067 to 0.019034 at 820 and 850 °C respectively (Figure 5-8 and 5-9).

Figure 5-10 shows the variation of produced molar hydrogen composition with time at coal feeding rate of 1.6 kg/h, S/F=0.5, at 850 °C and 820 °C. From the run completed with a coal mass flow rate of 1.6 kg/h, S/F ratio of 0.5, and temperature of 820 °C, the maximum molar hydrogen composition in the produced gas obtained is 0.1305. At the same mass rate of coal and steam to fuel ratio, but at 850 °C, the composition of maximum hydrogen produced obtained is 0.1718. The molar composition of the produced hydrogen increases with increasing temperature.



**Figure 5-10** Effect of bed temperature on the molar hydrogen compositions at coal feeding rate of 1.6 kg/h, 0.5 S/F

Figure 5-11 shows the variation of produced molar hydrogen composition with time at coal feeding rate of 1.6 kg/h, S/F=0.75, and at 850 °C and 820 °C, respectively, the maximum molar hydrogen compositions in this case are 0.1499 and 0.20539 respectively. It can be noticed that increasing temperature cause an increase in the molar composition of hydrogen produced.



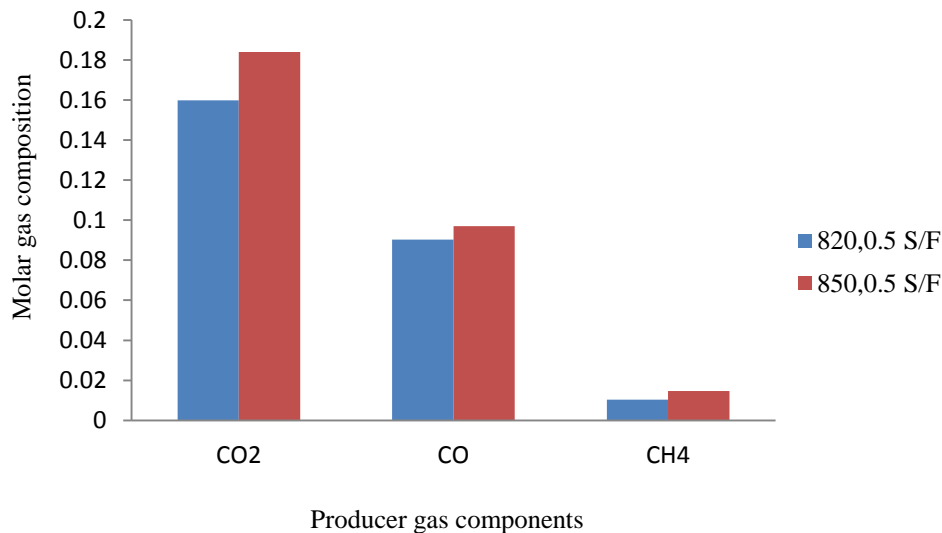
**Figure 5-11** Effect of bed temperature on the molar hydrogen compositions at coal feeding rate of 1.6 kg/h, 0.75 S/F

From the above 12 runs, the average hydrogen molar composition increases with increasing temperature and according to Le Chatelier's principle “**If a chemical system at equilibrium experiences a change in concentration,**

temperature, volume, or partial pressure, then the equilibrium shifts to counteract the imposed change and a new equilibrium is established”, after combustion reactions (1, 2, and 3) have been started the heat inside the gasifier will rise due to the heat from the oxidation reactions. Therefore; the endothermic reactions (6 and 7), and shift reaction (8) to the right direction will increase to consume the produced heat inside the gasifier and that explains the increase in the average molar composition of the produced hydrogen.

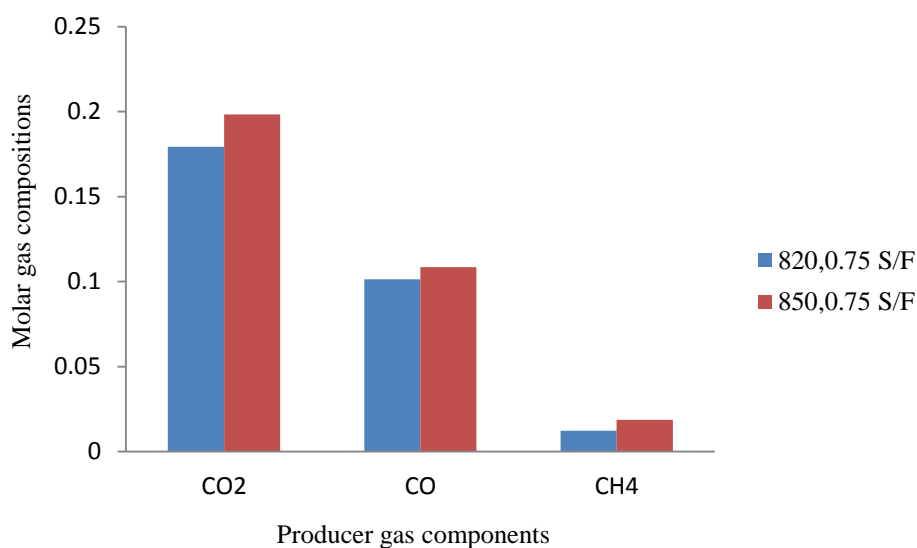
This tendency (higher temperatures produce higher H<sub>2</sub> concentrations) has been found by **Neogi et al., (1986); Xiao et al., (2006); and Gonzáleza et al., (2008)**.

Figure 5-12 shows the molar composition of CO<sub>2</sub>, CO, and CH<sub>4</sub> produced when running the gasifier with 1.6 kg/h, 0.5 S/F at 850 °C and 820 °C.



**Figure 5-12** Effect of bed temperature on the molar compositions of the produced gas component at run of 1.6 kg/h coal feed rate

Figure 5-13 shows the molar composition of CO<sub>2</sub>, CO, and CH<sub>4</sub> produced when running the gasifier with 1.6 kg/h, 0.75 S/F at 850 °C and 820 °C.



**Figure 5-13** Effect of bed temperature on the molar compositions of the produced gas component at run of 1.6 kg/h coal feed rate

The produced CO<sub>2</sub> is found to increase with increasing temperature from average molar composition of 0.159844 at 820 °C, 0.5 S/F ratio to 0.183927 at 850 °C, 0.5 S/F ratio and from 0.179247 at 820 °C, 0.75 S/F ratio to 0.198412 at 850 °C, 0.75 S/F ratio, while the produced CO and CH<sub>4</sub> is increasing with temperature. The average molar compositions for CO are 0.090233 and 0.096971 at 820 °C, 0.5 S/F ratio and 850 °C, 0.5 S/F ratio respectively, and when increasing the S/F ratio to 0.75 the average molar composition of CO increases from 0.101412 to 0.108606 at 820 °C and 850 °C respectively. CH<sub>4</sub> average molar compositions are increasing from 0.010321 at 820 °C, 0.5 S/F ratio to 0.014638 at 850 °C, 0.5 S/F ratio and at 0.75 S/F ratio the average molar compositions of CH<sub>4</sub> increased from 0.012354 to 0.018672 at 820 °C and 850 °C respectively.

When increasing the fuel feed rate from 1.28 kg/h to 1.43 kg/h and then to 1.6 kg/h with the same operating conditions of bed temperature of 820 °C and 850 °C and at S/F ratios of 0.5 and 0.75 the produced CO<sub>2</sub>, CO, H<sub>2</sub>, and CH<sub>4</sub> is increased with increasing temperature. The increase in CO<sub>2</sub> molar composition happens due to burning more coal by reaction 3 which results in more CO<sub>2</sub>, the produced CO<sub>2</sub> will react with the unconverted carbon producing more CO by reaction 6. The composition of hydrogen started to increase with time and its maximum molar

composition is obtained at the second hour then it is slightly decreased at the third and fourth hour so this trend in hydrogen composition is due to hydrogen reaction with the excess unconverted carbon producing more methane and that explains the increase in methane molar compositions.

### 5.2.2 Effect of steam to fuel ratio

Figure 5-14 shows the molar compositions of the produced gas component at the first hour when running with 1.43 kg/h coal feed rate and 0 S/F, at 850 °C. The experimental molar compositions for CO, CO<sub>2</sub>, H<sub>2</sub>, and CH<sub>4</sub> are 0.154, 0.137, 0.0829, and 0.0111 respectively.

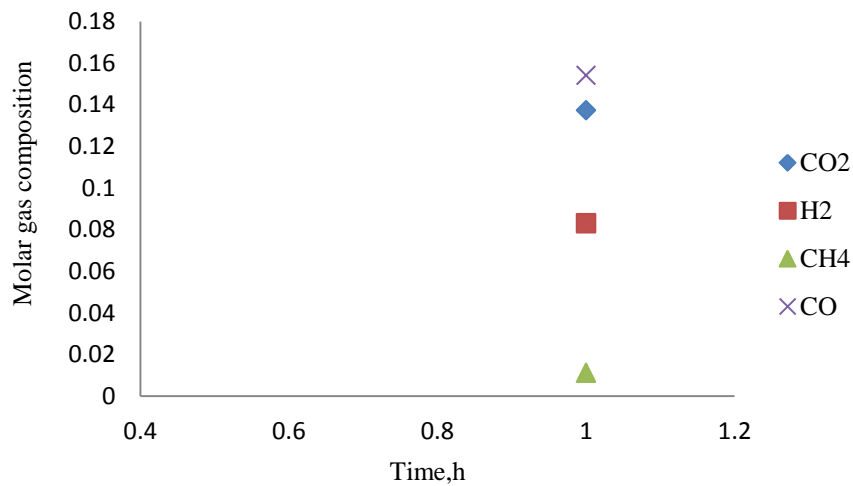


**Figure 5-14** Produced gas component distribution at the first hour of 1.43kg/h coal feed rate and 0 S/F, at 850 °C

Operating with a feed rate of 1.43 kg/h at a bed temperature of 850 °C and no steam result in a rapid increase in bed temperature to 1100 °C after two hours, this might be due to agglomeration of coal. Agglomeration and defluidization are major inhibitors to the use of fluidized-bed technology; agglomeration is generally caused when the bed temperature exceeds a critical temperature, which is sometimes referred to as the “sintering point”. Above the sintering point, bed particles enter a softened or sticky state. This reduces relative movement between particles and results in particle growth. Under worst-case conditions, the bed ceases to fluidize effectively or “defluidizes”. Controlling agglomeration and defluidization is thus

critical for any commercial fluidized-bed process; agglomeration at temperature above 850 °C is similar to the result obtained by **McCullough and Eyk, (2011)**.



**Figure 5-15** Photographic picture of the agglomerate collected after the run

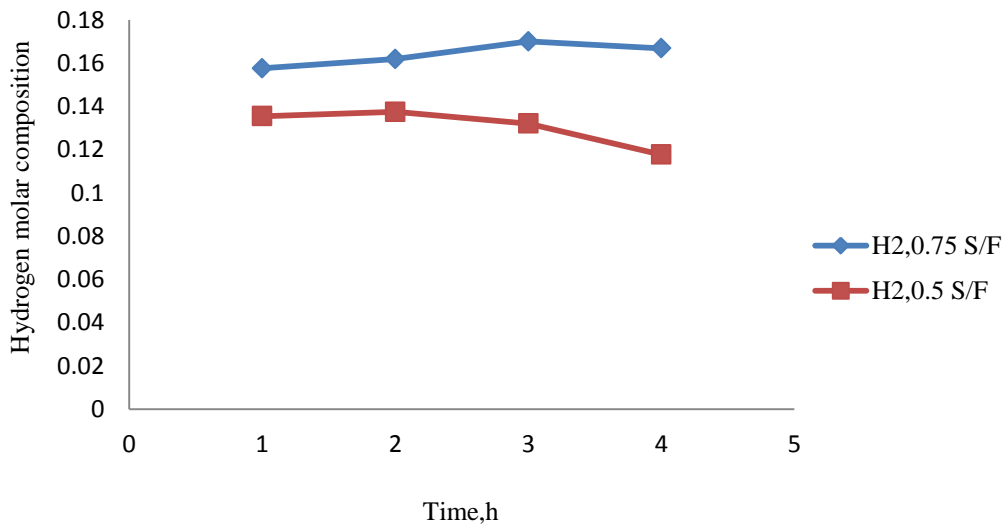
This agglomerate was analysed using Scanning Electron Microscopy (SEM) by Secondary Electron Detector (SE) and Backscattered Electron Detector (BSE) to know the compositions of materials in this agglomerate. Photographic pictures were taken under SE detector and the compositions of the resulted peaks were generated Figure E-1 and E-2.

Backscattered Electron Detector (BSE) was used to get information on the Z contrast of the sample ( $Z =$  atomic number), where regions that contain atoms with high  $Z$  will be viewed as bright regions, and conversely atoms with low  $Z$  as dark regions Figure E-3 and E-4.

Agglomeration during gasification of coal occurs due to defluidization, the bed temperature excess the “high- temperature defluidization limit” which means less value of superficial velocity to avoid defluidization case for a known bed temperature. Defluidization will lead to particle growth and will be in a stationary case in the annulus, while a channel in the spout region will form and the air could pass freely through. “Sintering point” will decrease by increasing the superficial velocity of the gas which increase the movement of the bed particles, or by decreasing the bed temperature.

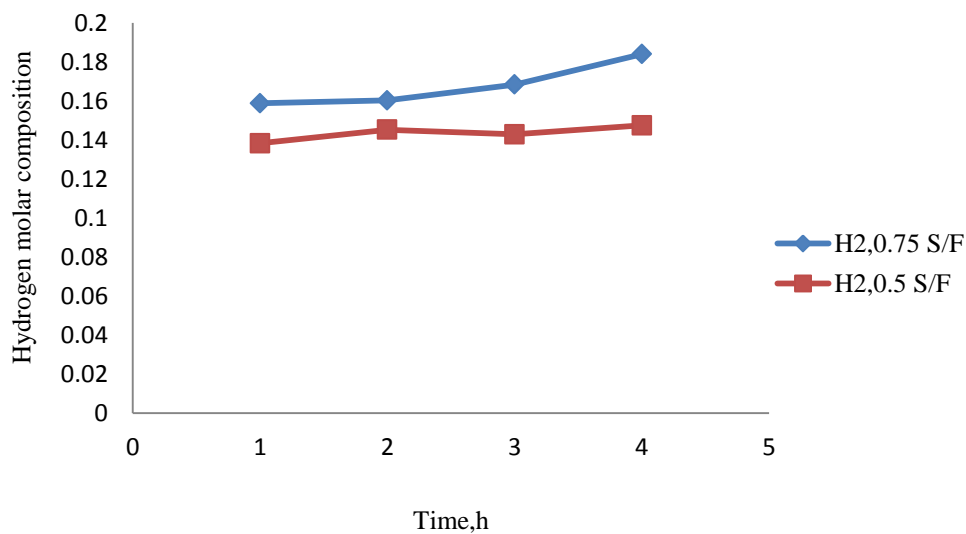
In the present study decreasing bed temperature was suggested by using (air-steam) gas mixture as gasification agent. Injection of steam through the gasifier with (0.5 and 0.75 S/F) will decrease the bed temperature due to the energy consuming for water evaporation.

Figure 5-16 shows the variation of hydrogen molar compositions in the produced gas for the coal mass rate of 1.28 kg/h, 820 °C, at 0.75 and 0.5 S/F. Increasing the S/F ratio causes the molar hydrogen composition to increase.



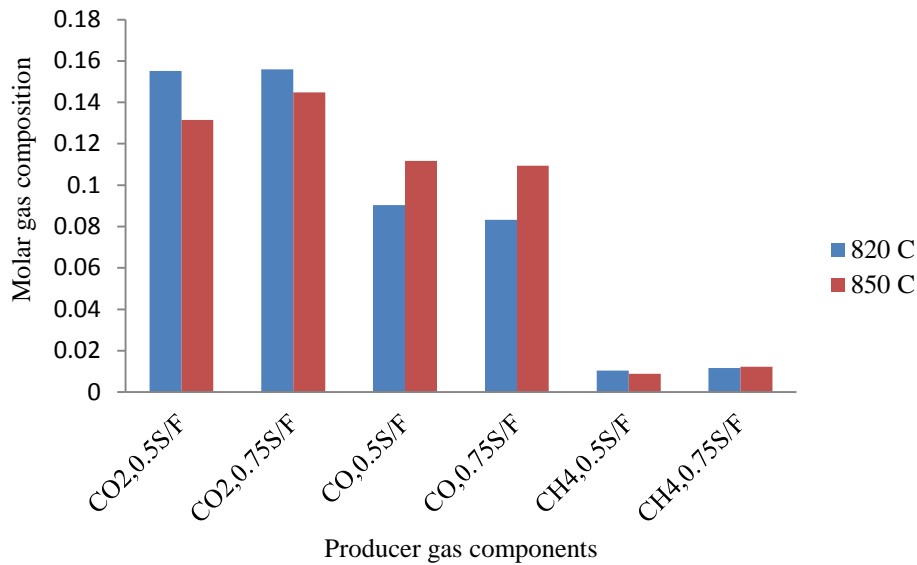
**Figure 5-16** Effect of S/F ratio on the molar hydrogen compositions at coal mass rate of 1.28 kg/h, 820 °C

Figure 5-17 shows the variation of hydrogen molar compositions in the produced gas for the coal mass rate of 1.28 kg/h, 850 °C, at 0.75 and 0.5 S/F respectively. Increasing the S/F ratio causes the molar hydrogen composition to increase.



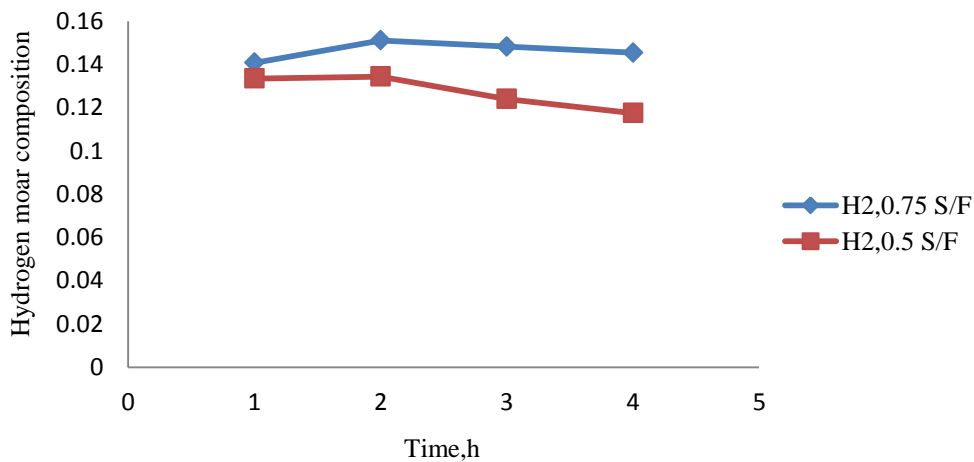
**Figure 5-17** Effect of S/F ratio on the molar hydrogen compositions at coal mass rate of 1.28 kg/h, 850 °C

Figure 5-18 shows the molar composition of CO<sub>2</sub>, CO, and CH<sub>4</sub> in the produced gas when running the gasifier with 1.28kg/h coal feed rate, 820 °C and 850 °C at 0.5 and 0.75 S/F respectively. At the same feed rate and temperature the molar compositions of CO<sub>2</sub> and CH<sub>4</sub> increase with increasing the S/F ratio. When operating the gasifier with coal feed rate of 1.28 kg/h, 820 °C, and S/F of 0.5, the average molar compositions for CO<sub>2</sub>, CO, and CH<sub>4</sub> are 0.155138, 0.090319, and 0.010384 respectively, while increasing the S/F to 0.75 with the same bed temperature and coal feed rate the average molar compositions of CO<sub>2</sub>, CO, and CH<sub>4</sub> are 0.156027, 0.08331, and 0.011679 respectively. Running with 850 C and 0.5 S/F, the average molar compositions of CO<sub>2</sub>, CO, and CH<sub>4</sub> produced are 0.13154, 0.111742, and 0.008779 respectively, increasing the S/F ratio to 0.75 at bed temperature of 850 °C, the average molar compositions of CO<sub>2</sub>, CO, and CH<sub>4</sub> obtained are 0.144742, 0.109389, and 0.01219 respectively.



**Figure 5-18** Effect of S/F ratio on the molar compositions of CO<sub>2</sub>, CO, and CH<sub>4</sub> at coal mass rate of 1.28 kg/h

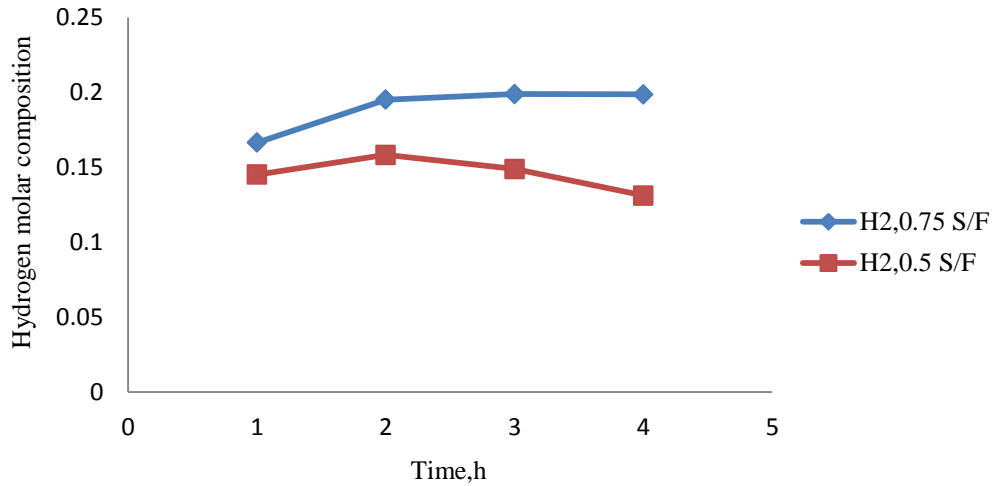
Figure 5-19 shows the hydrogen molar compositions in the produced gas for the coal mass rate of 1.43 kg/h, 820 °C, at 0.75 and 0.5 S/F respectively. The molar composition of hydrogen produced increases with increasing the ratio of steam to fuel.



**Figure 5-19** Effect of S/F ratio on the molar compositions of hydrogen at coal mass rate of 1.43 kg/h and 820 °C.

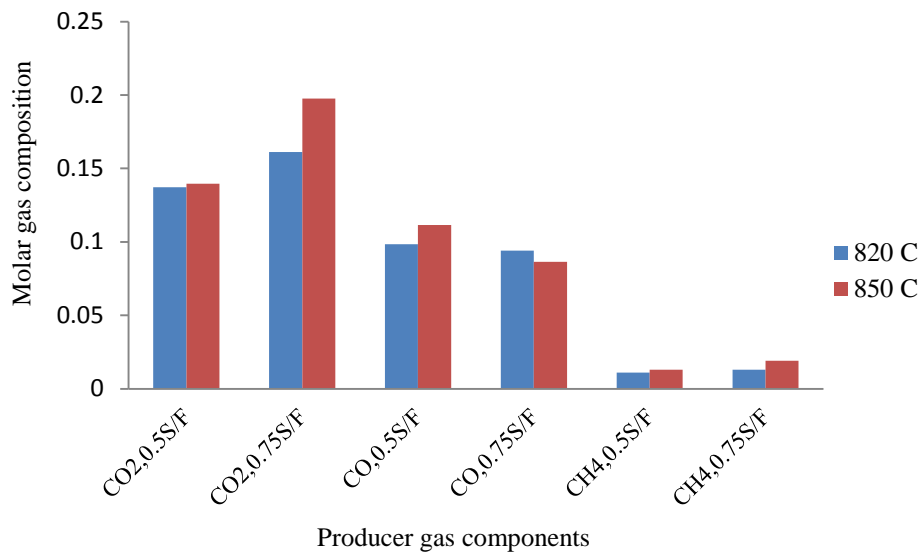
Figure 5-20 shows the molar compositions of hydrogen in the produced gas from the run with coal mass rate of 1.43 kg/h, 850 °C, at 0.75 and 0.5 S/F respectively. The composition of hydrogen in the produced gas was found to increase with increasing steam to fuel ratio from 0.5 to 0.75 at 820 °C and 850 °C.

This is due to increase in the right direction of reactions 5 and 7 and shift in reaction 8 to the right, consuming the excess amount of steam resulting in more hydrogen produced.



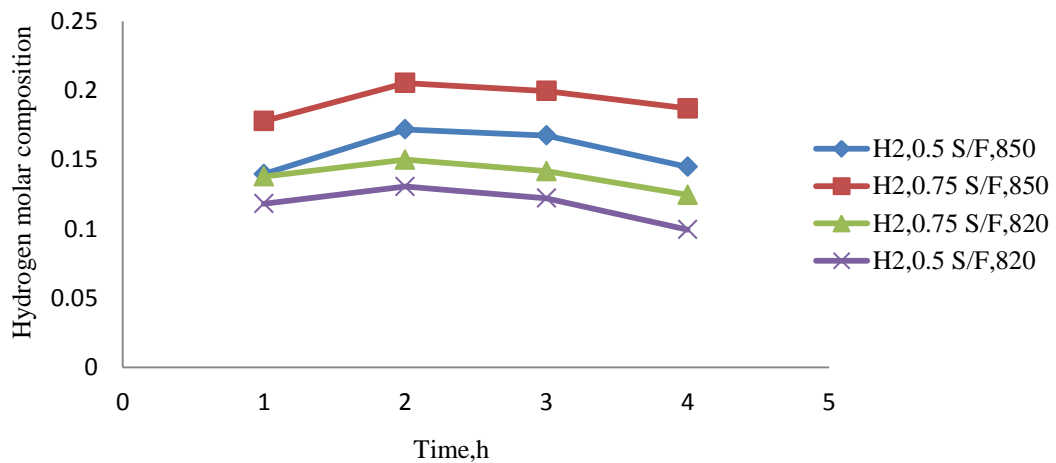
**Figure 5-20** Effect of S/F ratio on the molar compositions of hydrogen at coal mass rate of 1.43 kg/h and 850 °C

Figure 5-21 shows the molar compositions of CO<sub>2</sub>, CO, and CH<sub>4</sub> distribution in the produced gas when running with coal mass rate of 1.43 kg/h at two different ratios of S/F (0.5 and 0.75) and at temperature of 820 °C and 850 °C respectively. Running the gasifier with 1.43 kg/h and 820 °C bed temperature, the average molar compositions of CO<sub>2</sub>, CO, and CH<sub>4</sub> obtained are 0.13729, 0.098326, 0.011086 and 0.161112, 0.094026, 0.013067 at S/F ratios of 0.5 and 0.75 respectively. While at 850 °C bed temperature and with the same coal feed rate the average molar compositions of CO<sub>2</sub>, CO, and CH<sub>4</sub> obtained are 0.139534, 0.111467, 0.012946 and 0.19764, 0.086391, 0.019034 at S/F ratios of 0.5 and 0.75 respectively. The molar compositions of CO<sub>2</sub> and CH<sub>4</sub> increase when increasing the ratio of steam to fuel, while CO molar composition decreases with increasing S/F ratio.



**Figure 5-21** Effect of S/F ratio on the molar compositions of CO<sub>2</sub>, CO, and CH<sub>4</sub> at coal mass rate of 1.43 kg/h

Figure 5-22 shows hydrogen molar compositions distribution in the produced gas for the coal mass rate of 1.6 kg/h, 820 °C and 850 °C at 0.75 and 0.5 S/F respectively.



**Figure 5-22** Effect of S/F ratio on the molar compositions of hydrogen at coal mass rate of 1.6 kg/h

From the runs completed at 820 °C, as the S/F ratio is increased from 0.5 to 0.75, the CO<sub>2</sub> and CH<sub>4</sub> concentrations are also increased. This can be explained by a shift to the right in Reactions 5 and 7 due to excess water. A shift to the right in Reaction 7 should result in an increase in CO concentration, however the excess water present can then react with the CO produced (reaction 5) resulting in an

increase in CO<sub>2</sub> and H<sub>2</sub> production. The extra hydrogen produced can also interact with CO to produce CH<sub>4</sub> (Reaction 8) which explains the increase in CH<sub>4</sub>.

If the temperature is increased to 850 °C and with both 0.5 and 0.75 S/F and according to Le Chatelier's principle, endothermic reactions will increase in activity and exothermic decrease. A higher operating temperature would result in an increased production of CO by Reactions 6 and 7 which are endothermic. The excess H<sub>2</sub> and CO present is enough to force an increase in production of CH<sub>4</sub> by reaction 4 and 8.

Figure 5-23 shows the molar compositions of CO<sub>2</sub>, CO, and CH<sub>4</sub> distribution in the produced gas when running with coal mass rate of 1.6 kg/h at two different ratios of S/F (0.5 and 0.75) and at temperature of 820 °C and 850 °C respectively. Operating with 1.6 kg/h and 820 °C bed temperature, the average molar compositions of CO<sub>2</sub>, CO, and CH<sub>4</sub> obtained are 0.159844, 0.090233, 0.010321 and 0.179247, 0.101412, 0.012354 at S/F ratios of 0.5 and 0.75 respectively. While at 850 °C bed temperature and with the same coal feed rate the average molar compositions of CO<sub>2</sub>, CO, and CH<sub>4</sub> obtained are 0.183927, 0.096971, 0.014638 and 0.198412, 0.108606, 0.018672 at S/F ratios of 0.5 and 0.75 respectively.

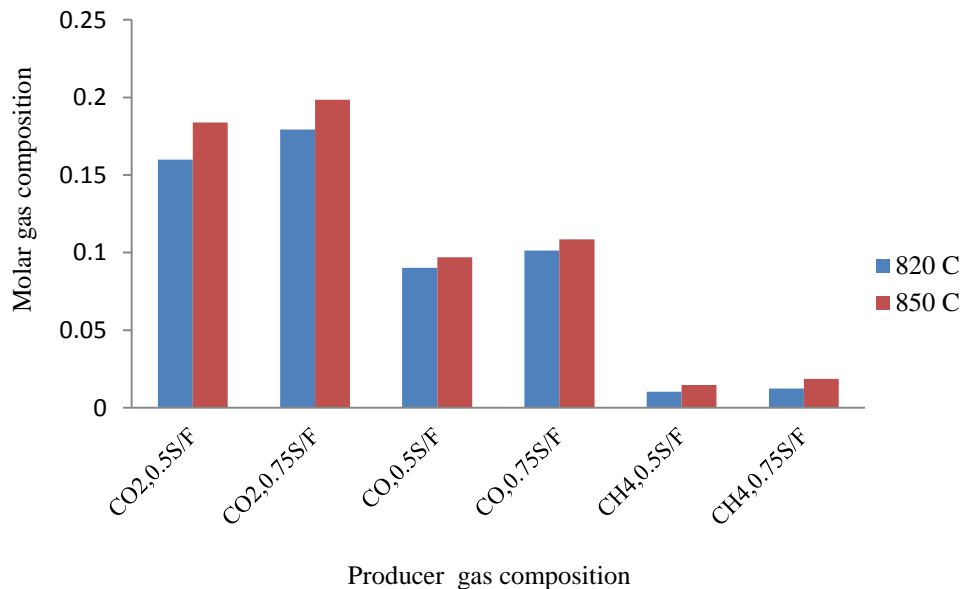
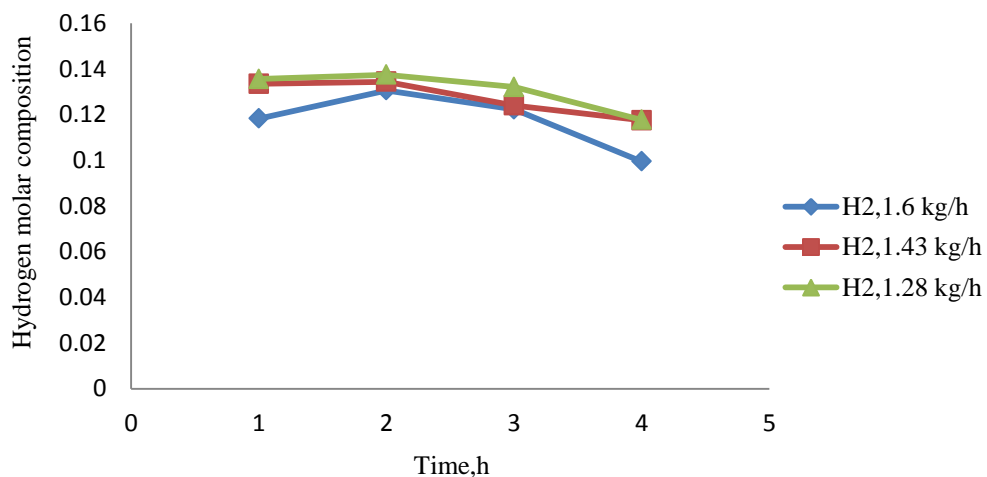


**Figure 5-23** Effect of S/F ratio on the molar compositions of CO<sub>2</sub>, CO, and CH<sub>4</sub> at coal mass rate of 1.6 kg/h

### 5.2.3 Effect of air to fuel ratio

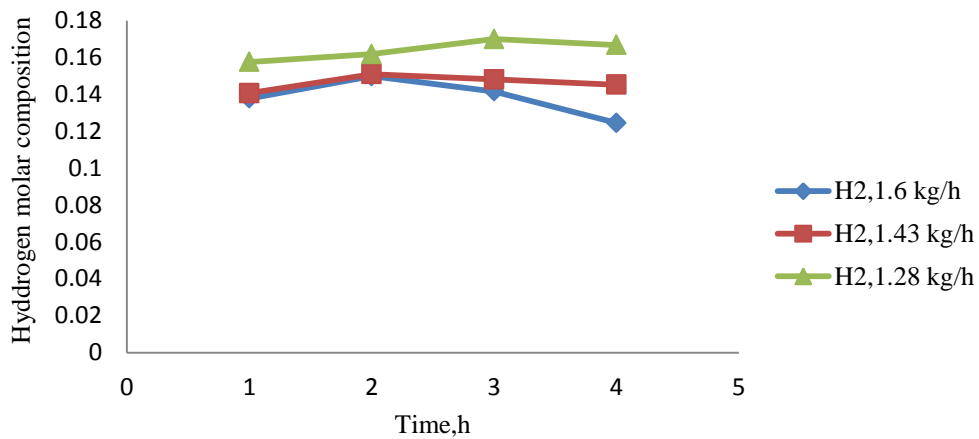
The air to fuel ratio is based on a dry air flow rate and the coal on a dry mass flow basis. Three different air to fuel ratios were compared (1.6, 1.8 and 2) at two different temperatures (820 °C and 850 °C) and two different steam to fuel ratios (0.5 and 0.75). These were achieved by altering the coal mass flow rate with a constant air flow rate of 35 l/min.

Figure 5-24 shows the molar compositions of hydrogen in the produced gas when running the gasifier with coal mass rate of (1.28, 1.43, and 1.6 kg/h) respectively with S/F of 0.5 and temperature of 820 °C. The concentration of hydrogen in the produced gas is increased with increasing air to fuel ratio when running with 820 °C. The average hydrogen compositions were 0.1176, 0.1273, and 0.1307 at 1.6, 1.8, and 2 A/F respectively with a S/F ratio of 0.5.



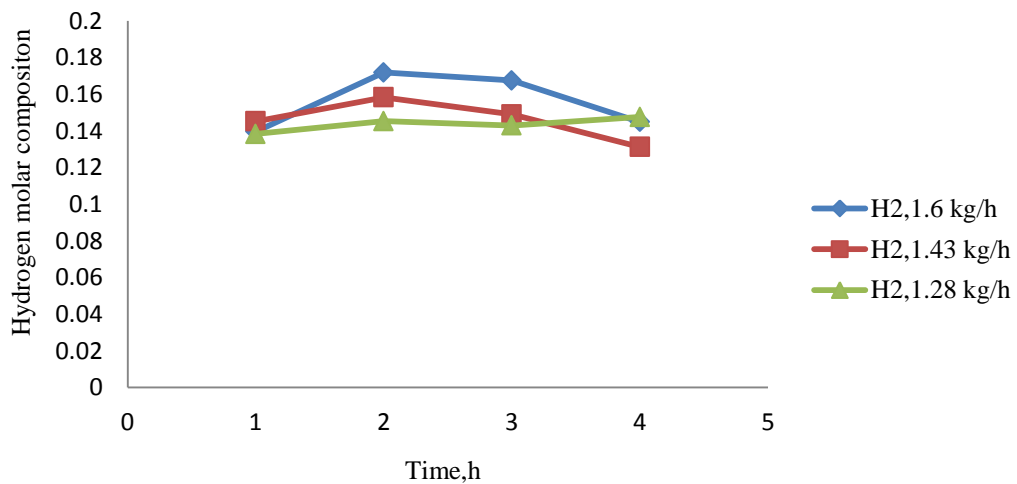
**Figure 5-24** Effect of A/F ratio on the molar compositions of hydrogen at S/F of 0.5 and 820 °C.

Figure 5-25 shows the molar compositions of hydrogen in the produced gas when running with coal mass rate of (1.28, 1.43, and 1.6 kg/h) respectively at S/F of 0.75 and at 820 °C. When running at the same temperature with 0.75 S/F the hydrogen compositions were found to be 0.1385, 0.146, and 0.1641 at A/F ratios of 1.6, 1.8, and 2 respectively. That increase in hydrogen produced at 820 °C is due to increase oxygen (A/F) that will shift reaction 5 and 8 to the right direction and more hydrogen.



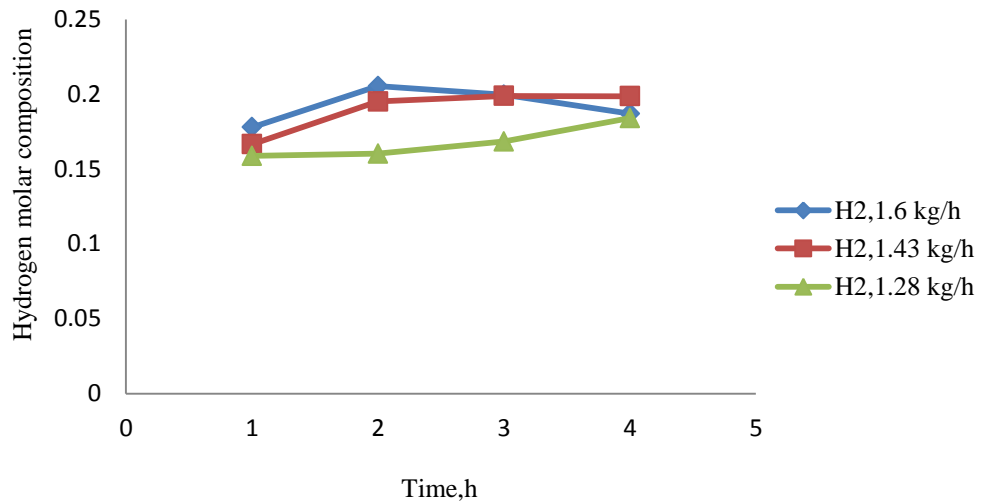
**Figure 5-25** Effect of A/F ratio on the molar compositions of hydrogen at S/F of 0.75 and 820 °C.

Figure 5-26 shows the molar compositions of hydrogen in the produced gas when running the gasifier with S/F of 0.5 and at 850 °C at A/F ratios of 1.6, 1.8, and 2 respectively. The average hydrogen compositions decrease with increasing air to fuel ratio and their values are (0.1559, 0.1459, and 0.143531 at A/F ratios respectively of 1.6, 1.8, and 2).



**Figure 5-26** Effect of A/F ratio on the molar compositions of hydrogen at S/F of 0.5 and 850 °C

Figure 5-27 shows the molar compositions of hydrogen in the produced gas when running the gasifier with S/F of 0.75 and at 850 °C at A/F ratios of 1.6, 1.8, and 2 respectively. At this case the average molar compositions of hydrogen are 0.1924, 0.1898, and 0.167903 at 1.6, 1.8, and 2 respectively.



**Figure 5-27** Effect of A/F ratio on the molar compositions of hydrogen at S/F of 0.75 and 850 °C

Figure 5-28 shows the molar composition of CO<sub>2</sub> produced when running the gasifier with A/F ratios of 1.6, 1.8, and 2 respectively, 0.5, and 0.75 S/F ratios, and at 850 °C and 820 °C, respectively.

At 0.75 S/F and 850 °C bed temperature, the average CO<sub>2</sub> compositions obtained are 0.198412, 0.19764, and 0.144742 at A/F ratios of 1.6, 1.8, and 2 respectively, when the bed temperature decreased to 820 °C and with 0.75 S/F ratio CO<sub>2</sub> average compositions are 0.179247, 0.161112, and 0.156027 at A/F ratios of 1.6, 1.8, and 2 respectively. When running with S/F ratio of 0.5 the average molar compositions of CO<sub>2</sub> at 850 °C are 0.183927, 0.139534, and 0.13154 at A/F ratios of 1.6, 1.8, and 2 respectively, and with the same S/F but with bed temperature of 820 °C the average CO<sub>2</sub> compositions obtained are 0.159844, 0.13729, and 0.155138 at A/F ratios of 1.6, 1.8, and 2 respectively.

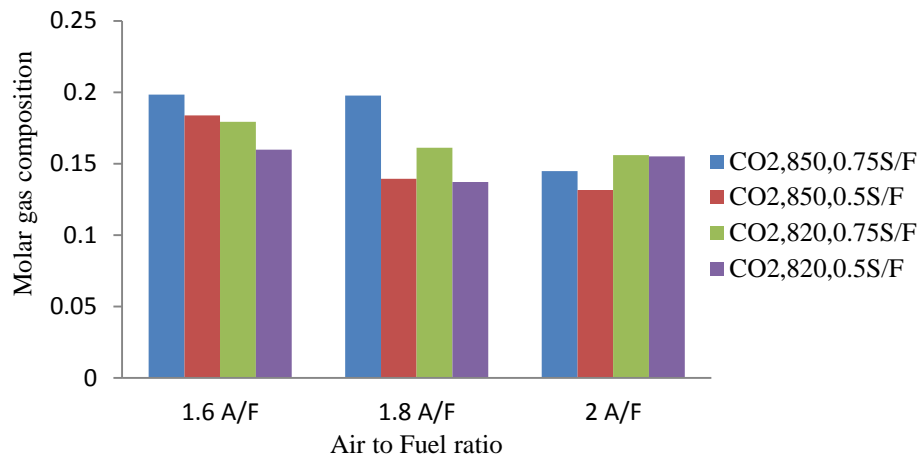


**Figure 5-28** Effect of A/F on the molar composition of CO<sub>2</sub> at S/F ratios of 0.5, and 0.75

The produced carbon dioxide decreases from an air to fuel ratio change of 1.6 to 1.8 in all cases except case (850 °C, 0.75 S/F). An increase in the oxygen available to react with carbon (A/F = 1.6 to A/F = 1.8) results in an increase in the production of CO by reaction 1. Reaction one is more favoured over 3 as it is less exothermic, which results in a shift to the right in reaction 5 increasing the production of CO<sub>2</sub> and H<sub>2</sub>. As the oxygen levels are further increased (A/F = 2), the amount of CO<sub>2</sub> produced by reaction 3 increases and the amount of CO converted to CO<sub>2</sub> by reaction 2 increases. This explains the increase in CO<sub>2</sub> from an A/F ratio of 1.8 to 2 in case (820 °C, 0.5 S/F). With extra steam present in the system, reaction 7 can reduce the amount of carbon available for reaction 3 resulting in reduced production of CO<sub>2</sub> (case, 820 °C, 0.75, A/F = 1.8 to A/F = 2). The amount of CO<sub>2</sub> produced in case three (850 °C, 0.5) can be explained in the same way as case (820 °C, 0.5) with a much higher CO<sub>2</sub> value resulting.

Figure 5-29 shows the molar composition of CO produced when operating with A/F ratios of 1.6, 1.8, and 2 respectively, S/F ratios of 0.5, and 0.75 at 850 °C and 820 °C respectively.

When running with A/F ratios of 1.6, 1.8, and 2 the average molar CO compositions obtained are 0.108606, 0.08639, and 0.1093 respectively at S/F ratio of 0.75 and 850 °C, and with the same A/F ratios and the same temperature and 0.5 S/F the average molar CO compositions obtained are 0.096971, 0.111467, and 0.111742 respectively. In the case of running with 820 °C and at S/F ratio of 0.75

the average compositions of CO are 0.101412, 0.094026, and 0.08331 at A/F ratios of 1.6, 1.8, and 2 respectively, and at 820 °C, 0.5 S/F the average CO compositions are 0.090233, 0.098326, and 0.090319 at A/F ratios of 1.6, 1.8, and 2 respectively.

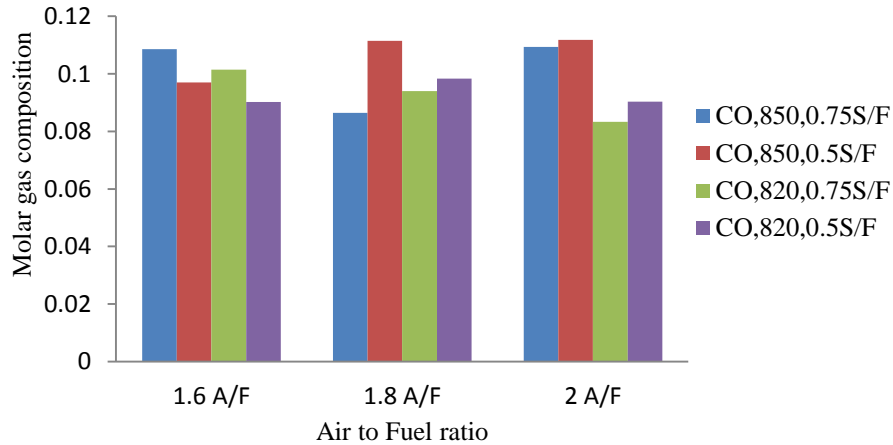


**Figure 5-29** Effect of A/F on the molar composition of CO at S/F ratios of 0.5 and 0.75

Figure 5-30 shows the molar composition of CH<sub>4</sub> produced when operating with A/F ratios of 1.6, 1.8, and 2 respectively, S/F ratios of 0.5, and 0.75 at 850 °C and 820 °C respectively. At 0.75 S/F and 850 °C bed temperature, the average CH<sub>4</sub> compositions obtained are 0.018672, 0.019034, and 0.01219 at A/F ratios of 1.6, 1.8, and 2 respectively, when the bed temperature decreased to 820 °C and with 0.75 S/F ratio the average CH<sub>4</sub> compositions are 0.012354, 0.013067, and 0.011679 at A/F ratios of 1.6, 1.8, and 2 respectively. When running with S/F ratio of 0.5 the average molar compositions of CH<sub>4</sub> at 850 °C are 0.014638, 0.012946, and 0.008779 at A/F ratios of 1.6, 1.8, and 2 respectively, and with the same S/F but with bed temperature of 820 °C the average CH<sub>4</sub> compositions obtained are 0.010321, 0.011086, and 0.010384 at A/F ratios of 1.6, 1.8, and 2 respectively.

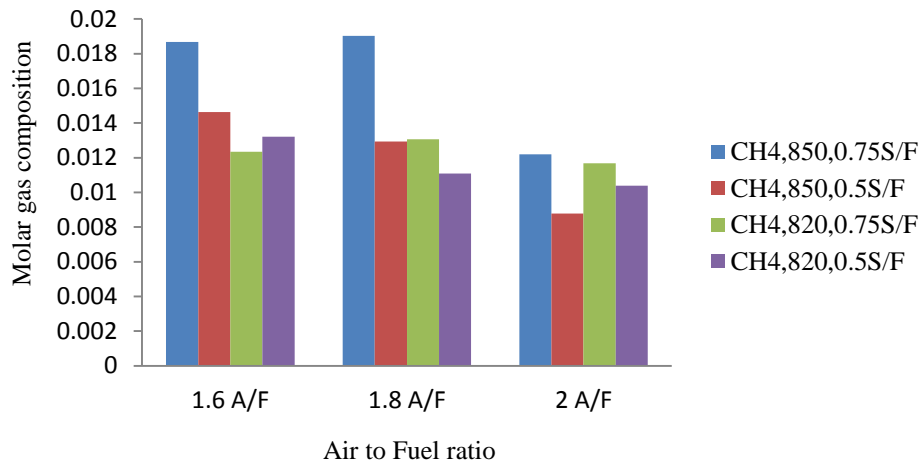


**Figure 5-30** Effect of A/F on the molar composition of CH<sub>4</sub> at S/F ratios of 0.5 and 0.75

At increased temperatures (850 °C) the opposite trend occurs. The less exothermic reactions are more favoured which results in more CO produced (Reaction 1) as the oxygen concentration increases, this reduces the amount of hydrogen produced by Reaction 7 and as the availability of oxygen is further increased the carbon dioxide produced by reaction 3 increases which will shift reaction 5 to the left further decreasing hydrogen concentrations and increasing carbon monoxide. The methane levels are dependent mainly on hydrogen levels in the reactor (reactions 4 and 8).

### 5.2.4 Carbon conversion

The carbon conversion, defined as the degree to which the carbon in the fuel has been converted into gaseous products, is an important parameter in deciding the performance of a gasifier (**Abdul Salam, 2006**). Carbon conversion calculations were completed based on the assumption that all nitrogen feed into the gasifier left in the gasifier in the producer gas. Using the assumptions of an atmospheric nitrogen concentration of 78% (molar percent), atmospheric pressure (101325 pa) and a temperature at the flow rate meter of 293.15 °C and a slightly altered version of the ideal gas law, equation (5.1), the flow rate of Nitrogen through the gasifier, and the total flow rate of the producer gas can be calculated from equation (5.2).

$$\dot{n}(N_2) = \frac{x(N_2)PV}{RT} \quad (5.1)$$

$$\dot{n}(total) = \frac{\dot{n}(N_2)}{C(N_{2,out})} \quad (5.2)$$

$\dot{n}(N_2)$  is the flow rate of Nitrogen into the gasifier,  $x(N_2)$  is the atmospheric molar concentration of  $N_2$  and  $C(N_{2, out})$  is the concentration of Nitrogen measured in the producer gas using the gas chromatogram.

The molar flow rates of carbon containing products in the producer gas can then be calculated and with the flow rate of carbon into the gasifier known an overall molar balance on carbon can be completed to find the carbon conversion, equation (5.3):

$$Carbon\ conversion = \frac{\dot{n}_{reacted}}{\dot{n}_{in}} \quad (5.3)$$

Where  $\dot{n}_{reacted}$  is total molar flow rate of converted carbon in the producer gas and  $\dot{n}_{in}$  is the molar flow rate of carbon fed to the gasifier,  $\dot{n}_{in}$  was calculated on a dry mass flow rate basis using the compositional information found in Table 4-1.

$$\dot{n}_{reacted} = \dot{n}(total) * [\sum x_i a_i] * M_{wt.}(C) = \dot{n}(gas), \left(\frac{g\ of\ carbon}{hr}\right) \quad (5.4)$$

$$\dot{n}(gas)_{in} = C\% \ in\ the\ fuel * fuel\ mass\ rate \quad (5.5)$$

C% in the fuel comes from ultimate analysis for the dry ash free.

Table A-14 shows the coal gasification experiments operating conditions and the % carbon conversion for each experiment. Figure 5-31 shows the values of % carbon conversion for coal gasification experiments.

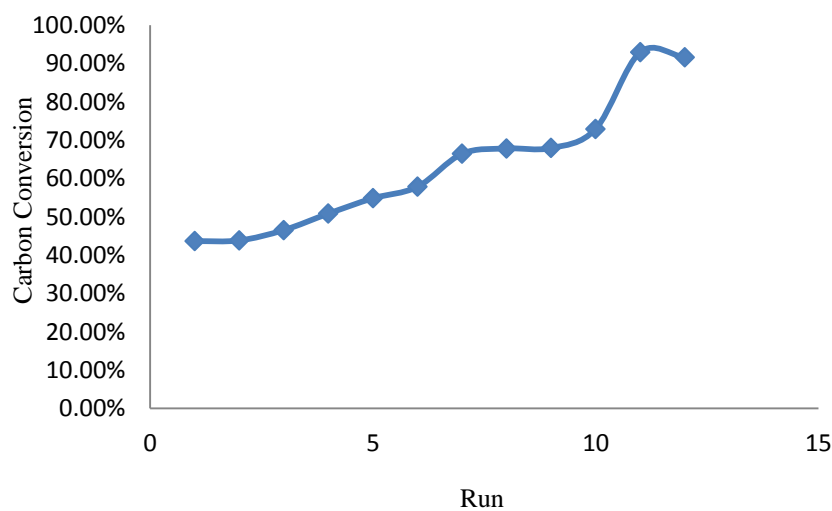


**Figure 5-31** Carbon conversion values for coal gasification experiments

The maximum value of carbon conversion and maximum H<sub>2</sub>:CO ratio are 92.9% and 2.197 respectively which are obtained at 1.8 A/F ratio, 0.75 S/F ratio, and at 850 °C bed temperature this indicates that these operating conditions are the optimum conditions for coal gasification.

### **5.3 Algae gasification**

Gasification experiments were conducted using algal biomass as a fuel source. Producer gas compositions were analysed to investigate the mechanism of gasification reactions present with an alternative source of carbon and how it differs to that of the mechanisms present in coal gasification. The first problem encountered with using the algae biomass was in the particle shape and size. The biomass particles were found to have a lower sphericity than the coal which affected the flow from the hoppers to the screw feeder. This generated an issue with feeding halting after approximately half an hour. To avoid this, the particle size diameter was reduced from between 1 and 3.35 mm to between 1 and 2 mm. The second major problem faced was with agglomeration of the bed during start up.

Experiments were conducted with a fuel mass rate of 1.43 kg/h, steam to fuel ratio of 0.5 at a temperature of 850 °C. The fuel was fed into the gasifier after bed temperature reached 450 °C. With coal this results in a temperature step increase in the reactor to approximately 840 °C however when this was done with the algae it was found the temperature reached a value of between 600 °C and 620 °C and stabilised. Agglomeration happened after feeding the fuel. As the bed material recovered was stuck together in clumps. Samples of raw algae and agglomerates from the gasification runs were analysed using SEM (Figures E-5, E-6, E-7, E-8, and E-9).

SEM images shown in Appendix E.2 show an excess amount of sodium, aluminium and magnesium chlorides and silica oxide. These could be from the water used to grow algae (sea water) which is high in salt content. The salt is likely to have crystallised during the drying process, which is what can be seen in Fig. E-8 and E-8a Silica oxide which is used as a heat carrier medium in the gasification

agglomerated in this case and formed clumps with the algae. Agglomeration may be due to the excess salt present in the algae. High levels of aluminium and magnesium also had been found which could have something to do with the chemistry occurring in the reactor.

A sample for the bed material from the run of agglomerated algae was analysed by SEM secondary electron detector to analyse the structure of this material (Figure E-9 a, b, c, and d).

From Figure E-9 an excess amount of sodium, aluminium and magnesium chlorides and silica oxide can be seen in the bed material resulting from algae gasification. Looking at the chemistry of Al and Cl there is a possibility that the sodium chloride is interacting with water to form  $\text{Cl}_2$ ,  $\text{H}_2$  and  $\text{NaOH}$ . The  $\text{Cl}_2$  produced is then free to react with Al to produce  $\text{AlCl}_3$  which forms a liquid at temperatures above  $192.4\text{ }^\circ\text{C}$ . It is also interesting to see that the reaction required for the formation of  $\text{AlCl}_3$  is favoured around  $650\text{-}750\text{ }^\circ\text{C}$  which is close to the temperature the gasifier reaches before agglomeration occurs.

In industry, elemental chlorine is usually produced by the electrolysis of sodium chloride dissolved in water. Along with chlorine, this chloralkali process yields hydrogen gas and sodium hydroxide, according to the following chemical equation (**Galatsis, 1999**).



Aluminium chloride is manufactured on a large scale by the exothermic reaction of aluminium metal with chlorine or hydrogen chloride at temperatures between  $650$  to  $750\text{ }^\circ\text{C}$  (**Greenwood and Earnshaw, 1984**).



Aluminium chloride is hygroscopic, having a very high affinity for water. It fumes in moist air and hisses when mixed with liquid water as the  $\text{Cl}^-$  ions are displaced with  $\text{H}_2\text{O}$  molecules in the lattice to form the hexahydrate  $\text{AlCl}_3 \cdot 6\text{H}_2\text{O}$  (white to yellowish in colour). The anhydrous phase cannot be regained on heating as  $\text{HCl}$  is lost leaving aluminum hydroxide or alumina (aluminum oxide):



On strong heating (~400 °C), the aluminum oxide is formed from the aluminum hydroxide by:



To ensure efficient gasification for the algae, leaching of raw algae is considered to dissolve the salt contained by this algae. Raw algae was examined by SEM secondary- electron detector to investigate the structural nature of the material before and after leaching. It was noticed that sodium chloride content in algae is decreased due to leaching Figures E-10 and E-11.

From Figure E-11, it can be shown that leaching of raw algae causes the salt content in raw algae to dissolve and that may prevent agglomeration problem from happening in the gasification experiments when using leached algae.

### **5.3.1 Co-gasification (Coal-Algae, gasification)**

Co-gasification was completed using 90% coal and 10% algae to study the mechanism of gasification reactions present for this fuel composition, and to investigate whether or not agglomeration would occur with a lower flow of biomass into the gasifier. The gasifier was operated with air and steam to fuel ratios of 2 and 0.5 respectively at a temperature of 820 °C. After beginning fuel feeding the temperature increases rapidly to 820 °C, gas samples were withdrawn at different periods (30, 45, 60, 75, and 90 minutes) . The bed temperature continued to rise steadily until the gasifier had to be shut down to prevent agglomeration.

Figure 5-32 shows the molar compositions of H<sub>2</sub>, CO<sub>2</sub>, CO, and CH<sub>4</sub> result from co-gasification experiment with 10% algae + 90% coal, with S/F and A/F ratios of 0.5 and 2 respectively and at 820 °C. The bed temperature fluctuating at different values starting from 830, 840, 850, 860, 870, and 880 °C, the increase in temperature is happening each 15 min, which means there is a problem within the bed inside the gasifier. The composition of hydrogen in the producer gas was noticed to decrease with time and with temperature increase and that trend is wrong,

according to gasification reactions and while the temperature increase the molar composition of hydrogen in the produced gas should increase.

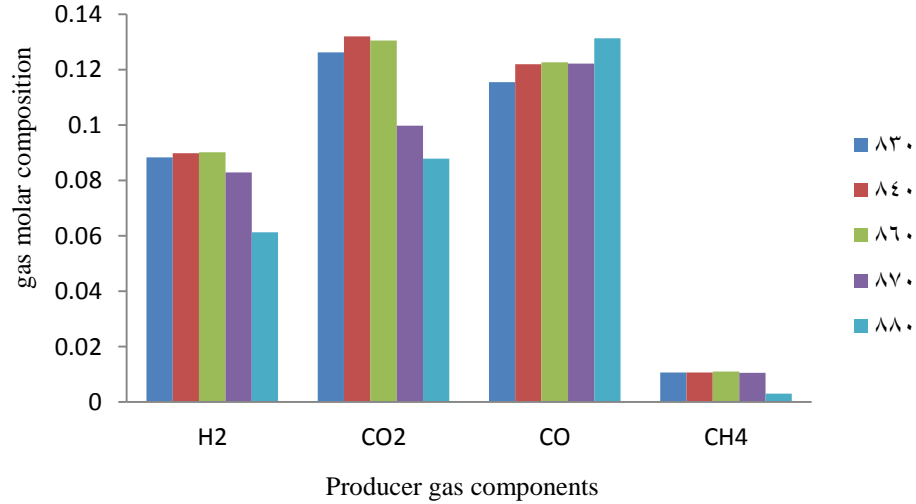


**Figure 5-32** Producer gas molar compositions from (algae-coal) gasification

Agglomeration doesn't occur however high levels of pressure and bed temperature were reached after 90 minutes. This might have resulted from decreased bed fluidisation, or it could have been due to interaction of potassium carbonate with minerals present in the coal at higher loadings. After the gasifier was cooled down, the bed material was recovered and there were no agglomerates found. The tubes for passing the producer gas were disconnected and found to be blocked with grey/black ash.



**Figure 5-33** Blockages in the outer tubes of the gasifier

A sample of the gray material blocking the pipes was taken and the salt content was tested. The salt level in the blockage was the same in the raw algae

which means that blockage lead to raw algae. The raw algae may be crushed in the screw feeder because it is soft and entered the gasifier as fine particles and smaller diameter than coal particles, and affecting by the air flow coming from the bottom of the gasifier and because the place of passing the producer gas nearer to the place of screw feeder more than the bed. The fine particles will pass easily through the outer tubes with the producer gas and gathered in these tubes with time and that will cause the inside gasifier temperature to increase with time because the producer gas will have a difficulty to pass through the out tubes and high pressure will results inside the gasifier. After 90 minutes the temperature reached to 950 °C and hydrogen composition in the producer gas was decreased with time.

#### **5.4 Co-gasification (coal-grape seeds gasification)**

First experiment was conducted with air to fuel and steam to fuel ratios of 2 and 0.5 respectively, 5 % grape seeds biomass at 820 °C. The fuel started to feed through the gasifier and the bed temperature started to increase gently, the samples were taken every 30 minutes after steady state. The hydrogen in the producer gas was increased at 30 to 60 minutes and the bed temperature was controlled. After the first hour the bed temperature started to increase rapidly with time and reached to 950 °C and the last gas sample was taken after 75 minutes and then the gasifier was shut down to prevent agglomeration. The bed material was removed after the gasifier had been cooled down, some sand particles were agglomerated. All the outer tubes were checked if any blockages might be happened and all of them were clean and empty. Therefore, the problem lead to the compositions of biomass because the coal was tested before with the same operating conditions of this experiment and succeeded. The air to fuel ratio of 1.8 was tested with 0.5 steam to fuel ratio at 820 °C, and 5% grape seeds, the temperature was increased further and faster than the previous case and 20 minutes after steady state the bed temperature increased to 990 °C and was shut down without taking gas sample.

Figure 5-34 shows the molar compositions of H<sub>2</sub>, CO<sub>2</sub>, CO, and CH<sub>4</sub> result from coal-grape seeds gasification with air to fuel and steam to fuel ratios of 2 and 0.5 respectively, 5 % grape seeds biomass at 820 °C.

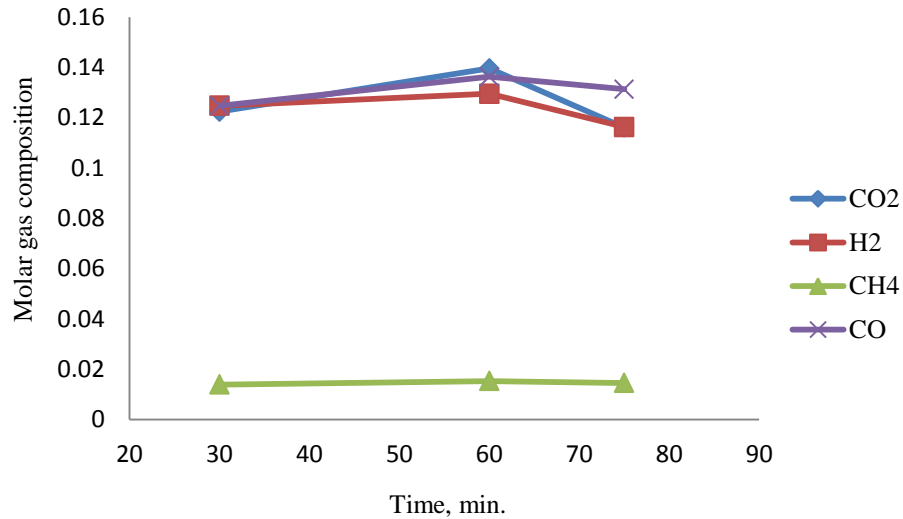


**Figure 5-34** Molar compositions of producer gas component result from Co-gasification.

It is concluded that the bed temperature increased rapidly with increasing the mass of fuel feeding to the gasifier or in other word with increasing the mass of biomass feeding to the gasifier. Looking at the chemical analysis of the biomass, (Table C-3) it noticed to contain much amount of potassium oxide which can be responsible for increasing the bed temperature. After the fuel was fed gasification reactions will start and the producer gas contains CO<sub>2</sub> which can react with potassium oxide in the grape seeds forming potassium carbonate K<sub>2</sub>CO<sub>3</sub> by the following reaction:



Potassium carbonate (K<sub>2</sub>CO<sub>3</sub>), formed in the char, can be reacting with silicon from the bed material leading to the formation of molten potassium silicates. A possible reaction to describe this process is:



The sodium analog of reaction (15) has been documented to form a liquid sodium silicate melt (Eyk, et al., 2009). So that the formation of molten potassium

and sodium silicate can be accumulated with time and form a layer on the top of the bed which prevent the gas to pass easily and also will lead to decrease or stop the gasification reactions to continue, and that will increase the temperature of the bed because defluidization will happen. To avoid this problem increasing the ratio of air to fuel was suggested to prevent or reduce the formation of the molten components in the bed.

Three ratios of air to fuel (2.1, 2.3, and 2.5) were performed in co-gasification with three steam to fuel ratios (0.25, 0.5, and 0.75) at different temperatures (800, 820, and 850 °C) with three different biomass to coal ratios (0.05, 0.11, and 0.25), set of the completed experiments are shown in Table 4-3. These experiments are done depending on Taguchi method of experiments design.

#### **5.4.1 Determination of Percentage Contribution of Individual Variables**

The carbon conversion producing biogas in a gasifier by nine set of gasification experiments (Table 4-3). From the experimental results carbon conversion has been calculated for each experiment and maximum value of carbon conversion is obtained at experiment number 8 which has a carbon conversion of 95.59345% which mean to have the best experimental conditions while the lowest conversion has been obtained at experiment number 5 and it is equal to 63.6665%. Taguchi method has been applied for the design of an experiment to study the best experimental conditions.

In Taguchi method, the signal-to-noise (S/N) ratio is used to measure the quality characteristics deviating from the desired value. The S/N ratios are different in terms of their characteristics, of which there are generally three types, i.e. smaller-the-better, larger-the-better and normal-the-better. According to the analysis for the case of ‘larger-the-better’, the mean squared deviations (MSD) of each experiment were evaluated using the following equation:

$$MSD = \frac{1}{n} \sum_{i=1}^n \left[ \frac{1}{y_i} \right]^2 \quad (5.6)$$

Where  $n$  is the number of repetitions of each experiment and  $y_i$  carbon conversion. Then, the S/N ratio was evaluated using the following equation (Taguchi, 1986):

$$\frac{S}{N} \text{ ratio} = -10 \log(MSD) \quad (5.7)$$

The S/N ratios for the nine sets of experiments are shown in Table 5-2. The mean carbon conversion and the mean S/N ratio are 82.72613% and 38.28649%, respectively. Experiment number 8 gave the highest conversion and had the largest S/N ratio.

**Table 5-2** % Carbon conversion, MSD, and S/N ratios for the nine set of gasification experiments

Experiment No.	% Carbon conversion	MSD	S/N
1	73.68429813	0.000184183	37.34749902
2	82.95197591	0.000145327	38.37653471
3	95.21793407	0.000110297	39.57437509
4	81.52657251	0.000150453	38.22598369
5	63.6665338	0.000246705	36.07822412
6	90.51054095	0.000122068	39.13398321
7	86.15732146	0.000134715	38.70584378
8	95.59345163	0.000109432	39.60856286
9	75.22657517	0.000176708	37.5274258
	Mean carbon conversion% = 82.72613374		Mean S/N ratio = 38.28649248

The mean S/N ratio was calculated from the effect of the variables and the interactions at assigned levels this means the average of all the S/N ratios of a set of control variables at a given level. For example, in the case of variable A and level 1, the mean S/N ratio (38.4328029) was calculated using the values (37.34749902, 38.37653471 and 39.57437509) from experiment numbers 1 to 3. In the case of parameter A and level 2, the mean S/N ratio (37.8127303) was calculated using the values (38.22598369, 36.07822412 and 39.13398321) from experiment numbers 4

to 6, and so on. The calculated values of the mean S/N ratios and the difference between two levels can be shown in Table 5-3 and 5-4 respectively.

**Table 5-3** Mean S/N ratios

Variables	Levels		
	1	2	3
<b>A</b> S/F ratio	38.4328029	37.8127303	38.61394415
<b>B</b> A/F ratio	38.0931088	38.0211072	38.74526137
<b>C</b> B/C ratio	38.6966817	38.04331473	38.119481
<b>D</b> Temperature, °C	36.984383	38.7387872	39.13630721

**Table 5-4** Difference between two levels

Parameters	Difference		
	$L_{2-1}$	$L_{3-1}$	$L_{3-2}$
<b>A</b> S/F ratio	-0.620072598	0.1811412	0.801213807
<b>B</b> A/F ratio	-0.072001596	0.6521525	0.724154136
<b>C</b> B/C ratio	-0.653366965	-0.5772007	0.076166263
<b>D</b> Temperature, °C	1.754404248	2.1519242	0.397519982

The contribution for each variable calculated from the maximum difference of mean S/N ratios between two levels for each variable Table 5-5.

**Table 5-5** % Contribution for each variable

Parameters	Max. difference	Contribution (%)
<b>A</b> S/F ratio	0.801213807	21.34601516
<b>B</b> A/F ratio	0.724154136	19.29298402
<b>C</b> B/C ratio	0.076166263	2.029228891
<b>D</b> Temperature, C	2.15192423	57.33177193
Total	3.753458435	100

The order of influence of the parameters in terms of the conversions is:

**D** Temperature, °C > **A** S/F ratio > **B** A/F ratio > **C** B/C ratio. Figure 5-35 shows the percentage contribution of individual variables on variation in carbon conversion.

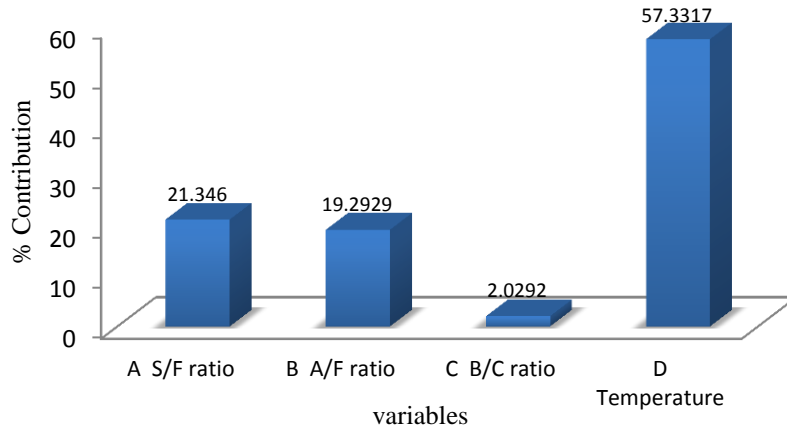
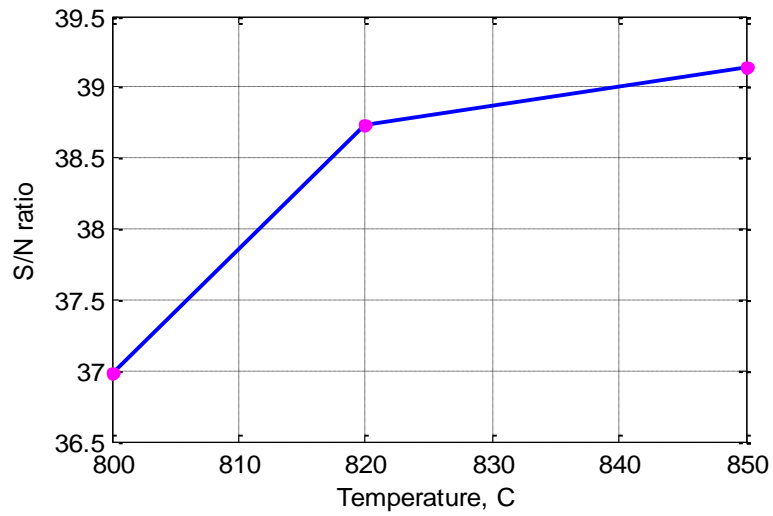


**Figure 5-35** Percentage contribution of individual variables on variation carbon conversion.

### 5.4.2 Determination of Best Experimental Condition by the Taguchi Method

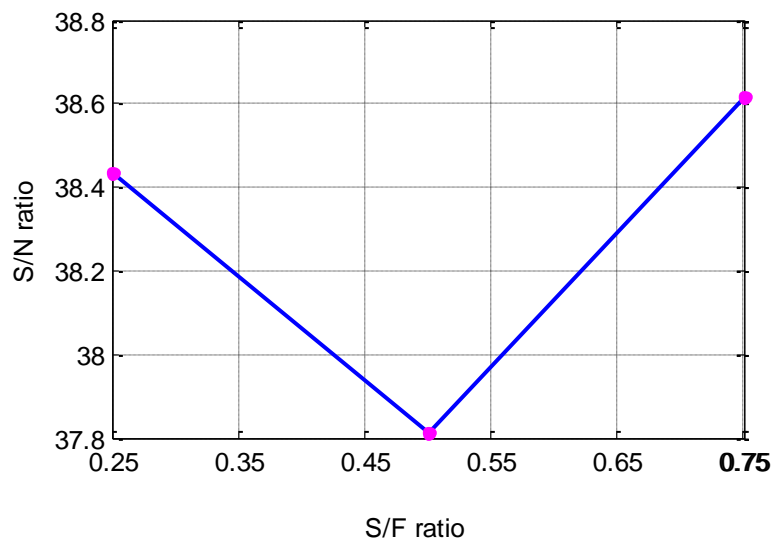
The effect of each control variable on the carbon conversion is indicated by the greater mean S/N ratio, the larger mean S/N ratio means the greater effect of the control variable. The bed temperature is the most influential variable on the carbon conversion.

A larger mean S/N ratio indicates a greater effect of the control variable at that level on the carbon conversion. The bed temperature is the most influential variable on the carbon conversion. Figure 5-36 shows that the greatest increase in the S/N ratio on the carbon conversion is obtained when increasing the bed temperature from 820 °C to 850 °C.



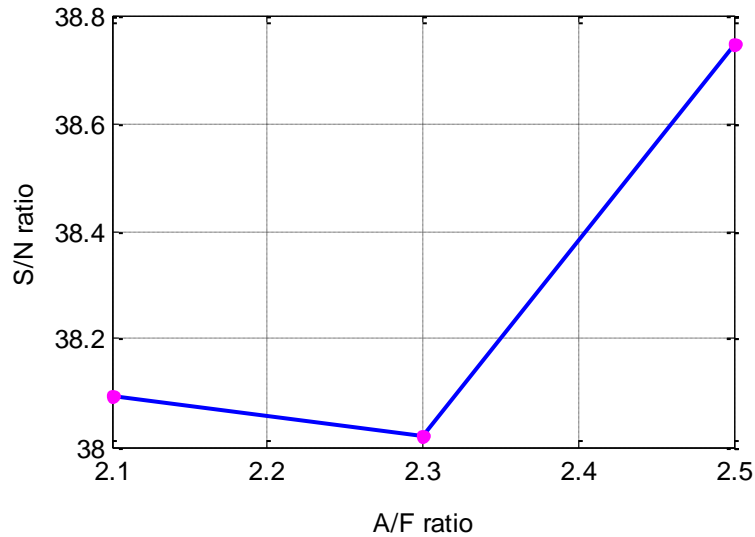
**Figure 5-36** Effect of bed temperature at different levels on the mean S/N ratio

Figure 5-37 shows the mean S/N ratios at different levels of S/F ratios. The S/N ratio decreased when changing the S/F ratio from 0.25 to 0.5 while the greatest increase in the S/N ratio on the carbon conversion is achieved when increasing the S/F ratio from 0.5 to 0.75.



**Figure 5-37** Effect of changing the S/F ratios on the S/N ratio

The effect of changing A/F ratio on S/N ratio can be seen in Figure 5-38, the increase in the A/F ratio from 2.1 to 2.3 decreased the S/N ratio, while the greatest S/N ratio obtained when increasing the A/F ratio from 2.3 to 2.5.



**Figure 5-38** Effect of changing A/F ratio on the S/N ratio

Figure 5-39 shows a decrease in the S/N ratio with increasing the B/C ratio from 0.05 to 0.11 while increasing the B/C ratio from 0.11 to 0.25 a slightly increase in the S/N is obtained. Changing the B/C ratio has a less significant effect on the carbon conversion.

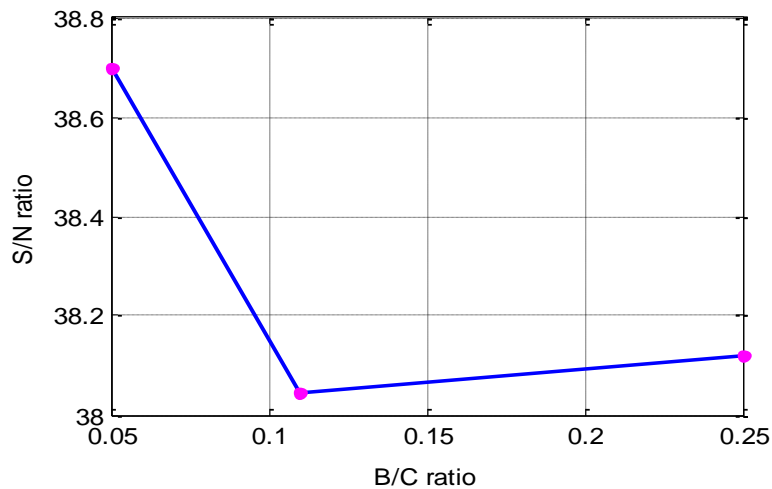


**Figure 5-39** Effect of changing the B/C ratios on the S/N

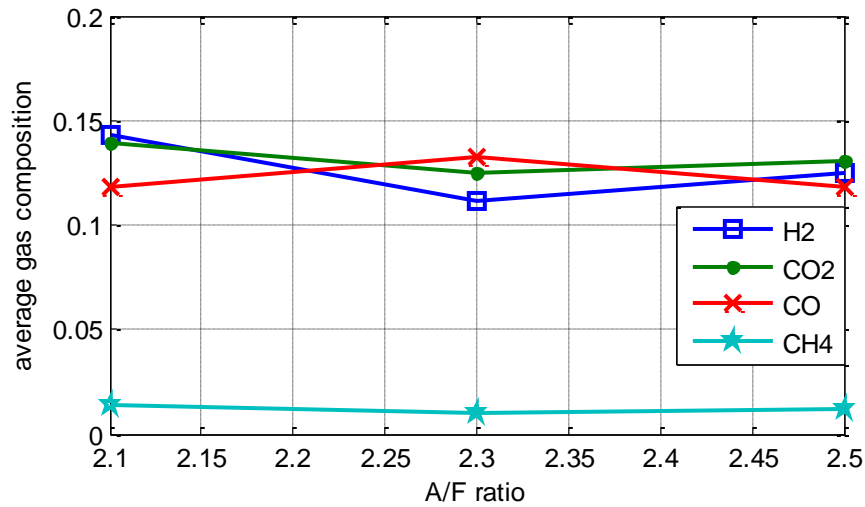
To check the trends of the mean S/N ratios with different levels of the studied variables the mean carbon conversion has been calculated with the three different levels and the results can be shown in Appendix F.

The best experimental conditions can be concluded from the previous figures and from figures F-1, F-2, F-3, and F-4. The arithmetic value of the maximum point in each graph indicates the best choice of the experimental conditions. Therefore, the best conditions for the largest carbon conversion are **A** Steam to fuel (S/F) ratio at level 3 (0.75), **B** Air to fuel (A/F) ratio at level 3 (2.5), **C** Biomass to coal (B/C) ratio at level 1 (0.05), and **D** Temperature, °C at level 3 (850 °C). In other words, the best experimental conditions are A3, B3, C1, and D3 in Table 5-3.

### **5.4.3 Effect of different variable levels on the average gas compositions**

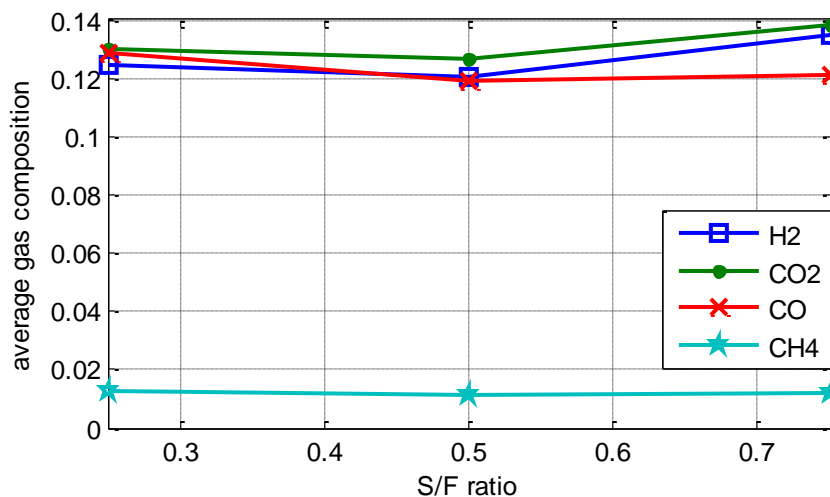
The gas produced from coal-garape seeds gasification contains CO<sub>2</sub>, CO, H<sub>2</sub>, CH<sub>4</sub> and less composition of the minor components (C<sub>2</sub>H<sub>2</sub>, C<sub>2</sub>H<sub>4</sub>, C<sub>2</sub>H<sub>6</sub>, H<sub>2</sub>S, COS, C<sub>3</sub>H<sub>6</sub>, and C<sub>3</sub>H<sub>8</sub>) reaches to about 0.004-0.0075. In this part the obtained average composition of CO<sub>2</sub>, CO, H<sub>2</sub>, and CH<sub>4</sub> will be discussed.

Figure 5-40 shows the average compositions of CO<sub>2</sub>, CO, H<sub>2</sub>, and CH<sub>4</sub> obtained when changing the A/F ratio. Increasing the A/F ratio from 2.1 to 2.3 led to increase the molar average composition of CO. Reaction 1 is more favourable than reaction 3 as it is less exothermic which explains the increase of CO and the decrease in CO<sub>2</sub>. Further increase in A/F ratio from 2.3 to 2.5 the reverse trend will happen; CO will decrease and CO<sub>2</sub> will increase that happens due to increase reaction 2 and 3 producing more CO<sub>2</sub> and consuming the excess of CO in the gasifier and the decrease in the produced CO can explain the increase in hydrogen composition by reaction 5. Methane composition will increase from A/F of 2.3 to 2.5 as it is mainly dependent on hydrogen compositions.



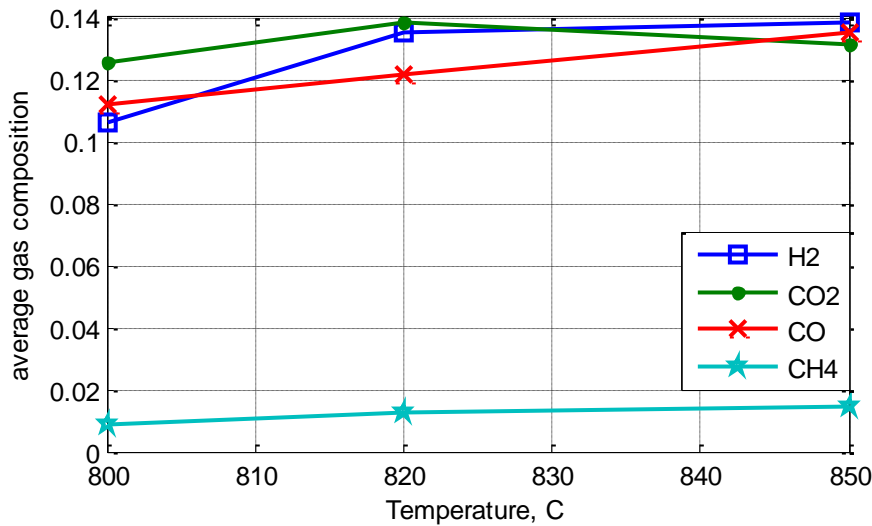
**Figure 5-40** Effect of A/F ratio on the average gas compositions

Figure 5-41 shows the average compositions of CO<sub>2</sub>, CO, H<sub>2</sub>, and CH<sub>4</sub> formed at different levels of S/F. A slight decrease in the average molar compositions is noticed with an increase the ratio of S/F from 0.25 to 0.5 while increasing the S/F from 0.5 to 0.75 causes the average molar compositions of CO<sub>2</sub> and H<sub>2</sub> to increase that explains reaction 5 is more rapid at higher S/F ratios. CO and CH<sub>4</sub> are slightly decreased due to their consumption by reaction 5 and 8 producing more hydrogen and carbon dioxide.



**Figure 5-41** Effect of S/F ratio on the average gas compositions

Figure 5-42 shows the average molar compositions of the produced carbon monoxide, carbon dioxide, hydrogen, and methane with changing the bed temperature. All the producer gas components obtained increased with temperature increase. The maximum increase for CO, H<sub>2</sub>, and CH<sub>4</sub> achieved at a bed temperature increase from 820 °C to 850 °C, at higher bed temperatures the endothermic reaction will be higher than the exothermic reactions, therefore higher CO and H<sub>2</sub> will be produced by reactions 6, 7, and 8 while decreasing CO<sub>2</sub> is due to its consumption by reaction 6 producing more CO.



**Figure 5-42** Effect of bed temperature on the average gas compositions

Figure 5-43 shows the values of the average composition of CO<sub>2</sub>, CO, H<sub>2</sub>, and CH<sub>4</sub> results with varying the B/C ratio at different levels. Both hydrogen and carbon monoxide decreased from B/C ratio of 0.05 to 0.11 and then slightly increase in hydrogen composition and slightly decreased in carbon monoxide composition have been occurred when increasing the B/C ratio from 0.25 to 0.5. While the compositions of carbon dioxide and methane are shown to increase with increasing B/C ratio and the maximum average composition obtained with an increase from 0.11 to 0.25. The increase in CO<sub>2</sub>, CH<sub>4</sub>, and H<sub>2</sub> is due to burning more carbon by reactions 3, 4, and 7 respectively, the produced CO by reaction 1 and 6 will be

consumed by reaction 2 producing CO<sub>2</sub> and reaction 5 producing CO<sub>2</sub> and H<sub>2</sub> which explains the increase in CO<sub>2</sub> and H<sub>2</sub> and the decreased in CO composition.

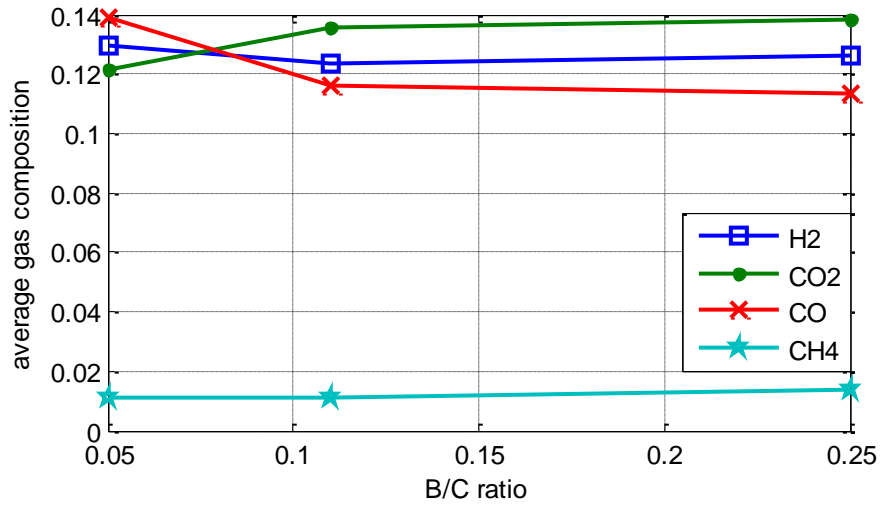


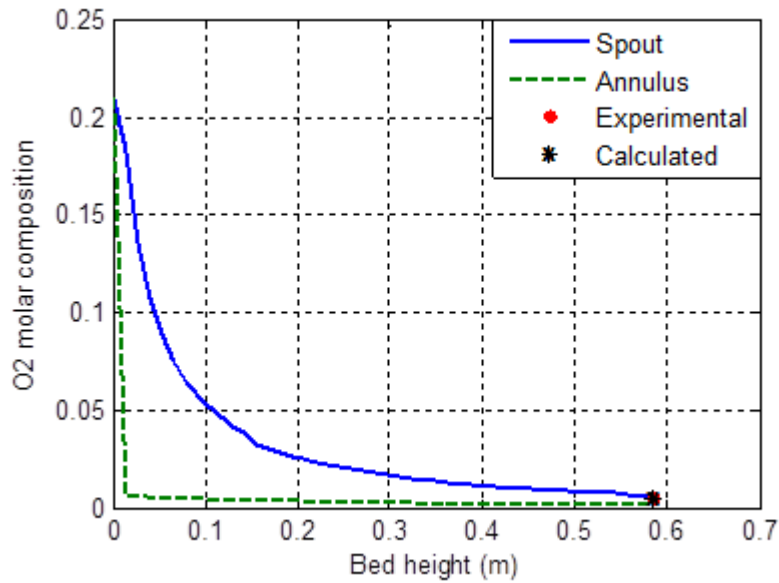
**Figure 5-43** Effect of B/C ratio on the average gas compositions

## **5.5 Theoretical modelling**

### **5.5.1 Distribution of gas compositions in the gasifier**

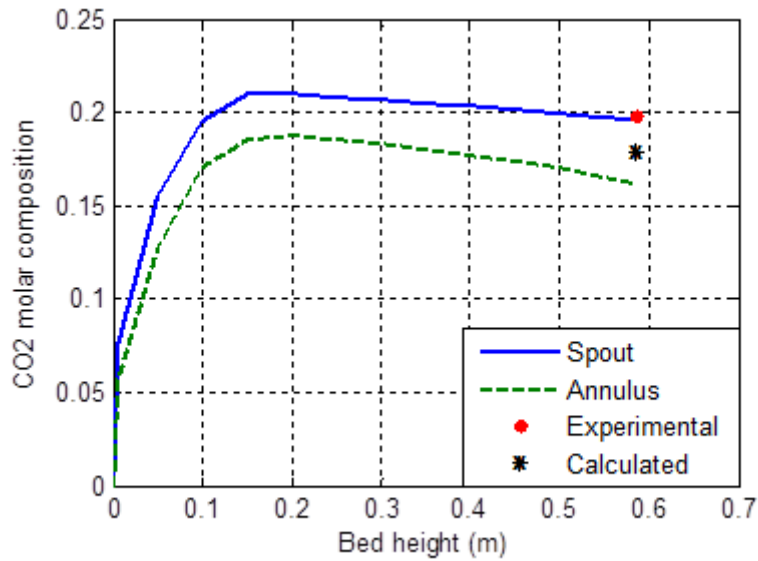
The gases concentrations in axial direction along the bed height were obtained by solving Equations 3.15, 3.17, and 3.24 numerically using finite difference method. The model calculates the gas concentration profile of O<sub>2</sub>, CO<sub>2</sub>, CO, H<sub>2</sub>, and H<sub>2</sub>O in the spout and annulus regions as a function of the bed height. The theoretical gas concentration profiles were compared against the experimental values of coal gasification process to examine the accuracy of the predicted model. The calculations were performed for constant bed temperature during the experiment of 850 °C, coal flow rate of 1.6 kg/h with steam to fuel ratio of 0.75.

Figure 5-44 shows the profile of oxygen concentration in the spout and annulus regions obtained theoretically and compared with experimental results. It can be noticed that oxygen is consumed rapidly in both regions but at different rates, oxygen composition in the spout at the bed exit is 0.0061 in the annulus and in the bed exit it is 0.0021. The fast depletion of oxygen concentration is due to the combustion reactions that are happening fast at the gasifier inlet producing carbon dioxide and carbon monoxide. The average experimental composition of the oxygen at the bed exit is 0.0045 where the average calculated composition from the predicted model is equal to 0.0041.



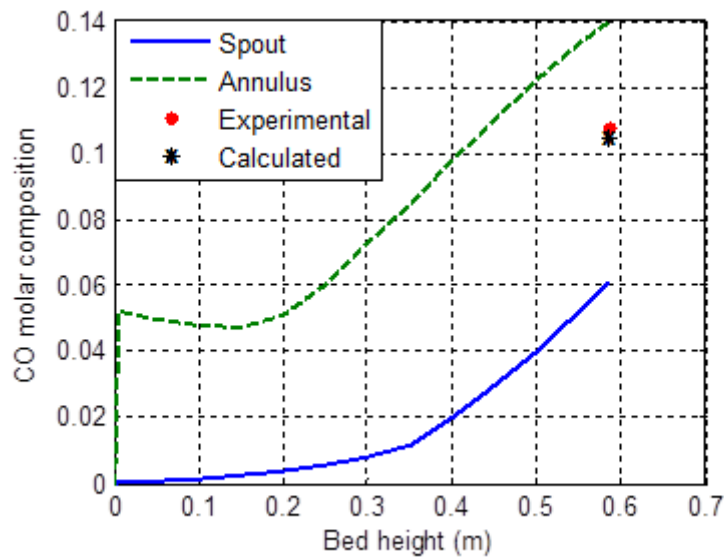
**Figure 5-44** Theoretical concentration profiles for oxygen in the spout and the annulus

Figure 5-45 shows the concentration profile of carbon dioxide in the spout and in the annulus regions and the average experimental composition of carbon dioxide at the bed exit. Carbon dioxide composition increased rapidly in both spout and annulus regions, and its value in the spout is higher than that in the annulus which indicates that complete oxidation is happening at the spout region and it is an exothermic region because the more exothermic reactions is happening at the spout region, so combustion reactions occurs in the spout producing more carbon dioxide. The value of carbon dioxide concentration at the bed exit in the spout region is 0.1959 and its value at the bed exit in the annulus region is 0.162, while the average experimental concentration of carbon dioxide is 0.198.



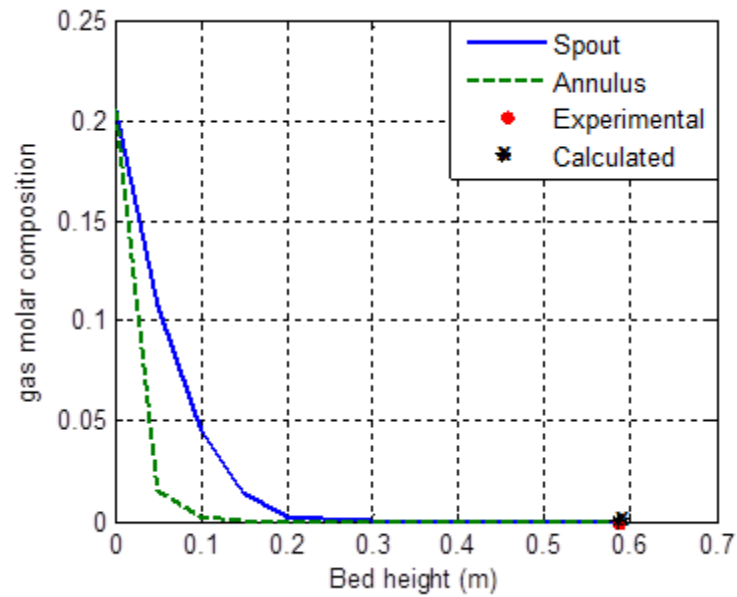
**Figure 5-45** Theoretical concentration profiles for carbon dioxide in the spout and the annulus

Figure 5-46 shows the composition profile of carbon monoxide with the bed height in the gasifier in both spout and annulus regions. It can be noticed from Figure 5-45 that complete oxidation happens at the spout region forming carbon dioxide, so the rest of oxygen will be consumed in the partial oxidation reaction forming carbon monoxide and that explains the excess amount of carbon monoxide in the annulus region. The value of CO composition at the bed exit in the annulus region is 0.14 while it's value at the bed exit in the spout region is 0.06. The average experimental composition of CO at the bed exit is 0.108.



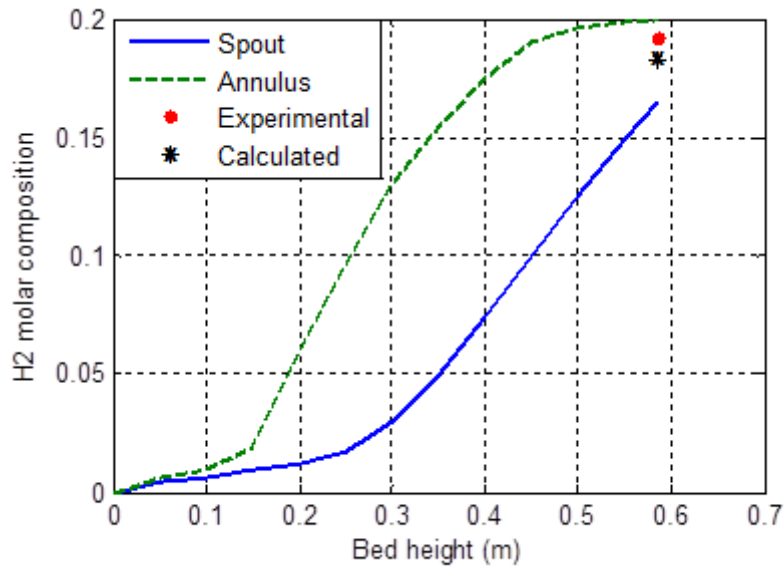
**Figure 5-46** Theoretical concentration profiles for carbon monoxide in the spout and the annulus

Figure 5-47 shows the theoretical composition profile for steam with the bed height in the spout and annulus regions. The steam is almost consumed rapidly in both regions but at different rates; more rapidly in the annulus than in the spout and its molar composition at the bed exit in the spout region is Nil, while it is Nil, and no steam is recorded in the experimental work. These trends suggest that the spout tends to be an oxidizing exothermic which is the same conclusion obtained from Figure 5-45, while the annulus behaves as a reducing endothermic region.



**Figure 5-47** Theoretical concentration profiles for steam in the spout and the annulus

Figure 5-48 shows the profile of hydrogen composition with the bed height in the spout and annulus regions. The composition of hydrogen at the bed exit in the spout region is 0.165 where it is value at the bed exit in the annulus region is 0.2. Because annulus region behaves as endothermic region, the steam will be consumed and endothermic reactions will increase producing more hydrogen and carbon monoxide in the annulus region. The average experimental hydrogen composition is obtained at the same conditions is 0.192.



**Figure 5-48** Theoretical concentration profiles for hydrogen in the spout and the annulus.

### 5.5.2 Comparison of Experimental and Isothermal Model results

The results from the isothermal model are compared with the experimental results obtained when running the gasifier with the same operating conditions. Table 5-6 shows the composition of the gases at the bed exit in both annulus and spout region and the average experimental composition at the bed exit. The average calculated gas compositions in Table 5-6 represent the average composition of each gas results from the spout and annulus regions at the bed exit.

**Table 5-6** Theoretical and experimental producer gas compositions at the bed exit

Gas components	Gas composition		Average gas composition		% Error
	Annulus	Spout	Calculated	Experimental	
O <sub>2</sub>	0.0021	0.0061	0.0041	0.0045	9.75609756
H <sub>2</sub>	0.2	0.165	0.1825	0.192	5.20547945
CO	0.14	0.06	0.1	0.108	8
CO <sub>2</sub>	0.1959	0.162	0.17895	0.198	10.6454317

Figure 5-49 shows comparison between the average compositions at the bed exit obtained from the isothermal model and the average experimental compositions

for the producer gas components at the same operating conditions of 850 °C bed temperature, 0.75 steam to fuel ratio, and 1.6 kg/h fuel rate.

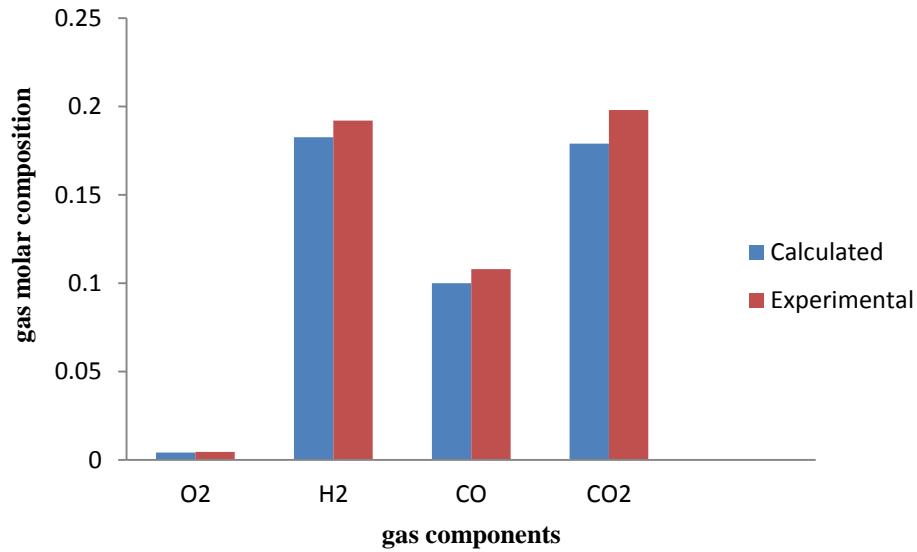


**Figure 5-49** Experimental and theoretical concentration profiles for CO<sub>2</sub>, CO, H<sub>2</sub>, and O<sub>2</sub> at the bed exit.

The above figure shows good agreement between the results obtained from the experiment and the results from the theoretical isothermal model. The % error between the average experimental and the average theoretical compositions is calculated from the following equation:

$$\% \text{ Error} = \frac{|Average\ composition_{EXP.} - Average\ composition_{THEO.}|}{Average\ composition_{THEO.}} * 100 \quad (5.8)$$

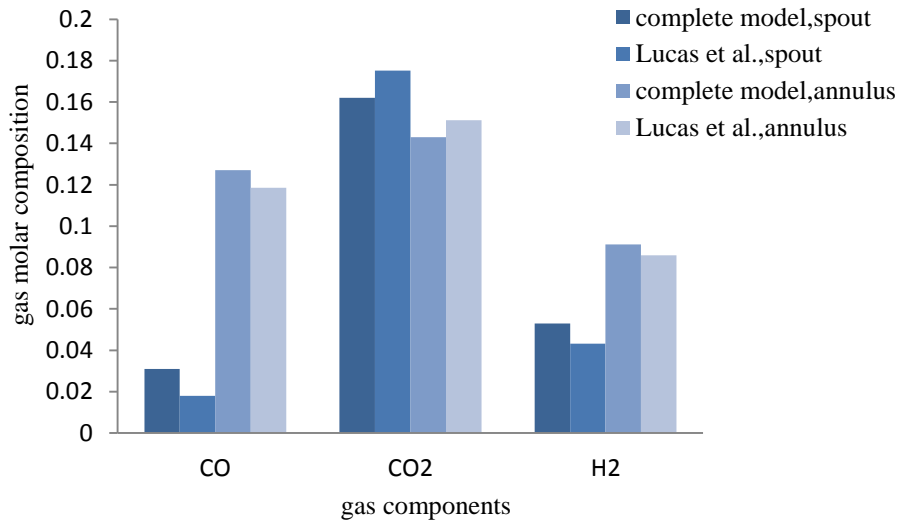
### 5.5.3 Checking the validity of the predicted isothermal Model

The validity and accuracy of the proposed isothermal model for gasification process using MATLAB (R2011a) are checked with the results obtained by **Lucas et al., (1991)** when using the same operating conditions of 925 °C bed temperature, 0.305 m column diameter, 0.61 m bed height, 0.00162 m particle diameter, and 27.50 kg/h coal feed rate. Table 5-7 shows the compositions of CO, CO<sub>2</sub>, and H<sub>2</sub> obtained by **Lucas et al., (1991)** and the compositions of these gases results from the completed isothermal model when using the same operating conditions. Figure 5-50 shows the comparison between the results obtained from the isothermal model

and the results obtained from **Lucas et al., (1991)** in both annulus and spout regions at the bed exit.

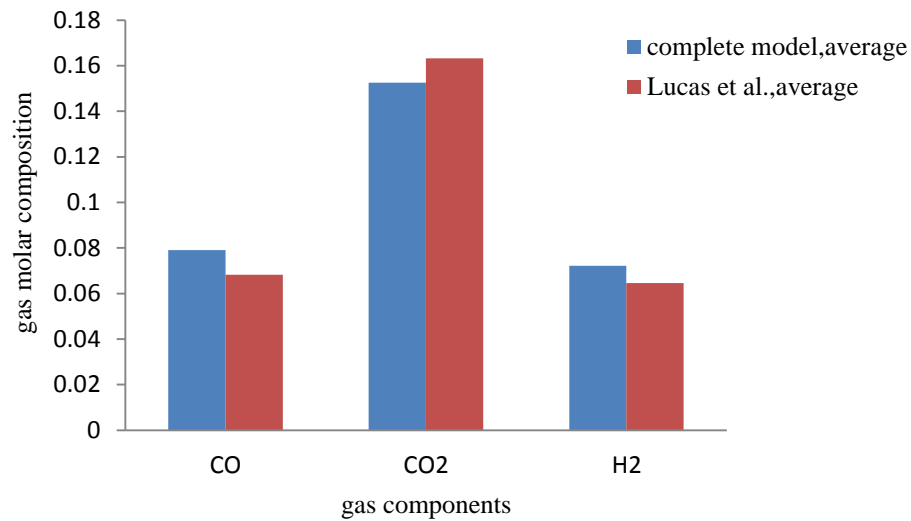
**Table 5-7** Producer gas compositions at the bed exit results from the completed model and the compositions obtained by Lucas et al., (1991) model.

Gas components	Complete model, spout	Lucas et al., spout	Complete model, annulus	Lucas et al., annulus	Complete model, average	Lucas et al., average	% Error
CO	0.031	0.018	0.127	0.1186	0.079	0.0683	13.5443038
CO <sub>2</sub>	0.162	0.1752	0.143	0.1512	0.1525	0.1632	7.01639344
H <sub>2</sub>	0.053	0.0432	0.09124	0.0859	0.07212	0.06455	10.4963949



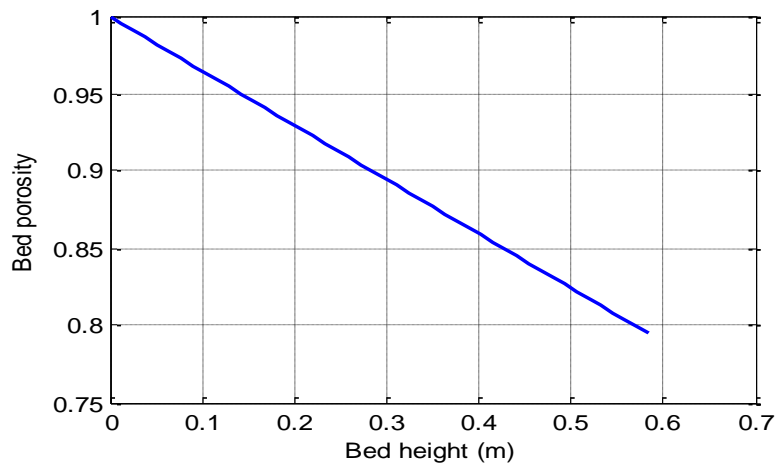
**Figure 5-50** CO, CO<sub>2</sub>, and H<sub>2</sub> concentration at the bed exit in both annulus and spout regions resulting from the completed model and Lucas et al., (1991) model.

Figure 5-51 shows the comparison between the average compositions for CO, CO<sub>2</sub>, and H<sub>2</sub> at the bed exit in both annulus and spout regions obtained from the completed model and results obtained from Lucas et al., (1991) model. Good agreement can be noticed between the results obtained from the isothermal model and that obtained by Lucas et al., (1991), 13.544% error for carbon monoxide compositions, 7.016% error for carbon dioxide compositions, and 10.496% error for hydrogen compositions.



**Figure 5-51** Average CO, CO<sub>2</sub>, and H<sub>2</sub> compositions at the bed exit in both annulus and spout regions resulting from the completed model and Lucas et al., (1991) model.

Figure 5-52 shows the bed porosity values along with the bed height calculated using equation D.16. It can be noticed that the bed porosity decreased linearly with increasing the bed height (**Smith et al., 1981**) due to the high flow rate of gasification agents at the gasifier inlet the space between particles will increase, so the porosity at this point will be 1 and decrease linearly with the axial distance.



**Figure 5-52** Bed porosity with the bed height

Figure 5-53 shows the velocity profile of the gas – phase at the annulus region calculated by equation D.17. The velocity of gas increased with the bed height (**Grbavcic et al., 1976**). The maximum velocity is found at the bed exit which

explains the trend of gasification agent motion because when entering the gasifier most of it will be in the spout and at the top of the spout region the solid particles will move on the annulus sides. This movement of particles may cause motion for the gasification agent and the velocity of gas will be high due to the high number of solid particles entering the annulus region.

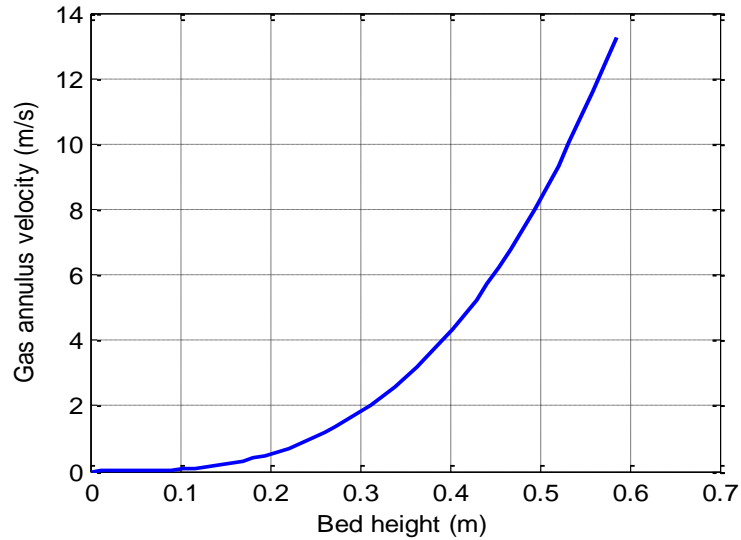


**Figure 5-53** Gas – phase velocity profile at the annulus region

# Chapter Six

## Conclusions and Recommendations

### 6.1 Conclusions

From the present work the effect of temperature, A/F ratio and S/F ratio on the composition of producer gas generated from coal, algae, coal-algae, and coal-grape seeds gasification processes in a 77 mm inside diameter spouted bed gasifier was investigated. The following conclusions can be drawn:

1. The average molar concentration of hydrogen obtained from coal gasification increases with increasing bed temperature to 850 °C.
2. At lower coal feed rate of 1.28 kg/h, the composition of the produced CO<sub>2</sub> decreases while that of CO and CH<sub>4</sub> increases with bed temperature increase. Increasing the coal feed rate to 1.43 and 1.6 kg/h results in considerable increase in the compositions of the produced CO<sub>2</sub>, CO, and CH<sub>4</sub>.
3. Operating without steam leads to an increase in the bed temperature to unstable high limit which is sometimes referred to as the “sintering point”. Above the sintering point, bed agglomeration occurred.
4. Agglomeration is prevented by using (air-steam) gas mixture as a gasification agent. Injection of steam through the gasifier with a S/F ratio of 0.5 or 0.75 decreased the bed temperature due to the energy consumption for water evaporation.
5. The average molar concentrations of CO<sub>2</sub>, H<sub>2</sub> and CH<sub>4</sub> increase when increasing the ratio of steam to fuel from 0.5 to 0.75, while CO average molar concentrations decreases.
6. Operating the gasifier with 820 °C bed temperature the average molar concentrations of the produced hydrogen increased with increasing the ratio of A/F, while at 850 °C the average concentrations of hydrogen decreased with increasing the A/F ratio.

7. The conversion of carbon increases with increasing mass rate of coal, bed temperature, and S/F ratio the maximum value of carbon conversion obtained is 92.9% at 1.8 A/F ratio, 850 °C bed temperature, and 0.75 S/F ratio.
8. Gasification of unleached algae results in bed agglomeration, apparently due to the high salt content of the raw algae. Leaching of raw algae is required to dissolve the salt content.
9. Co-gasification of coal-grape seeds with the same operating conditions applied with coal gasification results in the formation of molten potassium and sodium silicate which is accumulated with time stopping fluidization. Avoiding the formation of molten components achieved by increasing the A/F ratio.
10. According to the Taguchi method in design experiment of coal-grape seeds gasification the bed temperature is the most influential parameter on the carbon conversion while the ratio of B/C has low effect on carbon conversion and the best experimental conditions are 850 °C bed temperature, 0.75 S/F ratio, 2.5 A/F ratio, and 0.05 B/C ratio. For best conditions the carbon conversion is 96.1%.
11. Spout-fluid bed gasification is suitable for hydrogen production.
12. According to the isothermal model more carbon dioxide produced in the spout region while carbon monoxide and hydrogen produced more at the annulus region. These trends suggest that the spout tends to be an oxidizing exothermic region, while the annulus behaves as a reducing endothermic region. Good agreement is obtained between the experimental results and the isothermal model results.

## **6.2 Recommendations for the future work**

The following suggestions for future work can be considered:

1. Increase the production of hydrogen for fuel cells by steam gasification of different biomass types and by using catalysts such as  $\text{ZnCl}_2$  and dolomite.
2. Study the mechanisms of gasification reactions at high pressure and at different A/F ratios.
3. Feed the fuel nearer to the bed and increasing the height of column in algae gasification experiments to avoid the fuel elutriation and downstream gas outlet blockages.

## References

- Abadie, L.M., and Chamorro, J.M., “The Economics of Gasification: A Market-Based Approach”. *Energies Journal*, Vol. 2, 662-694; doi: 10.3390/en20300662, August (2009).
- Abdullah, S., and Yusup, S.,” Method for screening of Malaysian biomass based on aggregated matrix for hydrogen production through gasification”. *Journal of applied sciences* 10, 3301-3306, (2010).
- Abdul Salam, P., and Bhattacharya, S.C., “A comparative hydrodynamic study of two types of spouted bed reactor designs”. *Chemical Engineering Science* 61, 1946 – 1957, doi:10.1016/j.ces.2005.10.044, (2006).
- Abdul Salam, P., S., Kumar, and Siriwardhana, M., “Report on the status of biomass gasification”. October (2010).
- Agency, I.E., *World Energy Outlook Executive Summary*, (2011).
- Ammar, S. H., “Hydrodesulfurization of thiophene over Co-Mo/AlO catalyst using fixed-and fluidized-bed reactors”. PHD thesis, Baghdad university, (2009).
- Arnavat, M., P., Bruno, J., C., and Coronas, A., “Review and analysis of biomass gasification models”. *Renewable and Sustainable Energy Reviews* 14, 2841–2851, doi:10.1016/j.rser.2010.07.030, (2010).
- Basu, P., “Combustion and Gasification in Fluidized Beds-CRC Press.”. ISBN 0-8493-3396 2, 456 pages, (2006).
- Belgiorno, V., Feo, G. De, Della Rocca, C., and Napoli, R.M.A., “Energy from gasification of solid wastes”. *Science direct Journal*, 23, 1-15, (2002).
- Berkman, J., A., H., and Michael, G., “ALGAL BIOMASS”. Ebook, Chapter A7, *Biological Indicators Algal Biomass Indicators*, Version 1.0 (2007).
- Biba, V., Macak, J., Klose, E., Malecha, J., *Ind. Eng. Chem. Proc. Des. Dev.* 17, 92–98, (1978) as sign in Mendes et al., (2008).
- Boateng, A. A., Walawender, W. P., Fan, L.T. and Chee, C.S., “Fluidized bed gasification of rice hull”. *Bioresource Technology*, 40(3): 235-239, (1992).

- Bourgeois, P., Grenier, P., “The ratio of terminal velocity to minimum fluidising velocity for spherical particles”. *Canadian Journal of Chemical Engineering*, Volume 46, Issue 5, pages 325–328, October (1968).
- Bridgwater, A.V., Evans, G.D., “An Assessment of Thermochemical Conversion Systems for Processing Biomass and Refuse”. Energy Technology Support Unit (ETSU) on behalf of the Department of Trade, ETSU B/T1/00207/REP, (1993).
- Brown, J., “Biomass Gasification: Fast Internal Circulating Fluidised Bed Gasifier Characterisation and Comparison”. Master thesis in Chemical and Process Engineering, University of Canterbury, (2006).
- Brunello, G., Nina, G.D., Nunes, and F.C.S., Nascimento, C.A.O., “Minimum air requirement for spouting mixed particles”. *Canadian Journal of Chemical Engineering* 52, 170–173, (1974).
- Campbell, M., N., “Biodiesel: Algae as a Renewable Source for Liquid Fuel”. *Guelph Engineering Journal*, (1), 2 - 7. ISSN: 1916-1107, (2008).
- Cao, Y., Wang, Y., Rieley, J. and Pan, W., “A novel biomass air gasification process for producing tar-free higher heating value fuel gas”. *Fuel Processing Technology*, Vol. 87, 4, 343-353, (2005).
- Carlozz, P., “Closed Photobioreactor Assessments to Grow, Intensively, Light Dependent Microorganisms: A Twenty-Year Italian Outdoor Investigation”. *The Open Biotechnology Journal*, 2, 63-72, (2008).
- Carlsson, A., S., Beilen, J., B., V., Ralf, M., and Clayton, D., “UTILITY FOR INDUSTRIAL APPLICATIONS”. Outputs from the EPOBIO project, CNAP, University of York, September (2007).
- Chatterjee, P., K., Datta, A., B., and Kundu, K., M., “Fluidized bed gasification of coal”. *The Canadian Journal of Chemical Engineering*, Vol. 73, Issue 2, pages 204–210, 1995, DOI: 10.1002/cjce.5450730206, published MAR, (2009).
- Choi, M., and Meisen, A., “Hydrodynamics of shallow, conical spouted beds”. *The Canadian Journal of Chemical Engineering* 70, 916–924, (1992).

- Chopra, S. and A. Jain, “A Review of Fixed Bed Gasification Systems for Biomass”. *Agricultural Engineering International: the CIGR Ejournal*, Vol. IX, April, (2007).
- Ciferno, J. P., and Marano, J. J., “Benchmarking Biomass Gasification Technologies for Fuels, Chemicals and Hydrogen Production”. June (2002).
- Craig, K., R., and Margaret, K., M., “Cost and Performance Analysis of Biomass-Based Integrated Gasification Combined-Cycle (BIGCC) Power Systems”. DE-AC36-83CH10093, NREL/TP-430-21657, October (1996).
- Darby, R., “Chemical engineering fluid mechanics”. ISBN: 0-8247-0444-4, (2001).
- Deng, Z., Xiao, R., Jin, B., Huang, H., Shen, L., Song, Q., and Li, Q., “Computational Fluid Dynamics Modeling of Coal Gasification in a Pressurized Spout-Fluid Bed”. *Energy & Fuels*, 22, 1560–1569, (2008).
- Di, B., C., “Dynamic behaviour of stratified downdraft gasifier”. *Chemical Engineering Science* 55, 2931–2944, (2000).
- Dixit, R., and Shivanand P., “Fluidization Technologies: Aerodynamic Principles and Process Engineering”. *Journal of Pharmaceutical sciences* , VOL. 98, NO. 11, Wiley InterScience, DOI 10.1002/jps.21722, April (2009).
- Dogan, O. M., UYSAL B. Z. & GRACE J. R., “HYDRODYNAMIC STUDIES IN A HALF SLOT-RECTANGULAR SPOUTED BED COLUMN”. *Chem. Eng. Comm.*, 191: 566\_579, 2004, ISSN: 0098-6445 print/1563-5201online, DOI: 10.1080/00986440490277992, (2004).
- Du, W., Bao, Xu, X. J., and Wei, W., “Computational fluid dynamics (CFD) modeling of spouted bed: Assessment of drag coefficient correlations”. *Chemical Engineering Science* 61, 1401–1420, doi:10.1016/j.ces.2005.08.013, (2006).
- Eliasson, B., and Taylor, G., “The Future of the Hydrogen Economy: Bright or Bleak?”, ereport, [www.efcf.com/reports](http://www.efcf.com/reports), February (2005).
- Eng, J. H., Svrcek, W., Y., and Behie, L., A., “Dynamic Modeling of a Spouted Bed Reactor with a Draft Tube”. *Ind. Eng. Chem. Res.*, Vol. 28, No. 12, (1989).

- Ergudenler, A., “Gasification of Wheat Straw in a Dual-Distributor Type Fluidized Bed Reactor”. Ph.D. Thesis, Technical University of Nova Scotia, Nova Scotia, Canada, (1993).
- Eyk, P., J., V., Kosminski, A., and Ashman, P., J., “Control of Agglomeration and Defluidisation during Fluidised Bed Combustion of South Australian Low-Rank Coals”. Energy and Fuels Journal, DOI: 10.1021/ef2011518, (2011).
- Eyk, P., J., V., Muhlack, R., A., and Ashman, P., A., “Gasification of Grape Marc in a Circulating Fluidised Bed”. Proceedings of the Australian Combustion Symposium, the University of Queensland, December, (2009).
- Fogler, H., S., “Element of chemical reaction engineering”. Third edition, (1999).
- Gao, Y., Gregor., C., Liang, Y., Tang, D., and Tweed C., “Algae Biodiesel”. A Feasibility Report, BPRO 29000, (2009).
- Geankoplis, C., J., “Transport processes and unit operations”. Third edition, ISBN 0-13-045253-X, (1993).
- Global bioenergy partnership, “ALGAE-BASED BIOFUELS: A Review of Challenges and Opportunities for Developing Countries”. (2009).
- Goldemberg, J., “The Case for Renewable Energies”. Thematic Background Paper, February (2004).
- González, J., F., Román, S., Bragado, D., and Calderón, M., “Investigation on the reactions influencing biomass air and air/steam gasification for hydrogen production”. Fuel processing technology 89, 764- 772, (2008).
- Grace, J.R., In: Hetsroni, G. (Ed.), Handbook of Multiphase Systems. Hemisphere, New York, Chapter 8, (1982).
- Grbavcic, Z., B., Vuković D. V., Zdaaski F. K. and Littman H., Can. J. Chem. Engng 54 3, (1976).
- Greenwood N. N., Earnshaw A., Chemistry of the Elements, Pergamon Press, Oxford, United Kingdom, (1984).
- Heiskanen, L., “A study on rate correlations of gasification reactions”. Lappeenranta University of Technology Faculty of Technology Degree Program of Energy Technology, (2011).

- Hook, B., D., H. Littman, M.H. Morgan III, Y. Arkun, and Can. J. Chem. Eng. 70, 966–982, (1992) as sign in Mendes et al., (2008).
- Höök, M., “Coal fundamentals A brief overview”, (2007).
- Hoque, M. M., Bhattacharya S., C., “Fuel characteristics of gasified coconut shell in a fluidized and a spouted bed reactor”. Energy, 26, pp101–10, (2001).
- Hsu, D., D., “Life Cycle Assessment of Gasoline and Diesel Produced via Fast Pyrolysis and Hydroprocessing”. Technical Report, March (2011).
- Jackson, R. and Judd, M. R., Trans IChemE, 59, 119, (1981).
- Jin, H., Lu, Y., Liao, B., Guo, L., and Zhang, X., “Hydrogen production by coal gasification in supercritical water with a fluidized bed reactor”. International Journal of Hydrogen Energy, 35, 7151- 7160, (2010).
- Knoef, I. H. A. “BTG Biomass Gasification”. April (2008).
- Kong, L., L., G., ZHANG, B., HE, W., and WANG, H., “Hydrogen Production from Biomass Wastes by Hydrothermal Gasification”. Energy Sources, Part A, 30:1166–1178, Taylor & Francis Group, LLC, ISSN: 1556-7036 print/1556-7230 online, DOI: 10.1080/15567030701258246, (2008).
- Kreith, F., Boehm, R.F., “Heat and Mass Transfer”. Mechanical Engineering Handbook, (1999).
- Lettner, F., T., Helmut, H., Peter, “Biomass gasification – State of the art description”. Graz University of Technology - Institute of Thermal Engineering, Grant agreement no EIE/06/078/SI2.447511, December (2007).
- Lim, C., J., M., Sulaiman, H., and A., P., Watkinson, Can. J. Chem. Eng. 69, 596–606, (1991).
- Lim, M. T., and Alimuddin, Z., “Bubbling fluidized bed biomass gasification- Performance, process findings and energy analysis”. Science direct Journal, 33, 2339–2343, (2008).
- Limtrakul, S., Chalermwattanatai, A., Unggurawirote, K., Tsuji, Y., Kawaguchi, T., Tanthapanichakoon, W., “Discrete particle of solids motion in a gas–solid fluidized bed”. Chemical Engineering Science 58, 915–921, (2003), as sign in Limtrakul, S., Boonsrirat, A., and Vatanatham, T., “DEM modeling and

simulation of a catalytic gas–solid fluidized bed reactor: a spouted bed as a case study”.

- Li, Q., Zhang, M., Zhong, W., Wang, X., Xiao, R., and Jin, B., “Simulation of Coal Gasification in a Pressurized Spout-Fluid Bed Gasifier”. *The Canadian Journal of chemical engineering*, vol 87, April (2009).
- Littman , H., P.V. Narayan, A.H. Tomlins, and M.L. Friedman, *AIChE Symposium Series*, vol. 77, 174–180, (1981).
- Li, X.T., Grace, J.R., Lim, C.J., Watkinson, A.P., Chen, H.P., and Kim, J.R., “Biomass gasification in a circulating fluidized bed”. *Biomass and Bioenergy* 26, 171 – 193, doi:10.1016/S0961-9534(03)00084-9, (2004).
- Lucas, A., Arnaldos, J., Casal, J., and Puigjaner, L., “Improved equation for calculation of minimum fluidization velocity”. *Industrial & Engineering Chemistry Process Design and Development* 25, 426–429, (1986).
- Lucas, J.P., Lim, C.J., and Watkinson, A.P., “A nonisothermal model of a spouted bed gasifier”. *Fuel* Vol. 77, No. 7, pp. 683-694, PII:S 0016-2361(97)00237, (1998).
- Lucas, J. P., Watkinson, A. P. and Lim, C. J., “Mathematical Model of C.R.E. Gastjier”. Report of Contract CREICON 1035 to British Coal Corporation, (1991) as sign in Lucas et al., (1998).
- Lv, P., Chang, J., Xiong, Z., Huang, H., Wu, C., and Chen, Y., “Biomass Air-Steam Gasification in a Fluidized Bed to Produce Hydrogen-Rich Gas”. *Energy and Fuels*, 17, 677-682, (2003).
- Mahamuni, N.N. and Adewuyi, Y.G.. “Application of Taguchi Method to Investigate the Effects of Process Parameters on the Transesterification of Soybean Oil Using High Frequency Ultrasound”. *Energy Fuels*, 24, 2120-2126, (2010).
- Mamuro, T., and Hattori, H., *J. Chem. Engng Japan* (1968) as sign in Mendes et al., (2008).
- Matsui, D. K., Furusawa T., *Chem. Eng. J.* 18, 105–113, (1985) as sign in Mendes et al., (2008).

- Matsui I., Kunii D., Furusawa T., *Ind. Eng. Chem. Res.* 26, 91–95, (1987) as sign in Mendes et al., (2008).
- Mathur, K.B., and Gishler, P.E., “A technique for contacting gases with coarse solid particles”. *A.I.Ch.E. Journal* 1, 157–164, (1955).
- Mathur, K.B., Gishler, P.E., “A technique for contacting gases with coarse solid particles”. *A.I.Ch.E. Journal* 1 (1), 157–164, (1955).
- McCullough D. P., Eyk P. J., Ashman P. J., and Mullinger, “Investigation of Agglomeration and Defluidization during Spouted-Bed Gasification of High-Sodium, High-Sulfur South Australian Lignite”. Chemical engineering department, University of Adelaide, (2011).
- Mendes, A., Dollet, A., Ablitzer, C., Perrais, C., and Flamant, G., “Numerical simulation of reactive transfers in spouted beds at high temperature: Application to coal gasification”. *Science direct journal*, 82, 117–128, doi:10.1016/j.jaap.2008.02.001, (2008).
- Mermoud, F., Golfier, F., Salvador, S., Van de Steene and J Dirion, “Experimental and numerical study of steam gasification of a single charcoal particle”. *Combustion and Flame* 145 (2006) 59–79, (2006).
- Narvaez, I., Orto, A., Aznar, M. P., and Corella, J.,” Biomass Gasification with Air in an Atmospheric Bubbling Fluidized Bed. Effect of Six Operational Variables on the Quality of the Produced Raw Gas”, *Ind. Eng. Chem. Res.*, 35, 2110-2120,( 1996).
- Neogi D., Chang C.C., W.P., and Walawender L.T., “Study of coal gasification in an experimental fluidized bed reactor”. *AIChE Journal* (Vol. 32, No. 1), January (1986).
- Olazar, M., San Jose, M. J., Aguayo, A., T., Arandes, J., M., and Bilbao, J., “Design Factors of Conical Spouted Beds and Jet Spouted Beds”. *Znd. Eng. Chem. Res.*, 32, 1245-1250, (1993).
- Palacio, D., L., and Philippe B., “Hydrogen Energy and Fuel Cells”. Final report of the high level group, EUROPEAN COMMISSION, (2003).

- Purdy, M., J., Felder, R., M., and Ferrell, J., K., “Coal Gasification in a Pilot Scale Fluidized Bed Reactor, Gasification of a New Mexico Subbituminous Coal”. *Ind. Eng. Chem. Process Des. Dev.*, 23, 287-294, (1984).
- Rajvanshi, A., K., “BIOMASS GASIFICATION”. Director, Nimbkar Agricultural Research Institute, PHALTAN-415523, Maharashtra, India, (Published as a Chapter (No. 4) in book “Alternative Energy in Agriculture”. Vol. II, Ed. D. Yogi Goswami, CRC Press, 83-102, (1986).
- Riis, T., Elisabet, F., H., Vie, P., J., S., and Ulleberg, Q., “HYDROGEN PRODUCTION AND STORAGE”. INTERNATIONAL ENERGY AGENCY, OECD/IEA, (2006).
- Roos, C., J., “Biomass Drying and Dewatering for Clean Heat & Power”. WSU Extension Energy Program, September (2008).
- Sadaka, S. S., Ghaly, A. E., and Sabbah, M.A., “Two-phase biomass air-steam gasification model for fluidized bed reactors: Part III—model validation”. *Biomass and Bioenergy*, 22 479 – 487, (2002).
- Saito M., Sadakata M., Sakai T., *Combust. Sci. Technol.* 51, 109–128, (1983) as sign in Mendes et al., (2008).
- Salam, P. A., and Bhattacharya, S., C., “A comparative study of charcoal gasification in two types of spouted bed reactors”. *Energy* 31, 228–243, doi:10.1016/j.energy.2005.01.004, (2006).
- Sanchez, I., G., Mazza, G., Flamant, and D., Gauthier, *Chem. Eng. Sci.* 55, 193–202, (2000), as sign in Mendes et al., (2008).
- Secondary and Intermediate Energy Infobook, Project P.O. Box 10101, Manassas, VA 20108 1.800.875.5029, (2011).
- Smith, K., I., YAMAN, A., and HOWARD, L., “STUDIES ON MODELING AND CONTROL OF SPOUTED BED REACTORS-I REACTOR MODELING”. Department of Chemical Engineering and Environmental Engineering, Rensselaer Polytechnic Institute, Troy, NY 12181, U.S.A, (1981).
- Taglia, P., P.G., “Biogas: Rethinking the Midwest's Potential”. June (2010).

- Taguchi, G. *Introduction to Quality Engineering*; UNIPUB/Kraus International: White Plains, (1986), as sign in Mahamuni, N.N., et al., (2010).
- Tannous, K., “Contribution a letude hydrodynamique des lits fluidises de grosses particles. These de doctorat”. INP-Toulouse, France, (1993) as sign in Abdul Salam and Bhattacharya (2006).
- Tesner P.A., in: *Proceedings of the Eighth Symposium on Combustion*, p. 807, (1960 as sign in Mendes et al., (2008).
- Thamavithya, M., Sompop J., Animesh D., and Prabir B., “Experimental study on sawdust gasification in a spout–fluid bed reactor”. *Int. J. Energy Res.* 2012; 36:204–217, DOI: 10.1002/er.1796, (2010).
- The US Energy Information Administration (EIA), *International Energy Outlook* (2009).
- Thonglimp, V., Hiquily, N., Laguerie, C., “Vitesse minimale de fluidisation et expansion des couches fluidises par un gaz”. *Powder Technology* 38, 233–253, (1984).
- Tillman, D.A., “Biomass Combustion. Biomass: Regenerable Energy”. John Wiley and Sons, 203-219, (1987).
- TOSUN, I., “MODELLING IN TRANSPORT PHENOMENA”. *A Conceptual Approach*, (2002).
- Turare, C., “Biomass Gasification – Technology and Utilisation”. ARTES Institute, Glucksburg, Germany, (2002).
- Uemaki, O., Yamada, R., and Kugo, M., “Particle segregation in a spouted bed of binary mixtures of particles”. *Canadian Journal of Chemical Engineering* 61, 303–307, (1983).
- Wagner, L., “Biodiesel from algae oil, research report”. July (2007).
- Wang Y., Kinoshita C.M., *Solar Energy* 51, 19–25, (1993) as sign in Mendes et al., (2008).
- Weil, S.A., S.P. Nandi, D.V. Punwani and J.L. Johnson. “Peat hydrogasification”. (1978).

- Wellinger, A., “Algal Biomass: Does it save the world?”. Short reflections, Task 37, April (2009).
- Wen, C.Y., and Yu, Y.H., “Mechanics of fluidization”. Chemical Engineering Progress Symposium Series No. 62, 100–111, (1966).
- Wen, Z., and Michael B., J., “Microalgae as a Feedstock for Biofuel Production”. College of Agriculture and Life Sciences, Virginia Polytechnic Institute and State University, Publication 442-886, (2009).
- Werther, J., “Fluidized-Bed Reactors”. Ullmann’s Encyclopedia of industrial chemistry, Hamburg University of Technology, Hamburg, Germany, DOI: 10.1002/14356007.b04\_239.pub2, (2012).
- Wu, S.W.M., Lim, C.J., Epstein, N., “Hydrodynamics of spouted beds at elevated temperatures”. Chemical Engineering Communication 62, 251–268, (1987).
- Xiao, R., Zhang, M., Jin, B., and Huang Y., “High-Temperature Air/Steam-Blown Gasification of Coal in a Pressurized Spout-Fluid Bed” Energy & Fuels, 20, 715-720, (2006).
- Yang, W., C., “Modification and re-interpretation of Geldart's classification of powders”. Science direct Journal, Powder Technology 171 (2007) 69–74, DOI:10.1016/j.powtec.2006.08.024, (2006).
- Yu, L., Lu, J., Zhang, X., and Zhang, S., “Numerical simulation of the bubbling fluidized bed coal gasification by the kinetic theory of granular flow (KTGF)”. Fuel 86, 722–734, doi:10.1016/j.fuel.2006.09.008, (2007).
- Zedtwitz, P., V., and Steinfeld, A., “Steam-Gasification of Coal in a Fluidized-Bed/Packed-Bed Reactor Exposed to Concentrated Thermal Radiations Modeling and Experimental Validation”. Ind. Eng. Chem. Res., 44, 3852-3861, (2005).
- Zhang, Y., Xiao, J., and Shen, L.,” Simulation of Methanol Production from Biomass Gasification in Interconnected Fluidized Beds”. Ind. Eng. Chem. Res., 48, 5351–5359, (2009).
- Zhong, W., Rui , X., and Mingyao, Z., “Experimental Study of Gas Mixing in a Spout-Fluid Bed”. Thermoenergy Engineering Research Institute, Southeast

University, Nanjing 210096, China, DOI 10.1002/aic.10708, Wiley InterScience, (2005).

# Appendix A

## Experimental Data

### A.1 Coal gasification experiments results

**Table A-1** Experimental results for run with coal feed rate = 1.6 kg/h, S/F ratio= 0.5, and bed Temperature = 850 °C

Components	Time, h				Average Composition
	1h	2h	3h	4h	
C <sub>2</sub> H <sub>2</sub>	0.0021362	0.0035514	0.0027808	0.0035304	0.0029997
CO <sub>2</sub>	0.1517318	0.1927576	0.1939561	0.1972645	0.1839275
C <sub>2</sub> H <sub>4</sub>	0.0004582	0.0005101	0.0004368	0.0005146	0.0004799
C <sub>2</sub> H <sub>6</sub>	0.0008112	0.0019456	0.0016342	0.0019577	0.0015872
H <sub>2</sub> S	6.531E-05	0.0068521	0.0072179	0.0072147	0.0053375
COS	0.0004554	0.0002952	0.0003867	0.0003171	0.0003636
C <sub>3</sub> H <sub>6</sub>	0.0004999	0.0007362	0.0006989	0.0007583	0.0006733
C <sub>3</sub> H <sub>8</sub>	0.0001731	0.0007097	0.000665	0.0007206	0.0005671
H <sub>2</sub>	0.1396301	0.1718334	0.1675075	0.1448823	0.1559633
O <sub>2</sub>	0.0061795	0.0043048	0.0079389	0.0062531	0.0061691
N <sub>2</sub>	0.5426092	0.4787862	0.492676	0.5133664	0.5068595
CH <sub>4</sub>	0.0107394	0.0171409	0.0136193	0.017053	0.0146381
CO	0.1051754	0.0839117	0.0935535	0.1052449	0.0969714
total	0.9606649	0.9633349	0.9830717	0.9990777	0.9765373

**Table A-2** Experimental results for run with coal feed rate = 1.6 kg/h, S/F ratio= 0.75, and bed Temperature = 850 °C

Components	Time, h				Average Composition
	1h	2h	3h	4h	
C <sub>2</sub> H <sub>2</sub>	0.0026551	0.0046137	0.00425009	0.00378489	0.00382595
CO <sub>2</sub>	0.1896412	0.2092024	0.20066609	0.19413747	0.19841179
C <sub>2</sub> H <sub>4</sub>	0.0004137	0.0006825	0.00065435	0.00059865	0.0005873

C <sub>2</sub> H <sub>6</sub>	0.000973	0.0024642	0.00234675	0.0020704	0.00196359
H <sub>2</sub> S	0.0056036	0.0083047	0.00783754	0.00776265	0.00737712
COS	0.0006056	0.0005383	0.00045979	0.00045336	0.00051428
C <sub>3</sub> H <sub>6</sub>	0.0005686	0.0011682	0.00111059	0.0009768	0.00095605
C <sub>3</sub> H <sub>8</sub>	0.0002645	0.0008314	0.00083776	0.00076506	0.00067468
H <sub>2</sub>	0.1779318	0.2053905	0.19964419	0.18702279	0.19249732
O <sub>2</sub>	0.0031009	0.0061168	0.00549283	0.00335842	0.00451723
N <sub>2</sub>	0.4607383	0.4245824	0.43238922	0.4490296	0.44168489
CH <sub>4</sub>	0.0132555	0.022321	0.02058715	0.0185225	0.01867153
CO	0.1371875	0.09479	0.10028528	0.10216234	0.10860628
total	0.9929394	0.981006	0.97656163	0.97064494	0.98028801

**Table A-3** Experimental results for run with coal feed rate = 1.6 kg/h, S/F ratio= 0.5, and bed Temperature = 820 °C

Components	Time, h				Average composition
	1h	2h	3h	4h	
C <sub>2</sub> H <sub>2</sub>	0.002073767	0.002140653	0.0021117	0.001862877	0.00204725
CO <sub>2</sub>	0.155908934	0.166552357	0.1651651	0.151749009	0.159843862
C <sub>2</sub> H <sub>4</sub>	0.000312104	0.000305225	0.0003313	0.000290702	0.000309842
C <sub>2</sub> H <sub>6</sub>	0.000840015	0.000966932	0.0010061	0.000850825	0.000915965
H <sub>2</sub> S	5.50084E-06	0.003825397	0.004243	0.004395096	0.003117247
COS	0.000298081	0.000208234	0.0001483	0.000168188	0.000205711
C <sub>3</sub> H <sub>6</sub>	0.000431132	0.000416693	0.0004584	0.000453678	0.000439967
C <sub>3</sub> H <sub>8</sub>	0.000239627	0.000296508	0.0003246	0.000288215	0.000287243
H <sub>2</sub>	0.118252436	0.130595366	0.1222269	0.099508719	0.117645853
O <sub>2</sub>	0.008830154	0.016542355	0.0063513	0.004036361	0.008940034
N <sub>2</sub>	0.58231452	0.5736543	0.586993	0.60223	0.586297961
CH <sub>4</sub>	0.01042133	0.01065968	0.0104537	0.009748627	0.010320825
CO	0.113331264	0.083228798	0.0818728	0.082499626	0.090233129
total	0.993258864	0.989392498	0.9816863	0.958081923	0.980604888

**Table A-4** Experimental results for run with coal feed rate = 1.6 kg/h, S/F ratio= 0.75, and bed Temperature = 820 °C

Components	Time, h				Average composition
	1h	2h	3h	4h	
C <sub>2</sub> H <sub>2</sub>	0.002306325	0.002702543	0.002766973	0.00227486	0.00251268
CO <sub>2</sub>	0.158602112	0.194842072	0.186216757	0.17732584	0.1792467
C <sub>2</sub> H <sub>4</sub>	0.000342471	0.000386604	0.000445286	0.00036573	0.00038502
C <sub>2</sub> H <sub>6</sub>	0.000860847	0.001335741	0.001399712	0.00108894	0.00117131
H <sub>2</sub> S	6.96721E-05	0.009201496	0.009746378	0.0083191	0.00683416
COS	0.000312021	0.000266423	0.00027608	0.00017875	0.00025832
C <sub>3</sub> H <sub>6</sub>	0.000417355	0.000583298	0.000654722	0.00056779	0.00055579
C <sub>3</sub> H <sub>8</sub>	0.000218338	0.000470761	0.000487015	0.00037432	0.00038761
H <sub>2</sub>	0.137851367	0.149982132	0.141714564	0.12460911	0.13853929
O <sub>2</sub>	0.011008259	0.005985056	0.002801058	0.00413723	0.0059829
N <sub>2</sub>	0.550357031	0.530279292	0.522210201	0.54058395	0.53585762
CH <sub>4</sub>	0.011324644	0.013195418	0.013632404	0.01126458	0.01235426
CO	0.096082054	0.090226822	0.099359297	0.11998126	0.10141236
total	0.969752496	0.999457657	0.981710446	0.99107147	0.98549802

**Table A-5** Experimental results for run with coal feed rate = 1.43 kg/h, S/F ratio= 0.75, and bed Temperature = 850 °C

Components	Time, h				Average composition
	1h	2h	3h	4h	
C <sub>2</sub> H <sub>2</sub>	0.002265017	0.004744703	0.004424898	0.004243703	0.00391958
CO <sub>2</sub>	0.157375237	0.214339744	0.199394878	0.21944888	0.197639685
C <sub>2</sub> H <sub>4</sub>	0.000496941	0.000703129	0.000549707	0.000583399	0.000583294
C <sub>2</sub> H <sub>6</sub>	0.000777357	0.002375	0.001929071	0.001984774	0.00176655
H <sub>2</sub> S	0	0.008394918	0.004991976	0.00580703	0.004798481
COS	0.000662215	0.000426959	0.000328892	0.000319466	0.000434383
C <sub>3</sub> H <sub>6</sub>	0.000542127	0.001009879	0.000756137	0.00085429	0.000790608
C <sub>3</sub> H <sub>8</sub>	0.000155486	0.000632648	0.000476376	0.000538823	0.000450833

H <sub>2</sub>	0.166571164	0.195136255	0.198917333	0.198722869	0.189836905
O <sub>2</sub>	0.011837868	0.004249321	0.00786824	0.006234167	0.007547399
N <sub>2</sub>	0.515558541	0.443162276	0.456380055	0.460174214	0.468818771
CH <sub>4</sub>	0.011270936	0.022799118	0.02153337	0.020534257	0.01903442
CO	0.114267601	0.075244142	0.083976704	0.07207575	0.08639105
total	0.981780491	0.973218092	0.981527638	0.991521623	0.982011961

**Table A-6** Experimental results for run with coal feed rate = 1.43 kg/h, S/F ratio= 0.5, and bed Temperature = 850 °C

Components	Time, h				Average composition
	1h	2h	3h	4h	
C <sub>2</sub> H <sub>2</sub>	0.002458947	0.002622475	0.002594853	0.00247715	0.00253835
CO <sub>2</sub>	0.151362158	0.150986342	0.135391676	0.12039571	0.13953397
C <sub>2</sub> H <sub>4</sub>	0.000354014	0.000337106	0.000342797	0.00032101	0.00033873
C <sub>2</sub> H <sub>6</sub>	0.000990537	0.001073641	0.001111706	0.00104483	0.00105518
H <sub>2</sub> S	0.001413134	0.003335527	0.002398963	0	0.00178691
COS	0.000366918	0.000205746	0.000180629	0.00016375	0.00022926
C <sub>3</sub> H <sub>6</sub>	0.0004984	0.000456077	0.000433402	0.00040156	0.00044736
C <sub>3</sub> H <sub>8</sub>	0.000283417	0.000320087	0.000324001	0.00030637	0.00030847
H <sub>2</sub>	0.145178727	0.158290985	0.148948713	0.13122711	0.14591138
O <sub>2</sub>	0.011230844	0.00965902	0.02324855	0.03715	0.0203221
N <sub>2</sub>	0.550767421	0.543095895	0.55938098	0.566622	0.55496657
CH <sub>4</sub>	0.01233565	0.01333343	0.013306075	0.01280995	0.01294628
CO	0.114782567	0.112672283	0.109507736	0.108904	0.11146665
total	0.992022734	0.996388613	0.997170078	0.98182344	0.99185122

**Table A-7** Experimental results for run with coal feed rate = 1.43 kg/h, S/F ratio= 0.75, and bed Temperature = 820 °C

Components	Time, h				Average composition
	1h	2h	3h	4h	
C <sub>2</sub> H <sub>2</sub>	0.002290908	0.002448194	0.002960809	0.002773884	0.002618449

CO <sub>2</sub>	0.152889123	0.154567976	0.187780861	0.149209258	0.161111804
C <sub>2</sub> H <sub>4</sub>	0.0003486	0.000298078	0.000406734	0.000364547	0.00035449
C <sub>2</sub> H <sub>6</sub>	0.000837369	0.000875956	0.001407027	0.001150437	0.001067697
H <sub>2</sub> S	0.001123349	0.002576962	0.006595844	0.003382679	0.003419708
COS	0.000254837	0.000239174	0.000187502	0.000185131	0.000216661
C <sub>3</sub> H <sub>6</sub>	0.000434475	0.000374073	0.000595717	0.000419883	0.000456037
C <sub>3</sub> H <sub>8</sub>	0.000213029	3.0284E-06	0.000491216	0.000332592	0.000259966
H <sub>2</sub>	0.140757556	0.151077607	0.148181104	0.14536653	0.146345699
O <sub>2</sub>	0.014997592	0.010202098	0.004981379	0.017271372	0.01186311
N <sub>2</sub>	0.565715815	0.554421989	0.529894943	0.55443124	0.551115997
CH <sub>4</sub>	0.011498012	0.012378225	0.014589372	0.013802957	0.013067142
CO	0.092853912	0.098415563	0.088897158	0.095936954	0.094025897
total	0.984214577	0.987878923	0.986969666	0.984627464	0.985922657

**Table A-8** Experimental results for run with coal feed rate = 1.43 kg/h, S/F ratio= 0.5, and bed Temperature = 820 °C

Components	Time, h				Average composition
	1h	2h	3h	4h	
C <sub>2</sub> H <sub>2</sub>	0.002284047	0.002427051	0.002018163	0.00186619	0.00214886
CO <sub>2</sub>	0.164398047	0.137654492	0.140190666	0.10691734	0.13729014
C <sub>2</sub> H <sub>4</sub>	0.000353223	0.000295236	0.000263034	0.000189	0.00027512
C <sub>2</sub> H <sub>6</sub>	0.000943011	0.000886663	0.000832085	0.00055788	0.00080491
H <sub>2</sub> S	0	0.00142626	0.00252962	0	0.00098897
COS	0.000317103	0.000186032	0.000193642	0.0001427	0.00020987
C <sub>3</sub> H <sub>6</sub>	0.000488656	0.000329527	0.000366888	0.00018471	0.00034244
C <sub>3</sub> H <sub>8</sub>	0.000270254	0.000220753	0.000252463	0.00013656	0.00022001
H <sub>2</sub>	0.133470651	0.13438525	0.124005624	0.11747309	0.12733365
O <sub>2</sub>	0.012706017	0.017988239	0.010391684	0.01542534	0.01412782
N <sub>2</sub>	0.567602501	0.583102167	0.578469557	0.64078526	0.59248987
CH <sub>4</sub>	0.011439872	0.012407362	0.010243056	0.0102535	0.01108595
CO	0.095927292	0.098018216	0.100844835	0.09851455	0.09832622

total	0.990200672	0.989327249	0.970601317	0.99244612	0.98564384
-------	-------------	-------------	-------------	------------	------------

**Table A-9** Experimental results for run with coal feed rate = 1.28 kg/h, S/F ratio= 0.5, and bed Temperature = 850 °C

Components	Time, h				Average composition
	1h	2h	3h	4h	
C <sub>2</sub> H <sub>2</sub>	0.00156703	0.001665332	0.001742091	0.002005489	0.001744986
CO <sub>2</sub>	0.12938754	0.13305519	0.129811132	0.133905843	0.131539927
C <sub>2</sub> H <sub>4</sub>	0.000605584	0.000575692	0.000536466	0.000494923	0.000553166
C <sub>2</sub> H <sub>6</sub>	0.000335994	0.000377172	0.000392557	0.000438343	0.000386017
H <sub>2</sub> S	0	0.001144873	0.00108254	0.000910745	0.00078454
COS	0.000343163	0.000325521	0.000411018	0.000691383	0.000442771
C <sub>3</sub> H <sub>6</sub>	0.000270031	0.00028024	0.000288175	0.000299458	0.000284476
C <sub>3</sub> H <sub>8</sub>	3.24721E-05	3.42206E-05	3.73891E-05	4.34162E-05	3.68745E-05
H <sub>2</sub>	0.13834578	0.145317652	0.142922647	0.147538307	0.143531096
O <sub>2</sub>	0.020859627	0.013266659	0.014305532	0.009941028	0.014593212
N <sub>2</sub>	0.572083693	0.581105806	0.567357237	0.561495903	0.57051066
CH <sub>4</sub>	0.008055324	0.008315934	0.00879704	0.00994715	0.008778862
CO	0.107048352	0.100999939	0.117013246	0.121907197	0.111742183
total	0.978934591	0.98646423	0.984697071	0.989619186	0.984928769

**Table A-10** Experimental results for run with coal feed rate = 1.28 kg/h, S/F ratio= 0.75, and bed Temperature = 850 °C

Components	Time, h				Average composition
	1h	2h	3h	4h	
C <sub>2</sub> H <sub>2</sub>	0.001797012	0.002021935	0.002198579	0.00377329	0.0024477
CO <sub>2</sub>	0.127993714	0.143085875	0.137802666	0.17008391	0.14474154
C <sub>2</sub> H <sub>4</sub>	0.000695936	0.000648392	0.000544405	0.0005545	0.00061081
C <sub>2</sub> H <sub>6</sub>	0.000343338	0.000462851	0.000540218	0.00162855	0.00074374
H <sub>2</sub> S	0	0.00214765	0.001076735	0.00313484	0.00158981
COS	0.000360093	0.000405311	0.000387578	0.00031573	0.00036718

C <sub>3</sub> H <sub>6</sub>	0.000293095	0.000402739	0.000352261	0.0007069	0.00043875
C <sub>3</sub> H <sub>8</sub>	2.41037E-05	4.6104E-05	6.04185E-05	0.00039799	0.00013215
H <sub>2</sub>	0.158825849	0.160338081	0.168421954	0.18402552	0.16790285
O <sub>2</sub>	0.021301165	0.011379134	0.013942175	0.0140989	0.01518034
N <sub>2</sub>	0.547284468	0.523859175	0.535733988	0.48202189	0.52222488
CH <sub>4</sub>	0.009095732	0.010162501	0.010874465	0.01862816	0.01219022
CO	0.111167022	0.121315824	0.109373974	0.09569849	0.10938883
total	0.979181529	0.976275573	0.981309418	0.97506866	0.9779588

**Table A-11** Experimental results for run with coal feed rate = 1.28 kg/h, S/F ratio= 0.5, and bed Temperature = 820 °C

Components	Time, h				Average composition
	1h	2h	3h	4h	
C <sub>2</sub> H <sub>2</sub>	0.002173413	0.002218425	0.002115216	0.001800574	0.002076907
CO <sub>2</sub>	0.163552056	0.146507957	0.144876341	0.165615145	0.155137875
C <sub>2</sub> H <sub>4</sub>	0.0004595	0.000314957	0.000261291	0.000267157	0.000325726
C <sub>2</sub> H <sub>6</sub>	0.000906635	0.00083483	0.000785036	0.000836716	0.000840804
H <sub>2</sub> S	0	0	0	0.001746953	0.000436738
COS	0.000185161	0.000207783	0.000167635	0.000143466	0.000176011
C <sub>3</sub> H <sub>6</sub>	0.000503712	0.000371522	0.000291273	0.000386737	0.000388311
C <sub>3</sub> H <sub>8</sub>	0.000232634	0.000212736	0.000197015	0.000263894	0.00022657
H <sub>2</sub>	0.135551636	0.13748912	0.132089596	0.117726744	0.130714274
O <sub>2</sub>	0.015006184	0.021711073	0.016165124	0.013874408	0.016689197
N <sub>2</sub>	0.566495526	0.574816609	0.588652033	0.59086987	0.58020851
CH <sub>4</sub>	0.010814728	0.011077599	0.010604146	0.009040308	0.010384195
CO	0.095545146	0.097903941	0.08462492	0.083202968	0.090319244
total	0.991426332	0.993666552	0.980829625	0.98577494	0.987924362

**Table A-12** Experimental results for run with coal feed rate = 1.28 kg/h, S/F ratio= 0.75, and bed Temperature = 820 °C

Components	Time, h				Average composition
	1h	2h	3h	4h	
C <sub>2</sub> H <sub>2</sub>	0.002185814	0.002258338	0.002660507	0.00195213	0.0022642
CO <sub>2</sub>	0.161604257	0.166223209	0.146568554	0.14971002	0.15602651
C <sub>2</sub> H <sub>4</sub>	0.000493145	0.000310431	0.000371058	0.00028776	0.0003656
C <sub>2</sub> H <sub>6</sub>	0.000833926	0.000923381	0.001303391	0.00093343	0.00099853
H <sub>2</sub> S	0.002266008	0.004616646	0.003139344	0.00167178	0.00292344
COS	0.000406813	0.000368262	0.000181076	0.0001958	0.00028799
C <sub>3</sub> H <sub>6</sub>	0.000574422	0.000453856	0.000453243	0.00035868	0.00046005
C <sub>3</sub> H <sub>8</sub>	0.000178142	0.00027008	0.000391681	0.00030106	0.00028524
H <sub>2</sub>	0.157675892	0.161965526	0.170063044	0.1668724	0.16414422
O <sub>2</sub>	0.039825875	0.01346979	0.03104875	0.01637776	0.02518054
N <sub>2</sub>	0.532925205	0.551007488	0.542165228	0.52978354	0.53897037
CH <sub>4</sub>	0.011084671	0.011444995	0.013809083	0.01037549	0.01167856
CO	0.088330972	0.078557487	0.071019249	0.09533416	0.08331047
total	0.998385142	0.99186949	0.983174208	0.97415402	0.98689572

**Table A-13** Experimental results for run with coal feed rate = 1.43 kg/h, S/F ratio= 0, and bed Temperature = 850 °C

Components	Time, 1h
C <sub>2</sub> H <sub>2</sub>	0.0021617
CO <sub>2</sub>	0.1372455
C <sub>2</sub> H <sub>4</sub>	0.0004098
C <sub>2</sub> H <sub>6</sub>	0.0011761
H <sub>2</sub> S	0.0070084
COS	0.0002727
C <sub>3</sub> H <sub>6</sub>	0.0006377
C <sub>3</sub> H <sub>8</sub>	0.0003913
H <sub>2</sub>	0.0829505

O <sub>2</sub>	0.0037931
N <sub>2</sub>	0.5875139
CH <sub>4</sub>	0.0111526
CO	0.1540723
total	0.9887859

**Table A-14** Operating conditions for coal gasification experiments and % carbon conversion at each run

Run	Temperature, °C	S/F	Mass of coal, kg/h	H <sub>2</sub> /CO	% Carbon Conversion
1	850	0.5	1.28	1.284	43.61
2	820	0.5	1.28	1.447	43.8
3	820	0.75	1.28	1.970	46.5
4	850	0.75	1.28	1.534	50.8
5	820	0.5	1.6	1.303	54.8
6	820	0.5	1.43	1.295	57.8
7	850	0.5	1.43	1.309	66.4
8	820	0.75	1.6	1.366	67.8
9	820	0.75	1.43	1.556	67.9
10	850	0.5	1.6	1.608	72.9
11	850	0.75	1.43	2.197	92.9
12	850	0.75	1.6	1.772	91.6

## A.2 Algae – Coal gasification experiment results

**Table A-15** Compositions for gases result from co – gasification experiment with 10% algae + 90% coal, with S/F and A/F ratios of 0.5 and 2 respectively

Components	Bed temperature, °C				
	830	840	860	870	880
C <sub>2</sub> H <sub>2</sub>	0.0020744	0.0020464	0.002177	0.0019942	0.0004445
CO <sub>2</sub>	0.126217	0.1320851	0.1305432	0.0998472	0.0879027

C <sub>2</sub> H <sub>4</sub>	0.0002957	0.0002971	0.0003279	0.0002807	7.612E-05
C <sub>2</sub> H <sub>6</sub>	0.0009333	0.0009544	0.0011073	0.0009494	0.0002528
COS	0.0001934	0.0002265	0.0002074	0.0001878	0.0001731
C <sub>3</sub> H <sub>6</sub>	0.0003484	0.0003976	0.00046	0.0003666	0.000115
C <sub>3</sub> H <sub>8</sub>	0.0002394	0.0002756	0.0003329	0.0002739	8.819E-05
H <sub>2</sub>	0.088365	0.0898475	0.0901956	0.0829665	0.0613297
O <sub>2</sub>	0.0255543	0.015273	0.0200416	0.0352059	0.0274913
N <sub>2</sub>	0.6132412	0.6023133	0.6071987	0.6217058	0.6645218
CH <sub>4</sub>	0.0106833	0.0106714	0.011077	0.0105931	0.0030257
CO	0.1154998	0.1219568	0.1226874	0.1221649	0.1313257
total	0.983645	0.976345	0.986356	0.976536	0.9767466

### A.3 Grape seeds – coal gasification experiments results

**Table A-16** Average S/N ratios at different S/F ratios

S/F = 0.20	
Exp. run	S/N ratio
1	37.347499
2	38.3760347
3	39.0743701
Average S/N ratio	38.4328029
S/F = 0.5	
Exp. run	S/N ratio
4	38.2209837
5	36.0782241
6	39.1339832
Average S/N ratio	37.81273034
S/F = 0.75	
Exp. run	S/N ratio
7	38.70584378
8	39.60856286
9	37.5274258
Average S/N ratio	38.61394415

**Table A-17** Average S/N ratios at different A/F ratios

A/F=2.1	
Exp. run	S/N ratio
1	37.347499.2
4	38.22098379
7	38.7.084378
Average S/N ratio	38.931.883
A/F=2.3	
Exp. run	S/N ratio
2	38.37603471
5	37.07822412
8	39.60856286
Average S/N ratio	38.02110723
A/F=2.5	
Exp. run	S/N ratio
3	39.57437509
6	39.13398321
9	37.5274258
Average S/N ratio	38.74526137

**Table A-18** Average S/N ratios at different B/C ratios

B/C = 0.05	
Exp. run	S/N ratio
1	37.347499.2
6	39.13398321
8	39.7.084378
Average S/N ratio	38.7977817
B/C = 0.11	
Exp. run	S/N ratio
2	38.37603471
4	38.22098379
9	37.5274258
Average S/N ratio	38.04331473
B/C = 0.25	
Exp. run	S/N ratio
3	39.57437509

ο	36.07822412
γ	38.70584378
Average S/N ratio	38.119481

**Table A-19** Average S/N ratios at different bed temperatures

Bed Temp.800 °C	
Exp. run	S/N ratio
1	37.34749902
ο	36.07822412
9	37.0274208
Average S/N ratio	36.98438298
Bed Temp.820 °C	
Exp. run	S/N ratio
2	38.37603471
6	39.13398321
7	38.70584378
Average S/N ratio	38.73878723
Bed Temp.850 °C	
Exp. run	S/N ratio
3	39.57437509
4	38.22598369
8	39.60856286
Average S/N ratio	39.13630721

**Table A-20** Average carbon conversion results at different S/F ratios

S/F = 0.20	
Exp. run	Carbon conversion %
1	73.6842981
2	82.9019709
3	90.2179341
Average carbon conversion %	83.9014027
S/F = 0.5	
Exp. run	Carbon conversion %
4	81.0260720
ο	63.6660338
6	90.51054095

Average carbon conversion %	78.56788242
S/F = 0.75	
Exp. run	Carbon conversion %
۷	86.15732146
۸	95.59345163
۹	75.22657517
Average carbon conversion %	85.65911609

**Table A-21** Average carbon conversion results at different A/F ratios

A/F = 2.1	
Exp. run	Carbon conversion %
۱	۷۳.۶۸۴۲۹۸۱۳
۴	۸۱.۰۲۶۰۷۲۰۱
۷	۸۶.۱۰۷۳۲۱۴۶
Average carbon conversion %	۸۰.۴۰۶.۶۴.۰۳
A/F = 2.3	
Exp. run	Carbon conversion %
۲	۸۲.۹۰۱۹۷۰۹۱
۵	۶۳.۶۶۶۰۳۳۸
۸	95.59345163
Average carbon conversion %	80.73732045
A/F = 2.5	
Exp. run	Carbon conversion %
۳	95.21793407
۶	90.51054095
۹	75.22657517
Average carbon conversion %	86.98501673

**Table A-22** Average carbon conversion results at different B/C ratios

B/C = 0.05	
Exp. run	%Conversion
۱	۷۳.۶۸۴۲۹۸۱۳
۶	۹۰.۰۱.۰۴.۰۹۰
۸	۹۰.۰۹۳۴۰۱۶۳
Average carbon conversion %	۸۶.۰۹۶.۰۹۶۹

B/C = 0.11	
Exp. run	%Conversion
۲	۸۲.۹۰۱۹۷۰۹۱
۴	۸۱.۰۲۶۰۷۲۰۱
۹	75.22657517
Average carbon conversion %	79.90170786
B/C = 0.25	
Exp. run	%Conversion
۳	95.21793407
۵	63.6665338
۷	86.15732146
Average carbon conversion %	81.68059644

**Table A-23** Average carbon conversion results at different bed temperatures

Bed Temp.800 °C	
Exp. run	%Conversion
۱	۷۳.۶۸۴۲۹۸۱۳
۵	۶۳.۶۶۶۰۳۳۸
۹	۷۵.۲۲۶۰۷۰۱۷
Average carbon conversion %	۷۰.۸۵۹۱۳۵۷
Bed Temp.820 °C	
Exp. run	%Conversion
۲	۸۲.۹۰۱۹۷۰۹۱
۶	۹۰.۵۱۰۵۴.۹۵
7	86.15732146
Average carbon conversion %	86.53994611
Bed Temp.850 °C	
Exp. run	%Conversion
۳	95.21793407
۴	81.52657251
۸	95.59345163
Average carbon conversion %	90.7793194

**Table A-24** Average gas compositions at different S/F ratios

S/F = 0.20				
Exp. run	Gas compositions			
	CO	CO <sub>2</sub>	H <sub>2</sub>	CH <sub>4</sub>
1	0.12910056	0.12111307	0.12374301	0.1088137
2	0.12998207	0.13327810	0.11002903	0.1120029
3	0.12778107	0.13083108	0.13007147	0.1672024
Average gas composition	0.12870473	0.1300711	0.12474467	0.129023
S/F = 0.5				
Exp. run	CO	CO <sub>2</sub>	H <sub>2</sub>	CH <sub>4</sub>
4	0.11902109	0.13743330	0.14080269	0.1478719
5	0.10808408	0.12099973	0.18020397	0.0747106
6	0.129976674	0.122133382	0.130460289	0.010883692
Average gas composition	0.119194284	0.126855486	0.120505648	0.011013813
S/F = 0.75				
Exp. run	CO	CO <sub>2</sub>	H <sub>2</sub>	CH <sub>4</sub>
7	0.105452075	0.159020885	0.158884088	0.016506029
8	0.158466976	0.121288194	0.135098752	0.011369842
9	0.098483607	0.135236462	0.109567432	0.007881056
Average gas composition	0.120800886	0.13851518	0.134516757	0.011918976

**Table A-25** Average gas compositions at different A/F ratios

A/F = 2.1				
Exp. run	Gas compositions			
	CO	CO <sub>2</sub>	H <sub>2</sub>	CH <sub>4</sub>
1	0.12910056	0.12111307	0.123743014	0.10881371
4	0.119021094	0.137433346	0.140802687	0.14787187
7	0.10402070	0.109020885	0.108884088	0.016506029
Average gas composition	0.11804141	0.139189267	0.142776763	0.014024029
A/F = 2.3				
Exp. run	CO	CO <sub>2</sub>	H <sub>2</sub>	CH <sub>4</sub>
2	0.129982079	0.133278101	0.110029027	0.11200289
5	0.108084083	0.120999728	0.180203969	0.07471061
8	0.158466976	0.121288194	0.135098752	0.011369842
Average gas composition	0.132177876	0.125185358	0.111960583	0.010013897

A/F = 2.5				
Exp. run	CO	CO <sub>2</sub>	H <sub>2</sub>	CH <sub>4</sub>
۳	0.126681573	0.135831579	0.13506147	0.016625237
۶	0.129976674	0.122133382	0.130460289	0.010883692
۹	0.098483607	0.135236462	0.109567432	0.007881056
Average gas composition	0.118380618	0.131067141	0.12502973	0.011796662

**Table A-26** Average gas compositions at different B/C ratios

B/C = 0.05				
Exp. run	Gas compositions			
	CO	CO <sub>2</sub>	H <sub>2</sub>	CH <sub>4</sub>
۱	۰.۱۲۹۱۰۰۵۶	۰.۱۲۱۱۱۳۵۷	۰.۱۲۳۶۴۳۵۱۴	۰.۰۱۰۸۸۱۳۷ ۱
۶	۰.۱۲۹۹۷۶۶۷۴	۰.۱۲۲۱۳۳۳۸۲	۰.۱۳۰۴۶۰۲۸۹	۰.۰۱۰۸۸۳۶۹ ۲
۸	۰.۱۰۸۴۶۶۹۷۶	۰.۱۲۱۲۸۸۱۹۴	۰.۱۳۰۰۹۸۷۵۲	۰.۰۱۱۳۶۹۸۴ ۲
Average gas composition	۰.۱۳۹۱۹۸۰۷	۰.۱۲۱۰۱۱۷۱۰	۰.۱۲۹۷۳۴۱۸۵	۰.۰۱۱۰۴۴۹۶ ۸
B/C = 0.11				
Exp. run	CO	CO <sub>2</sub>	H <sub>2</sub>	CH <sub>4</sub>
۲	۰.۱۲۹۹۸۲۰۶۹	۰.۱۳۳۲۶۸۱۵۱	۰.۱۱۰۵۲۹۰۲۷	۰.۰۱۱۲۰۰۲۸ ۹
۴	۰.۱۱۹۰۲۱۰۹۴	۰.۱۳۷۴۳۳۳۴۶	۰.۱۴۵۸۰۲۶۸۷	۰.۰۱۴۶۸۶۱۸ ۷
9	0.098483607	0.135236462	0.109567432	0.007881056
Average gas composition	0.115995757	0.135312653	0.123633049	0.011255844
B/C = 0.25				
Exp. run	CO	CO <sub>2</sub>	H <sub>2</sub>	CH <sub>4</sub>
۳	0.126681573	0.135831579	0.13506147	0.016625237
۵	0.108084583	0.120999728	0.085253969	0.007471561
۷	0.105452075	0.159020885	0.158884088	0.016506029
Average gas composition	0.113406077	0.138617397	0.126399842	0.013534276

**Table A-27** Average gas compositions at different bed temperatures

Bed Temp.800 °C
-----------------

Exp. run	Gas compositions			
	CO	CO <sub>2</sub>	H <sub>2</sub>	CH <sub>4</sub>
1	0.12910056	0.12111307	0.123763014	0.01088137 1
5	0.108084083	0.120999728	0.080203969	0.00747106 1
9	0.098483607	0.130237662	0.090674332	0.00788100 6
Average gas composition	0.11190720	0.1205783203	0.07104972	0.00874477 3
Bed Temp.820 °C				
Exp. run	CO	CO <sub>2</sub>	H <sub>2</sub>	CH <sub>4</sub>
2	0.129982069	0.133278101	0.110029027	0.01120028 9
6	0.129976764	0.122133382	0.130460289	0.01088379 2
7	0.105452075	0.159020885	0.158884088	0.016506029
Average gas composition	0.121803606	0.138140806	0.134957801	0.012863336
Bed Temp.850 °C				
Exp. run	CO	CO <sub>2</sub>	H <sub>2</sub>	CH <sub>4</sub>
3	0.126681573	0.135831579	0.13506147	0.016625237
4	0.119521594	0.137433346	0.145802687	0.014686187
8	0.158466976	0.121288194	0.135098752	0.011369842
Average gas composition	0.134890048	0.131517706	0.138654303	0.014227089

**Table A-28** Experimental results for the best coal-grape seeds experiment with A/F = 2.5, S/F ratio= 0.75, B/C =0.05, and bed Temperature = 850 °C

H <sub>2</sub> /CO ratio = 1.57, Carbon conversion = 96.1 %	
Components	Average molar composition
C <sub>2</sub> H <sub>2</sub>	0.0021786
CO <sub>2</sub>	0.1184116
C <sub>2</sub> H <sub>4</sub>	0.0009147
C <sub>2</sub> H <sub>6</sub>	0.0009438
H <sub>2</sub> S	1.203E-05
COS	0.0003763
C <sub>3</sub> H <sub>6</sub>	0.0007018

C <sub>3</sub> H <sub>8</sub>	0.0001457
H <sub>2</sub>	0.1975575
O <sub>2</sub>	0.0147256
N <sub>2</sub>	0.5167189
CH <sub>4</sub>	0.0102136
CO	0.1257861
Total	0.9886862

## Appendix B

### Experimental calculations

#### B.1 Minimum fluidisation velocity experimental results

**Table B-1** Experimental results of pressure drop values for each superficial gas velocity

$U_0$ , m/s	0	0.01	0.035	0.053	0.071	0.089
$\Delta P$ , pa	2	70	358	503	794	1153
$U_0$ , m/s	0.096	0.107	0.179	0.250	0.322	0.393
$\Delta P$ , pa	950	670	683	646	700	772

#### B.2 Correction for minimum fluidization velocity

For two different gases the following equations are used to calculate the flow rates:

$$Q_1 \sqrt{\rho_1} = C_d A_2 \sqrt{\frac{2(-\Delta p)}{1 - \left(\frac{A_2}{A_1}\right)^2}} \quad (\text{B.1})$$

$$Q_2 \sqrt{\rho_2} = C_d A_2 \sqrt{\frac{2(-\Delta p)}{1 - \left(\frac{A_2}{A_1}\right)^2}} \quad (\text{B.2})$$

For a given value of the float position, the discharge coefficient  $C_d$ , the annular area  $A_2$ , and gas pressure drop  $-\Delta p$ , across the float are all constant then:

$$Q_1 \sqrt{\rho_1} = Q_2 \sqrt{\rho_2} \quad (\text{B.3})$$

$$\text{Or: } Q_2 = Q_1 \sqrt{\frac{\rho_1}{\rho_2}}$$

$$U_2 = U_1 \sqrt{\frac{\rho_1}{\rho_2}} \quad (\text{B.4})$$

Equation B.4 is used to correct the flow rate under different gases and temperatures (Ammar, 2009).

From figure 5-1 the velocity at minimum fluidization is 0.09 m/s at 25 °C, equation B.4 can be used to find the value of  $U_{mf}$  at 400 °C.

$$\rho = \frac{p.M}{R.T} \quad (B.5)$$

$$\rho_1 = \frac{101325 * 29}{8.314 * (25 + 273.15) * 1000}$$

$$\rho_1 = 1.185 \text{ Kg/m}^3 \text{ At } 25^\circ\text{C}$$

$$\rho_2 = \frac{101325 * 29}{8.314 * (400 + 273.15) * 1000}$$

$$\rho_2 = 0.525 \text{ Kg/m}^3 \text{ At } 400^\circ\text{C}$$

$$U_2 = 0.09 \sqrt{\frac{1.185}{0.525}}$$

$$U_2 = 0.135 \text{ m/s} \quad \text{At } 400^\circ\text{C}$$

### B.3 Steam calibration results

**Table B-2** Calibration data of water flow rate and mass flow rate

Reading (L/min)	0.07	0.08	0.1	0.115	0.13	0.15	0.16	0.18	0.2
Mass flow rate (g/h)	78	189	426	516	692	822.9	1047	1164	1357

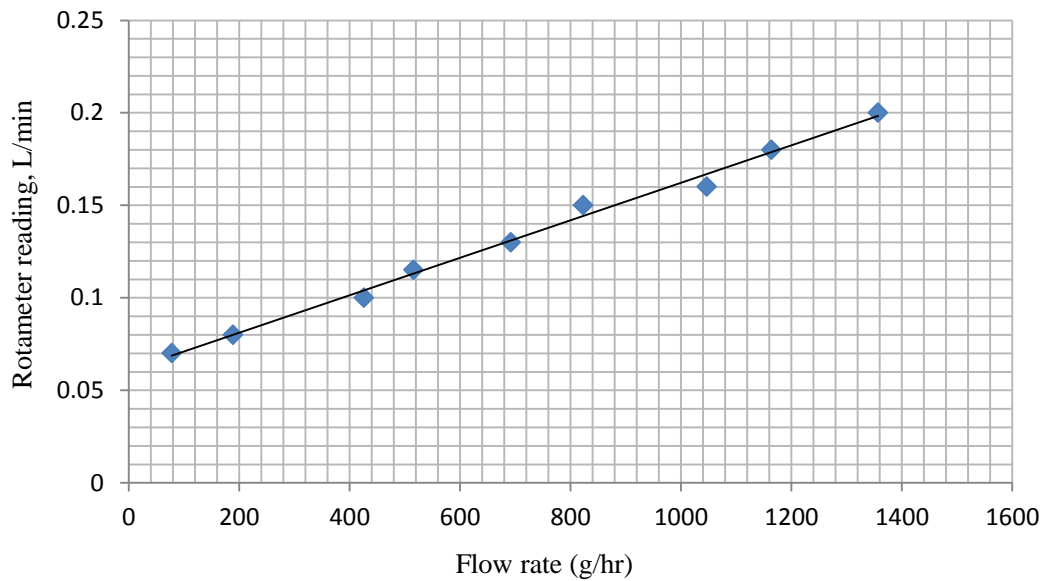


**Figure B-1** Relation between the mass flow rate of the water and rotameter readings

### B.4 Feeding velocity of the fuel

**Table B-3** Experimental results for the feed settling velocity experiment

Feed settling	1	2	3	4	5	6
Feed rate (g/h)	466.2	795	1137	1470	1700.4	2103

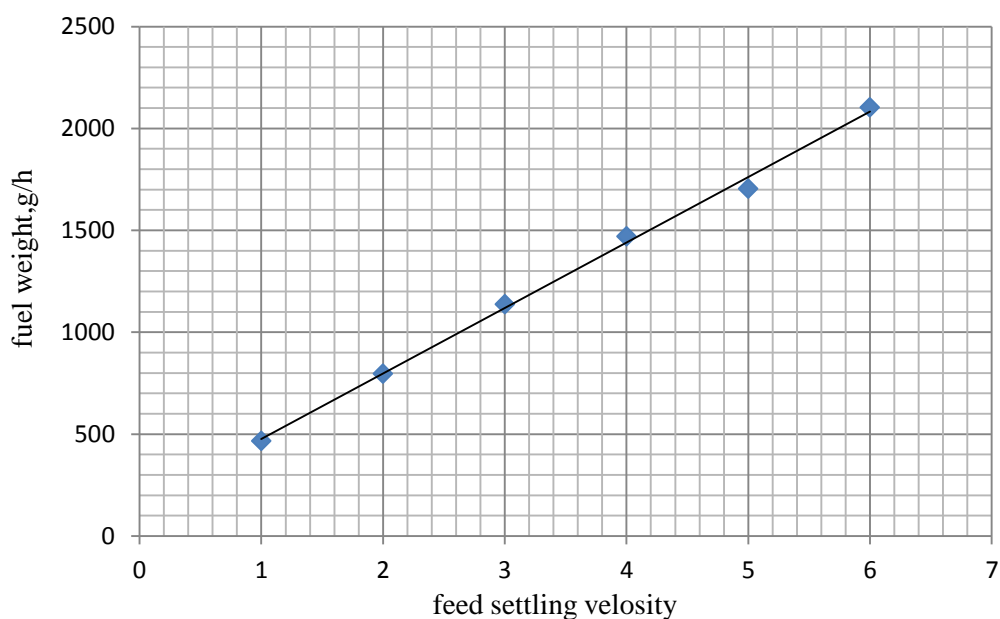


**Figure B-2** Relation between feed settler velocity and the weight of fuel

## B.5 Algae salt content calculation

**Table B-4** Experimental results for the volatile and non-volatile in the algae

Sample	Crucible weight, g	mass of crucible + algae before burning, g	Mass of algae (dry),g	mass of crucible + algae after burning, g	Mass of ash, g	Non volatile	Volatile
1	23.4018	25.7725	2.3707	24.3846	0.9828	0.4145611	0.5854389
2	27.4798	30.3689	2.8891	28.6698	1.19	0.411892977	0.588107
3	26.4015	28.9327	2.5312	27.4433	1.0418	0.411583439	0.5884166
4	22.3683	24.5571	2.1888	23.3006	0.9323	0.425941155	0.5740588

Non volatile (average) = 0.415995

Conductance readings (mS) = 0.457

Concentration of sodium chloride = 221.3759 mg/L

<http://www.scribd.com/doc/2751385/Conductivity-Measurement>

Mass of ash = Weight of crucible with algae after burning – Weight of crucible (B.6)

Mass of ash (average) = 1.036725 g

Mass of algae(average) = 2.49495 g

$$\% \text{ Non volatile} = \frac{\text{Mass of ash}}{\text{Mass of algae}} \quad (\text{B.7})$$

$$\% \text{ Volatile} = \frac{\text{Mass of algae} - \text{Mass of ash}}{\text{Mass of algae}} \quad (\text{B.8})$$

$\% \text{ Volatile} = 0.599$

$$\text{Nacl \%} = \frac{\text{Weight of salt}}{\text{Weight of algae}} * 100\% \quad (\text{B.9})$$

Weight of salt = Concentration of salt \* volume of solution  
(B.10)

$$\text{Weight of salt} = 221.3759 \frac{\text{mg}}{\text{L}} * \frac{1 \text{ L}}{1000 \text{ mL}} * 362.7 \text{ mL}$$

Weight of salt = 80.29303 mg = 0.08029303 g

Weight of leached algae = 0.93 g

$$\text{Nacl \%} = \frac{0.08029303 \text{ g}}{0.93 \text{ g}} * 100\%$$

Nacl % = 8.6336 %

Salt content = Nacl % \* Non volatile (B.11)

Salt content = 0.086336 \* 0.415995

Salt content = 0.035915

Ash = 1 - Volatile - Salt content (B.12)

Ash = 1 - 0.584005 - 0.035915

Ash = 0.38008

The salt content in algae was calculated before leaching with the same previous procedure and it was 42.7 %.

## Appendix C

### Kinetic rate expressions and fuel compositional information

#### C.1 Kinetic rate expression and kinetic constants for gasification reactions

**Table C-1** Gasification reaction rates expressions (Mendes et al., 2008)

No.	Reaction	Kinetic rate expression and kinetic constants, mol/m <sup>3</sup> .s	Reference
1	$C + \phi O_2 \rightarrow 2(1 - \phi)CO + (2\phi - 1)CO_2$ $0.5 \leq \phi \leq 1$	$R1 = \frac{6}{dp M_c} K1[O_2]$ $K1 = 11.34 * 10^3 \exp\left(\frac{-71160}{R_g T_p}\right)$	<b>Saito et al., (1983)</b>
2	$CO + 0.5O_2 \rightarrow CO_2$	$R2 = K2[CO][O_2]$ $K2 = 8.83 * 10^{11} \exp\left(\frac{-99800}{R_g T_g}\right)$	<b>Tenser, (1960)</b>
3	$C + 2H_2 \rightarrow CH_4$	$R3 = \frac{6}{dp} K3[H_2]$ $K3 = 2.08 * 10^3 \exp\left(\frac{-230274}{R_g T_p}\right)$	<b>Biba et al., (1978)</b>
4	$CO + H_2O \leftrightarrow CO_2 + H_2$	$R4 = K4,1 \left( [CO][H_2O] - \frac{[CO_2][H_2]}{K4,2} \right)$ $K4,1 = 2.778 \exp\left(\frac{-12560}{R_g T_g}\right)$ $K4,2 = 0.0265 \exp\left(\frac{32910}{R_g T_g}\right)$	<b>Biba et al., (1978)</b>
5	$C + CO_2 \leftrightarrow 2CO$	$R5 = \frac{K5,1[CO_2]}{1+K5,2[CO_2]+K5,3[CO]} \frac{\rho_p F_c}{M_c} (1 + 11X_c - 7.8X_c^2)$ $K5,1 = 4.89 * 10^{10} \exp\left(\frac{-268000}{R_g T_p}\right)$ $K5,2 = 6.6 * 10^{-2}$	<b>Matsui et al., (1985)</b>

		$K_{5,3} = 0.15 \exp\left(\frac{25500}{R_g T_p}\right)$	
6	$C + H_2O \rightarrow CO + H_2$	$R_6 = \frac{K_{6,1}[H_2O]}{1+K_{6,2}[H_2O]+K_{6,3}[H_2]+K_{6,4}[CO]} \frac{\rho_p F_c}{M_c} (1 + 11X_c - 7.8X_c^2)$ $K_{6,1} = 2.38 * 10^2 \exp\left(\frac{-129000}{R_g T_p}\right)$ $K_{6,2} = 3.16 * 10^{-2} \exp\left(\frac{-30100}{R_g T_p}\right)$ $K_{6,3} = 5.36 * 10^{-3} \exp\left(\frac{-59800}{R_g T_p}\right)$ $K_{6,4} = 8.25 * 10^{-5} \exp\left(\frac{-96100}{R_g T_p}\right)$	<b>Matsui et al., (1987)</b>
7	$CH_4 + H_2O \leftrightarrow CO + 3H_2$	$R_7 = K_{7,1} \left( [CH_4][H_2O] - \frac{[CO][H_2]^2}{K_{7,2}} \right) \frac{M_c}{\rho_c F_c}$ $K_{7,1} = 7.301 * 10^{-2} \exp\left(\frac{-36150}{R_g T_g}\right)$ $K_{7,2} = 5.12 * 10^{-14} \exp\left(\frac{27347}{T_g}\right)$	<b>Wang and Kinoshita, (1993)</b>

## C.2 Fuel compositional information

**Table C-2** Coal compositional information

Coal analysis	Composition
Ultimate Analysis(% db)	
carbon	56.4
Hydrogen	5.1
Sulphur	3.3
Nitrogen	0.6
Oxygen	23.4
Sodium in ash (%)	5.2
Ash Analysis (% in ash)	
SiO <sub>2</sub>	19.3
Al <sub>2</sub> O <sub>3</sub>	12.3
Fe <sub>2</sub> O <sub>3</sub>	1.68
TiO <sub>2</sub>	0.33
K <sub>2</sub> O	0.89

MgO	17.7
Na <sub>2</sub> O	12.4
CaO	13.0
SO <sub>3</sub>	23.2

**Table C-3** Grape seeds biomass compositional information

Grape seeds analysis	Composition
<b>Ultimate Analysis(%db)</b>	
C	54.8
H	6.3
N	2.43
S	0.14
Cl	0.05
Na	0.02
K	2.00
<b>Ash Analysis (% in ash)</b>	
LOI	10.5
SiO <sub>2</sub>	4.7
Al <sub>2</sub> O <sub>3</sub>	0.9
Fe <sub>2</sub> O <sub>3</sub>	0.6
TiO <sub>2</sub>	0.1
K <sub>2</sub> O	34.6
MgO	3.4
Na <sub>2</sub> O	0.4
CaO	15.3
SO <sub>3</sub>	2.6
P <sub>2</sub> O <sub>5</sub>	10.2
PbO	0.01
ZnO	0.02

## Appendix D

### Theoretical calculations

#### D.1 Spouting diameter ( $D_s$ )

The diameter of the spout can be calculated from **Hook et al., (1992)** correlation:

$$\frac{D_s}{D_c} = \left( \frac{2.028 \rho_g U_{in}'^2}{(\rho_p - \rho_g)(1 - \varepsilon_{mf})gD_c} \right)^{\frac{1}{4}} \quad (D.1)$$

Where:

$$U_{in}' = \frac{d_{in}^2 U_{in}}{D_c^2} \quad (D.2)$$

$U_{in}$  is the velocity of the gas at injection point and can be calculated from:

$$U_{in} = \frac{Q}{A_{in}} \quad (D.3)$$

$$A_{in} = \frac{\pi}{4} d_{in}^2 \quad (D.4)$$

$$A_{in} = \frac{\pi}{4} * (12.83 * 10^{-3})^2 = 1.29 * 10^{-4} m^2$$

$$U_{in} = \frac{5.83 * 10^{-4}}{1.29 * 10^{-4}} = 4.5 \frac{m}{s}$$

$$U_{in}' = \frac{(12.83 * 10^{-3})^2 * 4.5}{(0.077)^2} = 0.124 \frac{m}{s}$$

$$\rho = \frac{P.Mwt.}{RT} \quad (D.5)$$

$$\rho_{air} = \frac{101325 * 29}{8.314 * (850 + 273.15) * 1000} = 0.314 \frac{kg}{m^3}$$

$$\rho_{steam} = \frac{101325 * 0.0183}{8.314 * (850 + 273.15) * 1000} = 1.98 * 10^{-4} \frac{kg}{m^3}$$

$$mass\ of\ air = Q \cdot \rho_{air} \quad (D.6)$$

$$mass\ of\ air = 1.83 * 10^{-4} \frac{kg}{s}$$

$$\left( \frac{Steam}{Fuel} \right)_{ratio} = \frac{mass\ of\ fuel * Mc + mass\ of\ steam}{mass\ of\ fuel (1 - Mc)} \quad (D.7)$$

$$M_c = 0.19$$

$$\text{mass of steam} = 0.5 * 1.6 * (1 - 0.19) - 1.6 * 0.19 = 9.56 * 10^{-5} \frac{kg}{s}$$

$$Y_{air} = \frac{\text{mass of air}}{\text{mass of air} + \text{mass of steam}} \quad (D.8)$$

$$Y_{steam} = \frac{\text{mass of steam}}{\text{mass of steam} + \text{mass of air}} \quad (D.9)$$

$$Y_{air} = 0.657$$

$$Y_{steam} = 0.343$$

$$\rho_{gas} = 0.314 * 0.657 + 1.98 * 10^{-4} * 0.343 = 0.206 \frac{kg}{m^3}$$

$$\text{wt. Coal} = (1.6 * 4.5) = 7.2 \text{ kg}$$

$$\text{wt. Sand} = 0.2 \text{ kg}$$

$$\% \text{ Coal} = \frac{7.2}{7.4} = 0.97$$

$$\% \text{ Sand} = \frac{0.2}{7.4} = 0.03$$

$$\rho_{solid} = 672.28 * 0.97 + 1593.8 * 0.03 = 699.9 \cong 700 \frac{kg}{m^3}$$

$$D_s = 0.077 * \left[ \frac{2.028 * 700 * 0.124^2}{(700 - 0.206) * (1 - 0.45) * 9.81 * 0.077} \right]^{1/4}$$

$$D_s = 0.04 \text{ m}$$

## D.2 Spouting velocity ( $u_s$ )

$$u_s = \frac{Q}{A_s} \quad (D.10)$$

$$A_s = \frac{\pi}{4} * 0.04^2 = 1.25 * 10^{-3} \text{ m}^2$$

$$u_s = 0.46 \frac{m}{s}$$

## D.3 Bed porosity ( $\epsilon_s$ )

The spout voidage is assumed to decrease linearly with  $z$ , so it will be a variable and can be calculated at each axial distance point from the following equation (Smith et al., 1981):

$$\varepsilon_s(z) = 1 - 0.2 \frac{z}{H} \quad (\text{D.11})$$

$z$  represents the axial distance from the gas inlet, and  $H$  is the height of the bed inside the gasifier and it can be calculated using **Grbavcic, et al., (1976)** correlation:

$$u_{ms} = u_{mf} \left( 1 - \left( 1 - \frac{H}{H_m} \right)^3 \right) \quad (\text{D.12})$$

$u_{ms}$  represents the velocity of the gas – phase at minimum spouting conditions and can be calculated using **Wu, et al., (1987)** correlation:

$$u_{ms} = 10.6 \left[ \frac{d_p}{D_c} \right]^{1.05} \left[ \frac{d_{in}}{D_c} \right]^{0.266} \left[ \frac{H_c}{D_c} \right]^{-0.095} \left[ \frac{(\rho_p - \rho_g)}{\rho_g} \right]^{0.256} \sqrt{2gH_c} \quad (\text{D.13})$$

$u_{mf}$  is the velocity of the gas – phase at minimum fluidization conditions and can be calculated from **Littman et al., (1981)** correlation:

$$u_{mf} = 42.9(1 - \varepsilon_{mf}) \frac{\mu_g}{\rho_g D_p} \left[ \left\{ 1 + (3.111 * 10^{-4}) * \frac{\varepsilon_{mf}^3 Ar}{(1 - \varepsilon_{mf})^2} \right\}^{\frac{1}{2}} - 1 \right] \quad (\text{D.14})$$

Where:

$$Ar = \frac{d_p^3 \rho_f (\rho_p - \rho_f) g}{\mu_f^2}$$

The maximum spoutable height  $H_m$  can be calculated from **Wu et al., (1987)** correlation:

$$H_m = \left[ \frac{D_c^2}{d_p} \right] \left[ \frac{D_c}{d_{in}} \right]^{2/3} \left[ \frac{700}{B} \right] \left[ \sqrt{1 + 35.9 * 10^{-6} B} - 1 \right]^2 \quad (\text{D.15})$$

Where:

$$B = \frac{d_p^3 \rho_p (\rho_p - \rho_f) g}{\mu_f^2}$$

$$B = \frac{(2.1294 * 10^{-3})^3 * 700 * (700 - 0.206) * 9.81}{(4.2 * 10^{-5})^2} = 26303311.63$$

$$H_m =$$

$$\frac{0.077^2}{2.1294 * 10^{-3}} * \left[ \frac{0.077}{0.01283} \right]^{2/3} * \left[ \frac{700}{26303311.63} \right] * \left[ \sqrt{1 + 35.9 * 10^{-6} * 26303311.63} - 1 \right]^2$$

$$H_m = 0.211 \text{ m}$$

$$u_{ms} = 10.6 * \left[ \frac{2.1294 * 10^{-3}}{0.077} \right]^{1.05} * \left[ \frac{0.01283}{0.077} \right]^{0.266} * \left[ \frac{1.165}{0.077} \right]^{-0.095} * \left[ \frac{700 - 0.206}{0.206} \right]^{0.256} * \sqrt{2 * 9.81 * 1.165}$$

$$u_{ms} = 4.48 \frac{m}{s}$$

$$u_{mf} = 42.9(1 - 0.45) \frac{4.2 * 10^{-5}}{0.206 * 2.1294 * 10^{-3}} \left[ \left\{ 1 + (3.111 * 10^{-4} * \frac{0.45^3 * 7740.7}{(1 - 0.45)^2}) \right\}^{1/2} - 1 \right]$$

$$u_{mf} = 0.708 \frac{m}{s}$$

The bed height H can be calculated from equation (D.12):

$$H = 0.57 m$$

So, the bed porosity will be calculated from:

$$\varepsilon_s(z) = 1 - 0.2 * \frac{z}{0.57} \tag{D.16}$$

#### D.4 Annulus gas velocity

The superficial annular gas velocity is taken from the theories of **Mamuro and Hattori, (1968)** and **Grbavcic et al., (1976)**.

$$u_a(z) = 0.88 u_{mf} \left[ 1 - \left( 1 - \frac{z}{H_m} \right)^3 \right]$$

$$u_a(z) = 0.88 * 0.708 \left[ 1 - \left( 1 - \frac{z}{0.211} \right)^3 \right] \tag{D.17}$$

Table D-1 shows the values of bed porosity at the spout and the velocities of the gas phase at the annulus region.

**Table D-1** Values of bed porosity at the spout, and gas annulus velocities  $u_a$ 

$Z, m$	0	0.013	0.026	0.039	0.052
$\epsilon_s$	1	0.9954386	0.99087719	0.98631579	0.98175439
$u_{a,m/s}$	0	0.00014571	0.0011657	0.00393425	0.00932564
$Z, m$	0.065	0.078	0.091	0.104	0.117
$\epsilon_s$	0.97719298	0.97263158	0.96807018	0.96350877	0.95894737
$u_{a,m/s}$	0.01821414	0.03147403	0.0499796	0.07460511	0.10622486
$Z, m$	0.13	0.143	0.156	0.169	0.182
$\epsilon_s$	0.95438596	0.94982456	0.94526316	0.94070175	0.93614035
$u_{a,m/s}$	0.14571311	0.19394415	0.25179225	0.3201317	0.39983677
$Z, m$	0.195	0.208	0.221	0.234	0.247
$\epsilon_s$	0.93157895	0.92701754	0.92245614	0.91789474	0.91333333
$u_{a,m/s}$	0.49178174	0.59684089	0.7158885	0.84979884	0.99944621
$Z, m$	0.26	0.273	0.286	0.299	0.312
$\epsilon_s$	0.90877193	0.90421053	0.89964912	0.89508772	0.89052632
$u_{a,m/s}$	1.16570486	1.34944909	1.55155317	1.77289138	2.014338
$Z, m$	0.325	0.338	0.351	0.364	0.377
$\epsilon_s$	0.88596491	0.88140351	0.87684211	0.8722807	0.8677193
$u_{a,m/s}$	2.27676731	2.56105358	2.8680711	3.19869414	3.55379698
$Z, m$	0.39	0.403	0.416	0.429	0.442
$\epsilon_s$	0.86315789	0.85859649	0.85403509	0.84947368	0.84491228
$u_{a,m/s}$	3.93425391	4.34093919	4.77472711	5.23649195	5.72710799
$Z, m$	0.455	0.468	0.481	0.494	0.507
$\epsilon_s$	0.84035088	0.83578947	0.83122807	0.82666667	0.82210526
$u_{a,m/s}$	6.24744949	6.79839076	7.38080605	7.99556965	8.64355584
$Z, m$	0.52	0.533	0.546	0.559	0.572
$\epsilon_s$	0.81754386	0.81298246	0.80842105	0.80385965	0.79929825
$u_{a,m/s}$	9.3256389	10.0426931	10.7955927	11.5852121	12.4124254

## D.5 Boundary layer thickness

The mass transfer coefficient around a spherical pellet can be described by **Frössling correlation** (Fogler, 1999).

$$Sh = 2 + 0.6 Re^{1/2} Sc^{1/3} \quad (D.18)$$

Where:

$$Sh = \frac{kc dp}{D_{AB}} \quad (D.19)$$

$$Re = \frac{U \rho dp}{\mu} \quad (D.20)$$

$$Re = \frac{0.46 * 0.206 * 2.175 * 10^{-3}}{4.2 * 10^{-5}} = 4.9$$

$$Sc = \frac{\mu}{\rho D_{AB}} \quad (D.21)$$

$$Sc = \frac{4.2 * 10^{-5}}{0.206 * 0.73 * 10^{-5}} = 27.9$$

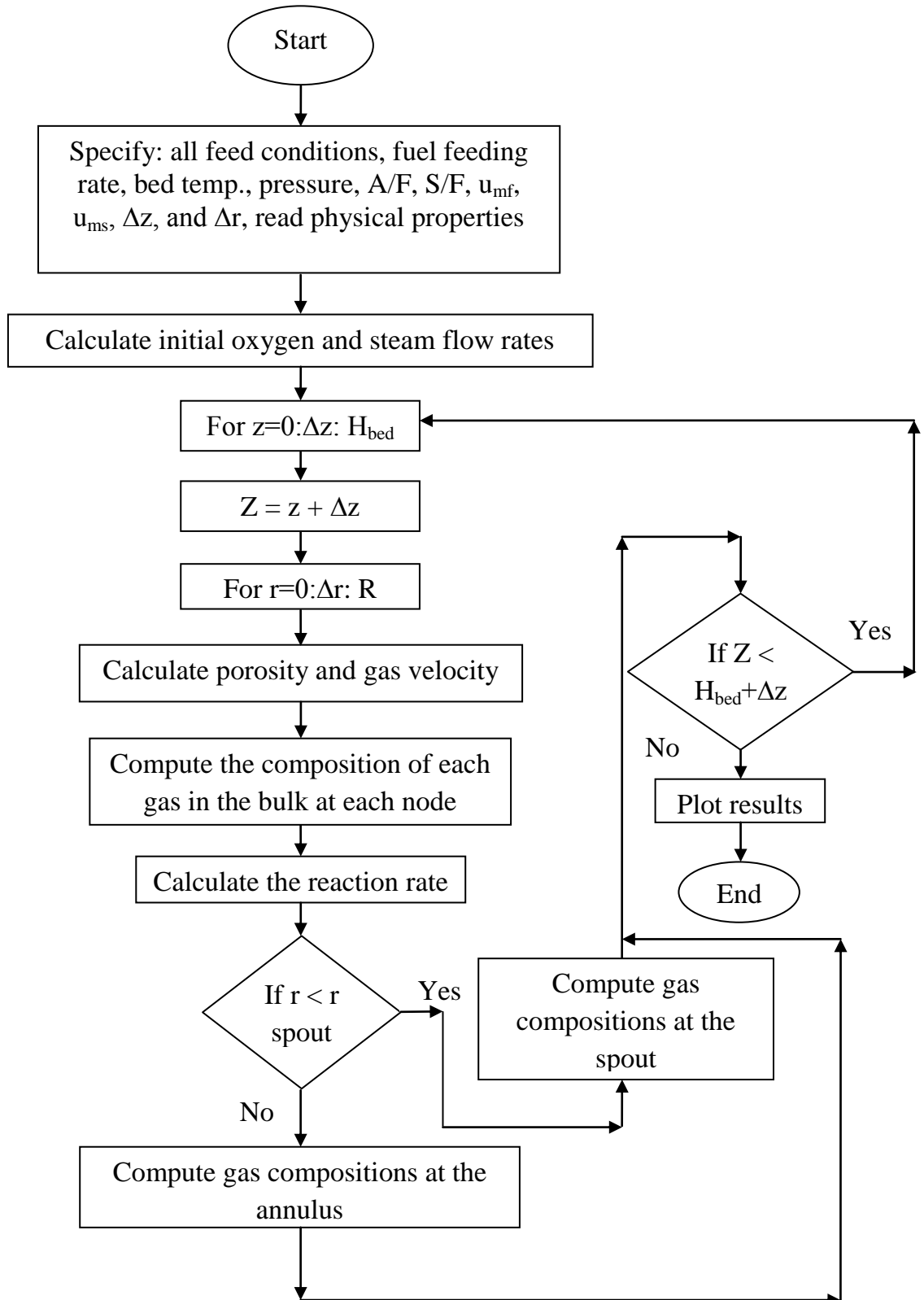
$$Sh = 2 + 0.6 * 4.9^{1/2} * 27.9^{1/3} = \frac{kc * 2.175 * 10^{-3}}{0.73 * 10^{-5}} \rightarrow kc = 0.02 \frac{m}{s}$$

The thickness of boundary layer can be calculated using:

$$Kc = \frac{D_{AB}}{\delta} \quad (D.22)$$

$$\delta = 3.65 * 10^{-4} m$$

## D.6 Block Diagram of Isothermal Model



## D.7 Concentration profile of gases at the spout and annulus program

```

                                %modelling of spouted bed reactor%
                                %spout region%
%program to estimate the concentration of the gas with the bed height
%concentration profile of the gas - phase at the spout region
clc
clear
%Diffusivity of gases at 805C in m2/s
DiCH4=(1.1*((850+273.15)/(500+273.15))^1.75)*10^-5;
DiH2=(0.611*((850+273.15)/(273.15))^1.75)*10^-5;
DiCO=(0.185*((850+273.15)/(273.15))^1.75)*10^-5;
DiCO2=(0.138*((850+273.15)/(273.15))^1.75)*10^-5;
DiH2O=(0.220*((850+273.15)/(273.15))^1.75)*10^-5;
%Diffusivity of oxygen in air at 805C in m2/s
Di=0.73E-5;
%average diameter of coal particles, m
dp=2.175E-3;
% the axial distance from the gas inlet to the free board above the bed
z=0:0.013:0.585;
i=1:1:307;
% voidage (v) in the gasifier is the porosity
for z=0:0.013:0.585;
%height of the bed is 0.57m
H=0.57;
v=1-(0.2*z/H);
% voidage=1-v=V
V=1-v;
dz=0.013;
a=(Di*v)/dz^2;
% uz is the velocity of gas - phase at the spout in m/s
uz=0.46;
e=uz*v/dz;
dr=6.4167E-3;
h=(Di*v)/dr^2;
% R is the porosity when i=i-1
% E is the porosity when i=i+1
R=v+0.0045;
E=v-0.0046;
c=(E+v)/dz;
d=[E-2*v+R]/dz^2;
for r=0.0001:0.00641:0.019245;
g=(Di*v)/(r*dr^2);
end
b=(2*Di)/dz;
% RO2, Rair are the flow rate of oxygen and air respectively,m^3/h
RO2=0.44016;
Rair=2.1;
Cl=RO2/ Rair;

```

```

%Cl=Cb1 at the gasifier entrance
Cb1=C1;
%%%OXYGEN%%%
Ca1= C1*[2*a+c*b-d*Di-e+2*h+g]-[a*Cb1-c*uz+h*Cb1]/[a+c*b-e+h+g];
Ci=(( (a*Ca1)+(a*Cb1)+(c*b*Ca1)-(e*Ca1)-
(c*uz)+(h*Ca1)+(h*Cb1)+(g*Ca1)/[(2*a)+(c*b)-(d*Di)-e+(2*h)+(g)]);
% Ca=C(i+1)which is the concentration of the gas phase for the node i+1
%Cb=C(i-1)which is the concentration of the gas phase for the node i-1
% C is the concentration of gas phase in the bulk at node i, spout region
Cb=Ci*[(2*a)+(c*b)-(d*Di)-e+(2*h)+g]-[(a*Ca1)+(c*b*Ca1)-(e*Ca1)-
(c*uz)+(h*Ca1)+(g*Ca1)]/[a+h];
Ca= Ci*[2*a+c*b-d*Di-e+2*h+g]-[a*Cb-c*uz+h*Cb]/[a+c*b-e+h+g];
C=(( (a*Ca)+(a*Cb)+(c*b*Ca)-(e*Ca)-
(c*uz)+(h*Ca)+(h*Cb)+(g*Ca)/[(2*a)+(c*b)-(d*Di)-e+(2*h)+(g)])/(Fr+Ar));
%dr is the distance between each two nodes from the centre to the wall of
the gasifier
dr=6.41666667E-3;
A1=(Di.*v)/dr^2;
A2=(2*Di.*v)/(r*dr);
%Mc is the molar mass of carbon (kg.mol^-1)
Mc=12;
Rg=8.314;
Tg=(850+273.15);
G=((12/dp*Mc)*11.34*10^3)*exp(-711600/(Rg*Tg));
L=(0.5*8.83)*exp(-99800/(Rg*Tg));
% equation of the gas - phase concentration on the solid surface
% CO2s is the concentration of O2 at the solid surface on the spout
% region
CO2s=((A2*(Ca-C))-(A1*(Ca-2*C+Cb)))/V*(G+L);
aCH4=(DiCH4*v)/dz^2;
% uz is the velocity of gas - phase at the spout in m/s
uz=0.46;
e=uz*v/dz;
dr=6.4167E-3;
%%% Methane %%%
hCH4=(DiCH4*v)/dr^2;
for r=0.0001:0.00641:0.019245;
gCH4=(DiCH4*v)/(r*dr^2);
end
bCH4=(2*DiCH4)/dz;
% C1CH4 is the concentration of methane at z<0.013 m
C1CH4=0;
%Cb1CH4 is the concentration of methane at the gasifier entrance
Cb1CH4=0;
% Ca1 is the concentration of methane at node where z>=0.013 m
Ca1CH4=C1CH4*[2*aCH4+c*bCH4-d*DiCH4-e+2*hCH4+gCH4]-[aCH4*Cb1CH4-
c*uz+hCH4*Cb1CH4]/[aCH4+c*bCH4-e+hCH4+gCH4];
CiCH4=(( (aCH4*Ca1CH4)+(aCH4*Cb1CH4)+(c*bCH4*Ca1CH4)-(e*Ca1CH4)-
(c*uz)+(hCH4*Ca1CH4)+(hCH4*Cb1CH4)+(gCH4*Ca1CH4)/[(2*aCH4)+(c*bCH4)-
(d*DiCH4)-e+(2*hCH4)+(gCH4)]));

```

```

CbCH4=CiCH4*[ (2*aCH4) + (c*bCH4) - (d*DiCH4) -e+ (2*hCH4) +gCH4] -
[ (a*Ca1CH4) + (c*bCH4*Ca1CH4) - (e*Ca1CH4) -
(c*uz) + (h*Ca1CH4) + (gCH4*Ca1CH4) ]/[aCH4+hCH4];
CaCH4=Ci*[2*aCH4+c*bCH4-d*DiCH4-e+2*hCH4+gCH4] - [aCH4*CbCH4-
c*uz+hCH4*CbCH4]/[aCH4+c*bCH4-e+hCH4+gCH4];
% C is the concentration of methane in the bulk
CCH4=(((aCH4*CaCH4) + (aCH4*CbCH4) + (c*bCH4*CaCH4) - (e*CaCH4) -
(c*uz) + (hCH4*CaCH4) + (hCH4*CbCH4) + (gCH4*CaCH4) / [ (2*aCH4) + (c*bCH4) -
(d*DiCH4) -e+ (2*hCH4) + (gCH4) ]));
%%% HYDROGEN %%%
% SOME VARAIBLES DEPEND ON THE PHYSICAL PROPERTIES
aH2=(DiH2*v)/dz^2;
hH2=(DiH2*v)/dr^2;
for r=0.000001:0.00641:0.019245;
gH2=(DiH2*v)/(r*dr^2);
end
bH2=(2*DiH2)/dz;
% C1 is the concentration of hydrogen at z=0
C1H2=(0.04)/(0.04+0.36);
%Cb1 is the concentration of hydrogen at the gasifier entrance
Cb1H2=C1H2;
% Ca1 is the concentration of hydrogen at node where z>=0.013 m
Ca1H2=C1H2*[2*aH2+c*bH2-d*DiH2-e+2*hH2+gH2] - [aH2*Cb1H2-
c*uz+hH2*Cb1H2]/[aH2+c*bH2-e+hH2+gH2];
CiH2=(((aH2*Ca1H2) + (aH2*Cb1H2) + (c*bH2*Ca1H2) - (e*Ca1H2) -
(c*uz) + (hH2*Ca1H2) + (hH2*Cb1H2) + (gH2*Ca1H2) / [ (2*aH2) + (c*bH2) - (d*DiH2) -
e+ (2*hH2) + (gH2) ]));
CbH2=CiH2*[ (2*aH2) + (c*bH2) - (d*DiH2) -e+ (2*hH2) +gH2] -
[ (aH2*Ca1H2) + (c*bH2*Ca1H2) - (e*Ca1H2) -
(c*uz) + (hH2*Ca1H2) + (gH2*Ca1H2) ]/[aH2+hH2];
CaH2=CiH2*[2*aH2+c*bH2-d*DiH2-e+2*hH2+gH2] - [aH2*CbH2-
c*uz+hH2*CbH2]/[aH2+c*bH2-e+hH2+gH2];
z=0:0.013:0.585;
% C is the concentration of hydrogen in the bulk
CH2=(((aH2*CaH2) + (aH2*CbH2) + (c*bH2*CaH2) - (e*CaH2) -
(c*uz) + (hH2*CaH2) + (hH2*CbH2) + (gH2*CaH2) / [ (2*aH2) + (c*bH2) - (d*DiH2) -
e+ (2*hH2) + (gH2) ]));
%%% CARBON MONOXIDE %%%
aCO=(DiCO*v)/dz^2;
hCO=(DiCO*v)/dr^2;
for r=0.0001:0.00641:0.019245;
gCO=(DiCO*v)/(r*dr^2);
end
bCO=(2*DiCO)/dz;
% C1 is the concentration of carbon monoxide at z=0
C1CO=0;
%Cb1 is the concentration of carbon monoxide at the gasifier entrance
Cb1CO=0;
% Ca1 is the concentration of carbon monoxide at node where z>=0.013 m
Ca1CO=C1CO*[2*aCO+c*bCO-d*DiCO-e+2*hCO+gCO] - [aCO*Cb1CO-
c*uz+hCO*Cb1CO]/[aCO+c*bCO-e+hCO+gCO];

```

```

CiCO=(((aCO*Ca1CO)+(aCO*Cb1CO)+(c*bCO*Ca1CO)-(e*Ca1CO)-
(c*uz)+(hCO*Ca1CO)+(hCO*Cb1CO)+(gCO*Ca1CO)/[(2*aCO)+(c*bCO)-(d*DiCO)-
e+(2*hCO)+(gCO)]));
CbCO=CiCO*[(2*aCO)+(c*bCO)-(d*DiCO)-e+(2*hCO)+gCO]-
[(aCO*Ca1CO)+(c*bCO*Ca1CO)-(e*Ca1CO)-
(c*uz)+(hCO*Ca1CO)+(gCO*Ca1CO)]/[aCO+hCO];
CaCO=CiCO*[2*aCO+c*bCO-d*DiCO-e+2*hCO+gCO]-[aCO*CbCO-
c*uz+hCO*CbCO]/[aCO+c*bCO-e+hCO+gCO];
% C is the concentration of carbon monoxide in the bulk
CCO=(((aCO*CaCO)+(aCO*CbCO)+(c*bCO*CaCO)-(e*CaCO)-
(c*uz)+(hCO*CaCO)+(hCO*CbCO)+(gCO*CaCO)/[(2*aCO)+(c*bCO)-(d*DiCO)-
e+(2*hCO)+(gCO)]));
%%% CARBON DIOXIDE %%%
aCO2=(DiCO2*v)/dz^2;
hCO2=(DiCO2*v)/dr^2;
for r=0.0001:0.00641:0.019245;
gCO2=(DiCO2*v)/(r*dr^2);
end
bCO2=(2*DiCO2)/dz;
%Cl is the concentration of carbon dioxide at z=0
C1CO2=0;
%Cb1 is the concentration of carbon dioxide at the gasifier entrance
Cb1CO2=0;
% Cal is the concentration of carbon dioxide at node where z>=0.013 m
Ca1CO2=C1CO2*[2*aCO2+c*bCO2-d*DiCO2-e+2*hCO2+gCO2]-[aCO2*Cb1CO2-
c*uz+hCO2*Cb1CO2]/[aCO2+c*bCO2-e+hCO2+gCO2];
CiCO2=(((aCO2*Ca1CO2)+(aCO2*Cb1CO2)+(c*bCO2*Ca1CO2)-(e*Ca1CO2)-
(c*uz)+(hCO2*Ca1CO2)+(hCO2*Cb1CO2)+(gCO2*Ca1CO2)/[(2*aCO2)+(c*bCO2)-
(d*DiCO2)-e+(2*hCO2)+(gCO2)]));
CbCO2=CiCO2*[(2*aCO2)+(c*bCO2)-(d*DiCO2)-e+(2*hCO2)+gCO2]-
[(aCO2*Ca1CO2)+(c*bCO2*Ca1CO2)-(e*Ca1CO2)-
(c*uz)+(hCO2*Ca1CO2)+(gCO2*Ca1CO2)]/[aCO2+hCO2];
CaCO2=CiCO2*[2*aCO2+c*bCO2-d*DiCO2-e+2*hCO2+gCO2]-[aCO2*CbCO2-
c*uz+hCO2*CbCO2]/[aCO2+c*bCO2-e+hCO2+gCO2];
% C is the concentration of carbon dioxide in the bulk
CCO2=(((aCO2*CaCO2)+(aCO2*CbCO2)+(c*bCO2*CaCO2)-(e*CaCO2)-
(c*uz)+(hCO2*CaCO2)+(hCO2*CbCO2)+(gCO2*CaCO2)/[(2*aCO2)+(c*bCO2)-
(d*DiCO2)-e+(2*hCO2)+(gCO2)]));
%%% STEAM (H2O) %%%
% SOME VARAIBLES DEPEND ON THE PHYSICAL PROPERTIES
aH2O=(DiH2O*v)/dz^2;
hH2O=(DiH2O*v)/dr^2;
for r=0.0001:0.00641:0.019245;
gH2O=(DiH2O*v)/(r*dr^2);
end
bH2O=(2*DiH2O)/dz;
% Cl is the concentration of steam at z=0 m = Cb1
C1H2O=(0.346)/(0.346+2.575);
%Cb1 is the concentration of steam at the gasifier entrance
Cb1H2O=C1H2O;
% Cal is the concentration of steam at node where z>=0.013 m

```



```

k10=7.301*10^-2 *exp((-36150)/(Rg*Tg));
k11=5.12*10^-14 *exp(27347/(Tg));
%%%%%%%%%%%%%%%%%%%%%%%%%%%%%%%%%%%%%%%%%%%%%%%%%%%%%%%%%%%%%%%%%%%%%%%%%
                    %methane%
%CCH4s is the concentration of methane at the spout
CCH4s=(( (A2*(CaCH4+CCH4)) - (A1*(CaCH4-
2*CCH4+CbCH4))) + ((CCO*CH2^2/k11)*H2)/k10*CH2O) * (G+L) /V;
                    %carbon monoxide%
%CCO is the concentration of carbon monoxide
%CCOs is the concentration of carbon monoxide at the solid - surface
BCO=(k1*CH2) + ((1/k3*CCO2*H1) / (1+k4*CCO2+k5)) + ((1/1+k7*CH2O+k8*CH2+k9) -
H2*(CH2^2/k11));
CCOs=(( (A2*(CaCO-CCO)) - (A1*(CaCO-2*CCO+CbCO))) + ((CO2s*CCH4s) /k2) -
(k10*H2*CCH4s*CH2O) /V*BCO;
                    %carbon dioxide%
%CCO2 is the concentration of carbon dioxide in the spout region
%CCO2s is the concentration of carbon dioxide in the spout
CCO2s=(( (A2*(CaCO2-CCO2)) - (A1*(CaCO2-
2*CCO2+CbCO2))) + (k2*((6/dp*Mc)*k1a*CO2s+k2a*CCOs*CO2s+k1*CCOs*CH2O)) /V*k1
*CH2;
                    %Hydrogen%
%CH2 is the concentration of hydrogen
%CH2s is the concentration of hydrogen in the spout
CH2s=(( (A2*(CaH2-CH2)) - (A1*(CaH2-2*CH2+CbH2))) + (-1*k1*CCOs*CH2O-
k10*CCH4s*CH2O) / ((6/dp)*k3a-
k1*CCO2/k2+ ((H1/1+k7*CH2O+k8+k9*CCOs) / (k6*CH2O))) /V;
                    %Steam%
%CH2O is the concentration of steam
%CH2Os is the concentration of steam in the spout
CH2Osc=(( (A2*(CaH2O-CH2O)) - (A1*(CaH2O-
2*CH2O+CbH2O))) + (k1*CCO2s*CH2s/k2) + (k10*CCOs*CH2s^2*H2/k11)) /V;
                    %%% corrected equation %%%
% methane %
CCH4sc=(( (A2*(CaCH4+CCH4)) - (A1*(CaCH4-
2*CCH4+CbCH4))) + ((CCOs*CH2s^2/k11)*H2)/k10*CH2Osc) * (G+L) /V;
%carbon monoxide%
BCO=(k1*CH2) + ((1/k3*CCO2*H1) / (1+k4*CCO2+k5)) + ((1/1+k7*CH2O+k8*CH2+k9) -
H2*(CH2^2/k11));
CCOsc=(( (A2*(CaCO-CCO)) - (A1*(CaCO-2*CCOs+CbCO))) + ((CO2s*CCH4sc) /k2) -
(k10*H2*CCH4sc*CH2Osc) /V*BCO;
%carbon dioxide%
CCO2sc=(( (A2*(CaCO2-CCO2)) - (A1*(CaCO2-
2*CCO2+CbCO2))) + (k2*((6/dp*Mc)*k1a*CO2s+k2a*CCOs*CO2s+k1*CCOs*CH2Osc)) /V*
k1*CH2s;
%Hydrogen%
CH2sc=(( (A2*(CaH2-CH2)) - (A1*(CaH2-2*CH2+CbH2))) + (-1*k1*CCOs*CH2Osc-
k10*CCH4sc*CH2Osc) / ((6/dp)*k3a-k1*CCO2/k2+ ((H1/1+k7*CH2Osc+k8+k9*CCOs) -
((k10*CCOsc^2)/k11) / (k6*CH2Osc))) /V;

```

```

% the concentration of the gas - phase on the solid surface in the
annulus region %
% ua is the velocity of the gas - phase at the annulus region, m/s
% umf is the minimum fluidization velocity of the gas - phase at the
annulus region, m/s
% Hm is the maximum spoutable height, m
for z=0:0.013:0.585;
Hm=0.211;
umf=0.708;
ua=0.88*umf*(1-(1-(z/Hm)^3));
end
b1=(v*ua)/dz;
c1=v/dz;
h=(2*Di*v)/(dr);
hCOa=(2*DiCO*v)/(dr);
hCO2a=(2*DiCO2*v)/(dr);
hH2a=(2*DiH2*v)/(dr);
hH2Oa=(2*DiH2O*v)/(dr);
hCH4a=(2*DiCH4*v)/(dr);
% ra is the radius where the nodes lie at the annulus region
for ra=0.019245:0.00641:0.0385;
z=0:0.013:0.585;
g1=(Di*v)/(ra*dr);
g1CO=(DiCO*v)/(ra*dr);
g1CO2=(DiCO2*v)/(ra*dr);
g1H2=(DiH2*v)/(ra*dr);
g1H2O=(DiH2O*v)/(ra*dr);
g1CH4=(DiCH4*v)/(ra*dr);
end
% Cga is the concentration of the gas - phase at the annulus region
for z=0.013:0.013:0.585;
uai=0.88*umf*(1-(1-(z/Hm)^3));
end
%%%% OXYGEN %%%
%Cba is the of the gas - phase in the annulus region at node i-1
%Cb1 is the initial concentration of the gas - phase in the annulus
region
Cba=Cb1;
%Cga is the initial concentration of the gas - phase at node i=1
Cga=C1;
Caa=(C1*[2*a-b1+2*h+g1]-a*Cba+c1*(uai-ua)-h*Cba)/(a-b1+h+g1);
for z=0:0.013:0.585;
Cga=[(a*Caa)+(a*Cba)-(b1*Caa)-c1*(uai-
ua)+(h*Caa)+(h*Cba)+(g1*Caa)]/[2*a-b1+2*h+g1];
% Cba1 is the concentration of the gas - phase in the annulus region for
% the nodes lie before the node i , i.e, for i-1
Cba1=(Cga*[a-b1+2*h+g1]+a*Caa+b1*Caa+c1*(uai-ua)-h*Caa-g1*Caa)/(a+h);
% Caa1 is the concentration of the gas - phase in the annulus region for
% the nodes lie before the node i , i.e, for i+1

```

```

Caa1=(Ci*[a-b1+2*h+g1]+a*Cba1+c1*(uai-ua)-h*Cba1)/a-b1+h+g1;
% Cga1 is the concentration of the gas - phase in the annulus region on
% the node i
Cga1=[(a*Caa1)+(a*Cba1)-(b1*Caa1)-c1*(uai-
ua)+(h*Caa1)+(h*Cba1)+(g1*Caa1)]/[2*a-b1+2*h+g1];
Ga=((12/dp*Mc)*11.34*10^3)*exp(-711600/(Rg*Tg));
La=(0.5*0.0883)*exp(-99800/(Rg*Tg));
% CO2s is the concentration of O2 at the solid surface on the annulus
% region
CO2a=((A1*(Caa1-Cga1))-(A2*(Caa1+2*Cga1+Cba1)))/V*(Ga+La);
%%% Steam %%%
CbaH2O=0;
CgaH2O=C1H2O;
CaaH2O=(C1H2O*[2*a-b1+2*hH2Oa+g1H2O]-a*CbaH2O+c1*(uai-ua)-
hH2Oa*CbaH2O)/a-b1+hH2Oa+g1H2O;
CgaH2O=[(a*CaaH2O)+(a*CbaH2O)-(b1*CaaH2O)-c1*(uai-
ua)+(hH2Oa*CaaH2O)+(hH2Oa*CbaH2O)+(g1H2O*CaaH2O)]/[2*a-b1+2*hH2Oa+g1H2O];
% Cba1 is the concentration of steam in the annulus region at
% node i-1
Cba1H2O=(CgaH2O*[a-b1+2*hH2Oa+g1H2O]+a*CaaH2O+b1*CaaH2O+c1*(uai-ua)-
hH2Oa*CaaH2O-g1H2O*CaaH2O)/a+hH2Oa;
% Caa1 is the concentration of steam in the annulus region at node
% i+1
Caa1H2O=(CgaH2O*[a-b1+2*hH2Oa+g1H2O]+a*Cba1H2O+c1*(uai-ua)-
hH2Oa*Cba1H2O)/a-b1+hH2Oa+g1H2O;
% Cga1 is the concentration of the gas - phase in the annulus region at
% the node i
Cga1H2O=[(a*Caa1H2O)+(a*Cba1H2O)-(b1*Caa1H2O)-c1*(uai-
ua)+(hH2Oa*Caa1H2O)+(hH2Oa*Cba1H2O)+(g1H2O*Caa1H2O)]/[2*a-
b1+2*hH2Oa+g1H2O];
% CCO2s is the concentration of H2O at the solid surface on the annulus
% region
CH2Oa=((A1*(Caa1H2O-Cga1H2O))-
(A2*(Caa1H2O+2*Cga1H2O+Cba1H2O)))/V*(Ga+La);
%%% carbon dioxide %%%
CbaCO2=0;
CgaCO2=C1CO2;
CaaCO2=(C1CO2*[2*a-b1+2*hCO2a+g1CO2]-a*CbaCO2+c1*(uai-ua)-
hCO2a*CbaCO2)/a-b1+hCO2a+g1CO2;
CgaCO2=[(a*CaaCO2)+(a*CbaCO2)-(b1*CaaCO2)-c1*(uai-
ua)+(hCO2a*CaaCO2)+(hCO2a*CbaCO2)+(g1CO2*CaaCO2)]/[2*a-b1+2*hCO2a+g1CO2];
% Cba1 is the concentration of carbon dioxide in the annulus region at
% node i-1
Cba1CO2=(CgaCO2*[a-b1+2*hCO2a+g1CO2]+a*CaaCO2+b1*CaaCO2+c1*(uai-ua)-
hCO2a*CaaCO2-g1CO2*CaaCO2)/a+hCO2a;
% Caa1 is the concentration of carbon dioxide in the annulus region at
node
% i+1
Caa1CO2=(CgaCO2*[a-b1+2*hCO2a+g1CO2]+a*Cba1CO2+c1*(uai-ua)-
hCO2a*Cba1CO2)/a-b1+hCO2a+g1CO2;
% Cga1 is the concentration of the gas - phase in the annulus region on

```

```

% the node i
Cga1CO2=[[ (a*Caa1CO2)+(a*Cba1CO2)-(b1*Caa1CO2)-c1*(uai-
ua)+(hCO2a*Caa1CO2)+(hCO2a*Cba1CO2)+(g1CO2*Caa1CO2) ]/[2*a-
b1+2*hCO2a+g1CO2]];
% CO2s is the concentration of CO2 at the solid surface on the annulus
% region
CCO2a=k1*CH2*((A1*(Caa1CO2-Cga1CO2))-
(A2*(Caa1CO2+2*Cga1CO2+Cba1CO2)))/V*(k2*((6/dp*Mc)*k1a*CO2s+k2a*CCOs*CO2s
+k1*CCOs*CH2Osc));
%%% carbon monoxide %%%
CbaCO=0;
CgaCO=C1CO;
CaaCO=(C1CO*[2*a-b1+2*hCOa+g1CO]-a*CbaCO+c1*(uai-ua)-hCOa*CbaCO)/a-
b1+hCOa+g1CO;
CgaCO=[(a*CaaCO)+(a*CbaCO)-(b1*CaaCO)-c1*(uai-
ua)+(hCOa*CaaCO)+(hCOa*CbaCO)+(g1CO*CaaCO) ]/[2*a-b1+2*hCOa+g1CO];
% Cba1 is the concentration of carbon monoxide in the annulus region at
% node i-1
Cba1CO=(CgaCO*[a-b1+2*hCOa+g1CO]+a*CaaCO+b1*CaaCO+c1*(uai-ua)-hCOa*CaaCO-
g1CO*CaaCO)/a+hCOa;
% Caa1 is the concentration of carbon monoxide in the annulus region at
node
% i+1
Caa1CO=(CgaCO*[a-b1+2*hCOa+g1CO]+a*Cba1CO+c1*(uai-ua)-hCOa*Cba1CO)/a-
b1+hCOa+g1CO;
% Cga1 is the concentration of the gas - phase in the annulus region at
% the node i
Cga1CO=[[ (a*Caa1CO)+(a*Cba1CO)-(b1*Caa1CO)-c1*(uai-
ua)+(hCOa*Caa1CO)+(hCOa*Cba1CO)+(g1CO*Caa1CO) ]/[2*a-b1+2*hCOa+g1CO]];
% COs is the concentration of CO at the solid surface on the annulus
% region
CCOa=((A1*(Caa1CO-Cga1CO))-(A2*(Caa1CO+2*Cga1CO+Cba1CO)))/V*BCO;
%%% Hydrogen %%%
CbaH2=0;
CgaH2=C1H2;
CaaH2=(C1H2*[2*a-b1+2*hH2a+g1H2]-a*CbaH2+c1*(uai-ua)-hH2a*CbaH2)/a-
b1+hH2a+g1H2;
CgaH2=[(a*CaaH2)+(a*CbaH2)-(b1*CaaH2)-c1*(uai-
ua)+(hH2a*CaaH2)+(hH2a*CbaH2)+(g1H2*CaaH2) ]/[2*a-b1+2*hH2a+g1H2];
% Cba1 is the concentration of hydrogen in the annulus region at
% node i-1
Cba1H2=(CgaH2*[a-b1+2*hH2a+g1H2]+a*CaaH2+b1*CaaH2+c1*(uai-ua)-hH2a*CaaH2-
g1H2*CaaH2)/a+hH2a;
% Caa1 is the concentration of hydrogen in the annulus region at node
% i+1
Caa1H2=(CgaH2*[a-b1+2*hH2a+g1H2]+a*Cba1H2+c1*(uai-ua)-hH2a*Cba1H2)/a-
b1+hH2a+g1H2;
% Cga1 is the concentration of the gas - phase in the annulus region at
% the node i
Cga1H2=[[ (a*Caa1H2)+(a*Cba1H2)-(b1*Caa1H2)-c1*(uai-
ua)+(hH2a*Caa1H2)+(hH2a*Cba1H2)+(g1H2*Caa1H2) ]/[2*a-b1+2*hH2a+g1H2]];

```

```

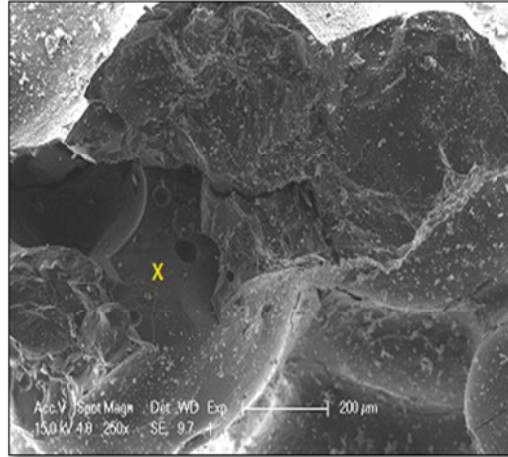
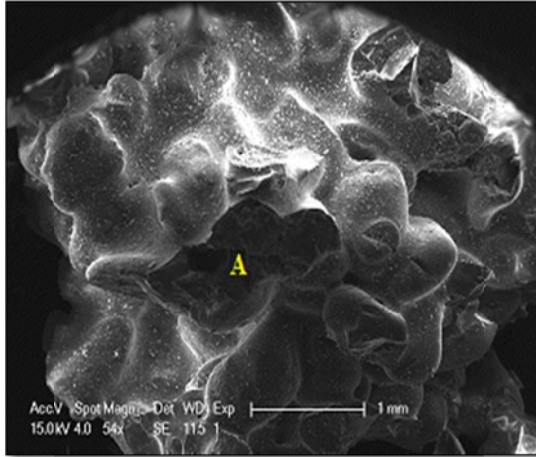
% CCO2s is the concentration of H2 at the solid surface on the annulus
% region
CH2a= ((6/dp)*k3a-k1*CCO2/k2+((H1/1+k7*CH2Osc+k8+k9*CCOs)-
((k10*CCOsc^2)+((A1*(Caa1H2-Cga1H2))-(A2*(Caa1H2+2*Cga1H2+Cba1H2)))/V*(-
1*k1*CCOsc*CH2Osc-k10*CCH4sc*CH2Osc))));
    end
end

```

# Appendix E

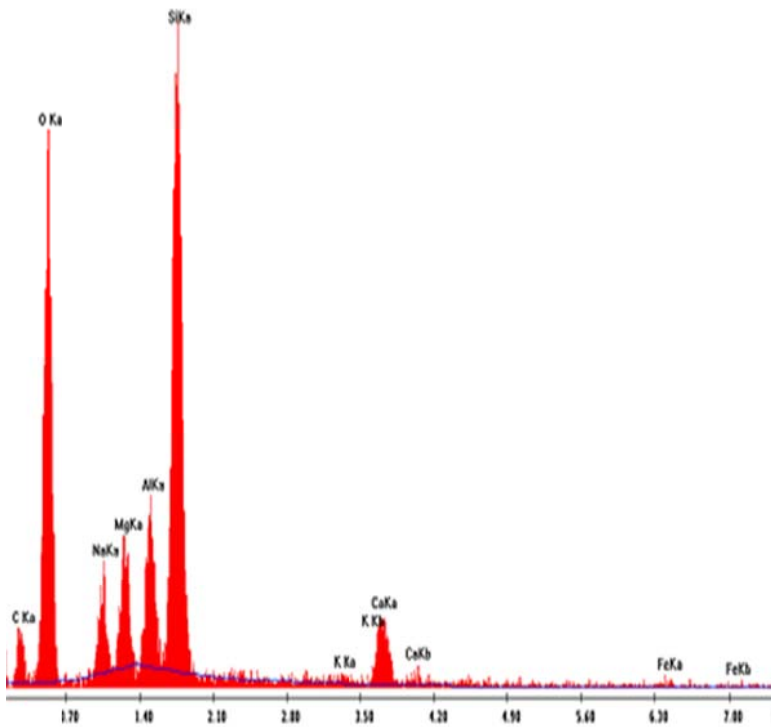
## SEM analysis results

### E.1 Micrograph of SE and BSE images for the agglomerate from coal gasification

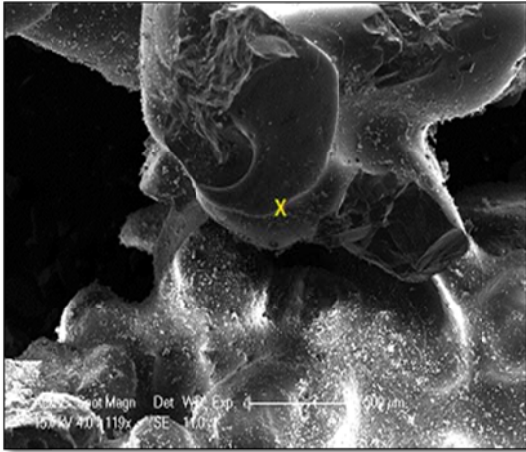


ion

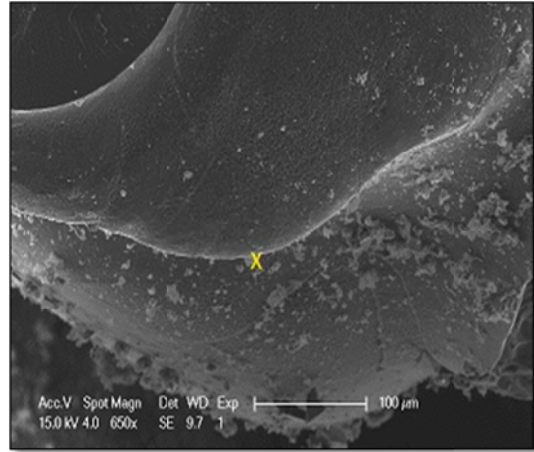
1



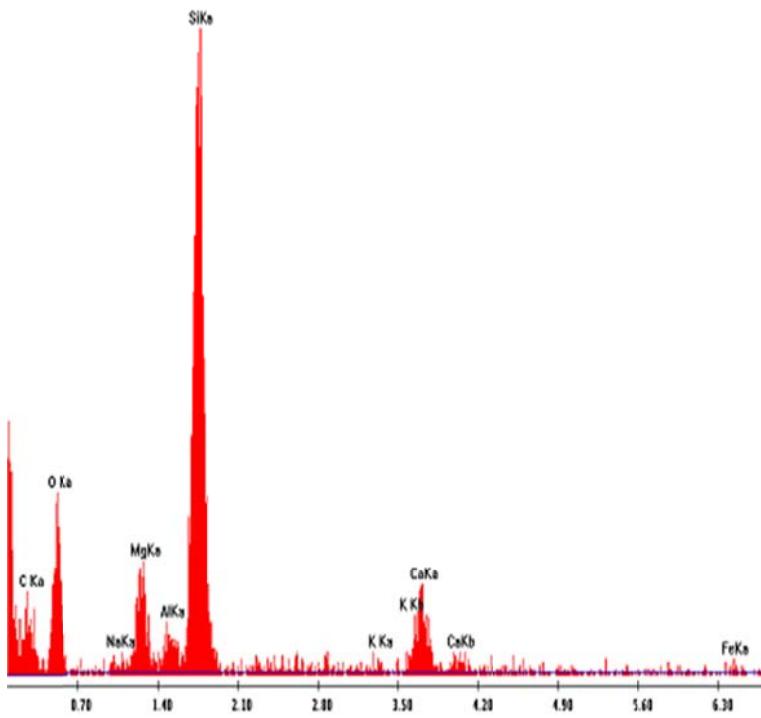
Element	Wt %
C	14.54
O	39.77
Na	3.6
Mg	4.49
Al	5.58
Si	24.67
K	0.76
Ca	5.33
Fe	1.26
Total	100



ion

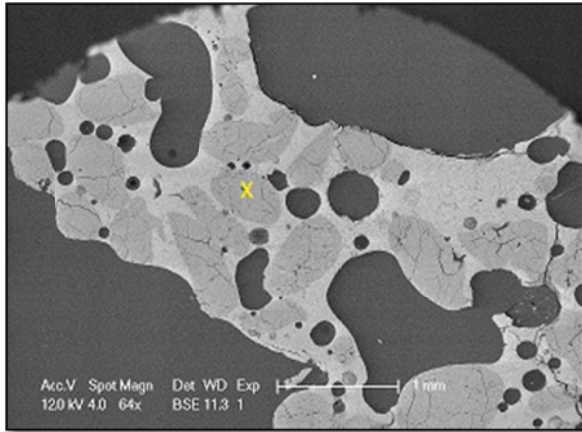


EM  
selected



Element	Wt%
C	31.77
O	21.83
Na	0.58
Mg	4.66
Al	1.79
Si	30.26
K	0.64
Ca	7.6
Fe	0.85
Total	100

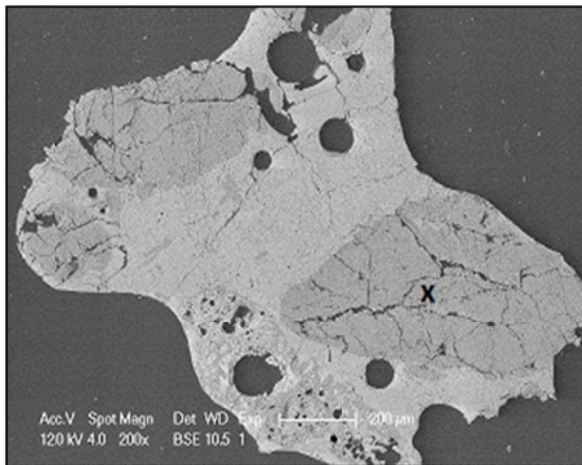
f the  
rt in



Element	Wt %
O	47.66
Na	0.35
Mg	0.35
Al	0.74
Si	49.28
S	0.39
Cl	0.4
K	0.22
Ca	0.6
Total	100

M  
of

3  
1

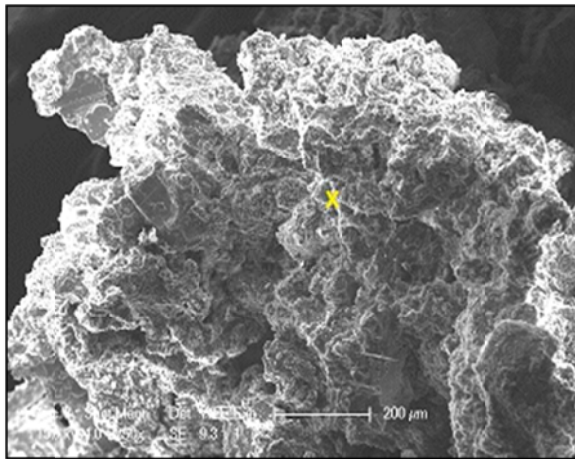


Element	Wt %
O	49.09
F	0
Na	0.43
Mg	0.39
Al	0.58
Si	48.99
P	0
S	0
Cl	0
K	0.12
Ca	0.39
Total	100

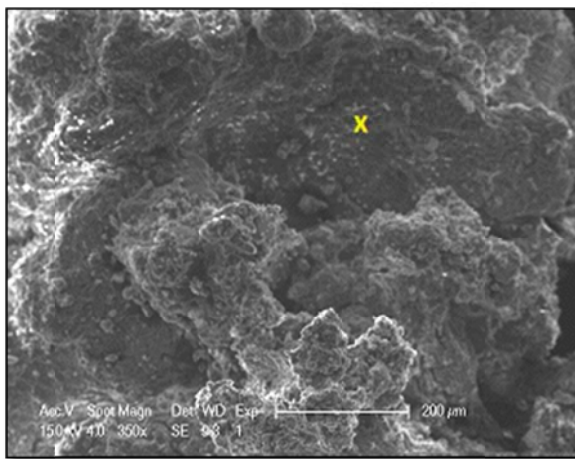
M  
1 of

## E.2 Micrograph of SE and BSE images for the agglomerate from algae gasification

Figures E-5 and E-6 show Micrographs of SEM secondary electronic images for the agglomerate obtained from the gasification of algae with 1.43 Kg/h algae feed rate, 0.5 S/F and a temperature of 850 °C. Analysis results for each selected section can be shown in front of each image.

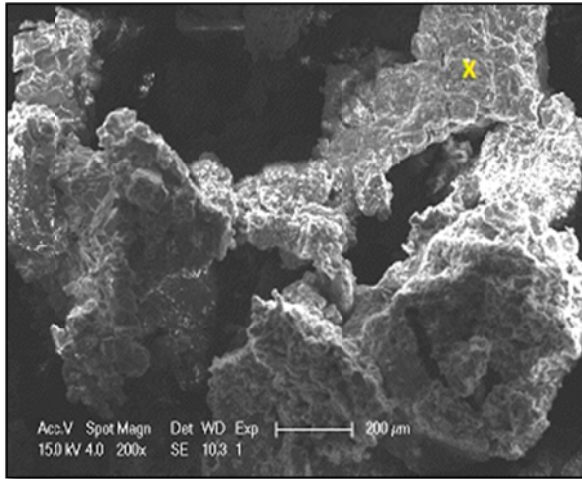


Element	Wt %
O	10.86
Na	4.97
Mg	1
Al	58.19
Si	3.11
P	0
S	1.89
Cl	15.17
K	1.61
Ca	2.24
Fe	0.97
Total	100



Element	Wt %
O	16.88
Na	15.97
Mg	7.42
Al	6.12
Si	2.06
P	1.3
S	2.84
Cl	37.38
K	3.97
Ca	2.76
Fe	3.29
Total	100

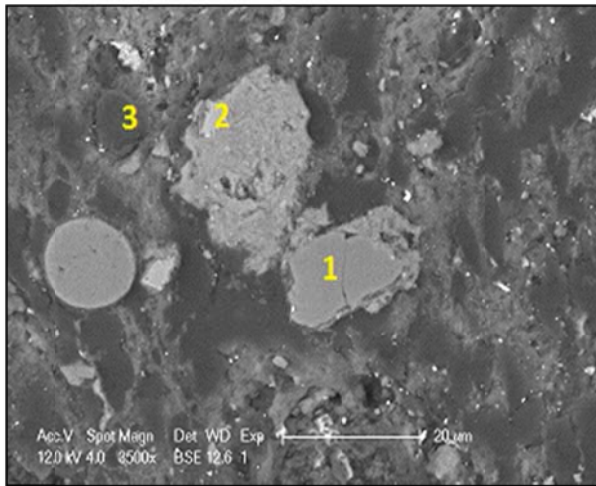
**Figure E-5** Micrographs of SEM secondary electronic images of agglomerate



Element	Wt %
O	20.95
Na	15.48
Mg	6.71
Al	4.68
Si	0.93
P	0.92
S	4.47
Cl	35.08
K	1.19
Ca	7.79
Fe	1.81
Total	100

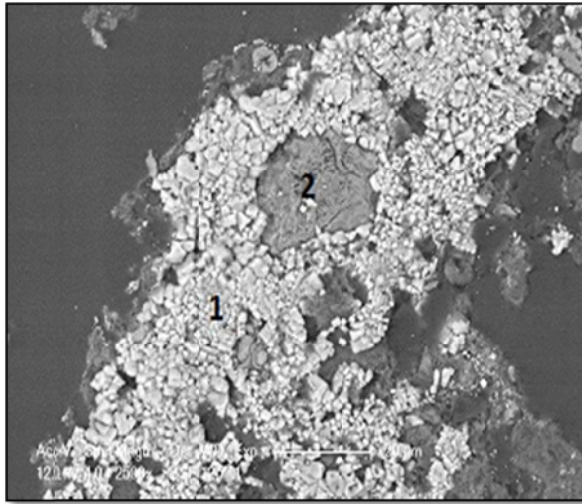
**Figure E-6** Micrographs of SEM secondary electronic images of agglomerate

Figures E-7 and E-8 shows Micrographs of SEM back scattered electron images for the agglomerate obtained from the gasification of algae with 1.43 Kg/h algae feed rate, 0.5 S/F and a temperature of 850 °C. Analysis results for each selected section can be shown in front of each image.



Element	Sec.1 Wt %	Sec.2 Wt %	Sec.3 Wt %
O	48.97	44.41	59.5
Na	0	2.85	4.13
Mg	0.41	4.32	6.85
Al	1.09	14.91	9.93
Si	47.45	20.8	3.32
P	0	0	4.23
S	0.41	0.32	3.89
Cl	0.46	1.51	5.82
K	0.42	2.69	0.95
Ca	0.79	8.2	1.38
Total	100	100	100

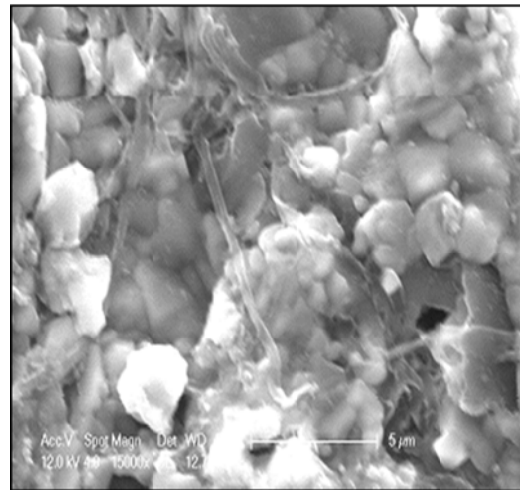
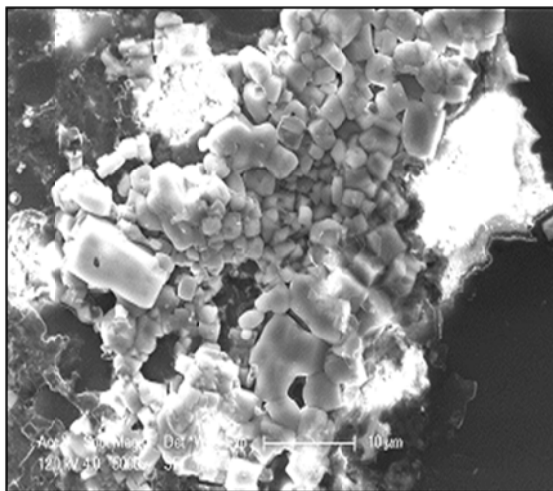
**Figure E-7** Micrographs of SEM back scattered electron images



Element	Sec.1 Wt %	Sec.2 Wt%
O	2.12	40.01
F	0	0
Na	33.74	3.08
Mg	0	20.39
Al	0.7	6.39
Si	0.73	20.66
P	0.82	0.89
S	1.75	0.67
Cl	58.56	4.24
K	0.79	1.17
Ca	0.79	2.51
Total	100	100

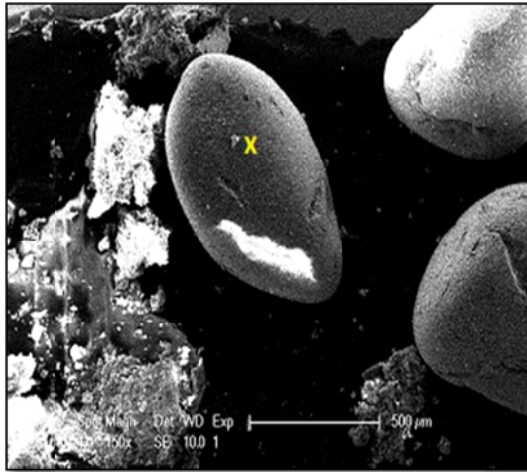
**Figure E-8** Micrographs of SEM back scattered electron images

Figure E-9 shows Micrographs of SEM back-scattered electron images zoom-in for section in the agglomerated algae results from the run with 1.43 Kg/h algae feed rate, 0.5 S/F, at 850 °C. The following images show how the salt crystals form in clusters sticking to each other during gasification.

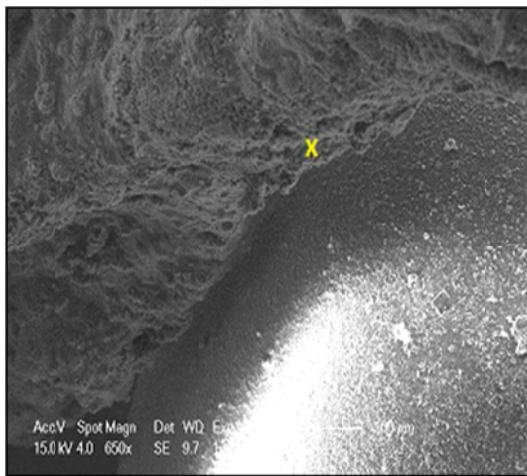
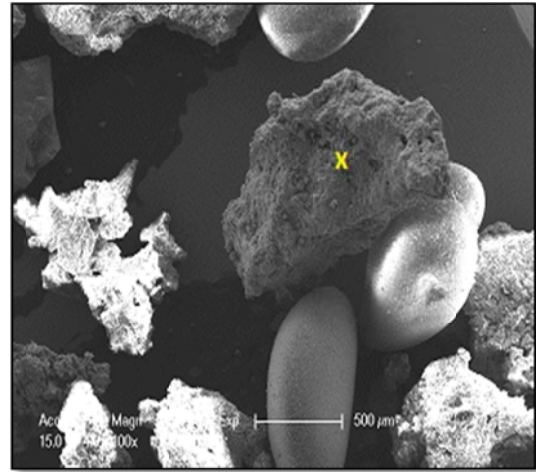


**Figure E-8a** Micrographs of SEM back-scattered electron images zoom-in for section 1 in Fig. E-8

Figure E-9a and b show micrographs of SEM back-scattered electron images for the bed material results from gasification of algae with fuel feed rate of 1.43 Kg/h, 0.5 S/F, at 850 °C. Figure E-9c and d show zoom-in micrographs of SEM back-scattered electron images for the bed material (section in contact between sand and algae articles in Figure E-9b).



a



c

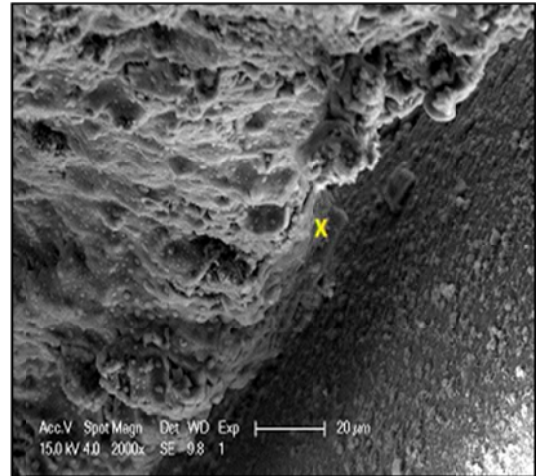


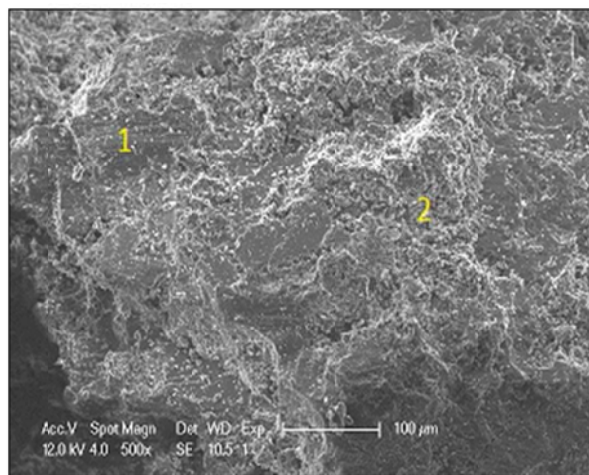
**Figure E-9** Micrographs of SEM back-scattered electron images for the bed material, with the results of analysis for the selected sections in images a, b, c, and d.

**Table E-5** Compositional information for the selected sections in Figure E-9a, b, c, and d

Element	Sec. a, Wt %	Sec. b, Wt %	Sec. c, Wt %	Sec. d, Wt %
O	39.05	5.91	10.43	6.49
Na	4.14	30.8	7.7	15.41
Mg	24.53	0	2.56	0
Al	0.79	1.04	27.87	38.96
Si	18.88	0.55	14.99	0.17
P	0	0.51	0.79	0.65
S	1.57	1.96	4.77	0.72
Cl	7.8	54.15	17	34
K	0.29	1.01	2.28	0.97
Ca	1.49	2.85	7.25	1.39
Fe	1.45	1.21	4.35	1.24
Total	100	100	100	100

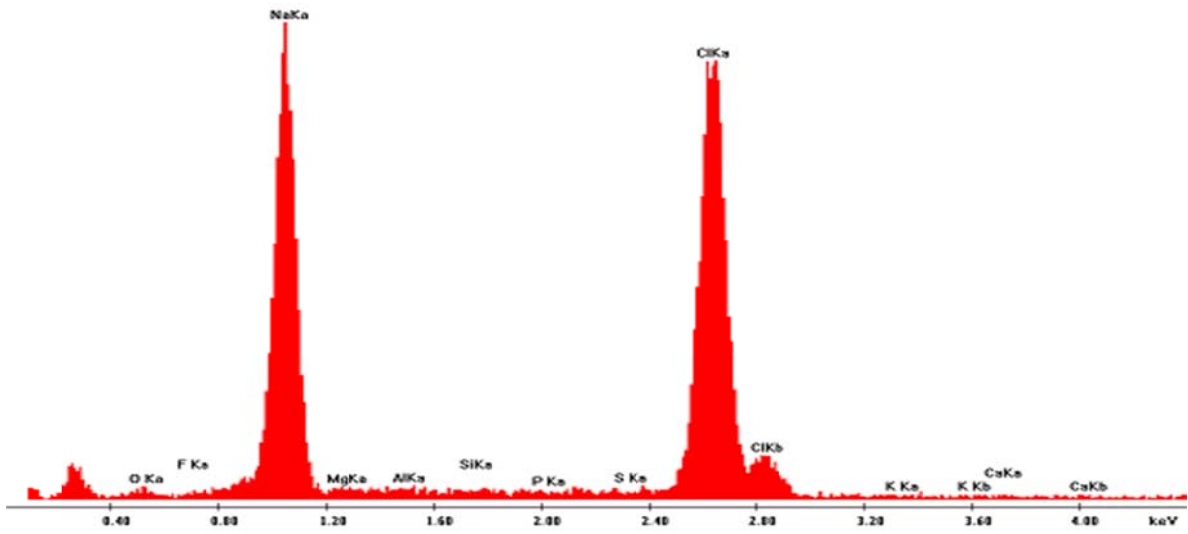
### E.3 Micrograph of SEM images for the raw algae before and after leaching

Figure E-10 shows micrographs of SEM secondary-electron images for the raw algae before leaching used in gasification with the compositions of components in sections 1 and 2.

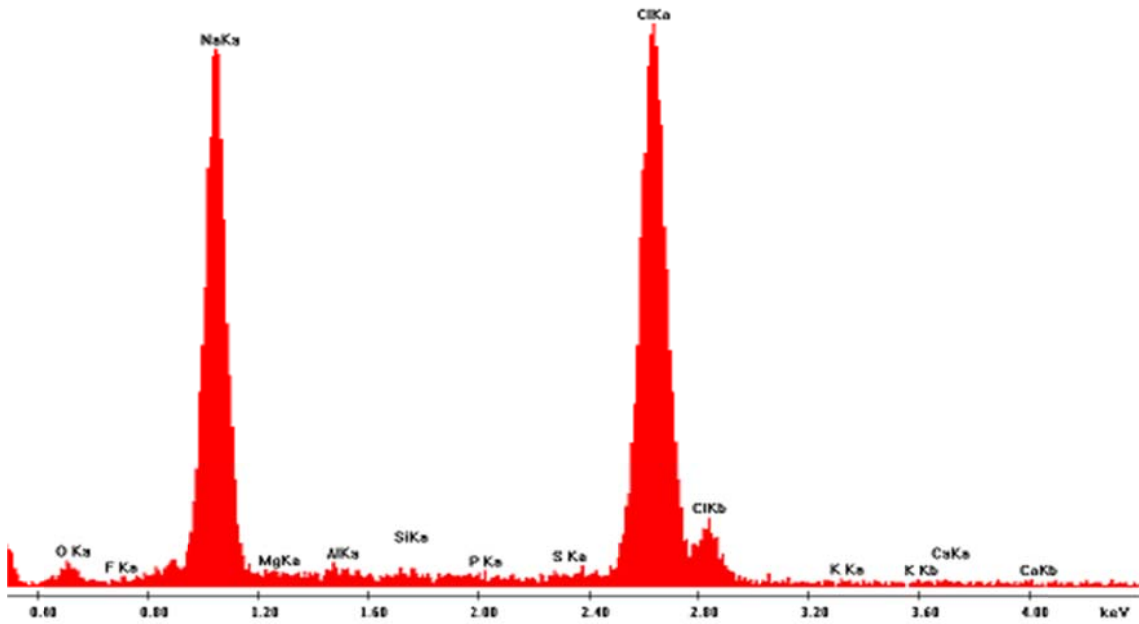


Element	Sec.1 Wt %	Sec.2 Wt %
O	1.99	4.36
F	0.35	0.12
Na	39	37.79
Mg	0	0
Al	0.49	0.73
Si	0.53	0.61
P	0.61	0.12
S	0.84	0.52
Cl	55.02	55.61
K	0.6	0
Ca	0.58	0.15
Total	100	100

**Figure E-10** Micrographs of SEM secondary- electron images and the composition of each component result from analysis in sections 1 and 2 of raw algae before leaching.

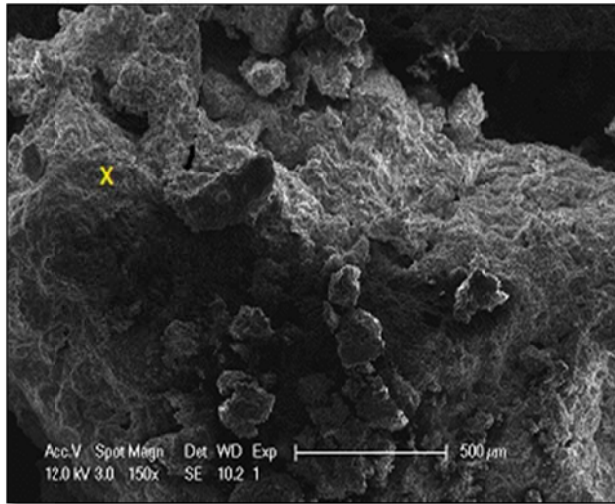


**Figure E-10a** Peaks for the compositions of raw algae before leaching at section 1 in Fig.E-10 taken under SE detector



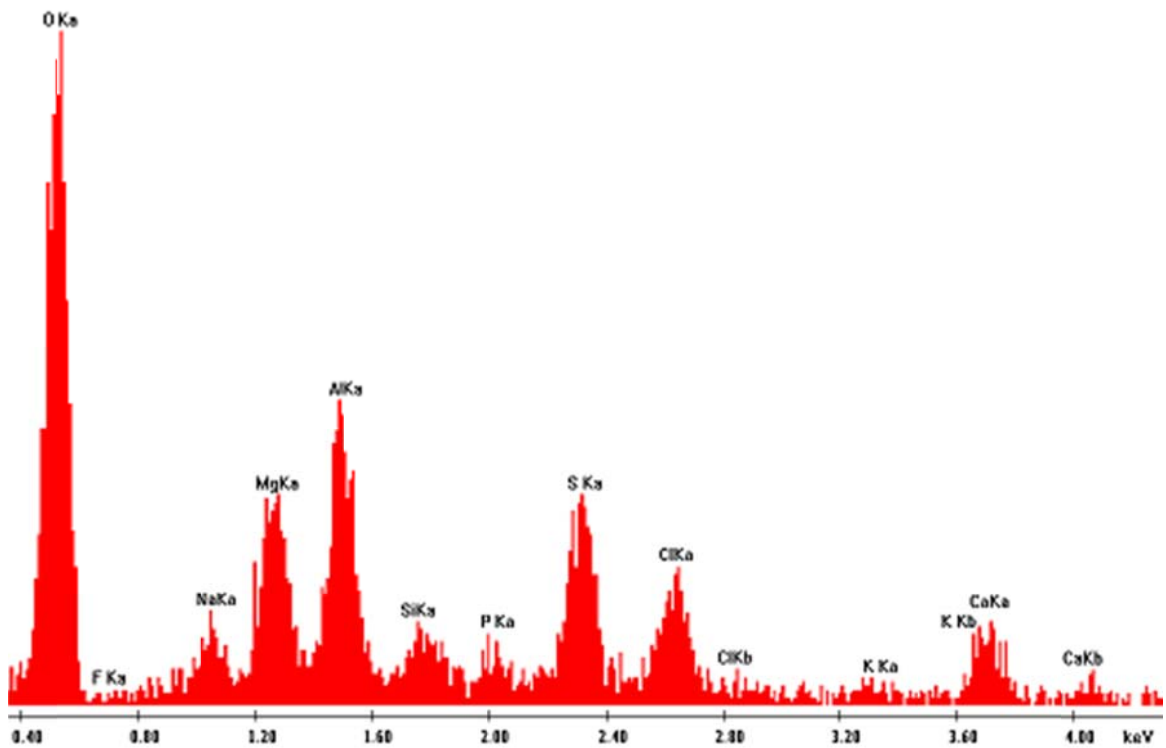
**Figure E-10b** Peaks for the compositions of raw algae before leaching at section 2 in Fig.E-10 taken under SE detector.

Figure E-11 shows micrographs of SEM secondary-electron images for the raw algae after leaching with the data results for the components in the selected section.



Element	Wt%
O	45.8
F	0
Na	3.01
Mg	6.38
Al	10.21
Si	1.41
P	1.91
S	12.26
Cl	8
K	1.55
Ca	9.48
Total	100

**Figure E-11** Micrographs of SEM secondary- electron images and the composition of each component result from analysis in the selected sections of raw algae after leaching.



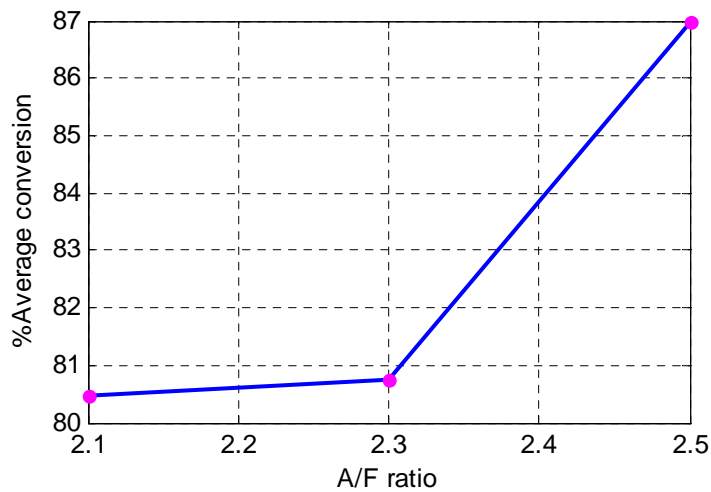
**Figure E-11a** Peaks for the compositions in the selected section in Fig. E-11 of raw algae after leaching taken under SE detector

## Appendix F

### Carbon conversion results for coal-grape seeds gasification

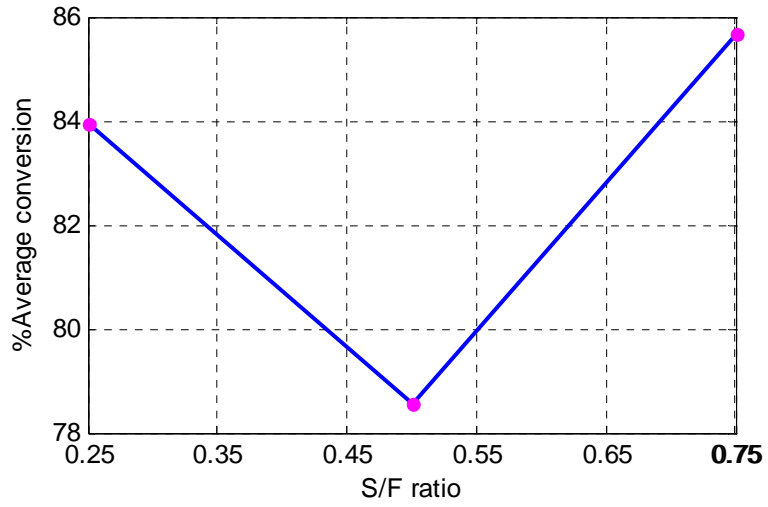
#### F.1 Carbon conversion results from coal-grape seeds gasification experiments at different levels of variables

Figure F-1 shows the values of the mean carbon conversion with changing the A/F ratios. The maximum mean carbon conversion achieved when increasing the A/F ratio from 2.3 to 2.5.



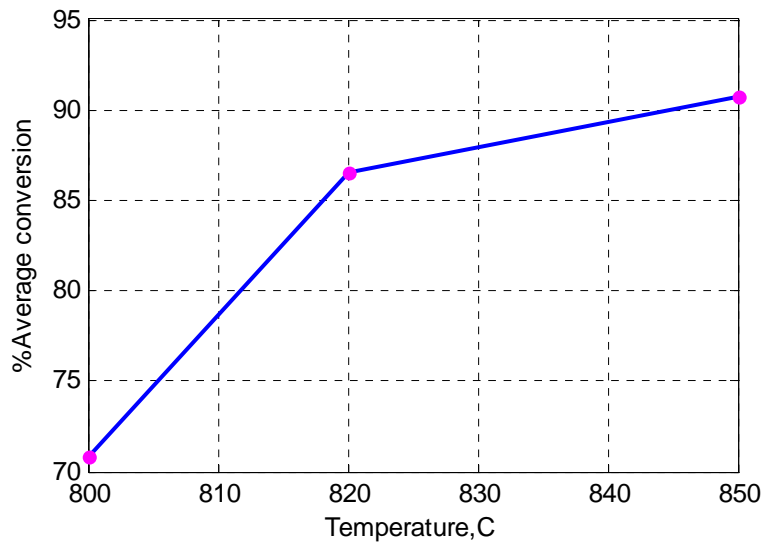
**Figure F-1** Effect of changing A/F ratio on carbon conversion

Figure F-2 shows the obtained mean carbon conversion values with different levels of S/F ratios. It can be noticed that carbon conversion decreased from S/F ratio of 0.25 to 0.5 while increasing the S/F ratio from 0.5 to 0.75 results in an increase in the carbon conversion.



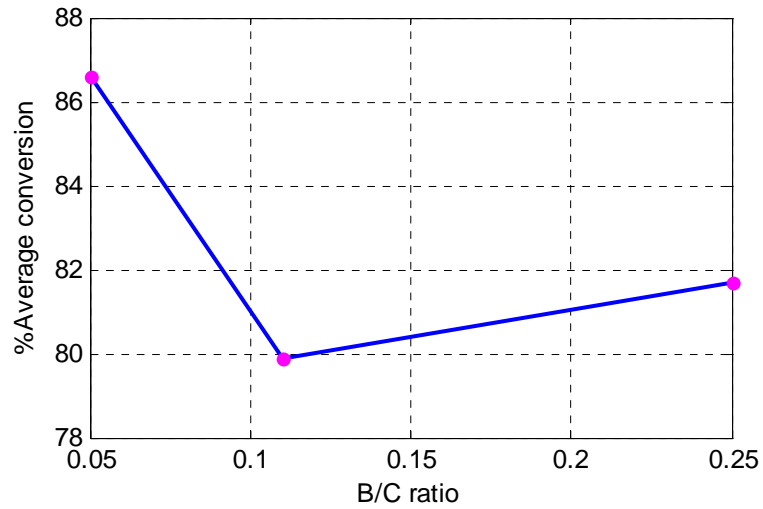
**Figure F-2** Effect of changing S/F ratio on carbon conversion

Figure F-3 shows the carbon conversion results when changing the bed temperature. The carbon conversion increased with increasing bed temperature and the maximum conversion achieved when increasing the temperature from 820 °C to 850 °C.



**Figure F-3** Effect of changing the bed temperature on carbon conversion

Figure F-4 shows the obtained carbon conversion values at different biomass to coal ratios. Changing the ratio of B/C from 0.05 to 0.11 decreased the carbon conversion while increasing the B/C from 0.11 to 0.25 results in slightly increase in the carbon conversion which concluded that changing the B/C ratio has a less effect on the carbon conversion.



**Figure F-4** Effect of changing the B/C ratio on carbon conversion

## الخلاصة

مع ارتفاع كلفة النفط الخام والحاجة المتزايدة لوقود النقل تم استخدام مواد خام قليلة الكلفة مثل الفحم وبقايا الكتلة العضوية كمصدر اقتصادي لانتاج وقود النقل أو لتوليد الطاقة الكهربائية باستعمال مفاعل الطبقة المميعة بعد ربطه مع محرك الغاز لتحويل الوقود الصلب، حيث يعتبر مفاعل الطبقة المميعة من التقنيات الراسخة والكثيرة الأستعمال.

العمل الحالي يهتم بدراسة آليات تفاعلات التحويل إلى الغاز لإنتاج الغاز الحيوي بتحويل الفحم، الطحالب، مشارك من طحالب-الفحم و بذور العنب-الفحم في مفاعل الطبقة المميعة المنطلق للتحويل الى الغاز تحت تأثير ظروف تشغيلية مختلفة. نظرياً، تم وضع موديل رياضي لحساب تراكيز الغازات الناتجة من عملية التحويل الى الغاز بثبوت الحرارة.

الجزء العملي يهتم بتحويل الفحم، الطحالب، والفحم- الطحالب الى الغاز الحيوي في مفاعل الطبقة المميعة المنطلق للتحويل الى الغاز باستخدام الرمل كوسط لنقل الحرارة وللمزج داخل المفاعل. تم دراسة تأثير تغيير الظروف التشغيلية مثل درجة الحرارة (٨٢٠، ٨٥٠) درجة سيليزية، نسبة البخار الى الوقود (0, 0.5, 0.75)، نسبة الهواء الى الوقود (1.6, 1.8, 2). أما في عملية تحويل الفحم- بذور العنب الى الغاز الحيوي فقد تم اعتماد طريقة تاجوشي في تصميم التجارب لدراسة مختلف الظروف التشغيلية مثل درجة الحرارة (٨٥٠، ٨٢٠)، نسبة البخار الى الوقود (0.25, 0.5, 0.75) ، نسبة الهواء الى الوقود (2.1, 2.3, 2.5) ، ونسبة البايوماس الى الفحم (0.05, 0.11, 0.25).

في عملية تحويل الفحم الى الغاز الحيوي، تركيز  $CO_2$  نقص عند زيادة درجة الحرارة في حالة كمية تغذية الوقود المنخفضة بينما تركيز  $H_2$ ،  $CO$ ،  $CH_4$  ازداد مع زيادة درجة الحرارة. في حالة زيادة كمية تغذية الوقود، تركيز  $CO_2$ ،  $CO$ ،  $H_2$ ،  $CH_4$  ازداد بزيادة درجة الحرارة.

اضافة البخار الى الهواء المتفاعل مع الوقود الصلب أدى الى منع حدوث تكثف للمادة المتفاعلة مع الرمل داخل المفاعل. زيادة نسبة البخار الى الوقود أدى الى زيادة تركيز  $H_2$ ،  $CO$  و  $CH_4$  ونقصان في تركيز  $CO$ . في درجات الحرارة المنخفضة تركيز غاز الهيدروجين ازداد بزيادة نسبة الهواء الى الوقود، أما في درجات الحرارة المرتفعة زيادة نسبة الهواء الى الوقود أدت الى نقصان تركيز غاز الهيدروجين الناتج. الظروف التشغيلية المثلى في عملية تحويل الفحم الى الغاز الحيوي هي: نسبة الهواء الى الوقود = ١.٨ ، نسبة البخار الى الوقود = ٠.٧٥ ، ودرجة الحرارة = ٨٥٠ درجة سيليزية. في هذه الظروف تم الحصول على اعلى نسبة تحول للكربون = 92.9% واعلى نسبة  $H_2:CO = 2.197$ .

عملية التحويل للغاز لوقود الطحالب الغير مرشحة و الفحم- الطحالب المرشحة أدى الى حدوث تكسر أو طحن لجزيئات الطحالب في وحدة التغذية وتحويلها الى جزيئات صغيرة الحجم تتطاير بسهولة عند دخولها المفاعل مما تسبب في حدوث انسداد في أنابيب مرور الغاز الناتج.

تجارب تحويل الفحم- بذور العنب الى الغاز الحيوي أثبتت ان درجة الحرارة هي المتغير الأكثر تأثيرا على نسبة تحول الكربون بينما نسبة البذور الى الفحم كان المتغير الأقل تأثيرا على نسبة تحول الكربون. نظريا، تم وضع موديل رياضي بثبوت درجة الحرارة لحساب تراكيز الغازات الناتجة مع ارتفاع المادة المتفاعلة داخل المفاعل. تم الوصول الى النموذج الذي يصف انتقال جزيئات الغاز خلال المفاعل عن طريق عمل موازنة ووضع معادلات تفاضلية تصف النظام. تقنية الاختلاف المحدود العددية استخدمت لحل هذه المعادلات باستخدام برنامج Matlab (R2011a) الذي تم عن طريقه حساب تراكيز الغازات الناتجة وحساب سرعة الغاز داخل المفاعل. بعد مقارنة النتائج العملية والنتائج التجريبية وجد أن هناك توافق جيد بينهما.

الحمد والشكر لله رب العالمين الذي هدانا لهذا وما كنا لنهتدي لولا أن هدانا الله والصلاة والسلام على النبي الأمين محمد وعلى آله وصحبه أجمعين ومن تبعه بإحسان الى يوم الدين وبعد:

أتقدم بجزيل الشكر والأمتنان إلى من تتجسد في عطاءه كل معاني الكرم والمروءة أستاذي الفاضل الدكتور باسم عبيد حسن/ رئيس قسم الهندسة الكيماوية / المشرف على الرسالة لما قدمه لي من نصح وتوجيهات سديدة وملاحظات علمية قيمة أسهمت في إنجاز هذا العمل بأفضل صورة ممكنة أسأل الله له عمراً مديداً، وعيشاً سعيداً إن ربي قريب مجيب. كما وأتوجه بالشكر والأمتنان الى الدكتور بيتر أشمان / جامعة أدليد / أستراليا لجهوده في توفير كافة المستلزمات لأتمام الجزء العملي. الشكر الجزيل للأستاذ الدكتور محسن جبر جويج / عميد كلية الهندسة لتعاونه مع الطلبة. شكري وتقديري الى الدكتور سعد حنش عمار لتعاونه أسأل الله له التوفيق كما وأشكر كادر الهندسة الكيماوية لتعاونهم وأتقدم بالشكر والحب والعرفان الى والدي، والدتي، أخوتي، أخواتي، وأصدقائي الأعراء وكل من تعرفت اليهم خلال فترة بحثي لتهيئة الظروف المناسبة وعلى تشجيعهم لي لمواصلة مسيرتي العلمية أسأل الله أن يوفقهم لكل ما يحبه ويرضاه وأن يحقق آمالهم.

